Copyright is owned by the Author of the thesis. Permission is given for a copy to be downloaded by an individual for the purpose of research and private study only. The thesis may not be reproduced elsewhere without the permission of the Author.



MASSEY UNIVERSITY
TE KUNENGA KI PŪREHUROA
UNIVERSITY OF NEW ZEALAND

Structure-function relationships in plant- and hybrid-protein processed cheese analogues: identifying drivers of functionality

A thesis presented in partial fulfilment of the requirements for the degree of

Doctor of Philosophy in Food Technology

at Massey University, Manawatū, New Zealand

Di Lu

2026



Abstract

Processed cheese was developed by blending natural cheese with emulsifying salts and applying heat, resulting in a stable product with an extended shelf life and versatile functionality across a wide range of applications. However, growing concerns regarding environmental impact, sustainability, health, and animal welfare have driven increasing interest in plant-based alternatives. As a result, the development of plant-based processed cheese analogues has accelerated, aiming to deliver comparable functionality and sensory properties while addressing these broader societal demands.

However, most commercial plant-based processed cheese analogues (PCAs) are primarily formulated with starch and vegetable oils. While starch contributes to viscosity and forms a gel-like network upon gelatinisation that can partially mimic dairy cheese structure, these systems often have low nutritional value and exhibit limited texture and functionality. In addition, substituting animal proteins with plant proteins remains challenging due to fundamental structural differences and functional limitations. Although the incorporation of plant proteins has led to some improvements, current formulation strategies remain largely empirical, and the underlying structure–function relationships are not well understood. Furthermore, the development of hybrid systems combining plant and milk proteins remains limited, and the mechanisms governing structure and functionality in such multiprotein systems are poorly defined.

To address these limitations, this doctoral thesis investigated the incorporation of plant proteins into processed cheese model systems, with a focus on their role in structure formation and functionality. Specifically, it aims to elucidate structure–function relationships in plant-based and hybrid cheese analogues at the multiscale and to develop strategies for modifying plant proteins to modulate their interactions and aggregation behaviour, thereby tailoring network formation and

improving functional performance, particularly in terms of microstructure, texture, meltability, and stretchability.

First, various plant proteins were evaluated within plant-based processed cheese analogues to elucidate structure–function relationships. The results demonstrated that plant-based processed cheese analogues generally lacked a continuous protein network, leading to poor melting and stretchability. Microstructure and textural properties were strongly dependent on protein type and aggregation behaviour.

Based on their distinct functional performance, mung bean protein and hemp protein were selected for further investigation in hybrid processed cheese systems formulated by blending with rennet casein at different ratios. The microstructure, texture, melting behaviour, and stretchability of these hybrid systems were characterised. The result indicated that both the type of plant protein and the blending ratio with casein significantly influenced structural organisation and functional performance. Mung bean protein–casein systems exhibited superior stretchability and viscoelasticity compared with hemp protein hybrid systems at equivalent incorporation levels, whereas hemp protein formulations showed greater meltability. These differences were primarily attributed to variations in protein aggregation size and structural composition.

Molecular interactions and structural changes were further examined using Raman microspectroscopy and synchrotron-based Fourier transform infrared (S-FTIR) spectroscopy, combined with chemometrics and machine learning approaches. The results showed that mung bean protein–casein systems induced microstructural segregation and changes in β-sheet content, whereas hemp protein–casein systems exhibited greater structural disorder and disulfide bond rearrangement. Increasing casein content reduced plant protein aggregation and promoted a more

flexible network, demonstrating that plant proteins are not functionally interchangeable and must be selected according to targeted functionality.

Furthermore, mung bean protein was subjected to enzymatic hydrolysis to evaluate physicochemical and structural modifications and to determine whether controlled enzymatic treatment could improve melting functionality in both PCAs and hybrid cheese systems. The results demonstrated that enzymatic hydrolysis effectively reduced the molecular weight and particle size of mung bean protein while increasing surface hydrophobicity, leading to improved meltability in PCA systems. Notably, enzyme specificity exerted a greater influence on functional outcomes than the degree of hydrolysis alone. These results demonstrate that controlled enzymatic modification can tailor functional performance, although optimisation requires balancing solubility, aggregation behaviour, and network continuity.

Overall, this PhD thesis demonstrates that the functionality of plant-based and hybrid processed cheese systems is governed by protein-specific interactions, aggregation behaviour, and the resulting network structure. In plant-based systems, different plant proteins generate distinct microstructures that influence texture, meltability, and stretchability. In hybrid cheeses, variations in plant protein–casein interactions lead to different microstructures and corresponding functional outcomes. Enzymatic modification provided an effective means to modulate these interactions and tailor melting behaviour. The findings from this thesis contribute to the rational design of high-plant-protein cheese analogues with improved texture and functional performance.

Keywords: Plant-based processed cheese analogues, hybrid processed cheese analogues, plant proteins, texture, meltability

Acknowledgements

I would like to sincerely thank all of my supervisors: Professor Aiqian Ye, Distinguished Professor Harjinder Singh, Associate Professor Alejandra Acevedo-Fani, and Dr Debashree Roy, for their continuous support, guidance, and encouragement throughout my PhD journey. I am especially grateful to my chief supervisor Professor Aiqian Ye, for giving me the opportunity to pursue this doctoral study. Your patience, insightful discussions, constructive feedback, and generous investment of time have shaped both this thesis and my development as a researcher. I truly appreciate the ideas, advice, and confidence you have shared with me over the years.

My heartfelt thanks go to Professor Mark Waterland for his valuable guidance in applying for funding for the synchrotron study. Your support made this important part of my research possible. I am also deeply grateful to Dr Cushla McGoverin, from University of Auckland, for her kind assistance with the Raman microscopy study and collaboration, and for the significant time and care she devoted to helping me navigate both the technical and practical aspects of the work.

I gratefully acknowledge the Riddet Institute, the Centre of Research Excellence, for funding this PhD project, providing me with a doctoral scholarship, and supporting my academic growth through conference travel grants. I also sincerely thank New Zealand Synchrotron Group Ltd for funding New Zealand researchers and students to access the Australian Synchrotron, which greatly enriched this research. I would also like to extend my sincere gratitude to the staff at the Australian Synchrotron, particularly Dr Pimm Vongsvivut and Dr Annaleise Klein, for organising the training and induction, setting up the equipment, and providing valuable suggestions on this work. I am also grateful to Mrs Clare Scott for coordinating the sample documentation and ensuring their smooth arrival.

I would like to extend my appreciation to the laboratory managers and technicians, Maggie Zou,, Michelle Tamehana, Adrain Koolarrd, Yu Zhang, Matthew Perrott, for their technical expertise, practical support, and readiness to help whenever challenges arose in the lab.

Finally, and most importantly, I thank my parents, my husband, and my child. Your unconditional love, understanding, and unwavering support have been my greatest source of strength. Completing this PhD would not have been possible without you beside me every step of the way.

Table of Contents

Abstract ..... **i**

Acknowledgements ..... **v**

List of publications, proposals, awards and presentations ..... **xii**

List of Figures ..... **xiv**

List of Tables ..... **xxi**

List of Abbreviations ..... **xxii**

Chapter 1 Introduction **1**

Chapter 2 Literature review – Plant-based cheese analogues: Bridging structure-function relationships towards improved function performance[1] **9**

Abstract 9

2.1. Introduction 12

2.2. Structure–function relationship 15

2.2.1. The role of starch in plant-based cheeses 16

2.2.2. The role of plant protein in plant-based cheeses 53

2.2.3. The role of vegetable oil in plant-based cheeses 54

2.2.4. Microstructure, texture, and functional properties of plant-based cheese analogues 55

2.3. Improvement strategies through tailoring input 65

2.3.1. Formulation strategies 65

2.3.2. Processing 78

2.3.3. Summary of recent developments 79

2.4. Future directions 81

2.4.1. Hybrid cheese 81

2.4.2. Disruptive technologies 90

2.5. Conclusion 92

Chapter 3 Investigation of various plant protein ingredients for processed cheese analogues: physical properties and microstructure compared with milk proteins[2] **96**

Abstract 96

3.1. Introduction 98

3.2. Materials and methods 100

3.2.1. Materials 100

3.2.2. Preparation of PCAs slices 100

3.2.3. Dynamic rheological analysis of PCAs 101
3.2.4. Texture profile analysis 102
3.2.5. Meltability of PCAs 103
3.2.6. Stretchability of PCAs 103
3.2.7. Microstructure of PCAs 103
3.2.8. Comparison of plant proteins in PCAs using principal component analysis and TOPSIS 104
3.2.9. Statistical analysis 105
3.3. Results and discussion 106
3.3.1. Formation of PCAs 106
3.3.2. Rheological properties 107
3.3.3. Texture profile 114
3.3.4. Meltability 116
3.3.5. Stretchability 117
3.3.6. Microstructure 120
3.3.7. Comparison of plant proteins in processed cheese analogues using principal component analysis and TOPSIS 123
3.4. Conclusion 126
3.5. Acknowledgements 126
3.6. Supplementary material 127
Chapter 4 Physical properties and microstructure of hybrid processed cheeses formulated with plant protein and milk protein ingredients[3] 130
4.1. Introduction 132
4.2. Materials and methods 135
4.2.1. Materials 135
4.2.2. Preparation of HPCAs 135
4.2.3. Sodium dodecyl sulphate–polyacrylamide gel electrophoresis (SDS–PAGE) 137
4.2.4. Dynamic rheological analysis 138
4.2.5. Microstructure 139
4.2.6. Texture profile analysis (TPA) 140
4.2.7. Meltability and Stretchability 140
4.2.8. Analysing protein structure with Fourier transform infrared (FTIR) spectroscopy 141
4.2.9. Statistical analysis 142

4.3. Results and discussion 142
4.3.1. Protein composition 142
4.3.2. Rheological properties of HPCAs 146
4.3.3. Microstructure 150
4.3.4. Texture profile of HPCAs 153
4.3.5. Meltability and Stretchability 157
4.3.6. Analysing protein structure with FTIR 160
4.3.7. Structure–functionality relationship proposed in plant protein-casein HPCAs 162
4.4. Conclusions 165
4.5. Acknowledgments 165
4.6. Supplementary material 167
Chapter 5 Distinguishing plant and milk proteins and their interactions in hybrid cheese using confocal Raman microscopy with machine learning[4] 171
5.1. Introduction 173
5.2. Materials and Methods 175
5.2.1. Materials 175
5.2.2. Preparation of HPCAs 175
5.2.3. Instrumentation and parameters 176
5.2.4. Raman imaging 177
5.2.5. Reference spectra of cheese ingredients 177
5.2.6. Raman imaging data processing using Quasar 177
5.2.7. Raman imaging data processing using CatBoost and transfer learning 181
5.2.8. Deconvolution of the amide I region 182
5.3. Results and Discussion 182
5.3.1 Overview of Raman spectra of components in HPCAs 183
5.3.2 Spatial distribution of components in both single- and dual-protein cheese systems 185
5.3.3. Distinguish plant proteins and caseins in dual-protein cheese systems 188
5.3.4. Protein–protein and protein–lipid interactions 196
5.3.5. Changes in protein secondary structures in MPI–RC cheese systems 199
5.3.6. Comparison of RC–MPI and RC–HPI interactions in dual-protein cheese systems. 200
5.4. Conclusions 201
5.5. Acknowledgements 202
5.6. Supplementary material 203

Chapter 6 Elucidating Protein–Lipid Microstructure and Interactions in Hybrid Processed Cheeses Using Synchrotron Macro ATR-FTIR Microspectroscopy[5] 210

6.1. Introduction 212

6.2. Materials and Methods 215

6.2.1. Materials 215

6.2.2. Preparation of HPCs 215

6.2.3. Synchrotron macro ATR-FTIR microspectroscopic measurements 216

6.2.4. Synchrotron FTIR analysis using Quasar 217

6.2.5. Deconvolution of the amide I region 221

6.3. Results and discussion 222

6.3.1. Overview of the FTIR spectra of HPCs components 222

6.3.2. Spatial distribution of components and protein structure in single-protein systems 225

6.3.3. Distinguish plant proteins and caseins in dual-protein cheese systems 228

6.3.4. Protein–lipid and protein–protein interactions 242

6.3.5. Complementary insights into Raman and S-FTIR results 246

6.4. Conclusions 249

6.5. Acknowledgments 251

6.6. Supplementary material 252

Chapter 7 A Hydrolysis-Based Strategy to Improve Meltability in Processed Cheese Analogues[6] 255

7.1. Introduction 256

7.2. Materials and Methods 259

7.2.1. Materials 259

7.2.2. Sample preparation and enzymatic hydrolysis 260

7.2.3. Degree of hydrolysis (DH) 261

7.2.4. Surface hydrophobicity of protein 261

7.2.5. Determination of hydrolysate particle size distribution 262

7.2.6. Sodium dodecyl sulphate–polyacrylamide gel electrophoresis (SDS–PAGE) 262

7.2.7. Characterization of MPI Hydrolysates by Size Exclusion and Reverse-Phase High-Performance Liquid Chromatography (SEC- and RP-HPLC) 263

7.2.8. Solubility of protein 264

7.2.9. Water-holding (WHC) and oil-holding capacity (OHC) of protein 264

7.2.10. Preparation of processed cheese analogues 265

7.2.11. Microstructure of PCAs 266
7.2.12. Rheological analysis 266
7.2.13. Meltability 267
7.2.14. Statistical analysis 267
7.3. Results and discussion 267
7.3.1. MPI hydrolysis using Alcalase 267
7.3.2. Processed cheese analogues with Alcalase hydrolysed MPI 276
7.3.3. Processed hybrid cheese using Alcalase hydrolysed protein and casein 284
7.3.4. Alcalase vs trypsin in plant-based cheese 290
7.4. Conclusions 293
Chapter 8 Overall discussion, conclusion, and future recommendations 294
8.1. Overall discussion and conclusions 294
8.1.1. Influence of plant protein type on structure and function of processed cheese analogues 295
8.1.2. Structure-function relationships in hybrid cheeses 296
8.1.3. Enzymatic modification as a structural engineering tool to improve cheese meltability 299
8.1.4. Conclusions 300
8.2. Future directions 302
8.2.1. Protein structure and synergistic blending 302
8.2.2. Balancing meltability and stretchability 302
8.2.3. Optimizing processing conditions 303
8.2.4. Exploring other types of cheese models 303
8.2.5. Digestibility and nutritional functionality 304
8.2.6. Pilot-Scale production of plant-based or hybrid cheese analogues 304
8.2.7. Sensory and consumer-relevant evaluation 305

List of publications, proposals, awards and presentations

Publications

Lu, D., Roy, D., Acevedo-Fani, A., Singh, H., & Ye, A. (2026). Plant-Based Cheese Analogues: Bridging Structure-Function towards Improved Functional Performance. Trends in Food Science & Technology, 105783. https://doi.org/https://doi.org/10.1016/j.tifs.2026.105783

Lu, D., Vongsvivut, J., Klein, A. R., McGoverin, C., Waterland, M., Zheng, Y., Acevedo–Fani, A., Roy, D., Singh, H., & Ye, A. (2026). Elucidating Protein–Lipid Microstructure and Interactions in Hybrid Processed Cheeses Using Synchrotron Macro ATR-FTIR Microspectroscopy. *Food Structure*, 100511. https://doi.org/https://doi.org/10.1016/j.foostr.2026.100511

Lu, D., McGoverin, C., Roy, D., Acevedo-Fani, A., Singh, H., Waterland, M., Zheng, Y., & Ye, A. (2026). Distinguishing plant and milk proteins and their interactions in hybrid cheese using confocal Raman microscopy with machine learning. *Food Chemistry*, *498*, 147102. https://doi.org/https://doi.org/10.1016/j.foodchem.2025.147102

Lu, D., Roy, D., Acevedo-Fani, A., Singh, H., Waterland, M., & Ye, A. (2026). Physical properties and microstructure of hybrid processed cheeses formulated with plant protein and milk protein ingredients. *Food Hydrocolloids*, *170*, 111688. https://doi.org/https://doi.org/10.1016/j.foodhyd.2025.111688

Roy, D., Lu, D., & Nag, A. (2026). Chapter 9 - Plant-based cheese alternatives: Production, physicochemical properties, nutritional value, sensory aspects, and opportunities. In A. Acevedo-Fani & H. Singh (Eds.), Alternative Dairy Products and Technologies (pp. 269-314). Academic Press. https://doi.org/https://doi.org/10.1016/B978-0-443-28890-6.00016-3

Lu, D., Roy, D., Acevedo-Fani, A., Singh, H., & Ye, A. (2025). Investigation of various plant protein ingredients for processed cheese analogues: physical properties and microstructure compared with milk proteins. *International Journal of Food Science and Technology*, *60*(1). https://doi.org/10.1093/ijfood/vvae018

Lu, D., Roy, D., Acevedo-Fani, A., Singh, H., & Ye, A. (2026). A Hydrolysis-Based Strategy to Improve Meltability in Mung Bean Protein Cheese Analogues (in preparation).

Awards & Granted proposals

First Place oral presentation, titled “Study the Microstructure of Hybrid Cheese Using Confocal Raman Microscopy with Machine Learning”, Riddet Institute Conference and Student Colloquium, 2025

Australian synchrotron beamtime proposal ID 22940: Investigating the spatial and microstructural distribution of plant protein, rennet casein and lipid in hybrid processed cheese products using synchrotron macro ATR-FTIR microspectroscopy, 2025

Conference presentations

Lu, D., McGoverin, C., Roy, D., Acevedo-Fani, A., Singh, H., Waterland, M., Zheng, Y., & Ye, A. (Oct 2025). Distinguishing Plant and Milk Proteins and Their Interactions in Hybrid Cheese Using Confocal Raman Microscopy with Machine Learning. Oral presentation at *4th Food Chemistry Conference*. Scotland, UK.

Lu, D., McGoverin, C., Roy, D., Acevedo-Fani, A., Singh, H., Waterland, M., Zheng, Y., & Ye, A. (Sep 2025). Study the Microstructure of Hybrid Cheese Using Confocal Raman Microscopy with Machine Learning. Oral presentation at *Riddet Institute Conference and Student Colloquium*. Wellington, New Zealand.

Lu, D., McGoverin, C., Roy, D., Acevedo-Fani, A., Singh, H., Waterland, M., Zheng, Y., & Ye, A. (Jun 2025). Distinguishing Plant and Milk Proteins and Their Interactions in Hybrid Cheese Using Confocal Raman Microscopy with Machine Learning. 3-Minute Pitch at *The New Zealand Institute of Food Science and Technology (NZIFST) Conference.* Palmerston North, New Zealand.

Lu, D., Roy, D., Acevedo-Fani, A., Singh, H., Waterland, M., & Ye, A. (Nov 2024). Investigation of the physical properties and microstructure in hybrid cheese formulated with plant protein and rennet casein. Oral presentation at *17th International Hydrocolloids Conference*. Palmerston North, New Zealand.

Lu, D., Roy, D., Acevedo-Fani, A., Singh, H., Waterland, M., & Ye, A. (Aug 2024). Investigation of the physical properties and microstructure in hybrid cheese formulated with plant protein and rennet casein. Oral presentation at *Riddet Institute Conference and Student Colloquium*. Palmerston North, New Zealand.

Lu, D., Roy, D., Acevedo-Fani, A., Singh, H., Waterland, M., & Ye, A. (Nov 2023). Evaluation of the functional properties of plant proteins for the formulation of processed cheese analogues. Poster and 90-second thesis video at *Food Structures, Digestion, and Health.* Queenstown, New Zealand.

Lu, D. (Nov 2022). *Riddet Institute Conference and Student Colloquium.* Napier, New Zealand.

List of Figures

Figure 2-1. Confocal laser scanning microscopy images (×40) of Cheddar cheese (a), processed dairy cheese (b), and plant-based cheese products A (c), B (d), C (e), and D (f) (top). Products A–D are commercial plant-based cheeses with no dairy ingredients and are mainly starch–oil-based systems; only product D contains pea protein isolate. The images show the distribution of fat globules (green) and protein (red). The scale bar represents 30 μm. Meltability of Cheddar (a), processed dairy cheese (b), and plant-based products A–D (c–f) after 5 min of heating in an oven at 232 °C (bottom). Adapted from (Grasso et al.), Future Foods, 2021, with permission from © Elsevier. 56
Figure 2-2. Confocal laser scanning microscopy (CLSM) images (×63; scale bar = 20 μm) of processed cheese analogues formulated with different protein sources (top). Fat and protein were stained red and green, respectively. PCA = processed cheese analogue; MPC = milk protein concentrate; RC = rennet casein; CPI = chickpea protein isolate; LPI = lentil protein isolate; MPI = mung bean protein isolate; PPI = pea protein isolate; SPI = soy protein isolate; HPI = hemp protein isolate; CAPI = canola protein isolate; QPI = quinoa protein isolate. Representative photographs comparing meltability of RC-based and chickpea-protein-based processed cheese analogues (bottom). Adapt from (Lu et al.), *International Journal of Food Science and Technology*, 2025, with permission from © Oxford University Press. 57
Figure 2-3. Comparison of commercial dairy cheese, commercial plant-based cheese, and high-protein plant-based cheese. (a) Texture profile analysis: (i) hardness (N), (ii) springiness (%), (iii) cohesiveness, and (iv) chewiness (N). (b) Meltability (%) and oil loss (%). (c) Stretchability (mm). Values are means ± SD; bars sharing the same letter within the same graph or row are not significantly different ($P > 0.05$; $n \geq 3$). (d–f) Synchrotron-based micro-computed tomography 3D renderings of whole cheese samples. Crystalline material (red) represents calcium phosphate or lactate crystals in dairy cheese and native starch granules in plant-based cheese. Adapted from(Dobson & Marangoni), *Food Structure*, 2025, with permission from © Elsevier. 59
Figure 2-4. Schematic overview of plant-based cheese structure formation and its relationship to texture, meltability, and stretchability. 63
Figure 2-5. Formulation design strategies to improve the structure, texture, and functionality of plant-based cheese. Reference for Plant protein-based system – zein: Grasso et al., 2023; Grasso et al., 2025; Mattice & Marangoni, 2020a, 2020b; Ozturk et al 2023; Salgado et al. 2023; Wahl and Hinrichs, 2006; Sutter et al., 2023; Xu et al., 2025; Protein modification: Xie et al., 2021; Lu et al., 2026; Zeng, 2021; Chuang et al., 2025; Zhu et al., 2022; Hu et al., 2024; Calcium addition: Grsso et al., 2024; Salgado et al., 2023; Hydrocolloid-dominated systems: Lyu et al., 2023; Ørskov et al., 2024; Sanders et al., 2024b; Dobson and Marangoni, 2023, 2024, 2025a, 2025b; Hanley et al., 2025; Yiu et al., 2026; Zhang et al., 2025; Grasso et al., 2023, 2024; Salgado et al., 2023. 66

Figure 3-1. Rapid visco analyzer curves for plant and dairy cheese analogues. PCA = processed cheese analogues; MPC = milk protein concentrate; RC = rennet casein; CPI = chickpea protein isolate; LPI = lentil protein isolate; MPI = mung bean protein isolate; PPI = pea protein isolate; SPI = soy protein isolate; CAPI = canola protein isolate; HPI = hemp protein isolate; QPI = quinoa protein isolate. 107
Figure 3-2. Storage modulus (G′) (A), loss modulus (G") (B), and tan δ (C) as a function of the frequency of processed cheese analogues (T = 20 ◦C, γ = 0.5%). Shear stress–strain curve of processed cheese analogues (D). PCA = processed cheese analogue; MPC = milk protein concentrate; RC = rennet casein; CPI = chickpea protein isolate; LPI = lentil protein isolate; MPI = mung bean protein isolate; PPI = pea protein isolate; SPI = soy protein isolate; CAPI = canola protein isolate; HPI = hemp protein isolate; QPI = quinoa protein isolate. Proteins of the same category are labelled with the same colour. 110

Figure 3-3. Storage modulus (G′) (A), Loss modulus (G") (B), and tan δ (C) as a function of temperature of processed cheese analogues (f = 1 Hz, γ = 0.5%). PCA: processed cheese analogue; MPC: milk protein concentrate; RC: rennet casein; CPI: chickpea protein isolate; LPI: lentil protein isolate; MPI: mung bean protein isolate; PPI: pea protein isolate; SPI: soy protein isolate; CAPI: canola protein isolate; HPI: hemp protein isolate; QPI: quinoa protein isolate. Proteins of the same category are labelled with the same colour. 113
Figure 3-4. Texture profile of processed cheese analogues containing different proteins: (A) hardness (with and without zein protein isolate), (B) springiness, (C) chewiness, and (D) resilience. No textural properties for canola and quinoa protein-based cheese samples were obtained due to softness. Values with the same letter are not significantly different (p <.05). PCA = processed cheese analogue; MPC = milk protein concentrate; RC = rennet casein; CPI = chickpea protein isolate; LPI = lentil protein isolate; MPI = mung bean protein isolate; PPI = pea protein isolate; SPI = soy protein isolate; ZPI = zein protein isolate; HPI = hemp protein isolate. Proteins of the same category are labelled with the same colour. ... 116
Figure 3-5. Stretchability derived from texture profile analysis of processed cheese analogues (PCA) containing rennet casein (RC), milk protein concentrate (MPC), soy protein isolate (SPI), and zein protein isolate (ZPI). 119
Figure 3-6. Confocal micrographs (CLSM) (A, top) with a scale bar of 20 μm and scanning electron microscope (SEM) (B, bottom) with a scale bar of 50 μm and magnification of 800 of processed cheese analogues containing different protein sources. Fat was stained in red, and protein was stained in green for CLSM analysis. No SEM for canola and quinoa protein-based samples. PCA = processed cheese analogue; MPC = milk protein concentrate; RC = rennet casein; CPI = chickpea protein isolate; LPI = lentil protein isolate; MPI = mung bean protein isolate; PPI = pea protein isolate; SPI = soy protein isolate; HPI = hemp protein isolate, CAPI = canola protein isolate; QPI = quinoa protein isolate. 122
Figure 3-7. Principal component analysis of processed cheese analogues containing different proteins was conducted using apparent viscosity and dynamic rheological results. MPC = milk protein concentrate; RC = rennet casein; CPI = chickpea protein isolate; LPI = lentil protein isolate; MPI = mung bean protein isolate; PPI = pea protein isolate; SPI = soy protein isolate; HPI = hemp protein isolate, CAPI = canola protein isolate; QPI = quinoa protein isolate. 124

Figure 4-1. SDS-PAGE profile of hybrid processed cheese analogues (HPCAs) made with mung bean protein (MPI) (A) or hemp protein (HPI) (B) and rennet casein (RC) at varying ratios. Ratios: MPI/HPI100 (100% plant protein), MPI/HPI70 (70% plant protein, 30% rennet casein), MPI/HPI50 (50% plant protein, 50 % rennet casein), MPI/HPI30 (30% plant protein, 70% rennet casein), RC100 (100% rennet casein). The samples were prepared under reducing (R) and non-reducing (NR) conditions. Molecular weight marker in kDa; αs1-CN: αs1-casein; αs2-CN: αs2-casein; β-CN: β-Casein; κ-CN: κ-Casein..... 145
Figure 4-2. Rheological properties of hybrid cheese analogues made with mung bean protein (MPI) or hemp protein (HPI) and rennet casein at varying ratios. Storage modulus (G′) and loss modulus (G″) vs. frequency at 20 °C, γ = 0.5% (A, B). G′ (C, D) and tan δ (E, F) vs. temperature (f = 1 Hz, γ = 0.5%). Ratios: MPI/HPI100 (100% plant protein), MPI/HPI70 (70% plant protein, 30% rennet casein), MPI/HPI50 (50 % plant protein, 50% rennet casein), MPI/HPI30 (30% plant protein, 70% rennet casein), RC100 (100% rennet casein). 148
Figure 4-3. Representative CLSM (A) and TEM (B) images of mung bean protein (MPI) and hemp protein-based (HPI) hybrid processed cheese analogues. Fat in red and protein in green in CLSM. MPI100: 100% mung bean protein in cheese (1); MPI70: 70% mung bean protein, 30% rennet casein (2); MPI50: 50% mung bean protein, 50% rennet casein (3); MPI30: 30% mung bean protein, 70% rennet

casein (4); RC100: 100% rennet casein (5); HPI100: 100% hemp protein in cheese (6); HPI70: 70% hemp protein, 30% rennet casein (7); HPI50: 50% hemp protein, 50% rennet casein (8); HPI30: 30% hemp protein, 70% rennet casein (9). CLSM images scale bars = 50 μm and TEM images scale bars = 5 μm. 152
Figure 4-4. Representative images (A) of hybrid processed cheese analogues (HPCAs) made with mung bean protein (MPI) or hemp protein (HPI) and rennet casein at varying ratios, after heating at 170 °C for 10 min, with melting index. Stretch distance of hybrid cheeses (B). Values within a row not having common superscripts differ significantly ($p < 0.05$). Ratios: MPI/HPI100 (100% plant protein), MPI/HPI70 (70% plant protein, 30% rennet casein), MPI/HPI50 (50% plant protein, 50% rennet casein), MPI/HPI30 (30% plant protein, 70% rennet casein), RC100 (100% rennet). 159
Figure 4-5. Secondary structure content of mung bean protein-based hybrid cheeses (A) and hemp protein-based hybrid cheeses (B) by FTIR. Referenced location of secondary structures: β-sheet (1610–1642 cm^{-1}), Random coil (1640–1650 cm^{-1}), α-helix (1650–1660 cm^{-1}) and β-turn (1660–1699 cm^{-1}) (Gawat et al., 2024; Sadat & Joye, 2020). All values are reported as the mean ± SEM, where N = 3 (3 replicates with 3 measurements). Values within a row not having common superscripts differ significantly ($p < 0.05$). Ratios: MPI/HPI100 (100% plant protein), MPI/HPI70 (70% plant protein, 30% rennet casein), MPI/HPI50 (50% plant protein, 50% rennet casein), MPI/HPI30 (30% plant protein, 70% rennet casein), RC100 (100% rennet casein). 162
Figure 4-6. A schematic diagram summarizing the development of the microstructure of mung bean protein (A) and hemp protein-based hybrid cheeses (B) at different plant protein-to-rennet casein ratios and the relationship between structure and functionality. Ratios: MPI/HPI100 (100% plant protein), MPI/HPI70 (70% plant protein, 30% rennet casein), MPI/HPI50 (50% plant protein, 50% rennet casein), MPI/HPI30 (30% plant protein, 70% rennet casein), RC100 (100% rennet casein). 164

Figure 5-1. Workflow for unsupervised analysis in Quasar (A). The 200–1800 cm−1 data were pre-processed with baseline correction, spike removal, Savitzky-Golay smoothing, and normalization (Box a). Hierarchical clustering grouped spectra into four clusters, with corresponding hyperspectral images (Box b). Principal Component Analysis (PCA) of PC1 and PC2 visualized cluster separation: PC1 separates the blue, red, and yellow clusters, while PC2 separates the green cluster (Box c). Loading plots from PC1 identified Raman shifts contributing to spectral variance (Box d), which were ranked by significance for feature selection (Box e). Workflow for supervised classification using CatBoost with Top-Ranked Feature Removal (TRFR) (B): pre-processed single-protein cheese samples trained the models, which were used to predict protein type in mixed cheese samples. Two predication evaluations were used to determine whether additional training cycles were required. 180
Figure 5-2. Raman images of processed cheeses formulated with 100% rennet casein (RC100), 50% rennet casein and 50% mung bean protein (MPI50), and 100% mung bean protein (MPI100). Distribution of fat (1730–1750 cm^{-1}), phenylalanine (Phe, 1001 cm^{-1}), amide I (1600–1700 cm^{-1}), amide III (1200–1300 cm^{-1}), and trisodium citrate (TSC, 834 cm^{-1}) is shown, with red indicating high and dark blue low concentration. The scale bars are each 15 μm in length..... 188
Figure 5-3. Average Raman spectra of mung bean protein, hemp protein, casein protein, and coconut oil extracted from cheese formulated with 100% mung bean protein (MPI100), 100% hemp protein (HPI100), and 100% rennet casein (RC100) by selecting the lipid and amide I regions with high intensity in the range of 200–1800 cm^{-1} (A), amide I region (1600–1700 cm^{-1}) (B), amide III region (1200–1300 cm^{-1}) (C), and tyrosine residues region (820–850 cm^{-1}) (D)..... 191
Figure 5-4. Raman images of MPI50 and HPI50 cheeses (top) and their average spectra data (bottom) using the CatBoost (left), hierarchical clustering (middle), and k-means models (right). The CatBoost model was trained using single-protein cheese samples – RC100, MPI100, and HPI100 – with predicted

RC shown in green, mung bean/hemp protein in blue, and fat in red in MPI50 and HPI50. MPI50 was imaged at low resolution (5 × 5 μm grid, 200 × 100 μm area) and HPI50 at high resolution (1.5 × 1.5 μm grid, 50 × 50 μm area). Colors indicate clusters from hierarchical clustering or k-means. Scale bars are 15 μm in length. MPI50: cheese formulated with 50% mung bean protein and 50% rennet casein. HPI50: cheese formulated with 50% hemp protein and 50% rennet casein. 193
Figure 5-5. Raman images of MPI50 and HPI50 based on PC1 scores for the 200–1800 cm^{-1} region (A & B, yellow = high, dark blue = low plant protein concentration), with corresponding loadings plots (C & D). Top 100 Raman shifts distinguishing RC from MPI or HPI are ranked (E & F), with lines connecting each shift (left axis) to its importance score (right axis, colour-coded). MPI50 was imaged at low resolution (5 × 5 μm grid, 200 × 100 μm), HPI50 at high resolution (1.5 × 1.5 μm grid, 50 × 50 μm). Key bands include Amide I (1600–1700 cm^{-1}), Amide III (~1250–1300 cm^{-1}), and bands associated with lipid (1745 cm^{-1}). MPI50: cheese formulated with 50 % mung bean protein and 50 % rennet casein. HPI50: cheese formulated with 50 % hemp protein and 50 % rennet casein. 195
Figure 5-6. Average spectra of RC from RC100, MPI50, and HPI50 (A), MPI from MPI100 and MPI50 (B), and HPI from HPI100 and HPI50 (C). Spectra were extracted using k-means clustering to evaluate structural changes upon mixing. RC100: cheese formulated with 100% rennet casein. MPI100: cheese formulated with 100% mung bean protein. MPI50: cheese formulated with 50% mung bean protein and 50% rennet casein. HPI100: cheese formulated with 100% hemp protein. HPI50: cheese formulated with 50% hemp protein and 50% rennet casein. 199

Figure 6-1. Workflow for S-FTIR map image data processing in Quasar, including single-protein (top) and dual-protein cheese systems (bottom). The pre–processed data with baseline correction retained spectra in the ranges of 3600–2800 and 1825–1000 cm^{-1} (Box a). Integrated peak mapping was performed using specific spectral regions (Box b), and hyperspectral images were generated after integration (Box c). Spectra were selected based on defined value conditions (Box d), and their average spectra were calculated (Box e). Hierarchical clustering was applied to group the spectra, and the corresponding hyperspectral images were generated after clustering (Box f), and the average spectra of selected regions were extracted (Box g). A scatter plot visualizing cluster separation was obtained after Principal Component Analysis (PCA) (Box h). PC2 was applied to rank protein-related variance (Box i). 219
Figure 6-2. A representative FTIR chemical image of the processed cheese formulated with 100% rennet casein (RC100). The distribution of lipids, proteins, and water was mapped using integrated areas under the peaks at 2950-2800 and 1745 cm^{-1}, 1700-1600 cm^{-1} and 3600-3200 cm^{-1}, respectively. Red and blue indicate high and low concentration, respectively, as shown by the colour intensity scale on the right. The scale bars are each 20 μm in length. 226
Figure 6-3. Average protein spectra of RC100, MPI100, and HPI100 cheese samples (A); corresponding second derivative spectra of the amide I region (B); and representative peak fitting of the amide I band for HPI (C), MPI (D), and RC (E). In the peak fitting, the black and yellow lines represent the experimental and final fitted spectra, respectively. The green, blue, red, and pink lines correspond to β-sheet, α-helix, random coil, and β-turn structures, respectively. RC100: cheese with 100% rennet casein; MPI100: cheese with 100% mung bean protein; HPI100: cheese with 100% hemp protein. 231
Figure 6-4. Representative FTIR chemical images of MPI50 (top) and HPI50 (bottom) using hierarchical clustering (left) and k-means models (right). Rennet casein is shown in green, mung bean/hemp protein in blue, and lipid in red in MPI50 and HPI50. Different colors represent clusters identified through hierarchical clustering or K-means. Scale bars are 20 μm in length. MPI50: cheese formulated with 50% mung bean protein and 50% rennet casein. HPI50: cheese formulated with 50% hemp protein and 50% rennet casein. 233

Figure 6-5. FTIR chemical images of MPI50 (A) and HPI50 (B). For MPI50: (A1) hierarchical clustering image, the red box shows region of interest (A2) PCA scatter plot or spectra within region of interest from A1, (A3) ranking based on PC2, (A4) average second derivative spectra of clusters, (A5) amide I region, and (A6) amide II region. For HPI50: (B1) hierarchical clustering image, (B2) PCA scatter plot, (B3) ranking based on PC2, (B4) average second-derivative spectra of clusters, (B5) amide I region, and (B6) amide II region. 240
Figure 6-6. FTIR spectra of (A) MPI (from MPI100 and MPI50), (B) HPI (from HPI100 and HPI50), and (C) RC (RC100, MPI50, HPI50) showing protein structural changes in dual-protein systems. Panels (D–F) present the corresponding second-derivative amide I spectra for MPI, HPI, and RC, respectively. 241

Figure 7-1. Degree of hydrolysis (DH) of mung bean protein isolates as a function of hydrolysis time (A); relationship between surface hydrophobicity and DH of Alcalase-treated hydrolysates (B); particle size distribution profiles (C); and corresponding volume-weighted mean diameters (D[4,3]) (D) of mung bean protein during hydrolysis. Sample numbers indicate hydrolysis time (min). 269
Figure 7-2. SDS-PAGE profiles (A), and RP-HPLC chromatograms (214 nm) (B) of mung bean protein and Alcalase-generated hydrolysates. Sample numbers represent hydrolysis time (min). 271
Figure 7-3. Solubility, water-holding capacity, and oil-holding capacity of mung bean protein and its Alcalase-generated hydrolysates as a function of degree of hydrolysis (DH). Sample numbers indicate hydrolysis time (min). 276
Figure 7-4. Representative CLSM (A) and TEM (B) images of plant-based cheeses formulated with non-hydrolyzed mung bean protein (MPI) and Alcalase-hydrolyzed MPI at different hydrolysis times. In CLSM images, fat is shown in red and protein in green. Scale bars: 50 μm for CLSM and 5 μm or 2 μm for TEM. Numbers indicate the Alcalase hydrolysis time (min). 278
Figure 7-5. Rheological properties of plant-based cheese formulated with non-hydrolyzed MPI and Alcalase-hydrolyzed MPI. Storage modulus (G′) (A) and loss modulus (G″) (B) vs. frequency at 20 °C, γ = 0.1 %. Tan δ vs. temperature (f = 1 Hz, γ = 0.1 %) (C). Numbers indicate the Alcalase hydrolysis time (min) 281
Figure 7-6. Representative images of plant-based cheese formulated with non-hydrolyzed MPI and Alcalase-hydrolyzed MPI, after heating at 170 °C for 10 min, with melting index (top). The relationship between the degree of hydrolysis and meltability (bottom). 284
Figure 7-7. Representative CLSM (A) and TEM (B) images of hybrid cheeses formulated with non-hydrolyzed mung bean protein and rennet casein (MPI50) and with 30-min Alcalase-hydrolyzed mung bean protein and rennet casein (MPI50_A30), compared with cheeses formulated solely with rennet casein (RC100) or mung bean protein (MPI100). Rheological properties of MPI50 and MPI50_A30 are shown as storage modulus (G′) and loss modulus (G″) as a function of frequency at 20 °C (γ = 0.1%) (C), and tan δ as a function of temperature (f = 1 Hz, γ = 0.1%) (D). Representative images of MPI50, MPI50_A30, RC100, and MPI100 cheeses after heating at 170 °C for 10 min, together with the corresponding melting index (E) 286
Figure 7-8. Profiles of mung bean protein hydrolysates produced by trypsin or Alcalase at comparable degrees of hydrolysis: SDS-PAGE profiles (A) and RP-HPLC chromatograms at 214 nm (B). Representative CLSM images of the corresponding plant-based cheeses (C). Rheological properties of the cheeses: storage modulus (G′) and loss modulus (G″) as a function of frequency at 20 °C (γ = 0.1%) (D), and as a function of temperature (f = 1 Hz, γ = 0.1%) (E). Representative images of cheeses after heating at 170 °C for 10 min, with the corresponding melting index (F). 292

Figure S 3-1. Schematic illustration of the process and visual appearance of processed cheese analogues containing different protein sources. PCA stands for processed cheese analogues. MPC: milk protein concentrate; RC: rennet casein; CPI: chickpea protein isolate; LPI: lentil protein isolate; MPI: mung bean protein isolate; PPI: pea protein isolate; SPI: soy protein isolate; CAPI: canola protein isolate; HPI: hemp protein isolate; QPI: quinoa protein isolate. (Zein-based PCA was excluded due to failure to prepare in RVA)..... 127
Figure S 3-2. Example photographs of the meltability comparison between RC-based and chickpea-protein-based processed cheese analogues. 128
Figure S 3-3. Photographs of melted processed cheese analogues (PCA) containing rennet casein (left), soy protein (middle), zein (right) during the stretchability test. 128

Figure S 4-1. SDS-PAGE profile of mung bean protein powder (A) and hemp protein powder (B). The samples were prepared in reducing (R) and non-reducing (NR) conditions..... 167
Figure S 4-2. Photo of the cheese stretchability rig, including in-house built post hooks and a base pot with dimensions. 168
Figure S 4-3. Example of FTIR Peak Fitting (top) and Second Derivative Analysis (bottom) of RC100 (A) and MPI100 cheese (B). 169

Figure S 5-1. Reference Raman spectra of ingredients used for making hybrid processed cheese analogues, including hydrated rennet casein (A), hemp protein isolate (B), mung bean protein isolate (C), coconut oil (D), trisodium citrate (E), calcium sulphate (F), and citric acid (G)..... 204
Figure S 5-2. Additional Raman images of processed cheeses formulated with 70% rennet casein and 30% mung bean protein (MPI30), 30% rennet casein and 70% mung bean protein (MPI70), and 50% rennet casein and 50% hemp protein (HPI50). The distribution of fat, amide I, amide III, phenylalanine (Phe), and trisodium citrate (TSC) was mapped using integrated spectral intensities at 1730–1750 cm^{-1}, 1600–1700 cm^{-1}, 1200–1300 cm^{-1} , and peak height of 1001 cm^{-1} and 834 cm^{-1}, respectively. MPI30 and MPI70 images were collected at low resolution with a 5 × 5 μm grid, covering a 200 × 100 μm area, while HPI50 images were collected at low resolution with a 5 × 2.5 μm grid, covering a 100 × 100 μm area. Red indicates a high concentration, while dark blue represents a low concentration, as shown by the colour intensity scale on the right. The scale bars are each 15 μm in length..... 205
Figure S 5-3. Top 10 Raman features ranking using Catboost model with top-ranked feature removal (TRFR) for cheese samples formulated with 50% rennet casein and 50% mung bean protein (MPI50) and 50% rennet casein and 50% hemp protein (HPI50)..... 206
Figure S 5-4. Additional Raman images of MPI30 and MPI70 cheeses using the CatBoost (left), hierarchical clustering (middle), and k-means models (right). The CatBoost model was trained using RC100, MPI100, and HPI100, with predicted RC shown in green, mung bean protein in blue, and fat in red in MPI30 and MPI70. MPI images were collected at low resolution with a 5 x 5 μm grid, covering a 200 x 100 μm area. Different colors represent clusters identified through hierarchical clustering or k-means. Scale bars are 15 μm in length. RC100: cheese formulated with 100% rennet casein. MPI100: cheese formulated with 100% mung bean protein. MPI70: cheese formulated with 70% mung bean protein and 30% rennet casein. MPI50: cheese formulated with 50% mung bean protein and 50% rennet casein. MPI30: cheese formulated with 30% mung bean protein and 70% rennet casein. HPI100: cheese formulated with 100% hemp protein. 206
Figure S 5-5. Representative Raman spectra showing the deconvoluted amide I bands (1600–1700 cm−1) of mung bean/rennet casein mixed cheese samples. For each peak fitting, the area under each peak is

presented as mean ± standard error, along with the corresponding Residual Sum of Squares (RSS), reduced chi-square, and R^2 values. RC100: cheese formulated with 100% rennet casein. MPI100: cheese formulated with 100% mung bean protein. MPI70: cheese formulated with 70% mung bean protein and 30% rennet casein. MPI50: cheese formulated with 50% mung bean protein and 50% rennet casein. MPI30: cheese formulated with 30% mung bean protein and 70% rennet casein. 207

Figure S 6-1. A representative S-FTIR chemical images of the processed cheese formulated with 100% mung bean protein (MPI100) and 100% hemp protein (HPI100). The distribution of lipids, proteins, and water was produced using integrated areas under specific bands at 2950-2800 and 1745 cm−1, 1700-1600 cm−1, and 3600-3200 cm−1, respectively. Red indicates a high concentration, while dark blue represents a low concentration, as shown by the colour intensity scale on the right. The scale bars are each 20 μm in length. 252

Figure S 6-2. Average coconut oil spectra obtained from HPI100, MPI100, and RC100 cheese samples. RC100: cheese with 100% rennet casein; MPI100: cheese with 100% mung bean protein; HPI100: cheese with 100% hemp protein. 253

List of Tables

Table 2-1. Structure-function relationships in plant-based cheese analogues: An overview of recent developments 18
Table 2-2. Overview of recent studies on hybrid cheese, summarising the main ingredients, objectives, formulation and processing, and types of cheese produced (2016-2026) 85

Table 3-1. Slopes from Log(G′)–Log(ω) and log(G")–log(ω) plots (data obtained from frequency sweep samples at 20 °C and γ = 0.5%). 110
Table 3-2. Mean values (n = 3) of the functional properties obtained from the cheese stretchability rig of processed cheese analogues containing MPC, RC, SPI, and ZPI. 118
Table 3-3. The scores of processed cheese analogues containing different proteins were evaluated using apparent viscosity, dynamic rheological measurements, and textural profile analysis results (without zein). 125

Table 4-1. Protein, fat, and moisture contents of processed hybrid cheese analogues. 136
Table 4-2. Textural profile of processed hybrid cheese analogues 156

Table 5-1. Typical Raman shifts of Raman bands and general assignments in protein and lipid structure in the range of 200–1800 cm^{-1}. 184
Table 5-2. Relative amount of protein secondary structures in MPI–RC cheese samples determined by peak fitting of the amide I in Raman Spectra 200

Table 6-1. Band assignment of FTIR absorption peaks typically found in most biological samples containing protein and lipid components (Barth, 2007; Bittante et al., 2022; Ørskov et al., 2023) 224
Table 6-2. Complementary insights of confocal Raman microscopy and S-FTIR for protein structure analysis in HPCs 246

Table 7-1. Molecular weight distribution of mung bean protein isolate (MPI) during Alcalase hydrolysis determined by size-exclusion chromatography (SEC) 272
Table 7-2. Effects of Alcalase and trypsin hydrolysis at comparable degrees of hydrolysis on molecular characteristics and functional properties of mung bean protein. 289

Table S 4-1. Particle size of mung bean protein and hemp protein dispersions (1% v/w) 167

Table S 5-1. Analysis of aromatic amino acid environment - Tyr (I_{850}/I_{830}) of the Raman spectra for HPCAs. 203

List of Abbreviations

DH	Degree of hydrolysis
FTIR	Fourier transform infrared spectroscopy
HPCs/HPCAs	Hybrid processed cheeses/Hybrid processed cheese analogues
HPI	Hemp protein isolate
MPC	Milk protein concentrate
MPI	Mung bean protein isolate
PCAs	Processed cheese analogues
RC	Rennet casein
RP-HPLC	Reversed-phase high-performance liquid chromatography
SDS-PAGE	Sodium dodecyl sulfate polyacrylamide gel electrophoresis
SEC-HPLC	Size exclusion chromatography-high performance liquid chromatography

Chapter 1 Introduction

Cheese is a traditional dairy gel-based food and has been consumed for thousands of years (Johnson, 2017). Processed cheese is produced by blending natural cheeses of different ages and degrees of maturity with water, fat, and emulsifying salts. The mixture is heated under constant agitation and shear to create a homogeneous, smooth, and shelf-stable emulsion (Kapoor et al., 2004). Processed cheese represents a widely consumed and commercially important product due to its consistent quality, extended shelf life, and desirable functional properties such as meltability, stretchability, and texture (Bouhlal & Capps, 2022). However, increasing concerns regarding global warming, greenhouse gas emissions, animal welfare, and human health have drawn attention to the environmental and societal impacts of producing and consuming animal-derived foods. As a result, consumer awareness has increased regarding dietary shifts from animal-based to plant-based foods, which are widely perceived as offering potential benefits for both climate sustainability and human health (Espinosa-Marrón et al., 2022; Popp et al., 2010; Springmann et al., 2016; Stehfest et al., 2009).

Plant-based cheese is one of the rapidly growing dairy alternative products. However, substituting animal proteins with plant proteins remains challenging due to fundamental structural differences and functional limitations (Day et al., 2022; Sim et al., 2021). In particular, plant proteins lack the unique casein micelle structure found in dairy systems, which plays a critical role in forming a dynamic, calcium-mediated network responsible for the meltability, stretchability, and cohesiveness of cheese. As a result, replicating the full physicochemical, functional, sensory, and nutritional profile of dairy cheese using plant-based ingredients remains difficult. Plant proteins often differ in solubility, aggregation behaviour, and intermolecular interactions, leading to less cohesive networks, poor fat distribution, and inferior texture and mouthfeel. Furthermore, there is

still a limited understanding of the structure–function relationships governing multiphase plant-based cheese systems. Consequently, plant-based cheeses often exhibit inferior sensory attributes, nutritional value, and functional performance compared with conventional dairy cheese.

To address these challenges, there is increasing interest in applying the principles of processed cheese systems to plant-based formulations. Processed cheese provides a well-defined and controllable matrix in which the relationships between composition, processing, and functionality can be systematically studied. Translating this framework to plant-based systems offers a promising approach to better understand how plant proteins and lipids interact to form structured and functional matrices. However, investigating these multiphase interactions requires model systems that allow precise control over thermal and mechanical processing conditions. A Rapid Visco Analyzer (RVA) was used as a processing tool due to its ability to precisely control temperature, shear, and viscosity during heating and cooling. Compared with traditional pilot-scale equipment, the RVA requires only small sample sizes, enabling rapid and cost-effective formulation screening. It allows simulation of key processing conditions encountered in industrial cheese manufacture while providing real-time viscosity measurements. This combination of controlled processing and analytical capability makes the RVA a versatile and efficient tool for developing and evaluating processed cheese analogues (Kapoor et al., 2004; Kapoor & Metzger, 2005; Onwulata et al., 2014; Prow & Metzger, 2005; Salunke & Metzger, 2022).

In designing plant protein–based processed cheese analogues, key quality and functional attributes include texture, microstructure, rheological behaviour, and melt and stretch properties, as these collectively determine consumer acceptability and functional performance. These attributes are therefore systematically evaluated in this thesis to establish the relationships between structure and functionality.

The performance of plant-based and hybrid processed cheese analogues depends on both ingredient composition and processing conditions. Common protein ingredients include soy protein, traditionally used to produce tofu, followed by pea protein, and more recently, novel proteins such as chickpea, mung bean, lentil, faba, and zein (Grasso et al., 2021; Hanley et al., 2025; Mattice & Marangoni, 2020b; Moradi et al., 2021; Zhang, Ling, et al., 2024). Although many studies have investigated these proteins in plant-based cheese formulations, comparative studies remain limited, which hinders the identification of suitable plant proteins for specific cheese applications. Furthermore, research on plant protein–casein interactions in hybrid processed cheeses is scarce, and the underlying mechanisms by which these interactions alter protein structure, microstructure, and overall functionality remain poorly understood. In addition, the potential of enzymatic modification to modulate protein behaviour and enhance the functional performance of processed cheeses has not been systematically explored.

The original contribution of this thesis is the establishment of a multiscale framework linking plant-protein type and molecular structure with aggregation, spatial organisation and the functional properties of plant-based and hybrid processed cheese analogues. This understanding provides a scientific basis for selecting and modifying proteins and designing cheese matrices to achieve targeted properties, particularly texture, meltability and stretchability.

Objectives

The main objective of this PhD thesis is to elucidate structure–function relationships in plant-based and hybrid cheese analogues at the multiscale and to develop enzymatic strategies for modifying

plant proteins to modulate their interactions and aggregation behaviour, thereby tailoring network formation and improving functional performance.

The specific objectives are:

1) To understand the functional and microstructural differences among various plant protein-based processed cheese analogues and to compare them with processed cheese formulated with dairy proteins (Chapter 3).
2) To develop hybrid processed cheese analogues formulated with mung bean protein isolate or hemp protein isolate blended with rennet casein at different ratios, and to investigate their spatial distribution, microstructure, and related physical properties (Chapter 4).
3) To elucidate changes in protein structure and interactions between plant protein and casein in hybrid processed cheese analogues using confocal Raman microscopy and synchrotron FTIR spectroscopy (Chapters 5 and 6).
4) To gain insight into the effect of enzymatically modified plant proteins in plant-based and hybrid processed cheese analogues, with a focus on improving meltability (Chapter 7).

The relevant literature background was presented in **Chapter 2**, and the key objectives were studied in **Chapters 3** to **7**:

To better understand the impact of different plant proteins on cheese analogues, several plant proteins were selected to develop processed cheese analogues (PCAs) in **Chapter 3**. These formulations were compared with dairy protein-based cheese analogues containing rennet casein (RC) and milk protein concentrate (MPC) in terms of rheological properties, texture, microstructure, meltability, and stretchability. The hypothesis is that different proteins contribute

to distinct microstructures, which in turn affect the texture and functional properties of cheese analogues. Based on this preliminary analysis, two plant proteins, mung bean protein isolate (MPI) and hemp protein isolate (HPI), exhibiting distinct microstructural, rheological, and textural properties in plant-based cheese analogues were selected for further study and optimization.

MPI consists of approximately 60% globulins and is rich in vicilin-type proteins, among which the 8S vicilin is the most extensively studied (Itoh et al., 2006; Mendoza et al., 2001; Tang & Sun, 2010). However, 8S vicilin lacks disulfide bonds due to the absence of sulfur-containing amino acids (methionine and cysteine), which is an important factor influencing the functional properties of mung bean protein (Yi-Shen et al., 2018). In contrast, hemp protein contains about 20–30% albumins and 60–80% globulins (primarily edestin), which are linked by disulfide bonds and therefore differ in structure and intermolecular interactions.

Because plant proteins struggle to mimic the structure and functionality of casein, blending plant proteins with casein to develop hybrid cheeses offers a potential solution to maintain desirable functional attributes while providing diverse nutritional benefits. Compared with conventional dairy cheeses, they can reduce overall dairy content while improving sustainability and broadening consumer appeal. In addition, hybrid formulations can enhance the nutritional profile by incorporating plant-based protein and fiber alongside dairy protein. These attributes make hybrid cheeses especially suitable for flexitarian consumers seeking products that combine functionality, taste, nutrition, and environmental benefits (Zhang, Jiang, et al., 2024). A range of plant proteins has been explored for incorporation into casein-based systems to develop hybrid cheeses, resulting in products with diverse textures, microstructures, and functional properties depending on the protein type and formulation ratio. **Chapter 4** investigates the effects of hybrid processed cheese analogues (HPCAs) formulated with MPI or HPI blended with RC at different ratios on their

textural and physicochemical properties. It is hypothesised that differences in structure and functionality among these hybrid cheese systems arise from the distinct properties of MPI and HPI and their interactions with RC.

The incorporation of plant proteins significantly altered the physical, textural, and microstructural properties of the cheese analogues. Building on the physicochemical results presented in **Chapter 4**, more advanced analytical techniques were employed to gain a deeper understanding of the underlying molecular interactions between plant and milk proteins. **Chapter 5** applied Raman spectroscopy combined with machine learning, while **Chapter 6** employed synchrotron FTIR spectroscopy with multivariate analysis, to provide molecular-level insights into the composition and structure of HPCAs and to enable comparison of RC-MPI and RC-HPI interactions within these systems. Both techniques enabled spatial mapping of key components in HPCAs and provided complementary information on changes in protein secondary structure, as well as protein–protein and protein–lipid interactions. These approaches offer valuable insight into the structural dynamics of mixed protein systems and can be extended to other plant proteins and food systems.

Plant proteins are structurally distinct from casein and tend to form large particles or aggregates during cheese-making, rather than creating a continuous network in which fat is evenly dispersed. In contrast, casein is highly disordered, and its network in cheese is plastic and flowable upon heating, whereas plant protein networks are typically rigid and less viscoelastic. Enzymatic hydrolysis is one approach to modify plant proteins and tailor their techno-functional properties. By cleaving the native proteins into smaller peptides and amino acids, enzymatic hydrolysis reduces molecular weight, weaker protein–protein interactions, increases solubility, enhances surface hydrophobicity, and exposes ionizable groups (Wouters et al., 2016). **Chapter 7**

investigated the effect of controlled enzymatic hydrolysis on improving the meltability of MPI-based cheese analogues. The effects of different hydrolysis times on MPI characteristics were analysed, and the resulting rheological properties and meltability of MPI-based and MPI/RC hybrid cheeses were evaluated. Two exogenous enzymes, Alcalase and trypsin, were used and compared at similar degrees of hydrolysis to elucidate how enzyme specificity influences cheese characteristics.

Together, these chapters provide a systematic investigation of structure–function relationships in plant-based and hybrid processed cheese analogues. **Chapter 8** provides an overview conclusion, highlighting how plant protein sources and plant protein–casein interactions influence microstructure and functionality, and how enzymatic strategies can modulate plant protein behaviour in processed cheese systems. The findings advance fundamental understanding of plant protein aggregation, hybrid protein interactions, and modification strategies. This work offers valuable insights for the rational design of plant-based and hybrid cheeses, supporting the development of sustainable, functional protein ingredients in food colloidal systems.

MASSEY UNIVERSITY
TE KUNENGA KI PŪREHUROA
UNIVERSITY OF NEW ZEALAND

GRADUATE RESEARCH SCHOOL

STATEMENT OF CONTRIBUTION
DOCTORATE WITH PUBLICATIONS/MANUSCRIPTS

We, the student and the student's main supervisor, certify that all co-authors have consented to their work being included in the thesis and they have accepted the student's contribution as indicated below in the Statement of Originality.

Student name:	Di Lu
Name and title of main supervisor:	Professor Aiqian Ye
In which chapter is the manuscript/published work?	Chapter 2

Describe the contribution that the student and members of the supervisory team have made to the manuscript/published work:[1]

Di Lu: Conceptualization, Visualization, Investigation, Literature search, Writing—original draft.
Debashree Roy: Supervision, Writing—review & editing.
Alejandra Acevedo-Fani: Supervision, Writing—review & editing.
Harjinder Singh: Supervision, Writing—review & editing.
Ye Aiqian: Conceptualization, Funding acquisition, Project administration, Supervision, Writing—review & editing.

Please select one of the following three options:

(●) The manuscript/published work is published or in press

Please provide the full reference of the research output:

Lu, D., Roy, D., Acevedo-Fani, A., Singh, H., & Ye, A. (2026). Plant-Based Cheese Analogues: Bridging Structure-Function towards Improved Functional Performance. Trends in Food Science & Technology, 105783. https://doi.org/https://doi.org/10.1016/j.tifs.2026.105783

( ) The manuscript is currently under review for publication

Please provide the name of the journal:

( ) It is intended that the manuscript will be published, but it has not yet been submitted to a journal

Student's signature:	Di LU Digitally signed by Di LU DN: cn=Di LU, o=Massey University, email=d.lu@massey.ac.nz Date: 2026.02.02 15:13:37 +13'00'	Main supervisor's signature:	Aiqian Ye Digitally signed by Aiqian Ye DN: cn=Aiqian Ye, o=Massey University, ou=Riddet Institute, email=A.M.YE@massey.ac.nz Reason: I am approving this document Date: 2026.02.27 11:35:20 +13'00'

This form should be placed at the beginning of each relevant thesis chapter.

[1] Refer to the Massey University Publishing and Authorship guidelines (OneMassey for staff, Stream for students) and/ or Contributor Roles Taxonomy (CRediT) guidelines for guidance.

Chapter 2 Literature review – Plant-based cheese analogues: Bridging structure-function relationships towards improved function performance[1]

Abstract

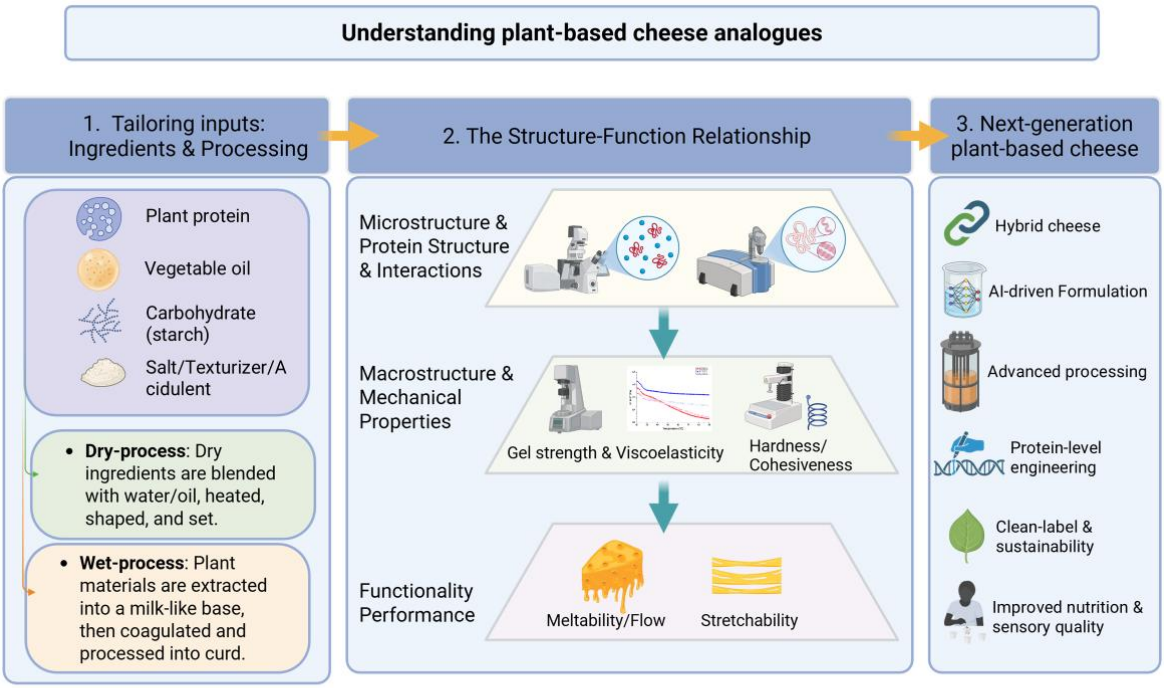
Background: Plant-based cheese has attracted increased attention owing to growing consumer concerns regarding the effects of animal-derived foods on health and the environment. However, the functional performance of plant-based cheese analogues is inferior to that of conventional dairy cheese. Although advances in formulation design and processing techniques have led to some improvements, the structure–function relationship in plant-based cheese systems remains unclear.

Scope and approach: This review provides a comprehensive overview of structure formation and network development in plant-based cheese and elucidates how these structural features govern key functional properties, particularly melting and stretchability, compared to those of conventional dairy cheese. Existing strategies for improving the texture and functionality of plant-based cheese are critically discussed. In addition, emerging trends are highlighted, including the development of hybrid cheese systems and the application of novel technologies.

Key findings and conclusion: The functionality of plant-based cheese depends on ingredient selection and the networks and interactions formed during processing. Existing strategies for improving texture and functionality mainly rely on hydrocolloid–protein–oil structures, wherein plant proteins often function as inert fillers. Non-covalent interactions are crucial for mimicking the functional properties of conventional cheese. Increasing protein concentration, selecting or blending suitable plant proteins, modifying protein structure to enable reversible thermal softening, and advancing processing technologies are key approaches to improving cheese functionality. Integrating these approaches with emerging technologies can accelerate the development of clean-

label, nutritious, and functional next-generation plant-based cheese while highlighting the importance of structure–function relationships for future research and industrial applications.

Graphic Abstract



2.1. Introduction

Cheese is a traditional gel-based dairy food with a long history and remarkable diversity, comprising more than 2000 varieties worldwide. It is commonly classified based on the manufacturing approach (e.g. rennet-coagulated cheese, fresh cheese and processed cheese), textural attributes (soft, semi-soft, semi-hard and hard) and milk origin (e.g. cow, goat and sheep). Despite this diversity, the functional properties of cheese, particularly melting, stretching, and textural performance, are fundamentally governed by the structure and interactions of the casein protein network formed during coagulation and ripening (Lucey et al., 2003). In addition, a large proportion of all cheese varieties (both natural and processed) is used as an ingredient (e.g. on pizzas, cheeseburgers, lasagna, cheese sticks and breads). In a majority of these applications, the physical and rheological characteristics of cheese are often more important than flavour attributes (Lucey et al., 2003).

In recent years, the demand for plant-based protein sources has significantly increased, driven by concerns regarding the sustainability and environmental impact of animal protein production and increased awareness of potential health risks associated with a high intake of animal-derived food (Salter, 2013). This increased demand has led to the rapid expansion of the plant-based protein sector, which has emerged as a key product category, aiming to replicate the taste, texture, and functionality of conventional dairy cheese.

Plant-based cheese analogues (or plant-based cheese/cheese alternatives) are typically designed to mimic traditional dairy cheese. Among them, cheddar- and mozzarella-type products are the most common owing to their popularity and functional significance (Kamath et al., 2022; Sözeri Atik &

Huppertz, 2025), especially for applications that require melting and stretching. In this thesis, functionality refers specifically to the melting behaviour, stretchability, firmness and structural integrity of processed cheese analogues. Numerous early-generation products heavily rely on starch-based matrices (5%–30%) and coconut oil (17%–28%), which often supply less protein, lack a casein-like protein network and exhibit limited cohesiveness, melting and stretching. Recent studies have increasingly focused on the development of high-protein plant-based cheese to address nutritional limitations (Dobson & Marangoni, 2023, 2024; Sutter et al., 2023). Typical formulations consist of plant proteins, vegetable oils, carbohydrates (e.g. starch), salts, acidulants and various texturising agents (Kovačević et al., 2024). The main ingredients are obtained either through tissue disruption of whole plant materials or through fractionation into functional components. For example, in tissue disruption, soybeans are typically soaked and mechanically disintegrated to form a colloidal dispersion containing oil bodies, cell fragments and solubilised biopolymers. In contrast, fractionation isolates functional ingredients such as proteins, starches and hydrocolloids from various plant sources, which are then often dried into powders. Two main processing methods are commonly used. In wet methods, plant raw materials are extracted to form a milk-like dispersion that is subsequently coagulated and processed into curd based on principles adapted from conventional cheesemaking. Conversely, dry methods involve blending dry ingredients with water and oil, followed by heating, shaping and setting. This process resembles the manufacturing process of processed cheese (Alehosseini et al., 2025; Grossmann & McClements, 2021; Sözeri Atik & Huppertz, 2025). Despite all these efforts, a majority of commercial plant-based cheese fail to fully replicate the complex physicochemical, functional, sensory and nutritional qualities of their dairy counterparts (Grasso et al., 2021; Grossmann & McClements, 2021), primarily owing to structural differences between casein and plant proteins

and functional limitations in plant proteins.

Existing strategies for manufacturing plant-based cheese often rely on empirical formulation adjustments, such as varying protein sources, starch types, fat levels or hydrocolloid combinations, without a fundamental understanding of the underlying mechanisms governing structure formation and functionality (Ahrné & Leser, 2025). In the case of dairy cheese, the mechanisms underlying casein micelle destabilisation, aggregation and network formation are reasonably well established on a qualitative level (Lucey et al., 2003). However, translating these mechanisms to plant-based systems is inherently challenging, as caseins are flexible, disordered proteins that undergo calcium-mediated aggregation, whereas most plant proteins are globular, structurally stable and require unfolding prior to aggregation. Distinct aggregation pathways and different sensitivities to pH, ionic strength, calcium, and thermal treatment introduce both thermodynamic barriers (higher energy input required for denaturation for plant proteins) and kinetic constraints, leading to fundamentally different network formation behaviour (Rashwan et al., 2025). Moreover, the gelation and network-forming behaviours of plant proteins in cheese analogues remain unclear (Ahrné & Leser, 2025). In particular, how plant protein networks form under cheese-like processing conditions and how these networks interact with hydrocolloids or lipids to determine macroscopic properties such as meltability and stretchability remain unclear. Furthermore, the structure–function relationships in plant-based cheeses are not clearly defined. Consequently, these proteins form composite matrices with functional properties fundamentally differing from those of dairy cheese. A mechanistic understanding of how ingredient selection and interaction and processing conditions influence microstructure and macrostructure and how these effects translate into functional performance is essential for the rational design of next-generation plant-based

cheeses.

This review critically examined plant-based cheeses from the perspective of structure–function relationships, with a particular focus on melting and stretching behaviours, which are among the most challenging functionalities to replicate. It highlights representative and mechanistically relevant studies, primarily from recent years (within 10 years), to provide insights into ingredient interactions and processing effects. The specific objectives of this review were as follows: (i) to discuss the relationships between the structure and network formation of proteins, starches and lipids in plant-based cheeses and their effects on functional properties, with explicit comparison to casein-based cheese systems and discussion of key analytical approaches; (ii) to evaluate existing ingredient- and process-based strategies used to improve the meltability and stretchability of plant-based cheeses and (iii) to briefly summarise future research directions, focusing on hybrid cheese development and emerging technologies, to advance the rational design of plant-based cheeses with dairy cheese–like functionality. The sensory and nutritional aspects of plant-based cheese are outside the scope of this review.

2.2. Structure–function relationship

Plant-based cheeses are complex systems, and their structure is determined by key ingredients, such as proteins, carbohydrates (e.g. starch) and fats, and processing conditions, such as temperature and pH. To better contextualise the diverse formulation strategies reported in the literature, plant-based cheeses can be broadly categorised according to their dominant structure-forming mechanisms into starch-dominated, protein-dominated, and hydrocolloid-structure (starch-protein-oil) systems. This progression reflects a shift from simple textural mimicry towards

more structurally and functionally optimised designs. A comparative summary of these systems, including their structural characteristics and associated functional performance, is presented in **Table 2-1**.

2.2.1. The role of starch in plant-based cheeses

From the earliest plant-based cheese formulations to those developed more recently, starch has remained a key component supporting the structure and functionality of plant-based cheeses (accounting for 5-30% of the plant-based cheese). In numerous studies, starch has been used as a partial or complete replacement for proteins and fats (Noronha, Duggan, Ziegler, O'Riordan, et al., 2008; Ørskov et al., 2021). Its widespread use is primarily attributed to its ability to increase viscosity and undergo gelatinisation upon heating, followed by the formation of a colloidal or gel-like structure during cooling. This behaviour enables the entrapment of water, fat and other components within a three-dimensional (3D) polysaccharide network, thereby mimicking the structural characteristics of conventional dairy cheese (Grossmann & McClements, 2021). Studies have investigated various starches, including native maize starch, wheat starch, potato starch, crosslinked starch, waxy starch, native rice starch, pre-gelatinised starch and modified starch with emulsifying properties (e.g. octenyl succinic anhydride [OSA]–modified starch). Among them, modified (e.g. oxidised starch) and waxy starches have been reported to exhibit improved melting properties (Dobson & Marangoni, 2023; Hanley et al., 2025; Lyu et al., 2023).

The textural, rheological and functional properties of starch-based cheese analogues are primarily influenced by amylose content rather than starch source or type (S. Liu et al., 2019). An increase in amylose content increases hardness, elasticity and rigidity, impeding meltability and flowability

(Mounsey & O'Riordan, 2008). Intermolecular hydrogen bonding and starch retrogradation lead to the formation of an ordered crystalline structure with increased rigidity. This irreversible retrogradation process (lack of thermoplasticity) reduces water mobility, increasing the rigidity and hardness of cheese and suppressing its melting ability. Conversely, amylopectin is preferred to enhance swelling capacity, viscoelasticity and gel reversibility, contributing to softer and more meltable textures (Dobson & Marangoni, 2023; S. Liu et al., 2019). Other factors, such as the shape, concentration and size of starch granules, may also influence texture and functionality by influencing water-binding and/or emulsifying capacities. For example, increasing starch concentration generally leads to higher hardness, reduced water mobility, and increased viscoelasticity (Noronha, Duggan, Ziegler, O'Riordan, et al., 2008), while starch granule size and gelatinisation behaviour further influence texture, with larger or pre-gelatinised starches often disrupting the protein matrix and reducing cohesiveness. In addition, interactions between starch, proteins, and lipids can alter fat distribution and melting behaviour, thereby affecting properties such as firmness, meltability, and flow (Dobson & Marangoni, 2024; Koekuyt et al., 2025; Mounsey & O'Riordan, 2008; Ørskov et al., 2021, 2024).

Table 2-1. Structure-function relationships in plant-based cheese analogues: An overview of recent developments

Network structure	Plant sources	Processing methods	Treatment/ Modification	Type of products	Purpose	Structure	Key functional outcomes	Reference
Starch-dominated	Modified maize starch, maize starch, modified potato starch, potato starch, tapioca starch	Fractionation/dry method		Processed cheese analogues compared to Cheddar	To evaluate the composition, structure, and physicochemical properties of commercial plant-based cheeses and to compare these properties with commercial dairy cheeses.		Functional properties of plant-based cheeses are dominated by starch and hydrocolloids rather than protein. High starch content generally leads to inferior melting performance compared to dairy cheese. Texture: Hardness for plant-based cheeses ranged 80.5-8.0 N. Higher hardness and firmness compared to Cheddar. Firmness between 73.3 and 95.4 N. Rheological properties: Temperature sweep (20-80°C): Plant-based cheeses remained solid-dominant throughout, showing no G' and G" crossover point unlike dairy Cheddar. Microstructure: CLSM and cryo-SEM revealed no continuous protein network; fat globules were stabilized by starch and hydrocolloids. Melt: Schreiber melt test: Plant-based cheeses showed	Grasso et al. (2021)

							low melt (5.59-21.00% expansion) compared to Cheddar (49.29%).	
Starch-dominated	Waxy potato starch, tapioca starch, potato starch, sweet potato starch, corn starch, glutinous rice starch, hydroxypropyl tapioca starch, acetylated distarch	Fractionation/dry method	Heating	Processed cheese analogues	To integrate machine learning analysis with rheological results to identify starches with meltability and stretchability characteristics in plant-based cheese analogues.	FTIR used; melt-stretch properties related to decreased ratio of crystalline to amorphous regions during pasting.	Machine learning using pasting and viscoelasticity identified melt-stretchable starches. Hydroxypropyl tapioca, waxy potato, and tapioca starches were superior. Texture: Waxy potato (4.16 N) and potato starches (3.67 N) showed higher hardness and fracturability than others (sweet potato, tapioca, hydroxypropyl tapioca). Rheological properties: G'	Yun et al. (2024)

	adipate starch, corn starch						decreased with temperature; a more pronounced decrease for waxy potato, tapioca, and hydroxypropyl tapioca starches. Melt & Stretch: Hydroxypropyl tapioca, waxy potato, and tapioca starches showed highest stretch length (e.g., 40.47 mm for hydroxypropyl tapioca).	
Transition from a casein-dominated to a starch-dominated continuous phase	Modified potato starch (Acetate starch, OSA-modified starch)	Fractionation/dry method		Processed cheese analogues compared to Mozzarella	To gain insights into the microstructure of imitation cheese, the system was examined for its transition from a casein-dominated to a starch-dominated phase, and how the continuous phase and fat emulsification influence microstructural stability and functionality.		Increasing starch concentration shifts the network from casein-dominated to starch-dominated. OSA-emulsifying starch reduces fat droplet size and improves stability at high starch levels. Texture: Hardness (N) and Young's Modulus (N/mm²) increased with starch concentration (Hardness: 8.50 N at 8% starch to 21.85 N at 25% starch). Rheological properties: Temperature sweep (20-90 °C): All samples remained solid-dominant (tan delta < 1) at 90 °C. G' decreased with temperature but remained above G".	Ørskov et al. (2021)

							Microstructure: As starch concentration increases, the microstructure undergoes a phase inversion from a protein-continuous network to a starch-dominated matrix where swollen, gelatinized starch granules coalesce to form the primary structural framework. In this starch-continuous system, residual protein and fat droplets are relegated to a dispersed filler phase, which fundamentally alters the material's mechanical strength and melting behavior. Melt: Highest melt at 17% starch A (231.57%); OSA-starch (Starch B) enabled stable cheese at 25% starch with lower melt (78.75%).	

Starch-dominated	Native potato starch (A) and chemically modified potato starches (starch acetates B-E, oxidized F-G, and starch acetate with OSA H)	Fractionation/dry method		Processed cheese analogues	To understand the impact of shifting from a casein-dominated to a starch-dominated continuous phase and related functionality.	Analyzed using FTIR and Raman spectroscopy. FTIR was more effective at detecting differences and interactions between starch, protein, and fat. PCA of FTIR showed clustering by starch modification.	OSA-modified starch improves component integration by acting as an emulsifier. Protein pre-hydration has a limited impact on final microstructure compared to starch modification. Texture: Hardness increased with starch and protein concentration. OSA-modified starch (Starch B) increased the hardness in 7% and 9% protein samples. Protein pre-hydration slightly reduced hardness. Rheological properties: Temperature sweep (40-95 °C): G* and phase angle (delta). Softening and increased phase angle during heating, indicating reduced elasticity. No crossover point reported. Microstructure: CLSM, SEM, and Cryo-SEM revealed OSA-starch as an emulsifier surrounding fat droplets.	Ørskov et al. (2023, 2024)

Transition from a starch-dominated to a protein-dominated network with increasing protein content Protein concentration: 8.68%-21.5%	Chickpea flour and chickpea protein concentrate	Fractionation/dry method		Processed cheese analogue	To assess the impact of protein concentration on the essential quality attributes of chickpea-based alternatives to cheese.	DSC (Differential Scanning Calorimetry) revealed a transition peak at ~30 °C for shea butter and a smaller peak at ~70 °C associated with chickpea starch gelatinization.	Increasing protein concentration significantly altered texture and microstructure. Texture: Hardness was highest (~45 N) at the lowest protein content (8.68% protein) due to high starch content and its retrogradation. Adhesiveness, springiness, and cohesiveness all increased significantly as protein content rose from 8.68% to 21.5%. All samples showed increased hardness after 1 month of storage at 4 °C Microstructure: CLSM confirmed a more extensive protein matrix at higher concentrations (up to 21.5% protein), which effectively encapsulated fat globules and prevented their coalescence compared to lower protein samples. Melt & Stretch: All formulations exhibited poor meltability in the Schreiber test. Starch gelatinization and subsequent water absorption led to a "drying out" effect and solidification rather than	Grasso et al. (2022)

							melting, with no significant increase in diameter upon heating.	
Transition from a starch-dominated to a protein-dominated network with increasing protein content	Zein, Pea protein isolate (PPI), Wheat gluten	Fractionation/dry method	Incubation at 40 °C for 30 min to allow network formation	Processed cheese analogue compared to Cheddar cheese	To investigate the fundamental structural and rheological properties of zein networks.	FTIR revealed that zein undergoes a structural reorganization from intermolecular to intramolecular beta-sheets during the first 24 h of storage. This transition	Zein (especially 30%) showed cheese-like softening (↓ G′, G″) and high stretchability (>125 mm), unlike PPI and gluten, which remained rigid and fractured. Functionality attributed to zein forming non-covalent networks above its glass transition (~45–50 °C). Networks stabilise over ~24 h, transitioning from viscous (G″ > G′) to more elastic structures. Structural shift from intermolecular to intramolecular β-sheets observed during ageing.	Mattice and Marangoni (2020a, 2020b)

						, driven by non-covalent hydrophobic interactions, is responsible for the stabilization and strengthening of the zein network.	Aged zein networks exhibit melt-softening similar to cheddar, highlighting strong potential for plant-based cheese applications.	
Composite network - pulse flour (where protein plays a more significant structural role) Protein	Yellow peas, faba beans (boiled and roasted flour)	Tissue disruption/ wet method	Boiled or roasted	Hard cheese analogue	To develop plant-based cheese analogues by evaluating the different types of pulse flour as raw materials.		Pulse-based cheese analogues were prepared using boiled and roasted yellow pea and faba bean flours. Flour-to-water ratio of 1:4 with 1% kappa-carrageenan was optimal for a firm and sliceable texture. Roasted pulse flours produced significantly harder and chewier textures than boiled flours.	Feraw ati et al. (2021)

concentration: 4-7%							Enhanced firmness likely due to ungelatinised starch and less denatured proteins forming stronger networks during processing. Both boiled and roasted flours showed higher water absorption (2–3 g/g) than raw flours (~1 g/g), supporting gel formation. Pulse flours contributed higher protein (4–7%) and dietary fibre (6–8%) compared to starch-based alternatives.	
A composite network (where starch and protein both play an improtant role) Protein concentration: 10%	Fava protein isolate	Fractionation/dry method	Extrusion	Processed cheese compared to Mozzarella	To investigate the effect of extrusion processing on improving the texture of fava bean protein–based cheese, particularly its stretchability and meltability.		Extrusion denatures proteins and aligns them, facilitating better fiber formation and stretching. Texture: TPA showed that the 10% extruded fava sample had lower maximum force (~2500 g) compared to commercial dairy-free mozzarella (~4000 g) and dairy mozzarella (~10,000 g), indicating a significantly softer and more fluid-like texture. Melt & Stretch: The 10% extruded fava sample achieved a stretch distance of 106.2 mm, which was higher	Zeng (2021)

							than both the unextruded sample (79.4 mm) and commercial dairy-free mozzarella (99.3 mm). Meltability slightly improved with extrusion (4.0 mm spread vs 3.5 mm for unextruded). However, fava-based cheeses were still less stretchy than dairy mozzarella (>200 mm). The study demonstrated that extrusion is a promising method to functionalize legume proteins, allowing for higher protein inclusion (10% vs <2% in commercial brands) while enhancing mozzarella-like stretch and melt properties.	
A composite network (where starch and protein both play an important role) (study on the protein)	Pea protein, soy, rice, zein, red quinoa flour (RQF)	Fractionation/dry method	Cold plasma	Processed cheese compared to Mozzarella	To evaluate different plant proteins (soy, pea, rice, and zein) to determine which is most suitable for vegan cheese production; to use cold plasma treatment as a physical modification method to improve the functional	Circular Dichroism revealed that cold plasma treatment at 130 W for 12 min caused tertiary structure unfolding (red shift in	Cold plasma treatment (130 W/12 min) significantly improved pea protein functionality: OHC, WHC (water holding capacity), solubility, and emulsifying ability. Structurally, tertiary structure unfolded, beta-turns increased (23.8% to 25.6%), and beta-sheets decreased (27.5% to 24.4%). Disulfide bond cleavage increased hydrophobicity. In vegan cheese, plasma-treated pea protein (PPC) showed higher hardness than untreated	Chuang et al. (2025)

					properties of plant proteins, making them more comparable to casein; to incorporate functional ingredients to improve nutritional value and functionality of vegan cheese	fluorescence). Secondary structure changed with beta-turns increasing (23.8% to 26.5%) and beta-sheets decreasing (27.5% to 23.3%).	(UPC). Flowability increased from 7.2% (UPC) to 10.3% (PPC) and stretchability from 4.33 to 4.67 cm. Increased hydrophobicity facilitated better protein-fat binding, leading to a more integrated matrix that enhanced melting properties.	
Protein-dominated network	Soy milk (from commercial soybeans)	Tissue disruption/ wet method	Fermentation	Soft cheese	To investigate the effect of Geotrichum candidum on the microbial, chemical, textural, and sensory features of soft soy cheese.	G. candidum possesses intense proteolytic and lipolytic activities. It breaks down the soy protein and fat into amino	Ripening with Geotrichum candidum significantly transformed soy cheese properties, turning it from brittle to soft and sticky. Hardness and chewiness decreased substantially during 35 days of ripening (e.g., from 512 g to 252 g at 10 °C). This softening was driven by G. candidum's intense proteolytic and lipolytic activity, which degraded soy proteins and fats, increasing amino nitrogen and free fatty acids. Microstructurally, the mold	Li et al. (2020)

						nitrogen and free fatty acids, which effectively "softens" the internal matrix	formed a uniform velvety-white coat on the surface. Sensory analysis showed that ripening at 10 °C for 28 days achieved the best flavor and texture balance while effectively masking the undesirable beany taste of soy.	
Protein-dominated network Protein concentration: 12%	Hemp (H), Yellow pea (P), Brown lentil (L)	Tissue disruption/ wet method	Glucono-delta-lactone (GDL), Transglutaminase (TG), or Heat (90 °C)	Soft gel - yogurt	The impact of mixing different ratios of hemp, pea, and lentil proteins using three different gelation methods on color, gel strength, and water-holding capacity (WHC) was investigated.	SDS-PAGE confirmed the presence of edestin and albumin in hemp, and legumin and vicilin in pea and lentil. Protein interactions in binary mixtures were hypothesized to form	Lentil protein formed the strongest gels under GDL and TG treatment. Pea protein behaved as a viscous solution rather than a gel at 90 °C heat. Binary mixtures of Pea-Lentil showed linear or synergistic gelling behavior, suggesting the formation of a joint gel network. In contrast, mixtures with Hemp often showed 'under-proportional' gelling due to a 'dilution effect' where hemp's weak gelling properties interrupted the stronger networks of pea/lentil. However, a synergistic effect was found in TG-induced Hemp-Pea gels at low hemp concentrations, where ~25% of pea protein could be replaced by hemp without losing gel strength. WHC was not directly linked to gel	Guidi et al. (2022)

						joint or independent networks depending on the gelling mechanism.	strength, with hemp protein generally showing lower WHC (41-69%) than pea/lentil (68-99%).	
Protein-dominated network Protein concentration: 16%	Zein protein isolate (ZPI); Chickpea protein concentrate (CPC)	Fractionation/dry method		Processed cheese analogue	To investigate binary blends of zein and chickpea protein and their combined effects on the development and physicochemical properties of plant-based cheese alternatives.		Blends of ZPI and CPC showed distinct properties Texture: Hardness (~23 N), springiness (~0.85), and cohesiveness (~0.5) were highest for the 100% ZPI (Zein Protein Isolate) sample. Adhesiveness (~18 N·s) was highest in the 100% CPC (Chickpea Protein Concentrate) sample, likely due to a different protein-fat matrix and carbohydrate profile Rheological properties: G' and G" decreased between 35 and 100 °C. Higher ZPI content increased tan delta at 80 °C, indicating greater flowability as zein transitioned to a viscoelastic plastic state above its glass	Grasso et al. (2023)

							transition temperature. Microstructure: CLSM showed zein forming a protein-rich layer around fat globules. Higher ZPI content promoted fat globule coalescence into larger, non-spherical pools, while CPC proteins were more homogeneously distributed. Melt & Stretch: Meltability improved with ZPI content, with 25% diameter expansion. Stretchability was also highest for the 100% ZPI sample, whereas high-CPC samples remained rigid and failed to stretch.	

Protein-dominated network Protein concentration: 32-33%	Zein; Pea protein isolate (PPI)	Fractionation/dry method	Arginine/Calcium hydroxide (texture modifier)	Processed cheese analogue compared to Mozzarella and Colby	To enhance the cohesive and viscoelastic properties of plant-based meat and cheese analogues by dispersion of zein into pea protein with calcium hydroxide as a modifier	FTIR revealed increased beta-sheet structures with Ca(OH)2 addition, contributing to the stronger matrix.	Dispersion of zein into pea protein was functionalized using alkaline agents Texture: Arginine treatment significantly increased elasticity, cohesiveness, and hardness while decreasing stickiness. Calcium hydroxide concentration was the primary tool for matching textural properties of commercial animal products. Increasing Ca(OH)2 from 1% to 5% significantly increased hardness, cohesiveness, and chewiness, while a decrease was observed at 7% likely due to calcium ion saturation. 1% Ca(OH)2 matched tilapia fish texture, 3% matched mozzarella/chicken nuggets, and 5% matched tuna fish and Colby cheese. Rheologically, alkaline-treated blends showed improved viscoelasticity even at room temperature, with higher G' and G" values.Higher Ca(OH)2 concentrations (up to 5%) increased complex modulus and elasticity (lower phase angle) due to enhanced calcium-protein and calcium-starch crosslinking, as	Ozturk et al. (2023); Salgado et al. (2023)

							confirmed by structural changes in FTIR (increased beta-sheets). Microstructure (SEM/CLSM) revealed that zein formed a network of viscoelastic fibrils that integrated with the pea protein matrix, especially when combined with boiling water. This fibril network held the structure together, providing the necessary cohesion for meat or cheese analogues without requiring high-temperature processing.zein formed a web-like viscoelastic network surrounding pea protein and rice starch; network rigidity and structural cohesion increased with higher Ca(OH)2 due to enhanced calcium-protein cross-linking. Stretch: Lubricated squeezing flow showed strain rate thickening behavior. Extensional viscosity, representing resistance to extension/stretch, increased with strain rate. Alkaline-treated blends exhibited higher extensional viscosity, which is indicative of	

							improved stretchability in cheese analogues.	

Protein-dominated network Protein concentration: 30%	Pea protein isolate (PPI); Zein	Fractionation/dry method	kappa-carrageenan (kC) + Calcium chloride (CC)	Processed cheese analogue compared to Mozzarella and Raclette	To explore the potential of using pea protein and zein as protein sources in the formulation of plant-based cheeses.		Rheologically, Amplitude sweep results showed that PPI only gels had high G' (~10^4-10^5 Pa) and fracture strain was independent of kC and CC concentrations. Blends containing zein had lower initial G' but exhibited temperature-dependent softening behavior. Melt: PPI-only formulations formed strong gels dominated by covalent bonds that did not weaken upon heating, resulting in poor meltability. In contrast, zein-based formulations (especially with 30% zein) showed significant temperature-dependent softening, with both G' and G" decreasing as temperature rose, mimicking the melting behavior of conventional cheese. This functionality is attributed to zein's non-covalent network which weakens at higher temperatures. Tribological analysis showed that all formulations reduced friction compared to buffer, but zein increased the friction coefficient due to its hydrophobicity. Combining	Sutter et al. (2023)

							zein and PPI (e.g., 20Z-10P) was identified as a promising strategy to balance meltability and oral lubrication. The inclusion of kC and CC did not significantly impact lubrication but strengthened the initial gel network.	

Protein-dominated network Protein concentration: 18%	Soy, pea, chickpeas, mung beans, lentils, quinoa, canola, hempseeds, zein protein isolates	Fractionation/dry method		Processed cheese analogue	To evaluate plant-based cheeses made from various plant proteins and compare them with milk protein–based cheeses in terms of rheological properties, texture, meltability, stretchability, and microstructure.		Lentil protein performed most similarly to casein when ranking physical properties. Overall, plant proteins formed coarser, less cohesive structures due to poorer emulsifying properties and the lack of a continuous protein network compared to milk proteins. Texture: Zein-based cheese analogue was the hardest (~35,616 g) and chewiest (~5,055 g) at room temperature. Legume cheese analouge (chickpea, mung bean, pea, soy, lentil) exhibited hardness (~30,000 g) comparable to rennet casein but had significantly lower springiness (~0.5), cohesiveness (~0.2), and resilience (~0.05) Rheological properties: All plant-based cheese analouges showed solid-like behavior (G' > G") with higher G' values than rennet casein. However, unlike milk proteins, plant-based cheese analogues (except zein) failed to soften upon heating, with tan delta remaining consistently low.	Lu et al. (2025)

							Microstructure revealed that plant proteins formed large, non-continuous aggregates and coarser structures. Fat separation was irregular, unlike the homogeneous network and uniform fat distribution seen in milk protein controls. Melt & Stretch: Legume-based cheese analogues lacked both melting and stretchability. Zein-based cheese analogue was the only plant protein to exhibit stretching behavior (~57 mm stable point) upon heating, though it did not undergo typical melting.	
Protein-dominated (both protein and starch are high, depending on the legume source used)	Chickpea, Red lentil, Quinoa, Faba bean flours; Avocado pulp	Using legume flours and then fermentaiton	Fermentation	Cream cheese analogue	To develop plant-based cream cheese analogues from chickpea, red lentil, quinoa, and faba bean flours, using avocado pulp as a fat source, and to evaluate the effects of		Fermentation significantly enhanced sensory and textural attributes. Firmness increased post-fermentation due to protein aggregation as pH reached the isoelectric point (pH ~4.5). Chickpea and red lentil plant-based cream cheese analogues showed superior adhesiveness and spreadability compared to quinoa or faba bean, closely	Palatzidi et al. (2025)

Protein concentration: 23-35%					fermentation with selected LAB starters on their nutritional and textural properties compared to non-fermented controls.		resembling commercial vegan cream cheese. Avocado pulp improved creaminess and provided healthy fats. Rheologically, G' increased significantly (from ~335 Pa to >1160 Pa for chickpea and >1300 Pa for lentil), indicating a transition to a solid-like gel. Emulsion stability improved as Turbiscan Stability Index values decreased from ~7.9 to ~4.2, reflecting better integration of lipids and proteins. The final products were nutritionally dense, with protein content reaching 35% in chickpea analogues.	
Protein-dominated network	Zein, Pea protein (Native pea protein, denatured pea protein)	Fractionation/dry method		Processed cheese analogue compared to Mozzarella, Camembert, Raclette, and Emmental	To investigate the effect of pea protein addition on the microstructure of zein–pea dispersions and the melting behavior of zein–pea–based cheese.		Native pea protein acted as a highly functional filler that hindered zein aggregation, resulting in firm (up to 64 N), less brittle, and more thermoreversible gels. In contrast, denatured F9 and C9 pea proteins acted as 'inert fillers' that provided a softer (3-40 N), more brittle, and less thermoreversible matrix. This difference is attributed to the higher water binding capacity (~48-63%) and larger hydrodynamic volumes of denatured proteins, which physically obstructed zein-	Wahl and Hinrichs (2026)

							zein interactions. CLSM confirmed that native pea protein integrated more homogeneously into the zein network, while F9/C9 formed larger, isolated aggregates. Native pea protein is thus identified as superior for creating firm yet meltable plant-based cheese hybrids.	
Hydrocolloid-structure (starch-dominated incorporating plant protein)	Oxidised potato starch (PS), maize starch (MS) pea protein isolate	Fractionation/dry method	Two heating methods: one-step (all mixed then heated) or two-step (emulsion/protein added after starch gelatinization).	Processed cheese analogues	To understand how oil and protein affect the structural and melting properties of starch-based gels.		Protein addition more effectively inhibits melting than oil. Both oil droplets and protein networks can reinforce the starch matrix, preventing complete collapse during heating. Rheological properties: Temperature sweep (20-100 °C). Native maize starch (MS) did not melt; oxidised potato starch (PS) melted completely at temperatures > 70 °C. Gel stiffness influenced by protein and oil content. Microstructure: consists of a continuous gelatinized starch matrix—predominantly oxidized potato starch—containing dispersed oil droplets and protein aggregates acting as filler particles. Confocal CLSM	Lyu et al. (2023)

							reveals that while oil droplets are typically small and uniformly distributed, proteins tend to form distinct clusters or interfacial films that can either reinforce or disrupt the starch network. Melt: Oxidised potato starch (PS) showed good melting properties.	
Hydrocolloid-structure (starch-dominated incorporating plant protein)	Tapioca starch (TS) (15%), Pea starch (PES), corn starch (CS), potato starch (POS), wheat starch (WHS), and waxy starch (WAS)	Fractionation/dry method		Processed cheese analogues	To develop a cheese alternative by comparing different ingredients to achieve high nutritional and textural characteristics consistently.	FTIR showed starch-protein-lipid interaction at 1700 cm-1.	Texture: TS, POS, and WHS showed higher hardness (~3000-4000 g). Rheological properties: Plant-based cheese (PC) showed higher elasticity and viscosity than commercial dairy (CDC) and commercial plant-based cheese (CPC). Microstructure showed dispersed starch granules partially encapsulated in protein forming a continuous matrix. Best recipe: 15% tapioca starch, 20% soy protein isolate (SPI), 7% gelatine, and 15% coconut oil. Lauric acid (from coconut oil) acts	Fan et al. (2023)

							as a bridge between starch and protein.	
Hydrocolloid-structure (starch-dominated incorporating plant protein)	Waxy maize starch pea protein isolate	Fractionation/dry method		Processed cheese analogues compared to Cheddar	A high-protein plant-based cheese (HPC) formula was developed and compared with existing commercial dairy and plant-based cheese alternatives.		HPC bridges the gap between dairy and commercial plant-based cheeses. Protein acts as a filler that disrupts the rigid starch network, allowing for more viscous flow, melting, and stretching. Texture: Dairy (~83 N) and HPC (~83 N) showed similar hardness; commercial plant-based cheese was softer (~56 N). HPC had higher cohesiveness (~0.4) than commercial plant-based (~0.3). Rheological properties: Dairy cheese crossed over (tan delta > 1) at 68 °C. HPC remained solid-dominant (tan delta < 1) but showed significant softening with tan delta = 0.71 at 80 °C; commercial plant-based cheese remained very rigid (tan delta = 0.08 at 80°C).	Dobson and Marangoni (2025a)

							Microstructure: Cold dairy and HPC showed high density of small fat globules. Melted HPC showed fat pooling and a continuous protein-starch matrix, similar to melted dairy; commercial plant-based cheese maintained an irreversible, rigid starch network. Melt & Stretch: Dairy melt ~184%, HPC melt ~110%, commercial plant-based cheese melt ~1%. Axial pull stretch: Dairy ~95 mm, HPC ~36 mm, commercial plant-based cheese ~8 mm.	
Hydrocolloid-structure (starch-dominated incorporating plant protein)	Waxy maize starch Plant protein: faba 1, faba 2, faba 3, pea 1, pea 2, soy 1, soy 2, chickpea, lupin, mung bean;	Fractionation/dry method		Processed cheese analogues compared to Cheddar	To assess cheese meltability, stretchability, hardness, and oil loss for formulations with different plant proteins, and relate these outcomes to protein properties.		Protein purity and solubility are key. Texture: Hardness (N) ranged from ~10 N to ~63 N. Higher hardness was associated with greater melt, stretch, and oil loss. Rheologically, Higher tan delta at 80 °C correlated with better melt. Microstructure showed high-purity proteins (>70%) act as passive fillers, while low-purity proteins disrupt the	Dobson and Marangoni (2025b)

							starch network. Melt & Stretch: High purity (>70%) and low solubility (<30% at pH 5.5) proteins result in better melt and stretch by allowing the starch to form a continuous network.	
Hydrocolloid-structure (starch-dominated incorporating plant protein)	Waxy maize starch Pea protein	Fractionation/dry method		Processed cheese analogues compared to Cheddar	To evaluate the effect of varying plant protein concentrations on meltability, oil loss, and texture of starch-based cheeses.		Protein addition (up to 7.5%) increases hardness and improves melt by weakening the starch network upon heating. Protein disrupts the starch matrix, reducing adhesiveness. Texture: Hardness increased with protein addition, peaking at 7.5% PPI (~100 N). 10% PPI sample was softer (~60 N). Cheddar control ~80 N. Melt & Stretch: Melt area increase peaked at 3% PPI (~130%) vs 0% PPI (~80%). Axial pull stretch: 0% and 3% PPI (~90 mm) were similar to Cheddar; 7.5% and 10% PPI showed lower stretch (~60 mm).	Sanders et al. (2024 b)

Hydrocolloid-structure (starch-dominated incorporating plant protein)	Waxy maize starch Pea, lentil, faba, soy protein isolate	Fractionation/dry method	Ball milling	Processed cheese analogues compared to Mozzarella	To characterize the physical and structural properties of plant proteins and their performance in plant cheese analogues.	FTIR for protein secondary structure. Ball milling-LP1 (lentil) showed a significant increase in random coils and beta-turns with a decrease in alpha-helix content. This suggests LP1 is particularly sensitive to milling-induced denaturation due to	Protein solubility and interactions are critical. Pea protein isolate (PP3) showed best performance (highest Water Holding Capacity. Ball milling enhances melt/stretch but reduces hardness) Texture: Hardness between 80.2-95.4 N. Ball milling significantly decreased hardness (by ~28.6-34.2%) by reducing protein particle size and disrupting the network. Microstructure showed protein source strongly influences the 3D organisation of oil and starch in plant-based cheese analogues, thereby affecting functionality. LP1 (lentil) and FP1 (faba) analogues contained high densities of small, well-stabilized oil droplets that were highly integrated into the matrix.Poorly Stabilized Systems: Conversely, PP3 (pea) analogues exhibited large, poorly stabilized oil bodies.Starch State: SP1 (soy) analogues contained the highest proportion of ungelatinized (native) starch	Hanley et al. (2025)

						hydrogen bond disruption.	granules (5.4%), which likely weakened the polysaccharide network and influenced melting behavior. These behaviours are governed by key mechanisms, including the role of low-solubility proteins as passive fillers that prevent over-structuring, the thermo-reversible nature of amylopectin-rich starch networks, and the extent of oil integration within the matrix, which collectively determine the balance between meltability, stretchability, and oil retention.	

Hydrocolloid-structure (starch-dominated incorporating plant protein)	Glutinous rice flour (GRF) Pea protein isolate	Fractionation/dry method		Processed cheese analogues compared to Cheddar and Mozzarella	To develop a dual-polysaccharide network incorporating plant proteins in plant-based cheese to mimic the meltability of dairy cheese upon heating.		A dual polysaccharide (kC and GRF) and PPI system allows for sequential melting and gelation. Texture: Hardness increased significantly with GRF content (from ~295 g at 0% GRF to ~836 g at 12% GRF). kC also increased hardness and cohesiveness. Samples showed enhanced springiness (~0.3-0.5) and chewiness. Rheological properties: Frequency sweep showed solid-dominant behavior (G' > G"). Temperature sweep showed kC melting (softening) at 50-75 °C, followed by GRF gelatinization (G' increase) at >80 °C. Final gel at 50 °C was strong and viscoelastic. Microstructure: kC provides initial structure that melts upon heating, while GRF gelatinization provides the required viscous flow and stretch. Melt & Stretch: Melt area increase peaked at 8% GRF (~190.5%). Extensibility increased with GRF, reaching	Yiu et al. (2026)

							~153% at 12% GRF and 0.6% kC. Samples outperformed commercial plant-based cheese in melt.	
Hydrocolloid-structure (starch-dominated incorporating plant protein) (oil study)	Waxy maize starch faba protein isolate	Fractionation/dry method		Processed cheese analogues compared to Cheddar	To study the incorporation of beeswax (BW), candelilla wax (CW), and ethylcellulose (EC) as gelators for coconut oil in plant-based cheese and how these gelators affect its structure and physical and functional properties.		Oil gelators (EC, BW, CW) significantly reduced oil loss during melting (from 53% in control to <20% in EC). EC increased hardness by strengthening the fat crystal network. Oil stabilization is achieved by trapping oil in a denser crystalline network or polymer matrix. Polarized light microscopy and fractal dimension (D). EC-oleogel fat network showed higher D (1.68) compared to control (1.40), indicating a more homogeneous and denser	Dobson and Marangoni (2024)

							crystal network. Melt diameter increase was ~100-120% for all samples. Axial pull stretch: ~20-30 mm; no significant difference between oleogels and control.	
Hydrocolloid-structure (starch-dominated incorporating plant protein) (oil study)	Waxy corn starch Pea protein	Fractionation/dry method		Processed cheese analogues compared to Mozzarella	To evaluate the effect of saturated and unsaturated fat on meltability, oil loss, and texture of starch-based cheeses.		Up to 75% of coconut oil (CO) can be replaced with sunflower oil (SO) without compromising texture, melt, and stretch properties. Texture: Hardness increased with CO content; 100% CO cheese ~106N. 25% CO sample showed unexpectedly high hardness (~81N). Rheological properties: No crossover point (tan delta < 1) observed for plant-based samples, indicating solid-dominant behavior. Melt & Stretch: 25% CO sample achieved 83mm stretch. Melt and stretch did not increase linearly with CO.	Sanders et al. (2024a)

Hydrocolloid-structure (starch-dominated incorporating plant protein) (protein-oil interaction)	Waxy maize starch Pea protein (PP1), pea protein isoalte, faba protein isolate, lentil protein isolate	Fractionation/dry method		Processed cheese analogues compared to Mozzarella	To evaluate the effects of different plant proteins on the physical characteristics of plant-based cheese		Protein-fat interactions are crucial. PP1 facilitates a more uniform distribution of oil droplets within the gelatinized starch and protein matrix. Specific proteins (like PP1) can maintain cheese functionality (melt, stretch) even when saturated fat is reduced to 25% of the total fat content. PP1 emulsifies both saturated and unsaturated fats similarly. This high oil-binding capacity prevents the liquid oil from leaking prematurely or weakening the starch-protein matrix, which typically happens when large, unstable fat globules form.	Sanders et al. (2025)
Protein-dominated network (protein-oil) Protein concentration: 10%	Pea protein isolate (PPI)	Tissue disruption/ wet method	Fermentation		To design of an optimal pea protein matrix for fermented plant-based cheese.		Fermentation-induced PPI gels were studied with 0-20% olive oil. Gel hardness (puncture test) decreased as olive oil content increased, dropping from ~280 g (0% oil) to ~180 g (20% oil). oil droplets acted as inactive fillers that disrupted the protein network. Conversely, WHC increased with oil content, possibly due to a filling effect. Microstructure revealed a bi-modal oil droplet distribution where larger droplets	Masiá et al. (2022)

							weakened the matrix. Gel hardness remained stable during 7 days of refrigerated storage. A matrix with 10% protein and 10% olive oil was found to be optimal, balancing firmness and mouthfeel without compromising gelling properties.	
Starch-oil-dominated	Pea protein , Potato fiber, Pea starch	Fractionation/dry method		Cream cheese analogue	To investigate the effect of the melting point of fat on the tribological properties of a pea-based cream cheese analogue.		Plant-based cream cheese emulsions were studied using various fats (sunflower oil, coconut fat, shea stearin). Solid fats (coconut, shea) significantly increased viscosity a G' at lower temperatures compared to liquid sunflower oil. Microstructure showed sunflower oil formed well-dispersed spherical droplets, whereas solid fats resulted in irregular fat crystal aggregates. Tribological analysis revealed that oil type and melting point greatly impacted the friction coefficient during oral processing. Emulsion stability was enhanced by interactions between amylose (from potato fibers) and lipids, which reduced syneresis and starch retrogradation. Overall, the physical state of the fat	Mefleh et al. (2022)

							(liquid vs solid) was the primary driver of rheological and textural differences.	

2.2.2. The role of plant protein in plant-based cheeses

Although starch or other polysaccharides play a dominant role in commercial plant-based cheeses, proteins (accounting for 0-5%) are important structural elements governing network formation depending on formulation and processing strategies. The plant protein sources most commonly used for the development of plant-based cheeses in recent studies include soy, pea, faba bean, chickpea, lentil, mung bean and zein (Ferawati et al., 2021; Grasso et al., 2021; Lu et al., 2025; Mattice & Marangoni, 2020a; Ozturk et al., 2023). However, plant proteins differ from casein in terms of molecular structure, aggregation behaviour and gelation mechanisms. Therefore, they often form weaker, less elastic, more particulate and more rigid networks with limited meltability, grainy texture, off-flavours, and nutritional limitations compared to casein-based systems. Consequently, plant proteins typically require physical, chemical and biological modifications to improve their functional properties, such as gelation and emulsification (Kovačević et al., 2024)

In contrast to the flexible and random-coil nature of casein, plant proteins usually exhibit globular structures, limited intrinsic flow and stretchability and strong sensitivity to processing conditions (Sözeri Atik & Huppertz, 2025). Their gelation is primarily driven by protein denaturation, hydrophobic interactions and aggregation, whereas casein gels through micellar disassembly mediated by reduced electrostatic interactions (Ahrné & Leser, 2025). Therefore, the functionality of plant proteins in cheese analogues relies on the formulation and manufacturing process. For example, the manufacturers often use functional ingredients such as modified starches or hydrocolloids, and emulsifying salts to mimic the elasticity of dairy cheese by creating a more continuous and flexible matrix. Several studies have emphasised the importance of non-covalent interactions in mimicking casein coagulation. In particular, the hydrophobicity and self-aggregating behaviours of zein, which are attributed to its high

proportion of non-polar amino acids, promote non-covalent interactions that lead to the formation of viscoelastic and cheese-like networks (Grasso et al., 2023; Grasso et al., 2025; Mattice & Marangoni, 2020a, 2020b). The limited water solubility of plant proteins is a significant factor restricting their application in food systems. Protein solubility is governed by intrinsic factors such as amino acid composition, structure and degree of denaturation, as well as extrinsic conditions including pH, ionic strength and temperature. Therefore, initial efforts typically focused on enhancing plant protein solubility through approaches such as optimisation of extraction methods, pH alteration, and enzymatic treatments, thereby improving their physicochemical properties (Zhu et al., 2022). However, solubility also plays a critical role in determining texture and mouthfeel in plant-based cheeses, where soluble proteins tend to form well-distributed and interconnected protein

2.2.3. The role of vegetable oil in plant-based cheeses

Several studies have investigated the effects of vegetable oils on plant-based cheeses (accounting for 17-28%)(Dobson & Marangoni, 2024; Michel et al., 2022; Sanders et al., 2024a; Sanders et al., 2025). Different types of oils, such as palm, soybean, sunflower, canola and olive oils, have distinct fatty acid compositions, which in turn influence the physicochemical and textural properties of plant-based cheese. Coconut oil is most commonly used because of its high saturated fat content (80%–90%) and a melting profile similar to that of milk fat, contributing to firmness when chilled (Grossmann & McClements, 2021; Kamath et al., 2022). However, health and sustainability concerns have driven interest in oil blends. For example, replacing 75% of coconut oil with sunflower oil can maintain hardness, meltability and stretchability (Sanders et al., 2024a; Sanders et al., 2025). Although starch- and oil-based systems can provide desirable textural attributes, their nutritional contribution is limited. Moreover, owing to the inherent structural differences between plant proteins and casein, plant

proteins alone cannot provide comparable functionality. Consequently, recent studies have increasingly focused on starch–protein–oil systems or polysaccharide–protein emulsion gels to better replicate the functionality of traditional dairy cheese while improving the nutritional value of plant-based cheeses (Dobson & Marangoni, 2023, 2024; Hanley et al., 2025; Lyu et al., 2023; Yiu et al., 2026).

2.2.4. Microstructure, texture, and functional properties of plant-based cheese analogues

The microstructure of cheese, which is modulated by ingredient composition and processing conditions, plays a crucial role in determining its texture and physicochemical properties.

The microstructure of plant-based cheeses markedly differs from that of conventional dairy cheese and can be described in terms of network continuity, phase behaviour and aggregate organisation. For example, the microstructure of cheddar cheese is characterised by large, clustered fat globules embedded within a compact and continuous protein matrix (Grasso et al., 2021; Ong et al., 2022). Conversely, commercial plant-based cheeses usually exhibit a non-continuous and less cohesive protein matrix with a heterogeneous structure (Grasso et al., 2021) (**Figure 2-1**). From a phase perspective, plant-based systems often show poor integration between components. In many formulations, vegetable oil droplets tend to coalesce, leading to phase separation and uneven fat distribution, which negatively affects texture and structural stability (**Figure 2-2**) (Lu et al., 2025). In addition, plant proteins commonly form large aggregates rather than a fine, interconnected network, further contributing to structural discontinuity. The organisation of these structural elements depends on the formulation strategy. In polysaccharide- or starch-based cheeses, a continuous 3D network entraps water, oil, and insoluble protein particles (Grossmann & McClements, 2021), whereas in plant protein-rich cheeses, aggregated protein phases provide structural support. Starch–protein–oil–based cheese systems represent another approach, where polysaccharides dominate network

formation, entrapping water, oil and protein particles to achieve desired textural properties and mimic the meltability and stretchability of processed dairy cheese (**Figure 2-3**) (Dobson & Marangoni, 2023, 2025b; Lyu et al., 2023). Overall, these systems behave as multiphase composites, and their functionality depends on the relative contributions and interactions of each structural component. **Figure 2-4** shows a schematic comparison of the microstructures of plant-based and casein-based cheeses, along with their associated textural and functional properties.

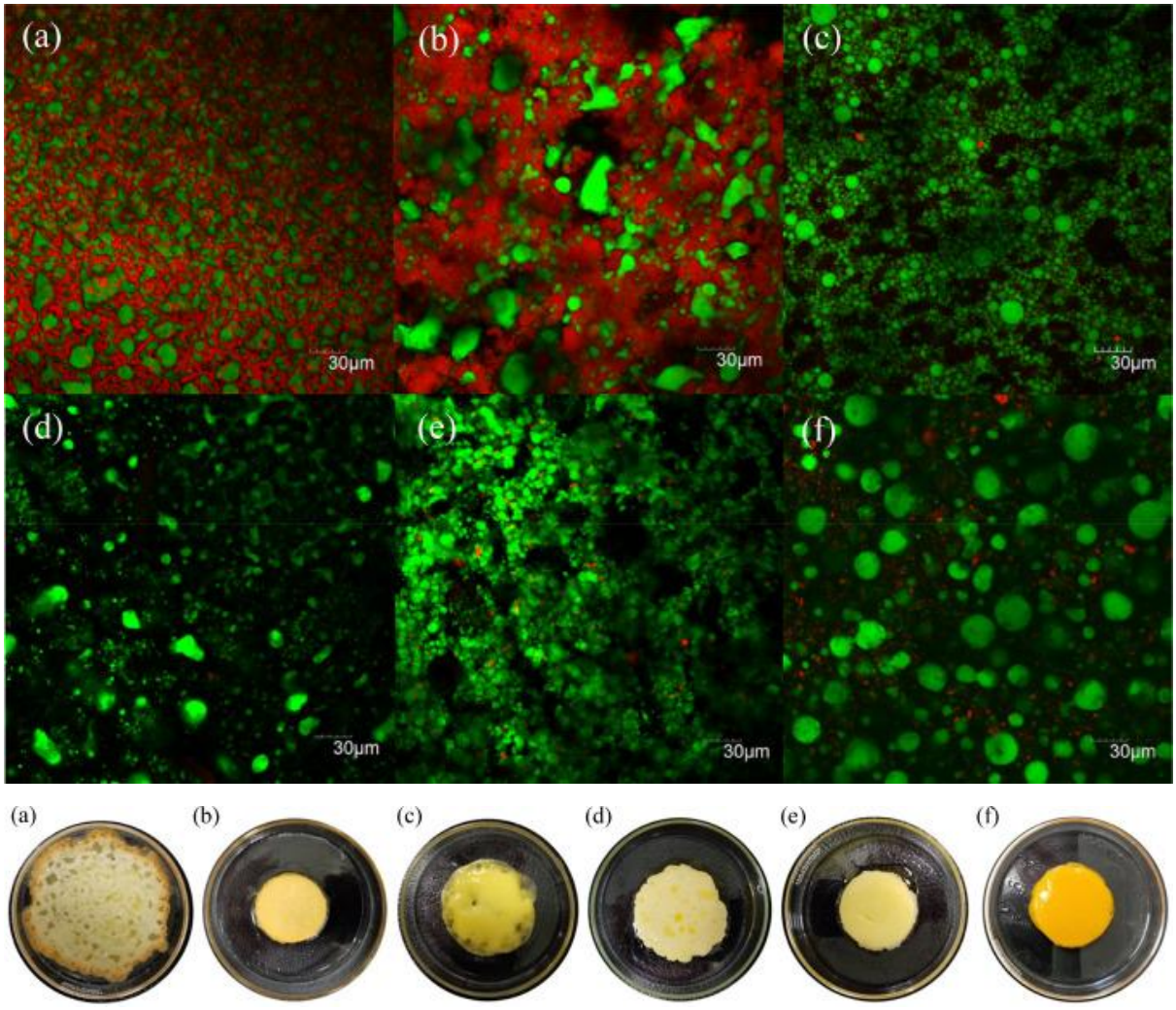


Figure 2-1. Confocal laser scanning microscopy images (×40) of Cheddar cheese (a), processed dairy cheese (b), and plant-based cheese products A (c), B (d), C (e), and D (f) (top). Products A–D are commercial plant-based cheeses with no dairy ingredients and are mainly starch–oil-based systems; only product D contains pea protein isolate. The images show the distribution of fat globules (green) and protein (red). The scale bar represents 30 μm.

Meltability of Cheddar (a), processed dairy cheese (b), and plant-based products A–D (c–f) after 5 min of heating in an oven at 232 °C (bottom). Adapted from (Grasso et al.), *Future Foods*, 2021, with permission from © Elsevier.

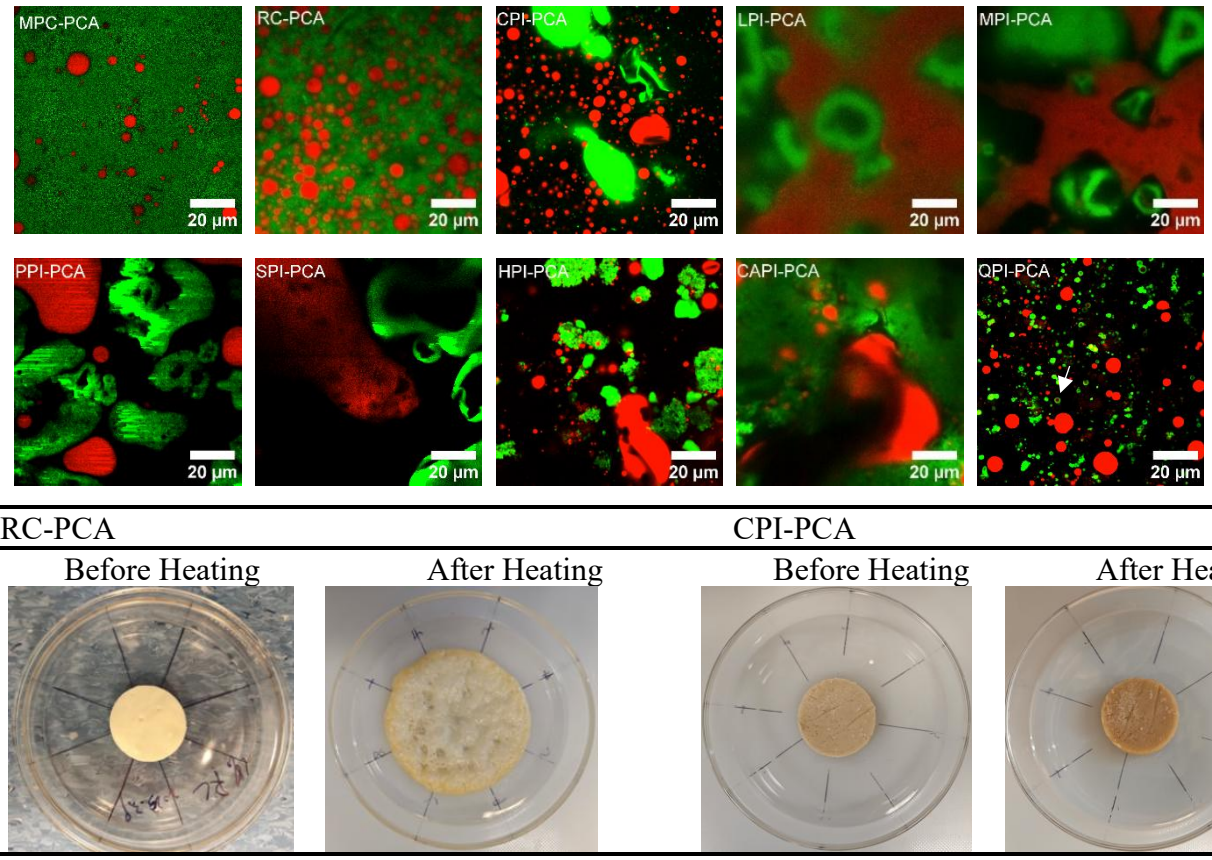
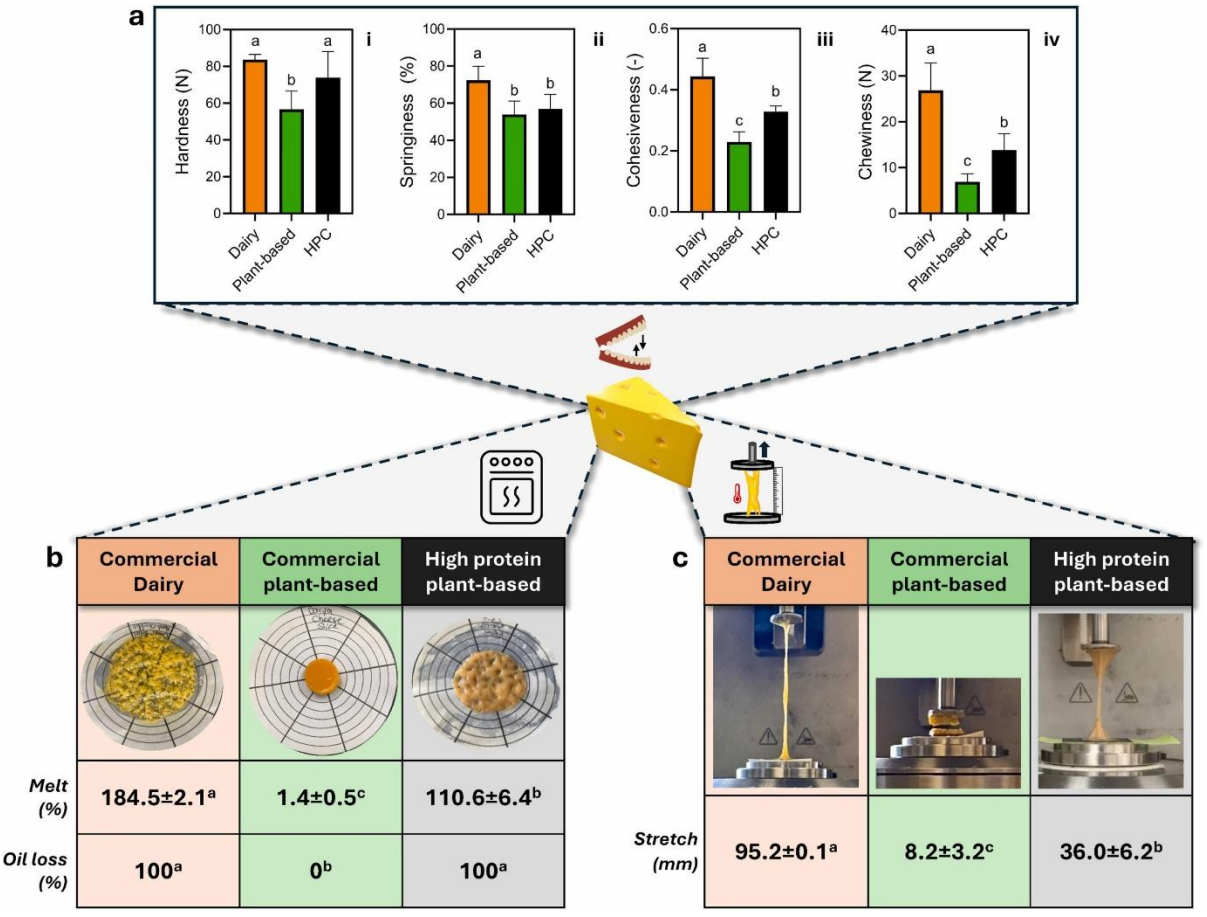


Figure 2-2. Confocal laser scanning microscopy (CLSM) images (×63; scale bar = 20 µm) of processed cheese analogues formulated with different protein sources (top). Fat and protein were stained red and green, respectively. PCA = processed cheese analogue; MPC = milk protein concentrate; RC = rennet casein; CPI = chickpea protein isolate; LPI = lentil protein isolate; MPI = mung bean protein isolate; PPI = pea protein isolate; SPI = soy protein isolate; HPI = hemp protein isolate; CAPI = canola protein isolate; QPI = quinoa protein isolate. Representative photographs comparing meltability of RC-based and chickpea-protein-based processed cheese analogues (bottom). Adapt from (Lu et al.), *International Journal of Food Science and Technology*, 2025, with permission from © Oxford University Press.

Conventional dairy cheeses exhibit a wide range of textures, from soft and spreadable to firm and crumbly, based on their intended end use. These properties are commonly measured using a texture analyser. Uniaxial compression is often used to assess firmness, whereas two-bite textural profile analysis is used to assess parameters such as hardness, springiness, cohesiveness, chewiness and adhesiveness. These methods have also been used to characterise plant-based cheeses. However, Braitmaier et al. (2024) indicated that lower deformation levels during compression (e.g. 25% rather than 80%) are required, as a majority of plant-based cheeses tend to fracture during testing. In addition, the storage modulus (G′, elasticity) at 20°C from oscillatory temperature sweep measurements can serve as an indicator of firmness, with higher G′ values corresponding to firmer samples (Braitmaier et al., 2024).



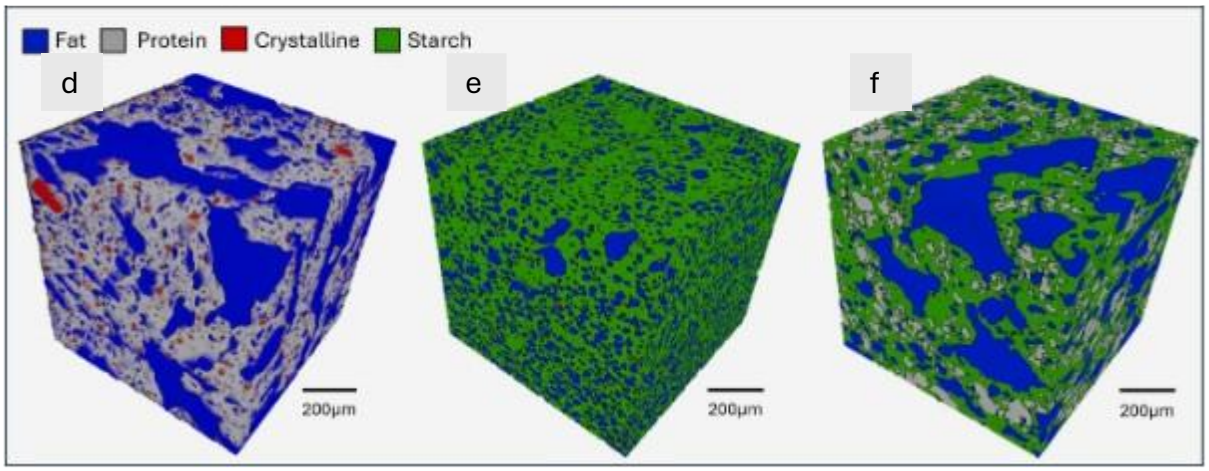


Figure 2-3. Comparison of commercial dairy cheese (23% w/w protein), commercial plant-based cheese (0% protein), and high-protein plant-based cheese (18% w/w protein, 12% waxy maize starch, 21% coconut oil). (a) Texture profile analysis: (i) hardness (N), (ii) springiness (%), (iii) cohesiveness, and (iv) chewiness (N). (b) Meltability (%) and oil loss (%). (c) Stretchability (mm). Values are means ± SD; bars sharing the same letter within the same graph or row are not significantly different ($P > 0.05$; $n \geq 3$). (d–f) Synchrotron-based micro-computed tomography 3D renderings of commercial dairy cheese, commercial plant-based cheese, and high-protein plant-based cheese, respectively. Crystalline material (red) represents calcium phosphate or lactate crystals in dairy cheese and native starch granules in plant-based cheese. Adapted from(Dobson & Marangoni), *Food Structure*, 2025, with permission from © Elsevier.

Cheese melting is a critical functional attribute and is commonly defined as the ability of cheese to soften, flow, and spread upon heating, accompanied by a visible loss of the integrity of individual shreds. Although the melting behaviour of cheese has been reasonably well described at a qualitative level, a fully quantitative and predictive mechanistic understanding remains lacking (Lucey et al., 2003). Upon heating, cheese undergoes a series of coupled structural and physicochemical transitions. One of the earliest and most influential changes is the solid-to-liquid transition of milk fat. The melted fat acts as a lubricant within the protein matrix, facilitating molecular mobility and promoting macroscopic flow. However, casein does not melt in a thermodynamic sense; rather, the pre-existing casein network progressively loses rigidity as temperature increases. Heating alters the balance of non-covalent interactions governing the casein network. Although intramolecular and intermolecular hydrophobic and electrostatic interactions may intensify at the molecular scale, increased thermal motion

reduces the effective contact area and stability of junctions between casein particles. Furthermore, colloidal calcium phosphate is progressively solubilised at elevated temperatures, weakening calcium-mediated crosslinks within and between casein micelles. Simultaneously, hydrogen bonds that contribute to the rigidity of the casein matrix are weakened. Altogether, these effects lead to a net reduction in gel strength and permit casein strands and aggregates to slide past one another (Atik & Huppertz, 2023). Melting is controlled by the local balance between attractive and repulsive forces within the casein matrix (Lucey et al., 2003). Continued heating influences the final appearance and texture of melted cheese through moisture loss, surface drying, fat coalescence and browning reactions such as the Maillard reaction.

Rheologically, the solid-to-liquid transition of cheese is commonly defined as a change from solid-like to liquid-like behaviour, characterised by the crossover of G′ and loss modulus (G″). Specifically, G″ is greater than G′ ($\tan \delta = G'' / G'$). This criterion provides an objective means of evaluating the inherent melting behaviour of dairy cheese. Accordingly, numerous studies have used small-amplitude oscillatory temperature sweeps to characterise the melting behaviour of plant-based cheeses using methodologies established for dairy cheese systems (Grasso et al., 2021; Yiu et al., 2026). However, in a majority of plant base cheeses, a $G'' > G'$ crossover is not observed during heating, indicating the absence of a true melt transition. Instead, only relative reductions in G′ are observed, reflecting progressive softening rather than melting. This distinction is critical and suggests that directly replicating casein-like melting behaviour with current plant-based formulations remains fundamentally challenging. Rather than targeting a true crossover, it may be more relevant to focus on rheological parameters that reflect functional performance, such as yield stress, flowability under large deformation, and the correlation between structural resilience (represented by the slope n of the linear region) and the deformation at the yield point, which together offer a more robust proxy for melt-like

functionality (Braitmaier et al., 2024). Furthermore, rheological measurements are typically conducted at temperatures below those encountered during cooking (e.g. oven heating at ~180°C). Therefore, Braitmaier et al. (2024) suggested that it is more appropriate to describe rheological changes in plant-based cheeses as a softening index rather than actual melting behaviour and that small-amplitude oscillatory measurements alone are insufficient to characterise meltability in these systems. Instead, the Schreiber test, which assesses changes in sample diameter during heating, is the most commonly used empirical method owing to its straightforward application. Braitmaier et al. (2024) compared two temperature–time combinations (232°C for 5 min versus 180°C for 10 min) and concluded that the Schreiber test was the most suitable method for describing the melting behaviour of plant-based cheese. A temperature of 180°C is preferred, as it more closely reflects the conditions of domestic oven systems. Furthermore, large-amplitude oscillatory shear measurements recorded at 60°C were correlated with the Schreiber test results obtained at 180°C. This approach may serve as a complementary tool for characterising flow and melting behaviour; however, further studies are required to validate this relationship.

Stretchability is another critical functional attribute of cheese and remains particularly challenging to replicate in plant-based cheeses. In dairy cheese, stretchability refers to the ability of the casein network to deform under applied stress without fracture, which requires a continuous, well-connected casein matrix. This behaviour results from a balance between energy storage and dissipation within the protein network (Lucey et al., 2003). Although this behaviour is widely observed in cheeses such as mozzarella, the underlying relaxation mechanisms and durations and their relationships with both frequency and temperature remain unclear. Upon heating, enhanced hydrophobic interactions promote partial contraction and rearrangement of the casein network, thereby increasing molecular mobility while maintaining

network connectivity. When mechanical energy is applied, the network can elongate and stretch as intermolecular bonds dynamically break and reform. Therefore, at the molecular level, stretchability is governed by the reversible relaxation of non-covalent interactions within the casein matrix and affected by the concentrations of intact casein and calcium (Dobson & Marangoni, 2023; Grasso et al., 2024; Lucey et al., 2003; Salgado et al., 2023). In contrast to conventional dairy cheese, plant based cheeses lack this protein network, exhibiting fracture under deformation and negligible stretching behaviour.

Despite its importance, a standardised method for quantifying the stretchability of cheese remains lacking. Traditional methods, such as the fork test or texture analysis, are subjective and highly variable (Grasso et al., 2023; Salunke et al., 2022). Dobson and Marangoni (2023) developed an extensional rheological method to quantify cheese stretchability. According to the authors, this method provides higher accuracy by maintaining constant heat and elongation speed. However, key limitations include uncertainty in repeatability for heterogeneous samples, constraints on maximum measurable extension that may prevent the detection of break points and limited adoption and standardisation across studies. Lu, Roy, et al. (2026) developed a modified cheese stretchability rig using a texture analyser with a post-comb and base pot. The maximum pull force, total work and stable stretch distance were measured; however, the analyser's limited sensitivity prevented the detection of the stretch-breaking point. An ideal standardised method should combine controlled temperature with constant extensional rates and sufficient sensitivity to capture both elongation and fracture. Given the anisotropic and heterogeneous nature of cheese, reproducible sample geometry and alignment during stretching are essential. Key parameters should include stretch distance, fracture strain and energy to break, enabling consistent comparison across studies.

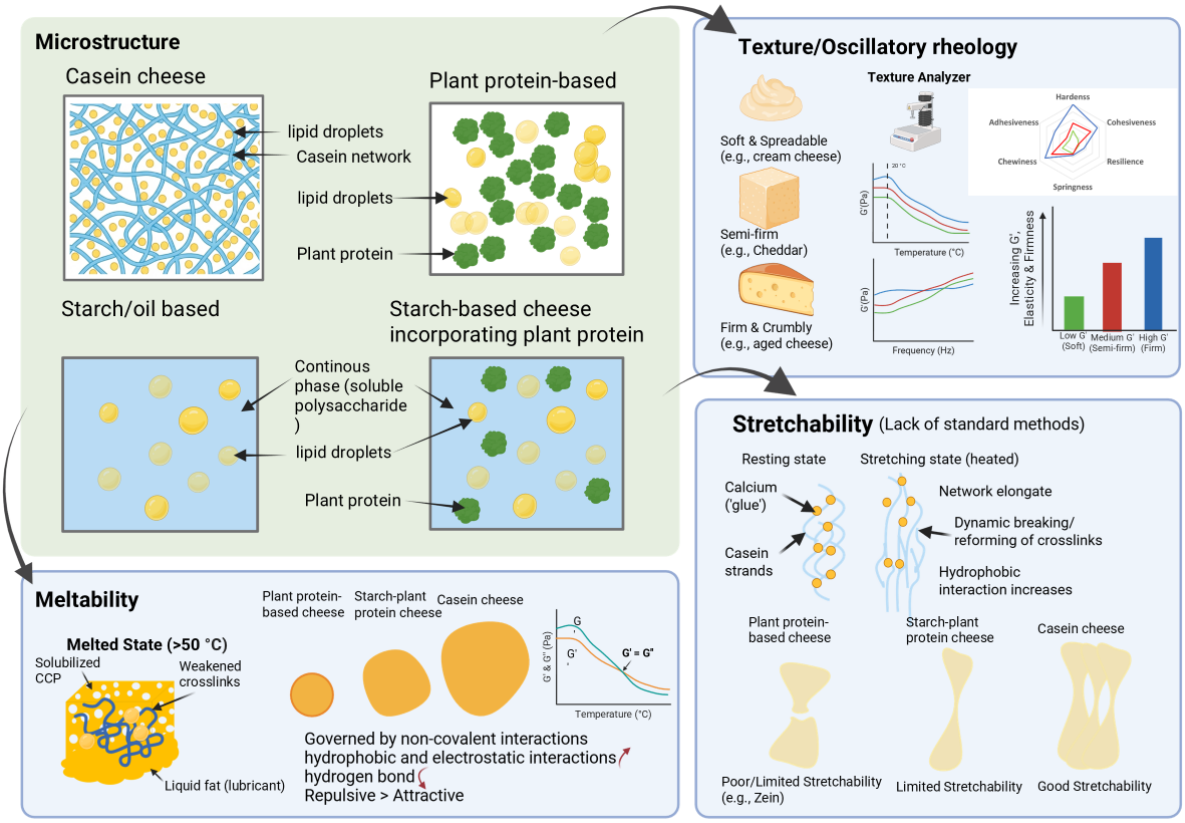


Figure 2-4. Schematic overview of plant-based cheese structure formation and its relationship to texture, meltability, and stretchability.

Conventional dairy cheeses exhibit a wide range of textures, from soft and spreadable to firm and crumbly, based on their intended end use. These properties are commonly measured using a texture analyser. Uniaxial compression is often used to assess firmness, whereas two-bite textural profile analysis is used to assess parameters such as hardness, springiness, cohesiveness, chewiness and adhesiveness. These methods have also been used to characterise plant-based cheese analogues. However, Braitmaier et al. (2024) indicated that lower deformation levels during compression (e.g. 25% rather than 80%) are required, as a majority of plant-based cheese analogues tend to fracture during testing. In addition, the storage modulus (G′, elasticity) at 20°C from oscillatory temperature sweep measurements can serve as an indicator of firmness, with higher G′ values corresponding to firmer samples (Braitmaier et al., 2024).

2.3. Improvement strategies through tailoring input

Understanding the fundamental differences in ingredients, structure and functionality between plant-based and traditional dairy cheeses provides insights into how raw materials and processing conditions can be modified to improve microstructure, texture and melting and stretching properties.

2.3.1. Formulation strategies

Numerous researchers have focused on formulation strategies to improve plant-based cheese functionality, such as the selection of appropriate plant protein assemblies with casein, blending of different protein sources, protein modification, use of hydrocolloids and ion modulation. These formulation designs are summarised in **Figure 2-5**.

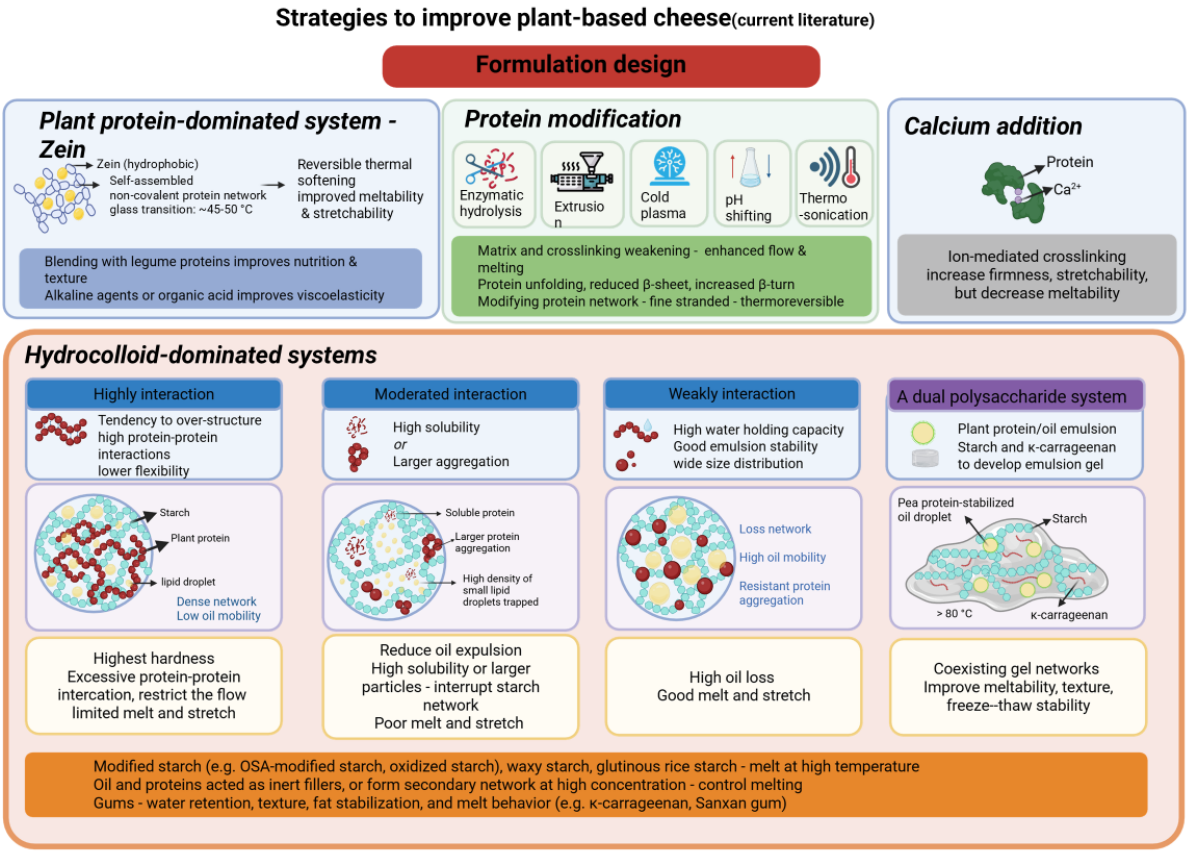


Figure 2-5. Formulation design strategies to improve the structure, texture, and functionality of plant-based cheese. Reference for Plant protein-based system – zein: Grasso et al., 2023; Grasso et al., 2025; Mattice & Marangoni, 2020a, 2020b; Ozturk et al 2023; Salgado et al. 2023; Wahl and Hinrichs, 2006; Sutter et al., 2023; Xu et al., 2025; Protein modification: Xie et al., 2021; Lu et al., 2026; Zeng, 2021; Chuang et al., 2025; Zhu et al., 2022; Hu et al., 2024; Calcium addition: Grsso et al., 2024; Salgado et al., 2023; Hydrocolloid-dominated systems: Lyu et al., 2023; Ørskov et al., 2024; Sanders et al., 2024b; Dobson and Marangoni, 2023, 2024, 2025a, 2025b; Hanley et al., 2025; Yiu et al., 2026; Zhang et al., 2025; Grasso et al., 2023, 2024; Salgado et al., 2023.

2.3.1.1. Plant protein–based systems

Although various plant proteins have been used to develop cheese analogues, none have been shown to fully replicate the structure and functionality of casein (refer to Table 2-1). Legume proteins, such as soy and pea proteins, typically form covalently linked, gel-like networks that remain structurally stable at elevated temperatures (e.g. ~60°C), resulting in limited thermal softening and poor meltability. On the contrary, zein has emerged as a promising alternative, exhibiting cohesiveness, viscoelasticity and improved meltability and stretchability at elevated temperatures (Grasso et al., 2023; Mattice & Marangoni, 2020a, 2020b). Zein is a hydrophobic prolamin protein that self-assembles into a continuous, non-covalently bonded protein network within cheese-like matrices, enabling reversible thermal softening. After heating above 45°C–50°C (glass transition temperature), zein transitions from a glassy to a rubbery state, increasing chain mobility and weakening hydrogen bonds without complete network disruption (Sutter et al., 2023). Thermal treatment promotes β-sheet formation and fibrillation, resulting in a fibrillar, viscoelastic network. This behaviour contrasts with typical globular proteins, which require irreversible unfolding and aggregation to form stable networks (Sadat et al., 2022).

Zein-based cheeses containing approximately 30% zein exhibit enhanced viscosity and stretchability comparable to those of cheddar cheese (Mattice & Marangoni, 2020a, 2020b).

However, zein alone is nutritionally limited (limiting essential amino acid profile) and often produces brittle and firm textures. Blending zein with other plant proteins has therefore been explored to tailor both functionality and microstructure. Integration of globular plant proteins (e.g. chickpea and pea proteins) generally follows two principles: the secondary protein phase modulates the continuity and mobility of the zein network. In zein–chickpea protein cheeses, a hierarchical structure emerges in which zein forms a stabilizing layer around fat globules, facilitating flow at elevated temperatures. Textural properties also vary with formulation, with samples containing 100% zein showing the highest hardness and those containing 100% chickpea protein exhibiting higher adhesiveness, springiness and cohesiveness (Grasso et al., 2023; Grasso et al., 2025). In zein-pea protein blends (90:10, 80:20,70:30, zein: pea), functionality is strongly influenced by the physical state and ratio of pea protein (Wahl & Hinrichs, 2026). Native pea protein, which aggregates upon heating, and its denatured variants with high water-binding capacity that form extended hydrodynamic volumes act as physical barriers that disrupt the continuity of the zein network. This interference results in a softer, less brittle matrix with compromised meltability. Conversely, denatured pea protein with low water-binding capacity allows greater solvent availability, enabling zein particles to move and interact while preserving a continuous, thermoreversible network. This process results in a firmer, more brittle cheese that retains good meltability and flowability.

Beyond protein composition, the transition of these blends from brittle to cohesive solids is governed by the chemical environment. Alkaline agents (e.g., calcium hydroxide) enhance β-sheet content, supporting viscoelasticity at room temperature (Ozturk et al., 2023), whereas acid treatments disrupt hydrogen bonds and hydrophobic interactions to create a denser, more flexible

network, reducingthe glass transition temperature and proventing greasy or leaky textures (Xu et al., 2025). With these principles, zein–pea formulations with adjusted calcium hydroxide concentrations achieve textures comparable to mozzarella (3%) and Colby cheese (5%), forming well-incorporated, web-like networks that support cohesiveness and viscoelasticity (Salgado et al., 2023). Overall, formulations containing a total protein content of approximately 30% from combined zein and pea protein show strong potential in mimicking the melting behaviour of conventional dairy cheese (Sutter et al., 2023).

Emerging approaches have also explored plant-based casein micelle analogues such as those derived from potato protein, which can form colloidal structures with some similarities to casein micelles. However, these systems still differ in aggregation behaviour and lack the full functional complexity of dairy casein, indicating that further development is required before they can be considered true functional equivalents (Chen et al., 2026).

2.3.1.2. Protein modification

A majority of plant-based cheeses rely on commercial plant protein concentrates or isolates, which exhibit diverse physicochemical properties. To improve functionality, plant proteins can be modified using physical (e.g. ultrasound, extrusion and pulsed electric fields), chemical (e.g. pH shifting, acylation and phosphorylation) and biological (e.g. enzymatic hydrolysis, crosslinking and fermentation) approaches.

For example, Xie et al. (2021) used Flavourzyme to partially hydrolyse soymilk and incorporated the hydrolysed soymilk into fresh milk to produce a cheese analogue. Among the hydrolysis

conditions tested, the optimum treatment of 50 °C, 0.5% (w/v) Flavourzyme and 6 h produced a degree of hydrolysis of 15.1% and the greatest stretch length of 95 mm. Meltability showed slightly increased by less than 3 mm and reaching 32 mm under the optimum treatment; however, this system was not fully plant-based. On the contrary, Lu et al (2026) (unpublished data) suggest that hydrolysed mung bean protein using Alcalase and trypsin and used the modified protein to prepare plant-based cheeses. Meltability increased with an increase in the degree of hydrolysis, with Alcalase-treated samples exhibiting better meltability than trypsin-treated samples at identical hydrolysis levels. This behaviour is attributed to hydrolysis-induced weakening of the protein matrix through reduced intermolecular crosslinking and the formation of smaller peptides, as evidenced by decreased elasticity and thermal stability. Differences between the two enzymes are likely related to variations in peptide profiles and hydrophobicity, influencing protein–protein and protein–matrix interactions. CLSM results supported these findings, showing a more fragmented and finely dispersed protein network in hydrolysed samples, which facilitated matrix deformation and flow during heating.

In contrast to enzymatic hydrolysis, which reduces network strength, extrusion is used to texturise plant-based proteins, as high temperatures and shear levels induce protein unfolding followed by reassociation and alignment along the flow direction during cooling (Kovačević et al., 2024). Zeng (2021) reported that extrusion of faba bean protein improved the stretchability and meltability of plant-based cheese by disrupting the tertiary and quaternary structures of the protein. This unfolding exposes hydrophobic residues, enhancing their interactions with fats and starches, whereas shear-induced alignment produces a less rigid, more fluid-like network that favours melting and stretching compared to the network formed by native proteins.

Unlike bulk restructuring methods such as extrusion, cold plasma is a non-thermal processing technology operated at atmospheric pressure that generates highly reactive species, including electrons, ions, UV light and reactive oxygen and nitrogen species (ROS/RNS). These reactive species can modify protein structure and intermolecular interactions, thereby altering protein functionality (S. Zhang et al., 2022). Chuang et al. (2025) reported that cold plasma treatment disrupted the tertiary structure of pea protein, leading to protein unfolding and exposure of hydrophobic functional groups. In addition, cold-plasma treatment at 130 W for 12 min led to changes in secondary structures, including a decrease in β-sheet content (from 27.5 to 24.4%) and an increase in β-turn content (from 23.8 to 26.5%), and altered surface hydrophobicity, which enhanced oil-holding capacity from approximately 2.1 to 2.9 mL/g, corresponding to an increase of about 40% compared with untreated pea protein. Plasma-treated pea protein (130 W for 12 min) exhibited increased hardness and improved heating behaviour, closely mimicking the melting characteristics of commercial vegan cheese.

In addition, chemical approaches such as pH-shifting provide a relatively simple and scalable strategy to modify protein conformation and functionality. Zhu et al. (2022) found that pea protein extracted through ammonium sulfate precipitation formed thermally reversible and transparent gels. This reversibility results from a fine-stranded protein network stabilised primarily by hydrogen bonds, which dissociate upon heating and reform during cooling, in the absence of strong hydrophobic or covalent interactions. The gels exhibited excellent viscoelasticity and melt–set transitions within a narrow acidic pH range (2.4–4.2) and at moderate protein concentrations (10%–15%). Similarly, Hu et al. (2024) converted faba bean protein into amyloid-like fibrils

through thermosonication or conventional heating, producing gels with a reversible gel–sol transition at approximately 68.5°C. In both systems, thermal reversibility resulted from the disruption and reformation of non-covalent interactions, particularly hydrogen bonds stabilising β-sheets. These findings suggest that inducing a reversible solid–liquid transition in protein matrices is a promising strategy for improving the meltability and stretchability of plant-based cheeses. However, the practical application of this strategy remains challenging owing to pH and salt constraints that may limit flavour and processing flexibility. Although numerous studies have modified plant proteins through various approaches and investigated the effects of modified proteins on physicochemical properties, the application of these proteins in the development of plant-based cheeses remains limited.

Overall, these modification strategies improve plant protein functionality through different mechanisms. Enzymatic hydrolysis reduces molecular size and crosslinking, yielding softer and more meltable but less structured matrices. In contrast, physical methods such as extrusion promote protein unfolding and alignment, forming more continuous networks that enhance stretchability, while non-thermal approaches like cold plasma primarily alter surface chemistry and secondary structure to improve interfacial interactions and oil binding. pH-shifting allows proteins to unfold and refold into fine-stranded networks through reversible non-covalent interactions. Despite these differences, a common modification principle includes partial unfolding while preserving the ability to reorganise into a continuous, non-covalently stabilised network that is most effective in achieving casein-like behaviour. No single approach is sufficient; therefore, combining chemical, physical and biological strategies, alongside optimisation of processing conditions, is essential to balance network integrity, mobility and functionality.

2.3.1.3. Hydrocolloid-based systems

Starch-based hydrocolloid systems are widely used in PCA formulations; however, starch usually increases hardness and restricts melting owing to the formation of a compact particle network, the presence of large fat droplets, emulsion destabilisation and resistance to flow upon heating (Lyu et al., 2023; Mounsey & O'Riordan, 2008). The use of modified starches, such as starch acetate and OSA-modified starch, has been shown to improve emulsification by reducing fat droplet size and retaining meltability (Ørskov et al., 2024). These modifications introduce steric hindrance or amphiphilic groups, enhancing starch swelling, reducing retrogradation, and improving interfacial activity, thereby promoting better interactions with both proteins and lipids (Gałkowska et al., 2023). Oxidised potato starch forms an entangled polymer network without visible granules, indicating complete melting. At low concentrations (5%), oil droplets and proteins act as inert fillers; however, at high concentrations (10-15%), they form a secondary network that restricts starch gel melting. These findings indicate that the melting behaviour of starch gels can be controlled through the development of an additional protein network (Lyu et al., 2023).

To address nutritional limitations while maintaining functionality, recent studies have shifted focus towards plant polysaccharide–protein–based cheese systems, wherein plant proteins are incorporated into polysaccharide-dominated networks (Sanders et al., 2024b). For example, Dobson and Marangoni (2023) developed a high-protein plant-based cheese analogue containing 18% fava bean protein, 12% waxy starch and 21% coconut oil using a controlled sequence of heating and shear. Low-shear mixing promoted native starch swelling and viscosity development, and subsequent high-shear treatment disrupted starch granules and enhanced the viscoelasticity of

waxy starch. The protein was hydrated before heating. Gradual heating induced starch gelatinisation, with longer heating durations increasing hardness through greater granule disruption. Short high-shear steps reduced viscosity and increased stickiness, and maintaining temperatures below 80°C prevented protein denaturation. The resulting gel consisted of protein and fat molecules dispersed within a continuous starch matrix, which enhanced meltability and stretchability by improving phase connectivity. Texture analysis revealed a hardness of 15–90 N, indicating the versatile applicability of the gel in different dairy products. The plant-based cheeses showed 2–3 times higher meltability and stretchability than commercial alternatives, resembling traditional dairy cheese. Rheological analysis indicated a higher tan δ value (up to 0.7), reflecting better meltability. However, a limitation of the product was that high amounts of oil loss occurred during melting. This loss can be mitigated by incorporating oil gelators to modify the crystal network microstructure of coconut oil. To better understand meltability, the authors compared microstructural changes before and after heating with those of commercial dairy cheese. Although the plant-based cheese contained larger fat globules and protein aggregates in the cold state, both plant-based and dairy cheeses exhibited pronounced microstructural changes after heating, characterised by fat pooling and yielding of the continuous matrix (Dobson & Marangoni, 2025b). The authors highlighted that effective melting requires a network that yields upon heating, allowing fat to pool while maintaining matrix connectivity to prevent oil leakage. Therefore, balancing protein–fat interactions, emulsion stability and network integrity is critical for achieving both meltability and structural stability in plant-based cheeses.

These findings align with broader evidence that starch–lipid interactions are critical in determining functionality. Starch networks can stabilise lipid phases and control melt behaviour through phase

connectivity and matrix rigidity (Dobson & Marangoni, 2024). In addition, lipid complexation with high-amylose starches can modify starch gel structure via amylose–lipid complex formation, altering crystallinity and nanoscale organisation (Koekuyt et al., 2025). Similarly, appropriate starch-structured matrices can maintain meltability and extensibility even at reduced saturated fat levels, highlighting the interplay between lipid crystallisation and the surrounding biopolymer network(Sanders et al., 2024a). On the other hand, lipid crystallisation and solid fat content (SFC) play an important role in balancing melt behaviour and oil retention. Higher SFC promotes the formation of a dense, fine crystal network with increased surface area, enhancing oil binding and retention, but also increasing hardness and limiting melt. In contrast, lower SFC results in greater fluidity and improved meltability, but with a higher risk of oil leakage due to insufficient structural support. Crystal size and distribution are also critical, with smaller, well-dispersed crystals improving oil retention, whereas larger or poorly connected crystals promote fat pooling during heating (Dobson & Marangoni, 2024; Masiá et al., 2022; Michel et al., 2022; Sanders et al., 2024a). Overall, optimal functionality requires a balance between sufficient crystallinity to retain oil and adequate lipid mobility to enable matrix yielding and flow, governed by both fat composition and its interactions with the surrounding starch–protein network.

Further studies demonstrated that protein functionality in these systems depends on their role as fillers rather than network formers. For example, evaluations of various legume proteins in plant-based cheeses under the same conditions showed that higher cheese hardness was correlated with greater meltability, stretchability and oil loss, with tan δ positively associated with meltability in kinetic tests. Structural analyses (FTIR spectromicroscopy and synchrotron computed tomography) confirmed that the proteins acted as passive fillers in the waxy starch matrix. High-purity (>70%)

proteins with low solubility (<30% at pH 5.5) resulted in the best melting performance, supporting the concept that starch governs thermal behaviour while proteins provide mechanical reinforcement (Dobson & Marangoni, 2025a).

These findings were confirmed by Hanley et al. (2025), who reported that waxy maize starch–based networks containing embedded, low-solubility protein particles (<3.7% solubility at pH 5.0) show promise in developing plant-based mozzarella analogues with desirable functionality. The authors found that differences in the performance of cheese analogues were primarily driven by protein type and physical characteristics rather than protein secondary structure. Hydrophobicity and structural conformation govern interactions with water, starch and fat. Protein isolates strongly influence cheese microstructure by regulating oil droplet size and starch network strength, which in turn control melting behaviour. Proteins that promote the formation of a high density of small and well-stabilised oil droplets strongly retain oil within the starch matrix, limiting matrix yielding, reducing meltability and minimising oil loss. However, proteins forming larger particles or weakly stabilised oil droplets disrupt starch network continuity, facilitating fat pooling during heating and enhancing meltability but often increasing oil loss. Proteins with high water-holding capacity, good emulsifying ability and resistance to aggregation allow the starch network to soften and yield upon heating while maintaining connectivity, resulting in improved meltability and stretchability. Conversely, reducing particle size, such as through ball-milling, can increase protein-protein interactions, leading to a harder sample with significantly reduced melt. Therefore, excessive starch–protein/protein–protein interactions produce excessively rigid networks that entrap oil and restrict structural rearrangement, suppressing meltability and extensibility.

Gums, such as alginate, carrageenan and guar gum, are often added to plant-based cheeses formulations to control water retention, texture, fat stabilisation and meltability, compensating for the limitations of plant proteins and starch in mimicking the functionality of dairy cheese (Ferawati et al., 2021; Grossmann & McClements, 2021; Monga et al., 2022; Sözeri Atik & Huppertz, 2025). For example, a formulation composed of pea protein isolate, κ-carrageenan and glutinous rice starch has been shown to form two distinct but coexisting gel networks at different thermal and temporal stages (Yiu et al., 2026). This behaviour results from heating across the temperature gap between the helix-to-coil transition of κ-carrageenan and the gelatinisation of starch, enabling controlled network formation. The resulting microstructure, consisting of an interpenetrating polysaccharide–protein matrix with stabilised fat droplets, led to improved meltability, tailored textural properties and excellent freeze–thaw stability, suggesting that the prepared formulation can be used to develop plant-based cheeses. Another study investigated the effects of Sanxan gum on hemp protein–based plant cheese (L. Zhang et al., 2025). Increasing Sanxan gum content enhanced hardness, springiness and chewiness while decreasing adhesiveness. It also improved water- and oil-holding capacities, reduced oil separation and increased storage stability and shelf life. At a Sanxan gum content of 0.9 g/100 g, the prepared cheese exhibited textural properties closely similar to those of commercial mozzarella, with a fine structure, good formability and excellent slicing performance. Microscopy revealed that Sanxan gum created a more compact microstructure and led to uniform fat distribution.

Overall, these results emphasise that plant-based cheeses function as multiphase composites, where meltability and structural stability are governed by the coupled interactions between starch, lipids, and proteins across multiple length scales.

2.3.1.4. Calcium addition

In milk, casein forms micelles stabilised by colloidal calcium phosphate, which bridges casein molecules and enables the formation of a porous, elastic gel network (Lucey et al., 2003). Similarly, the addition of calcium salts to plant-based cheese can modulate textural and functional properties. Studies have shown that the hardness, adhesiveness, springiness and cohesiveness can be fine-tuned by adding different calcium salts, such as calcium chloride and calcium citrate (Grasso et al., 2024), with fortification enhancing stretchability but reduce meltability, as calcium ions promote stronger interactions between proteins and starch (Grasso et al., 2024; Salgado et al., 2023). However, the behaviour of calcium in plant-based cheeses differs substantially from that in casein-based systems. Unlike casein, plant proteins lack phosphoserine clusters and often require unfolding or modification for effective calcium-mediated crosslinking, making these interactions more sensitive to pH, protein concentration and processing conditions. As a result, the optimal calcium levels vary by protein types. For example, soy protein gels can form at 6–9% protein with 10–20 mM calcium, where higher calcium increases gel opacity and aggregate size, and higher protein improves water-holding capacity and elasticity (Maltais et al., 2005). In zein–pea systems, adjusting calcium hydroxide between 3–5% can shift texture from Mozzarella-like elasticity to firmer, Colby-like structures (Salgado et al., 2023). In casein-based processed cheese, citrate and phosphate emulsifying salts sequester calcium, weaken calcium-mediated casein associations and increase protein hydration and dispersion, thereby influencing the balance between structural integrity and meltability (Grasso et al., 2024; Silva et al., 2018). Despite its importance, systematic studies on calcium-mediated structuring in plant-based cheeses remain limited. Understanding calcium speciation, concentration, and interactions with proteins and starch is essential to design

plant-based cheese with optimal stretchability, meltability, and structural stability.

2.3.2. Processing

In addition to formulation design, processing conditions can influence the texture and functionality of plant-based cheeses; however, research in this area is limited. Fermentation is commonly used to convert a liquid protein suspension into a firm curd by decreasing pH, reducing electrostatic repulsion and promoting protein unfolding and aggregation, thereby enhancing the nutritional value, flavour and texture of the product. (Kamath et al., 2022; Li et al., 2013; Masiá et al., 2022). In addition, fermentation can improve rheological properties by increasing G′, emulsion stability, spreadability and firmness, with outcomes depending on plant protein type, starter culture or acidifying agent type and fermentation duration (Palatzidi et al., 2025). For example, Luo et al. (2025) found that fermenting a soymilk–soy protein isolate blend with kefir grains resulted in a firmer, more water-retentive and more thermally stable cheese compared to that obtained through fermentation with yogurt starters, primarily owing to exopolysaccharide production and enhanced protein network formation. Li et al. (2013) combined fermentation with glucono-δ-lactone addition, along with enzymatic hydrolysis, to produce a soy cheese spread with improved stability, reduced brittleness and enhanced sensory acceptability. However, the effect of this treatment on meltability and stretchability remained limited, suggesting that additional strategies are required to replicate dairy cheese–like functionality. Industry players, such as Daiya and Armoured Fresh, focus on fermentation-based approaches to produce plant-based cheeses with enhanced sensory, textural, melting and stretching properties.

The enzyme transglutaminase (TG) has been used to catalyse covalent crosslinking between

protein molecules, thereby increasing cheese yield and improving texture. PM et al. (2024) reported that microbial TG enhanced the hardness, cohesiveness and springiness of cashew-based cheese incorporated with pea protein. Low TG concentrations (0.1%–0.25%) combined with short incubation durations (30 min) were optimal conditions for maintaining meltability, whereas prolonged incubation promoted excessive crosslinking, resulting in an excessively rigid matrix that impaired meltability. Guidi et al. (2022) examined the impact of mixing pea, lentil and hemp proteins on colour, gel strength and water-holding capacity using glucono-δ-lactone, TG and heat treatment. Notably, TG-induced gels showed synergistic interactions, particularly between lentil and pea proteins, resulting in good compatibility with a negligible decrease in gel strength. As discussed above, Dobson and Marangoni (2023) found that a controlled sequence of heating and shear treatment effectively modulated the rheological and textural properties of starch-based cheese analogues.

Overall, a majority of existing studies aimed at improving the functionality of plant-based cheeses have focused on formulation strategies, such as ingredient selection and compositional design, rather than the modification of processing routes or conditions. Although some processing methods (e.g. cold plasma treatment, pH shifting and enzymatic modification) have been used to alter plant protein functionality, these treatments are typically performed at the ingredient level, with the modified proteins subsequently incorporated into cheese formulations. Consequently, these methods do not fundamentally alter processing conditions, and studies investigating true process-driven strategies for developing plant-based cheeses remain lacking.

2.3.3. Summary of recent developments

Recent advances in plant-based cheese formulation have demonstrated that the commonly reported inferior melting and stretching behaviour of these systems can be significantly improved through the rational design of composite matrices (Dobson & Marangoni, 2023). In particular, hydrocolloid-based structuring strategies have shown considerable potential to achieve meltability and stretchability approaching those of dairy cheese analogues. In these systems, starch and other hydrocolloids play a critical role in forming a continuous viscoelastic matrix that can soften and flow upon heating, thereby contributing to meltability. Simultaneously, interactions between hydrocolloids, lipids, and proteins influence water distribution, phase behaviour, and network integrity, which collectively determine the extent of stretchability (Dobson & Marangoni, 2025a; Hanley et al., 2025; Yiu et al., 2026).

Despite these promising developments, important differences remain between plant-based systems and dairy cheese. Variations in composition, such as lower or different protein content, distinct protein structures, and differences in total solids, can influence the formation and stability of the network. In many hydrocolloid-dominant systems, plant proteins often act as dispersed phases or fillers rather than primary structure-forming components. In addition, their contribution to functionality is highly dependent on their physicochemical properties, including solubility, particle size, aggregation state, and degree of denaturation. Moreover, plant proteins from different sources exhibit markedly different behaviours, and their functionality can be further altered by extraction, modification and processing methods. This variability makes it challenging to generalise their role within composite matrices and highlights the need for systematic investigations. Future research should focus on elucidating the structure–function relationships of plant proteins within hydrocolloid-based systems, as well as optimising their interactions with starch and lipids to

achieve more consistent and desirable functional properties. Overall, while recent studies demonstrate significant progress toward achieving dairy-like meltability and stretchability in plant-based cheeses, further work is required to elucidate and predict the complex interplay between composition, processing, and microstructure.

2.4. Future directions

Despite the growing research interest in plant-based cheeses, they substantially differ from traditional dairy cheeses in terms of structure, functionality and sensory properties. These gaps highlight significant opportunities for future research and innovation. Future studies should focus on advancing the mechanistic understanding of structure–function relationships, identifying more suitable ingredients and optimising formulations and processing strategies. In particular, protein-level engineering is required to improve meltability, and advanced technologies are required to achieve closer functional alignment with conventional dairy cheese. In addition, to meet consumer demands, the production of next-generation plant-based cheeses should prioritise clean-label and sustainable formulations while enhancing nutritional value, sensory quality and desired functionality.

2.4.1. Hybrid cheese

Hybrid cheeses combining plant and dairy proteins can improve the functionality of plant-based cheeses while reducing the overall dairy content. The complementary properties of plant proteins and casein result in better melting, stretching and texture than those of fully plant-based systems. In conventional dairy cheeses, they can reduce overall dairy content while improving sustainability and broadening consumer appeal. In addition, hybrid formulations can enhance the nutritional

profile by incorporating plant-based protein and fiber alongside dairy protein. These attributes make hybrid cheeses especially suitable for flexitarian consumers seeking products that combine functionality, taste, nutrition, and environmental benefits (Zhang, Jiang, et al., 2024). Similar to plant-based cheeses, hybrid cheeses can be produced using either wet or dry processing methods. Wet processing involves blending plant protein dispersions or plant milks with bovine milk, followed by enzymatic or acid-induced coagulation using acids, calcium salts, starter cultures or rennet. Conversely, dry processing involves blending plant protein powders with milk powders or natural cheeses, which are subsequently heated, mixed and moulded to form a cohesive matrix that sets upon cooling. Across acid-induced gelation systems, plant proteins and casein usually form separate networks, with plant proteins acting as space-filling gels and casein providing the primary acid-responsive matrix (Mession et al., 2017; Silva et al., 2018). Heat treatment and enzymatic crosslinking can enhance plant protein unfolding and heterologous interactions, improving gel strength and water retention capacity (Beghdadi et al., 2022; Mession et al., 2017; Zhou et al., 2022). The overall gel properties depend on plant protein type, protein ratio, pH and processing conditions. These mechanisms explain the structure–function relationships in hybrid cheeses, wherein the interactions between plant and milk proteins determine microstructure, texture and overall functional properties. A schematic diagram is presented in Figure 4, and recent studies are summarised in **Table 2-2**.

Soy protein has been the most extensively investigated plant protein in the context of hybrid cheese. Partial replacement of milk proteins with soy protein in soft-to-hard cheese varieties has been shown to improve yield, nutritional value and shelf life (Khiabanian et al., 2022; Mazinani et al., 2021; Pratap et al., 2019; Sarker et al., 2026; Ushkalova et al., 2025). Recent studies have extended

this approach to other plant proteins, faba bean protein (Garcia-Fontanals et al., 2023; Rodrigues et al., 2021; Sarker et al., 2026), mung bean protein (Lu, Roy, et al., 2026; Tojan et al., 2024; Ushkalova et al., 2025), chickpea protein(Grasso et al., 2022; Lu et al., 2025; Palatzidi et al., 2025), lentil protein (Moradi et al., 2021) and brewery side-stream flours (containing a combination of protein and fiber) (Palatzidi et al., 2024). Low-to-moderate substitution levels (typically <10%) maintain acceptable texture, microstructure and sensory quality, whereas higher substitution levels often increase firmness or hardness while compromising cohesiveness, elasticity, meltability and stretchability. These effects are commonly associated with plant protein aggregation, phase separation and disruption of the continuous casein network (Mazinani et al., 2020; Omrani Khiabanian et al., 2020; Tojan et al., 2024).

Targeted formulation and processing strategies, such as hydrocolloid addition, pH shifting, enzymatic treatment and fermentation, can mitigate the abovementioned limitations. For example, hydrocolloids can enhance intermolecular bonding and network cohesion (Monga et al., 2022; Moradi et al., 2021), whereas pH shifting and fermentation (Alrosan et al., 2023) improve plant protein solubility, digestibility and compatibility with casein, resulting in hybrid cheeses with improved texture and sensory acceptance.

Recent studies have highlighted that the type of plant protein plays a role in determining the functionality of hybrid cheese. Comparative studies on mung bean, hemp, soy, pea and faba bean proteins have reported that differences in aggregation size, secondary structure and protein–protein interactions strongly influence meltability and stretchability (Lu, Roy, et al., 2026; Sarker et al., 2026; Ushkalova et al., 2025). Larger, rigid aggregates tend to restrict casein network relaxation,

enhancing stretchability but limiting meltability, whereas smaller, more uniformly dispersed aggregates promote network flexibility and meltability while compromising stretchability. These findings highlight that hybrid cheese functionality is governed by a balance between protein interactions and microstructural organization, rather than a single structural state. Advanced spectroscopic and machine learning methods have further revealed that changes in protein secondary structures are also responsible for these functional outcomes (Lu, McGoverin, et al., 2026). Despite growing interest, systematic strategies for investigating protein structure–function relationships in hybrid cheeses remain limited. Overall, hybrid cheeses offer a valuable intermediate strategy to bridge the functionality gap between conventional dairy and fully plant-based cheeses while informing the development of next-generation plant-based cheese alternatives with improved performance and consumer acceptance.

Table 2-2. Overview of recent studies on hybrid cheese, summarising the main ingredients, objectives, formulation and processing, and types of cheese produced (2016-2026)

Plant sources	Cow milk	Objectives	Formulation and processing	Coagulant	Type of products	Reference
Soy milk	Skim milk	To measure the composition and sensory attributes of the enzyme-modified cheese by blending soymilk and cow milk.	Skim milk–soy milk blend (1:1; final protein 4.5 %); starter culture (0.2 DCU/L), $CaCl_2$ (1 mM), rennet (0.18 IMCU/mL) at pH 6.4 to induce simultaneous casein and soy protein aggregation (curd formation). Curd mixed with fat, water, NaCl, and emulsifying salts; heated at 80 °C for 10 min. Proteases (Protease M, Protease P, ProteAX, Neutrase, Flavourzyme), Peptidase R, or lipases (AY, MER, DF) are added. TPC: 27.1–31.7 %.	Calcium chloride	Enzyme-modified cheese	Ali et al. (2017)
Soy milk	Skim milk	To investigate the effect of enzymatically hydrolyzed soymilk on rennet induced gelation of skim milk.	Soy milk (5, 10, 15, 20, 25 %, w/w) blended with skim milk; soy milk unhydrolysed or hydrolysed to a low or high degree using Flavourzyme; rennet (0.1 %).	Rennet	Cheese curd	K. Li et al. (2018)

Soy milk		To develop and characterize probiotic-based soy cheese spread, and to study the rheological behaviour of the same during storage	Soymilk (from soybeans), residue (okara) powder, soybean oil, sucrose; emulsification, culturing, coagulation The one with skim milk to soy milk (50:50 v/v)	Starter culture	Cream cheese	Giri et al. (2018)
Soy milk	Standardized milk	To investigate the physicochemical, antioxidant, and sensory characteristics of khoa prepared from blends of soy milk and standardized milk	Milk and soymilk ratio 100:0, 50:50, 60:40, 70:30 TPC: 17.67-18.66 %		Khoa (India cheese)	Pratap et al. (2019)
Pea protein isolate	Milk protein concentrate	To investigate the effects of partially replacing milk protein with pea protein isolate on the composition, microstructural, rheological properties, and sensory attributes of feta-cheese.	Milk protein concentrate: pea protein blends (12:0, 10:2, 9:3, 8:4, 7:5, 6:6; w/v, dry basis; total protein 12 %), cream powder, homogenized, pasteurized (78 °C, 1 min), cooled to 35 °C, inoculated with mixed starter cultures (1 %), and coagulated with calf rennet (0.005 %).	Starter culture Rennet	feta-cheese	Omrani Khiabanian et al. (2020)
Pea protein isolate	Milk protein concentrate	To investigate the effects of partially replacing milk protein with pea protein isolate on the microstructural and rheological properties of feta-cheese.	Milk protein concentrate: pea protein blends (12:0, 10:2, 9:3, 8:4, 7:5, 6:6; w/v, dry basis; total protein 12 %), cream powder, homogenized, pasteurized (78 °C, 60 s), cooled to 35 °C, inoculated	Starter culture Rennet	feta-cheese (soft)	Mazinani et al. (2020)

			with starter culture (1 %), salted, fermented to pH 5.3, then coagulated with rennet (0.3 g/kg) at 42 °C.			
Soy protein isolate	Milk protein concentrate	To investigate the effects of partially replacing milk protein with soy protein isolate on the microstructural and rheological properties of feta-cheese.	Milk protein concentrate: soy protein blends (12:0, 10:2, 9:3, 8:4, 7:5, 6:6; w/v, dry basis; total protein 12 %), cream powder, homogenized, pasteurized (78 °C, 60 s), cooled to 35 °C, inoculated with starter culture (1%), salted, fermented to pH 5.3, then coagulated with rennet (0.3 g/kg) at 42 °C.	Starter culture Rennet	feta-cheese	Mazinani et al. (2021)
Fava bean Pea Lentil	Milk protein concentrate	To evaluate the effect of partially replacing milk protein with pulse proteins in the production of creamy cheese on texture and physicochemical properties	25 % plant proteins:75 % milk protein concentrate	Lactic acid	requeijão (a Brazilian cream cheese)	Rodrigues et al. (2021)
lentil milk	cow milk	To partially replace cow milk with lentil milk to obtain a feta cheese analogue with desired flavour and texture	0,10,20 % lentil milk with cow milk, 0, 3.5,7 % inulin TPC: 18.23-26.33 %	Acetic acid	Feta cheese	Moradi et al. (2021)

Pea protein	Dairy milk	To create a cottage cheese-like product named pEaneer by combining fresh green peas and dairy milk in different proportions.	Pea protein/milk protein (100:0, 80:20, 60:40, 40:60, 20:80 and 0:100 w/w), MgCl2, gellan gum, pectin (for study their effect on texture of pEaneer) TPC - 42.07-60.34 %	MgCl2	pEaneer (soft)	Monga et al. (2022)
Soy protein isolate	Milk protein concentrate	To develop a whey-less feta cheese by combining milk protein with varying levels of soy protein, and to evaluate its structural and rheological properties	Milk protein concentration: soy protein (12:0, 10:2, 9:3, 8:4, 7:5, 6:6 % w/v)	Starter culture	Feta cheese	Khiabanian et al. (2022)
faba bean flour (FBL)	Milk protein concentrate (MPC)	To develop a hybrid spreadable cheese with dairy protein replaced by insect flour (IF) (T. Molitor) and faba bean flours.	7.1% MPC/FBL/IF (insect flour) - C1 (100/0/0), C2(50/50/0), C3(0/50/50), C4(50/0/50), C5(75/0/25), C6(75/25/0), C7(25/50/25), C8(25/25/50), C9(50/25/25), 49 % water, 42.8 % veg oil, 0.4 % stabiliser, 0.6 % salt, 0.1 % trisodium citrate, pH 4.6-4.8 TPC:4.2-5.18 %	Citric acid	Spreadable cheese analogue	Garcia-Fontanals et al. (2023)
Fermented side-streams (spent yeast and malt rootlets)		To develop hybrid cheese using fermented brewery side-streams and dairy milk and evaluate their biochemical and textural properties.	Spent yeast and malt rootlets were fermented with *Rhizopus oligosporus* on soybean flour (20:80 w/w side-stream:soybean) to produce soy yeast flour and malt rootlets flour (protein	Rennet		Palatzidi et al. (2024)

			37.9% and 31.3%). Flours (3.5–7.5%) were added to pasteurized, partially skimmed milk with or without rennet (15 mL/100 L), mixed to coagulate. The curds were fermented until pH 5.2–5.6, brined (20% NaCl), and stored at 4 °C. A control cheese without flour was also produced.			
Mung bean	Skim milk	To identify the possibility of developing paneer by partially replacing milk with mung bean protein	70 % skim milk:30 % mung bean protein (3.3 %) TPC: 22.27 %	Citric acid	Paneer (cottage cheese)	Tojan et al. (2024)
Mung bean Hemp	Rennet casein	To assess the performance of hybrid cheeses containing mung bean or hemp protein with rennet casein and the influence of microstructure on functionality.	Plant protein: rennet casein (0:10, 2:8, 3:7, 5:5, 7:3, 8:2, 9:1, 10:0); Protein (18 %), coconut oil (20 %), water, sodium chloride, calcium sulphate, potassium sorbate, trisodium citrate, citric acid; controlled heating TPC: 18 %		Processed cheese	Lu, Roy, et al. (2026)

TPC – total protein concentration.

2.4.2. Disruptive technologies

Artificial intelligence (AI) is increasingly recognised as a powerful tool in the food industry, particularly for accelerating formulation optimisation and guiding product design in complex food systems (Pennells et al., 2025). For example, Yakoubi (2024) combined molecular docking with deep-learning algorithms to design novel plant-based cheese formulations, improving texture, nutritional value and flavour through molecular dynamic simulations. Similarly, Yun et al. (2024) used rheological features and machine learning to screen starches with favourable melt–stretch behaviour for application in plant-based cheeses. Industrial efforts, including those by start-ups such as Climax Foods, further highlight the potential of AI-driven approaches to rapidly explore large formulation spaces and identify ingredient combinations that can accurately replicate the functionality and flavour of conventional dairy cheese (Pennells et al., 2025). Furthermore, NotCo developed an AI platform for plant-based product formation using generative models and data. Despite these advances, the application of AI in plant-based cheese research remains limited, particularly in the development of predictive frameworks that link formulation variables to microstructure and, eventually, functional performance.

3D printing is a rapidly advancing additive manufacturing technology that converts digital designs into physical objects through layer-by-layer material deposition. In the food industry, this technology offers unique opportunities to produce personalised products tailored to consumer preferences and nutritional requirements. Extrusion-based printers are most commonly used to process plant-based proteins, and numerous studies have focused on a range of plant-derived materials suitable for 3D printing, including proteins from soy, pea and other legumes, particularly in the development of plant-based meat analogues (Qiu et al., 2023). Companies such as Revo

Foods and SavorEat are well known for their 3D-printed meat analogues, and their technology platforms are increasingly being explored for the production of plant-based cheeses with complex, hierarchical textures through high-precision 3D structuring. Despite this potential, studies on 3D-printed plant-based cheeses remain limited, and significant challenges persist, particularly in achieving the physicochemical properties required for printability while maintaining structural integrity and shape stability after printing. Furthermore, the integration of cellular agriculture with 3D printing represents a promising strategy for the customisation of sustainable dairy-free foods; however, advances are required to address challenges associated with scalability, cost efficiency and public acceptance of lab-grown products (Kanwal et al., 2025).

With the advancement of innovative technologies, precision fermentation and molecular farming have emerged as promising strategies for producing dairy-free components for plant-based cheeses. Precision fermentation aims to produce high-value compounds using genetically engineered microorganisms, such as bacteria and yeast. Balasubramanian et al. (2025) reported that plant-based casein can be produced in *Escherichia coli* through bacterial kinase expression or phosphomimetic substitutions, with proper phosphorylation. This strategy allowed the protein to bind to calcium, form cheese-like structures and retain digestibility. The authors consider this achievement a transformative advance for the alternative protein industry, which can meet both functional and sustainability demands in food production. Various companies (e.g. Change Foods, New Culture, Formo, Remilk and Imagindairy) are attempting to produce real dairy protein analogues with functional properties (e.g. meltability, stretchability and texture) similar to those of traditional dairy cheese (Harvey, 2023). Although precision fermentation can produce bioidentical casein, the protein lacks inherent functionality in its non-micellar state. Achieving the

necessary meltability and stretchability requires the assembly of these proteins into micelle-like structures through biomimetic engineering or colloidal science. In this context, Antuma et al. (2024) reported that the formation of artificial casein micelles is a feasible strategy for developing functional, animal-free cheese alternatives from recombinant milk proteins. Precision fermentation is promising but faces challenges in terms of scaling up and price compatibility.

Molecular farming is an alternative method for producing dairy-like casein for plant-based cheeses, addressing the high cost and scalability limitations of precision fermentation. This approach uses genetically engineered plants or seeds to express complex milk proteins (Turetta et al., 2025). Start-ups such as NewMoo, Finally, Foods, Nobell Foods and Mozza Foods have applied this strategy to different host systems: NewMoo expressed multiple caseins in soy to generate a liquid, cheese-ready base. Finally, Foods used potatoes combined with AI-guided design to produce functional caseins at scale; Nobell Foods engineered soy to produce plant-grown casein for cheese with authentic meltability and stretchability and Mozza Foods produced milk proteins directly within plants, aiming to form casein micelles that simplify downstream processing. Although molecular farming offers advantages in terms of cost, scalability and environmental sustainability, challenges associated with protein purification efficiency, regulatory approval and public acceptance remain to be addressed that may slow commercial adoption (Bobo, 2024).

2.5. Conclusion

Plant-based cheese development has accelerated, driven by intense academic research and growing industrial investment. Although plant-based cheeses have historically been considered inferior to dairy cheese in terms of nutritional quality, sensory attributes, and functional performance,

substantial progress has been achieved in recent years. In particular, advances in formulation and processing have enabled the development of systems that increasingly approximate key functionalities such as melting and stretching.

Across different PCA categories, clear structure–function relationships can be identified. Starch-dominated systems provide structural integrity through gelatinised polysaccharide networks but are often limited by rigidity and restricted melt–stretch behaviour. Protein-dominated systems improve nutritional value but remain constrained by the intrinsic properties of plant proteins, which tend to form less cohesive and less extensible networks. Notably, hydrocolloid-structured systems incorporating proteins, polysaccharides, and lipids have demonstrated significant advances, as their multiphase composite structures allow more effective control of microstructure and functionality. In such systems, hydrocolloid-based matrices can successfully mimic the viscoelastic behaviour of dairy cheese by forming continuous, flexible networks, while proteins and fats act as active or passive fillers to modulate texture and melting behaviour. These developments indicate that desirable meltability and stretchability are increasingly achievable through rational design of phase interactions and network architecture.

These insights highlight that functionality in plant-based cheeses arises from the synergistic interactions between components rather than from individual ingredients alone. Building on this understanding, several research priorities emerge. Future work should focus on combined protein modification strategies to tailor aggregation and gelation under cheese-relevant processing conditions. In parallel, establishing quantitative links between microstructure, macroscopic

properties, and component interactions, supported by advanced analytical techniques and modelling, will be essential for transitioning from empirical formulation to mechanism-driven design. Additionally, improved standardisation of functional testing methods and stronger integration between academic research and industrial application will support more efficient translation of scientific insights into commercial products. Collectively, these advances position plant-based cheeses as a rapidly evolving category with increasing capability to deliver products that closely mimic the functionality and sensory experience of dairy cheese while meeting sustainability and nutrition goals.

MASSEY UNIVERSITY
TE KUNENGA KI PŪREHUROA
UNIVERSITY OF NEW ZEALAND

GRADUATE RESEARCH SCHOOL

STATEMENT OF CONTRIBUTION
DOCTORATE WITH PUBLICATIONS/MANUSCRIPTS

We, the student and the student's main supervisor, certify that all co-authors have consented to their work being included in the thesis and they have accepted the student's contribution as indicated below in the Statement of Originality.

Student name:	Di Lu
Name and title of main supervisor:	Professor Aiqian Ye
In which chapter is the manuscript/published work?	Chapter 3

Describe the contribution that the student and members of the supervisory team have made to the manuscript/published work:[1]

Di Lu: Conceptualization, Data curation, Formal analysis, Investigation, Methodology, Writing—original draft.
Debashree Roy: Supervision, Writing—review & editing.
Alejandra Acevedo-Fani: Supervision, Writing—review & editing.
Harjinder Singh: Supervision, Writing—review & editing.
Ye Aiqian: Conceptualization, Funding acquisition, Project administration, Supervision, Writing—review & editing.

Please select one of the following three options:

- (●) The manuscript/published work is published or in press

  Please provide the full reference of the research output:

  Lu, D., Roy, D., Acevedo-Fani, A., Singh, H., & Ye, A. (2025). Investigation of various plant protein ingredients for processed cheese analogues: physical properties and microstructure compared with milk proteins. International Journal of Food Science and Technology, 60(1). https://doi.org/10.1093/ijfood/vvae018

- ( ) The manuscript is currently under review for publication

  Please provide the name of the journal:

- ( ) It is intended that the manuscript will be published, but it has not yet been submitted to a journal

Student's signature:	Di LU Digitally signed by Di LU DN: cn=Di LU, o=Massey University, email=d.lu@massey.ac.nz Date: 2026.02.02 15:45:33 +13'00'	Main supervisor's signature:	Aiqian Ye Digitally signed by Aiqian Ye DN: cn=Aiqian Ye, o=Massey University, ou=Riddet Institute, email=A.M.YE@massey.ac.nz Reason: I am approving this document Date: 2026.02.27 11:37:01 +13'00'

This form should be placed at the beginning of each relevant thesis chapter.

[1] Refer to the Massey University Publishing and Authorship guidelines (OneMassey for staff, Stream for students) and/ or Contributor Roles Taxonomy (CRediT) guidelines for guidance.

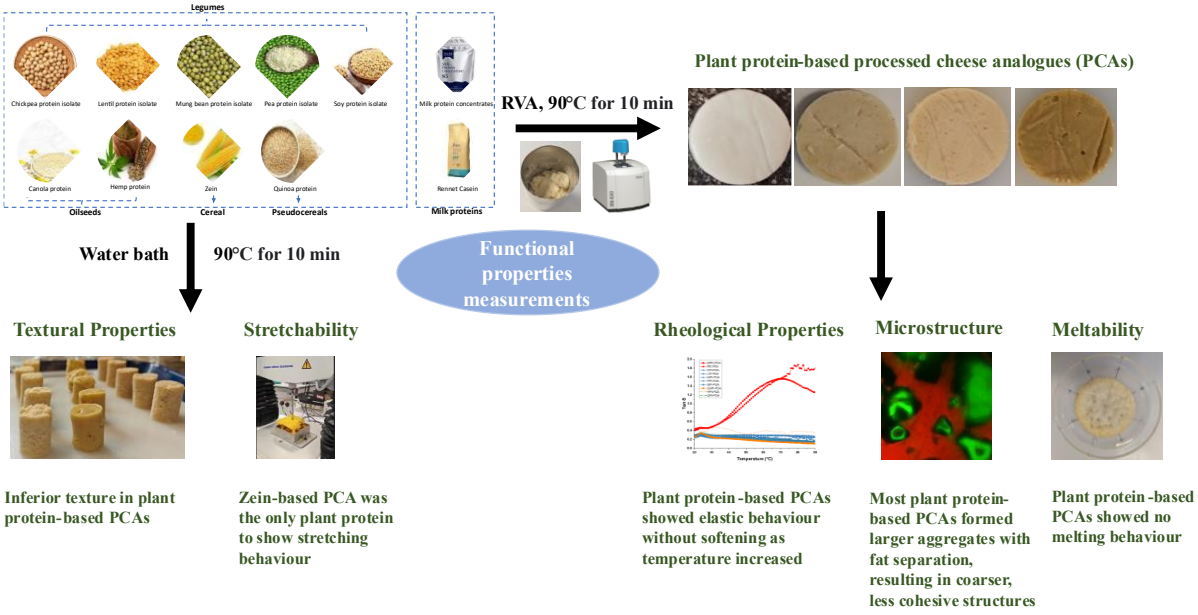
Chapter 3 Investigation of various plant protein ingredients for processed cheese analogues: physical properties and microstructure compared with milk proteins[2]

Abstract

This chapter evaluated various structural and physical properties of several plant proteins in the context of processed cheese analogues (PCAs). A total of 9 plant protein sources were selected to formulate PCA samples. The samples were processed at 90 °C for 10 min using either a rapid visco analyzer or water bath for different tests. Rheological analysis revealed that PCA samples formulated with plant proteins all exhibited solid-like behaviour. PCAs containing legume proteins had a higher storage modulus (G′) than that of rennet casein (RC) cheese samples, while canola protein samples showed the lowest G′ values. Zein-based PCA had the highest hardness and chewiness but softened when subjected to heat during the stretchability test. In contrast, PCAs containing chickpea, mung bean, or pea proteins exhibited similar hardness to RC-based cheeses but had poorer springiness, cohesiveness, and resilience. Plant protein-based PCAs also lacked melting and stretchability properties due to the absence of a continuous protein network. When ranking all proteins in PCAs based on viscosity, rheological, and textural properties, lentil protein scored the highest, followed by hemp and quinoa proteins, performing most similarly to casein protein. The presented comparison of different plant proteins in PCAs provides valuable insights for cheese analogue development.

[2]This chapter has been published as Lu, D., Roy, D., Acevedo-Fani, A., Singh, H., & Ye, A. (2025). Investigation of various plant protein ingredients for processed cheese analogues: physical properties and microstructure compared with milk proteins. *International Journal of Food Science and Technology*, *60*(1).

Graphic Abstract



3.1. Introduction

Cheeses made from animal milk are widely consumed for their exceptional nutritional value. However, the dairy industry faces many challenges, such as the environmental impact of animal farming, animal welfare concerns (Mazac et al., 2023), personal health concerns, and dairy allergies (Espinosa-Marrón et al., 2022; Mazac et al., 2023; Notarnicola et al., 2017; Springmann et al., 2016). Consequently, consumers are increasingly considering plant-based alternatives to replace dairy products, and the global market for plant-based dairy substitutes is projected to continue growing (Fact.MR, 2023).

Plant-based cheese analogues are products prepared from plant ingredients (starch, plant protein, vegetable oil) that are designed to have a similar appearance, texture, and flavour as animal-based cheeses (Grossmann & McClements, 2021). Commercially, many formulations of plant-based cheese rely more heavily on non-protein ingredients, such as starch and coconut oil, to provide structure and functionality to the final product, sacrificing the nutritional value (Grasso et al., 2022; Grasso et al., 2021). For instance, the protein content of conventional cheeses (about 18–25%) is considerably higher than that of plant-based cheeses (0.6–3%) in the market. Indeed, designing plant-based products with a high protein content that matches the texture, composition, and functionality of conventional cheeses presents significant challenges, mainly due to different protein structures and functional properties (Zhang, Jiang, et al., 2024).

Previous studies have investigated the use of plant proteins as the primary structure to develop plant-based cheese, primarily focusing on soy milk for cream cheese types (Ali et al., 2017; Li et al., 2013; Li et al., 2020; Zulkurnain et al., 2008) or pea-based cheeses (Ferawati et al., 2021; Masiá et al., 2022; Mefleh et al., 2022; Michel et al., 2022). Zein has been studied and used in

plant-based cheeses alone or combined with other plant proteins such as pea or chickpea by several research groups due to its melt-stretch and viscoelastic properties, similar to those of Cheddar cheese (Grasso et al., 2023; Grasso et al., 2024; Mattice & Marangoni, 2020a, 2020b; Ozturk et al., 2023; Salgado et al., 2023). Although zein shows promise, its poor solubility, limited nutritional value, flavour issues and processing challenges make it less desirable for plant-based cheese products (Dobson & Marangoni, 2023). Since a high-protein plant-based cheese with optimal physicochemical properties has yet to be developed, gaining a more comprehensive understanding of the impact of various plant proteins on cheese analogues could be significant for guiding food industry applications. Currently, aside from soy protein cheese analogues, studies on the effects of other plant proteins on the rheological properties, texture, microstructure, and melt and stretch properties of plant-based cheese analogues are limited, and comparative studies investigating the influence of different plant proteins on these properties are scarce (Zhang, Jiang, et al., 2024).

In this chapter, several plant proteins were selected, including soybeans, peas, chickpeas, mung beans, lentils proteins (legumes), quinoa (pseudocereals), canola, hempseeds (oilseeds), and zein (cereals), to develop processed cheese analogues. These were then compared to dairy-protein-based cheese analogues containing rennet casein (RC) and milk protein concentrate (MPC) regarding rheological properties, texture, meltability, stretchability, and microstructural characteristics. Rennet casein (RC) and milk protein concentrate (MPC) are commonly used in the processed cheese analogues (Warncke et al., 2021). Although RC is the preferred choice due to its intact casein micelle structure, which provides better textural and functional properties, MPC is widely used in PCA manufacturing for its cost-effectiveness (Khiabanian et al., 2022). This preliminary study attempted to uncover the similarities and differences among various cheese analogues made with plant proteins, while also benchmarking them against milk protein-based

cheeses. To the best of our knowledge, no previous studies have conducted such a comprehensive comparison. We hypothesize that the plant protein microstructure plays a crucial role in determining cheese analogue properties, providing valuable guidance for selecting ingredients in plant-based cheese products.

3.2. Materials and methods

3.2.1. Materials

Rennet casein (RC; SureProteinTM 779) containing 82% protein was obtained from Fonterra Co-operative Group Ltd., New Zealand. Milk protein concentrate (81%; MPC) was obtained from Waiu Dairy Ltd., New Zealand. Soy protein isolate (91%; SPI), pea protein isolate (82%; PPI), and mung bean protein isolate (85%; MPI) were purchased from Bulk Powders New Zealand. Maize zein protein isolate (90%; ZPI) was obtained from Flo Chemical Corp., USA. Lentil protein isolate (88%; LPI) and chickpea protein isolate (83%; CPI) were purchased from Yantai T.full Biotech Co., Ltd., China. Canola protein isolate (CanolaPRO®, 90%; CAPI) was purchased from DSM, New Zealand. Hemp protein isolate (70%; HPI) and coconut oil were purchased from Davis Trading Company, New Zealand. Quinoa protein (80%; QPI) was purchased from Qingdao Chibio Biotech Co., Ltd., China. Potassium sorbate was purchased from PureNature NZ, New Zealand. All chemicals used were of analytical grade and were obtained from Sigma Chemical Co., unless otherwise specified.

3.2.2. Preparation of PCAs slices

The formulation used for the processed cheese analogues was based on Ye et al. (2009) with some modifications. Specifically, the formulation contained 18% protein, 20% coconut oil, 0.5% sodium chloride, 0.5% calcium sulfate, 0.1% potassium sorbate, 2.8% trisodium citrate, 0.7% citric acid,

and 57.4% water on a weight ratio basis. A constant trisodium citrate concentration was applied to all formulations to provide a common processing condition for comparing the different protein ingredients. This concentration was not individually optimised for each protein. Therefore, because the mineral composition and ion-binding behaviour of the commercial ingredients were not determined, an equivalent physicochemical effect of trisodium citrate across all formulations cannot be assumed. To achieve an 18% protein concentration, the protein powder amount was adjusted to accommodate variations in protein content among different sources. The processed cheese slice samples were prepared using a Rapid Visco Analyzer (RVA-4; Newport Scientific Pty Ltd, Warriewood, NSW, Australia), which can mix and heat a 30 g sample in an aluminum with a polycarbonate paddle and was used to make PCAs for measurement of apparent viscosity (Ye et al., 2009). All dry ingredients and oil were manually blended with water for 5 minutes and hydrated for 1 h at room temperature. The mixtures were heated to 90 °C over 4 minutes and held at 90 °C for 10 minutes, then cooled to 50 °C with mixing at a shear speed of 300 rpm from the heating to the cooling stage. The sample was then rolled into a slice with a uniform thickness of approximately 2.2 mm and sealed in a plastic bag. The slices were immediately cooled to 4 °C in a fridge and stored at 4 °C until further analysis. The preliminary trial showed that zein mixtures underwent liquid phase separation, with the liquid splattering out in the RVA. Therefore, the results for zein from RVA were excluded. The pH of all samples was controlled at 5.4 ± 0.5. The schematic illustration of process and appearances of all samples are shown in **Figure S 3-1.**

3.2.3. Dynamic rheological analysis of PCAs

The rheological properties were measured using a stress-controlled rheometer (Physica MCR 302, Anton Paar, Austria) equipped with a 20 mm diameter parallel plate with a 2.0 mm gap. Cheese samples were carefully cut into 20 mm diameter discs using a cylindrical cutter and equilibrated

at room temperature in a plastic bag for 1 hour before the experiment. The cheese discs were glued to the surface of the lower plate. The upper serrated plate (parallel plate) was lowered until it reached a 2 mm gap distance, and the sample was trimmed and left to rest for 15 min in the rheometer. The exposed edge of the samples was coated with a thin layer of mineral oil to minimize moisture loss during the measurement. The linear viscoelastic range was obtained by performing an amplitude sweep at 1 Hz as the percentage of strain values varied from 0.01% to 100%. The linear region was then selected (0.5% of strain amplitude), and a frequency sweep was performed at 20 °C with frequency varying from 0.01 to 10 Hz. This was followed by a temperature sweep, performed at a constant frequency of 1 Hz and a constant strain amplitude of 0.5%. The temperature was increased from 20 to 90 °C at 3 °C/min using a Peltier heating element. The storage modulus (G′), loss modulus (G"), and loss tangent (tan δ) were determined.

3.2.4. Texture profile analysis

Texture profile analysis (TPA) was performed with TAXT.plus (Stable Micro Systems Ltd., Godalming, Surrey, UK). A 50 mm compression cylinder probe (P/50) attached to a 50 kg load cell was utilized for all TPA measurements. Cheese samples were prepared using the formulation described in section 3.2.2 but heated in a water bath at 90 °C for 10 min, producing a larger sample size compared to RVA (which only generated 30 g per sample). The cheese samples were then stored overnight at 4 °C. The following day, the cheese samples were cut into cylinders 20 mm in height and 15 mm in diameter. Two compression–decompression cycles were carried out with a pre-test speed of 1.00 mm/s, test speed of 5.00 mm/s, and post-test speed of 5.00 mm/s, in order to compress the cheese sample to 75% of its initial height. TPA parameters were measured as hardness, fracturability, springiness, chewiness, and resilience. The standard deviation of the results was calculated.

3.2.5. Meltability of PCAs

The meltability of the processed cheeses prepared with RVA was measured using a modified Schreiber melt test (Kosikowski, 1977). Cheese discs of about 5 mm thickness and 30 mm diameter were put on glass Petri dishes and heated in an oven at 170 °C for 10 min. The radii in four directions (0°, 90°, 180°, and 270°) were measured after cooling to 20 °C. The melt index was the average value of the four radius readings. The tests were replicated 4 times.

3.2.6. Stretchability of PCAs

A stretchability test was performed using a TA.HD plus Texture analyzer (Stable Micro Systems Ltd., Godalming, Surrey, UK) with a modified cheese stretchability rig including a post comb/fork and a base pot. Only cheese samples containing MPC, RC, zein, and soy protein were tested for stretchability, as the first three proteins have been reported to exhibit stretchability, and the soy protein sample was included for comparison. These samples were prepared using the formulation described in section 3.2.2, but heated in a water bath at 90 °C for 10 min, allowing for the production of a larger sample size. The samples (150 g) were weighed and evenly distributed in the pot. The base pot and post comb with the cheese sample were heated for 15 min in the oven at 95 °C. To minimize drying during heating, the cheese was covered with an aluminum dish. The comb–sample–pot assembly was placed on the TA, and a thermometer (temperature probe) was inserted into the cheese. Once the temperature reached 60 °C, the test was initiated by pulling the comb out of the melted sample. The test speed and distance were set to 10 mm/s and 220 mm, respectively.

3.2.7. Microstructure of PCAs

Confocal microscopy (CLSM) and scanning electron microscopy (SEM) analyses were conducted at the Manawatu Microscopy and Imaging Centre (Massey University, Palmerston North, New Zealand). For CLSM, fresh cheese samples were cut into thin layers and stained 1% Nile Red (1 mg/ml in acetone, to stain fat), and 1% Fast Green FCF (1 mg/ml in Milli-Q water, to stain protein) for 10 minutes before imaging. Fast Green FCF and Nile Red were excited with He–Ne laser at 633 nm and argon laser at 488 nm, respectively, using a ZEISS LSM 900 microscope (Auty et al., 2001; Gallier et al., 2012). Representative images were captured using a 63× objective lens.

For SEM, all processed cheese samples for SEM were cut into rectangular strips measuring 1 cm × 1 cm × 5 mm—except for quinoa and canola protein samples, as they were soft and could not be fixed and mounted—and were analyzed within 2 weeks of the same day. The cheese strips were fixed by immersing them in a prepared modified Karnovsky's fixative (3% glutaraldehyde and 2% formaldehyde in 0.1 M phosphate buffer at pH 7.2) and washed in phosphate buffer. Next, the samples were dehydrated using a graded series of ethanol washes. Critical point drying was performed using the Polaron E3000 series II critical point drying apparatus (Quorum, Laughton, UK). Samples were mounted onto aluminum stubs using double-sided tape and sputter coated with 100 nm of gold for 110 seconds using a Baltec SCD 050 sputter coater (Balzers, Liechtenstein). The mounted and coated samples were viewed using an FEI Quanta 200 environmental scanning electron microscope (FEI, Hillsboro, Oregon, USA) at an accelerating voltage of 20 kV and different magnifications (Gunn et al., 2022; Li et al., 2013).

3.2.8. Comparison of plant proteins in PCAs using principal component analysis and TOPSIS

3.2.8.1. Principal component analysis

Principal component analysis is one of the simplest yet widely used dimensionality reduction algorithms. It linearly decomposes the data into principal components that explain the variances in the data (Hwang & Yoon, 1981). The data preparation and analysis were done in Google Colab using Python 3.10.12, with packages including Pandas, NumPy, and Scikit-learn (sklearn). All plots were created using the Seaborn and Matplotlib libraries. The original data was stored in an Excel file and loaded into the Colab environment using Pandas. Data collected from the rheological analysis and apparent viscosity results were concatenated horizontally, so each row of data represented a single sample. The processed data was then fed into the sklearn PCA model to calculate the normalized top three principal components.

3.2.8.2. Technique for order of preference by similarity to ideal solution (TOPSIS)

Technique for order of preference by similarity to ideal solution (TOPSIS) is implemented by establishing an ideal solution and calculating the Euclidean distances of each feature between the samples and the ideal solution. The sample closer to the ideal solution is ranked with a higher score (Fan et al., 2023; Hwang & Yoon, 1981). The rheological, apparent viscosity and texture profile analysis results (without zein) were used for comparison. The missing texture results for CAPI and QPI were imputed with zeros, indicating no data was acquired. The distances between samples were then calculated using NumPy, with equal weights assigned to all features.

3.2.9. Statistical analysis

All experiments were performed in triplicate (unless otherwise specified). The results are reported as mean values and standard deviations. The data were subjected to one-way ANOVA analysis using SPSS, followed by Tukey's comparison difference. Differences were considered significant at a level of $p < 0.05$.

3.3. Results and discussion

3.3.1. Formation of PCAs

The changes in viscosity during processing in the RVA indicated the mixture of ingredients and formation of the cheese structure, as shown in **Figure 3-1**. The data collected during the first 90 s of mixing (when the stirring speed was being increased) are meaningless and, thus, were ignored. However, once the maximum stirring speed of 300 rpm had been reached, useful data were obtained. Specifically, as the temperature increased, the apparent viscosity of the mixtures (paste-like) made with plant proteins consistently remained low and stable. Among the legume proteins, chickpea, lentil, mung bean, pea, and soy showed similar viscosities, while canola, hemp, and quinoa proteins consistently exhibited lower viscosities. In contrast, the RVA curves of the MPC and RC mixtures differed from those of the plant protein mixtures. The apparent viscosity increased with rising temperature due to enhanced hydrophobic interaction between casein molecules, resulting in contraction of the protein network (Lamichhane et al., 2018; Lucey et al., 2003), where RC mixtures contained higher casein and showed higher viscosity than MPC mixtures. MPC mixtures displayed a few peaks during temperature increase, which may be due to the presence of whey protein interrupting casein-casein interactions. RC mixtures exhibited a single peak, with viscosity decreasing sharply thereafter, indicating that the protein network begins to soften after reaching 90 °C. Holding the temperature at 90 °C weakens the casein matrix, although hydrophobic interactions increase, the overall effect may be a weakening of the matrix due to a reduction in the contact area between casein molecules. Additionally, electrostatic repulsion increases while hydrogen bonding decreases (Atik & Huppertz, 2023). The results showed a similar trend as the studies by Prow et al.(Prow & Metzger, 2005) and Kapoor et al.(Kapoor & Metzger, 2005). However, the plant protein mixtures tended to have lower viscosity

during mixing and temperature rise, suggesting that they did not undergo significant structural alterations compared to milk protein mixtures (Salunke & Metzger, 2022). Upon cooling to 50 °C, RC and MPC mixtures formed a cheese matrix through the formation of a protein network and had much higher viscosity than plant protein mixtures.

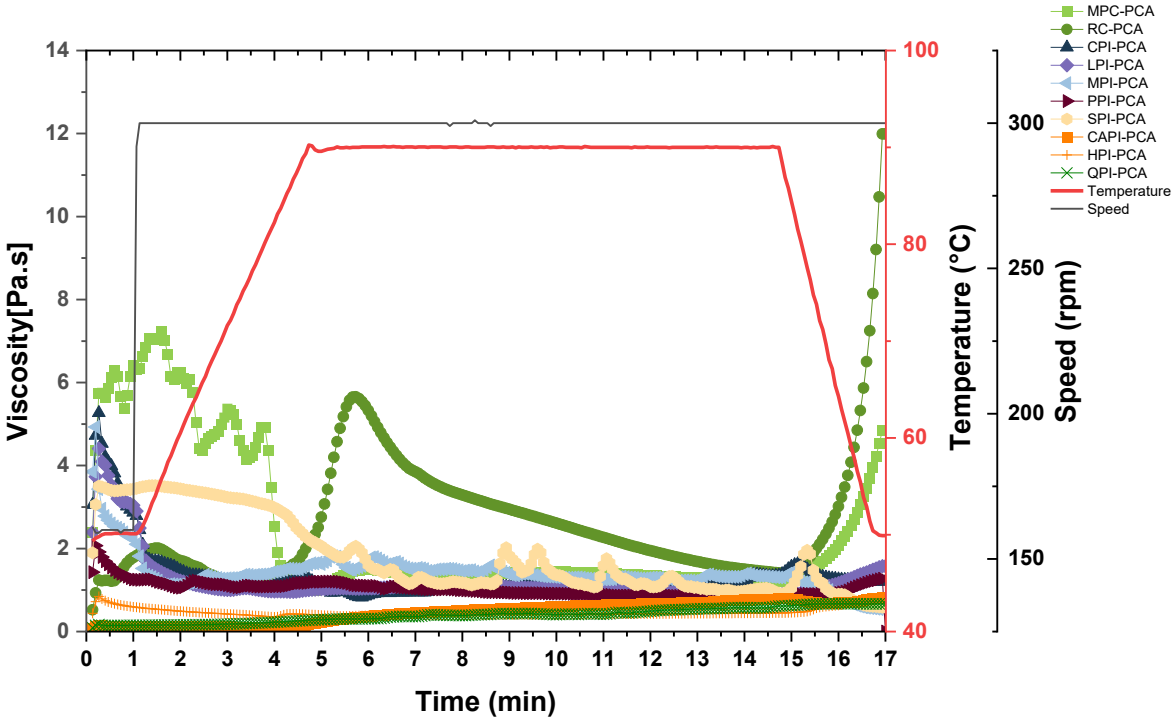


Figure 3-1. Rapid visco analyzer curves for plant and dairy cheese analogues. PCA = processed cheese analogues; MPC = milk protein concentrate; RC = rennet casein; CPI = chickpea protein isolate; LPI = lentil protein isolate; MPI = mung bean protein isolate; PPI = pea protein isolate; SPI = soy protein isolate; CAPI = canola protein isolate; HPI = hemp protein isolate; QPI = quinoa protein isolate.

3.3.2. Rheological properties

3.3.2.1. Frequency sweep test

To better understand the differences in the overall viscoelastic properties of PCAs prepared with different protein sources using the RVA, a frequency sweep test from 0.01 to 10 Hz was conducted within the linear viscoelastic region at a 0.5% strain level. The results are shown in **Figure 3-2**. In general, all tested samples exhibited a solid-like behaviour, as indicated by the storage modulus (G') consistently surpassing the loss modulus (G") across the entire frequency range, in agreement with other studies (Rinaldoni et al., 2014; Salgado et al., 2023). This solid-like behaviour implies that the PCAs possess a certain degree of structural integrity. However, there were differences in the magnitudes of G' and G" between the cheese samples derived from plant proteins and those derived from milk proteins (RC and MPC).

From Figures **Figure 3-2A and B**, PCAs containing pea, chickpea, mung bean, and soy proteins exhibited relatively high values of G' and G", higher than those of cheese samples formulated with MPC and RC. Ben-harb (2018) also reported similar results when they investigated the properties of acid gels made from pure pea, pure milk, and a mixture of pea and milk (1:1) with the aim of creating cheese-like gels with a protein content of 14.8%. Hemp protein, quinoa protein, and lentil protein cheese samples demonstrated similar G' and G" values, which were higher than those of RC and MPC samples under lower frequencies (0.01–1 Hz) and remained similar as the frequency increased from 1 Hz to 10 Hz. On the other hand, the cheese samples incorporating canola protein exhibited the lowest values of G' and G", suggesting that canola-protein-based cheeses had weaker gel-like behaviour than the other samples.

The tan δ value measures the ratio of energy lost to energy stored as a function of frequency in processed cheeses containing different protein sources, offering insights into their viscoelastic nature (**Figure 3-2C**). A low value of tan δ (<1) indicates a more elastic behaviour, while a high value (>1) indicates a viscous-like behaviour (Mazinani et al., 2020). PCAs with plant proteins

exhibited consistent and lower tan δ values across all frequencies, suggesting a predominant elastic nature. Milk-protein-based PCA samples (RC and MPC) showed higher tan δ values, indicating both viscosity and elasticity contributions with complex structure and interactions. The mechanical consistency of plant-protein-based PCAs over various frequencies is also evidenced by their shallower G′ slopes, as provided in

Table 3-1, ranging from 0.10 to 0.13 (compared to 0.26 and 0.27 for MPC and RC, respectively). These shallower slopes in plant-protein-based PCAs indicate a lower frequency dependence, showing that non-covalent bonds including hydrophobic interactions and hydrogen bonds might be controlling the gel network (Zhu et al., 2021), suggesting a more stable and solid-like structure (Beliciu & Moraru, 2013; Grygorczyk et al., 2014; Roesch & Corredig, 2006; Salgado et al., 2023). The consistency in these slope values within plant-protein-based PCA samples further implies similar intermolecular interactions and system stability.

The shear stress values were obtained during amplitude sweeps at T = 20 °C and were plotted against shear strain, as shown in **Figure 3-2D**. These stress–strain curves indicate the brittle behaviour of various networks. In this context, the term "brittle" describes the irreversible damage or breakage of the material upon reaching its maximum stress level (Mattice & Marangoni, 2020b). Among plant proteins, brittleness was observed in legume proteins (i.e., chickpea, mung bean, pea, soy, and lentil), with the peak occurring at a strain of 10%. In contrast, other plant proteins, including canola, hemp, and quinoa, as well as milk proteins, demonstrated more ductile material properties.

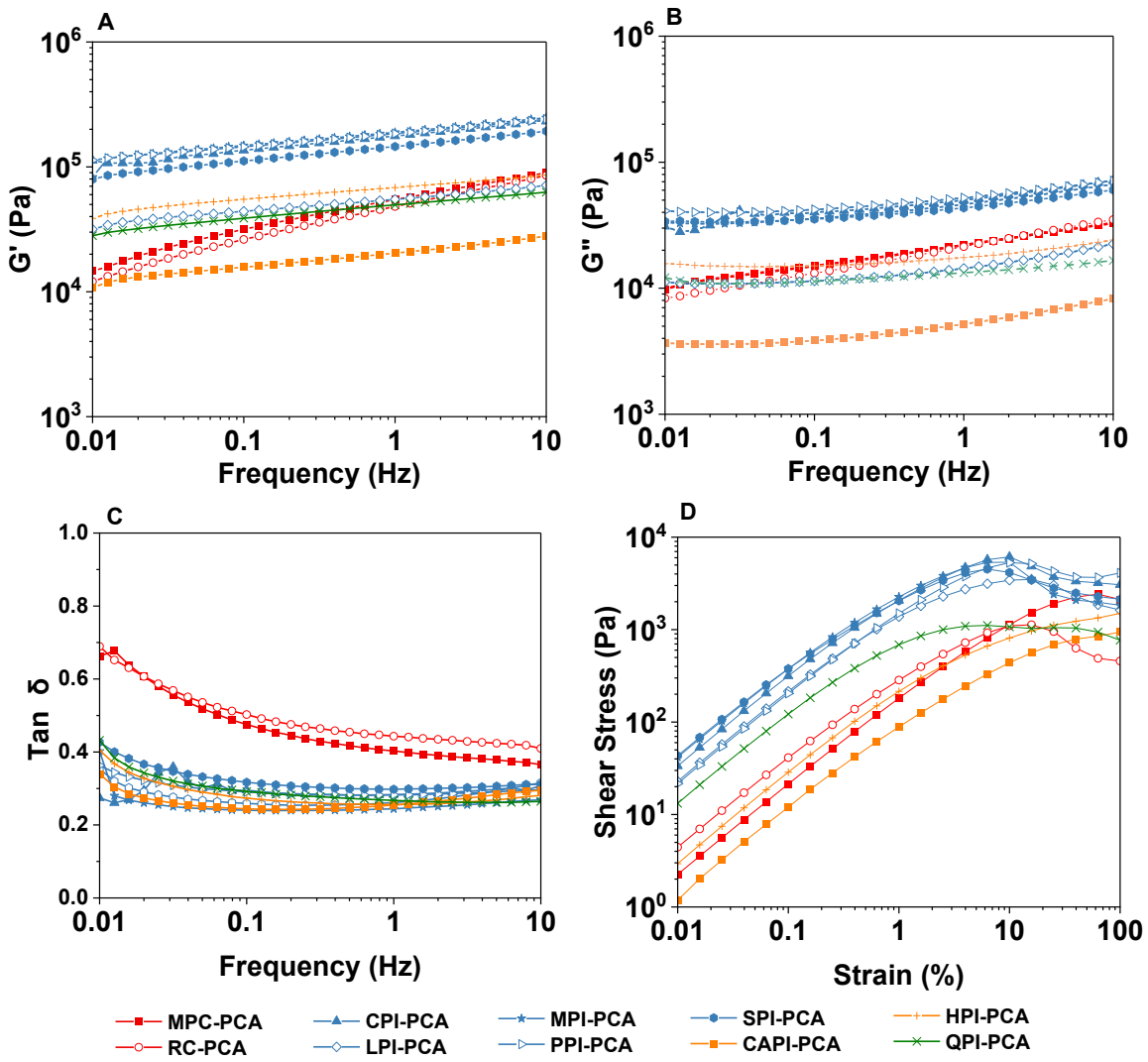


Figure 3-2. Storage modulus (G′) (A), loss modulus (G") (B), and tan δ (C) as a function of the frequency of processed cheese analogues (T = 20 ◦C, γ = 0.5%). Shear stress–strain curve of processed cheese analogues (D). PCA = processed cheese analogue; MPC = milk protein concentrate; RC = rennet casein; CPI = chickpea protein isolate; LPI = lentil protein isolate; MPI = mung bean protein isolate; PPI = pea protein isolate; SPI = soy protein isolate; CAPI = canola protein isolate; HPI = hemp protein isolate; QPI = quinoa protein isolate. Proteins of the same category are labelled with the same colour.

Table 3-1. Slopes from Log(G′)–Log(ω) and log(G")–log(ω) plots (data obtained from frequency sweep samples at 20 °C and γ = 0.5%).

Slope	MPC-PCA	RC-PCA	CPI-PCA	LPI-PCA	MPI-PCA

G′	0.26 ±0.01[a]	0.27 ±0.01[a]	0.12 ±0.01[b]	0.10 ±0.01[b]	0.11 ±0.01[b]
G"	0.17±0.02[a]	0.21±0.01[a]	0.12±0.04[e]	0.10±0.02[bcde]	0.11[ec]

Slope	PPI-PCA	SPI-PCA	CAPI-PCA	HPI-PCA	QPI-PCA
G′	0.11 ±0.01[b]	0.12 ±0.01[b]	0.12 ±0.01[b]	0.10 ±0.01[b]	0.11[b]
G"	0.09±0.01[bcde]	0.09±0.01[bcde]	0.12±-0.01[ec]	0.06±0.01[d]	0.06±0.01[d]

Note. Values with the same superscript letter are not significantly different ($P < 0.05$). G′: storage modulus; G": loss modulus; ω: angular frequency PCA: processed cheese analogue; MPC: milk protein concentrate; RC: rennet casein; CPI: chickpea protein isolate; LPI: lentil protein isolate; MPI: mung bean protein isolate; PPI: pea protein isolate; SPI: soy protein isolate; CAPI: canola protein isolate; HPI: hemp protein isolate; QPI: quinoa protein isolate.

3.3.2.2. Temperature sweep test

The rheological melting profiles for PCAs were conducted from 20 to 90 °C at a constant frequency of 1 Hz and a strain of 0.5% on cheese samples after the frequency sweep. The storage modulus (G'), the loss modulus (G") and Tan δ (G"/G') were measured as a function of temperature, and the results are presented in **Figure 3-3**. Milk-protein-based (RC and MPC) PCAs and plant-protein-based PCAs exhibited vastly different melting profiles. From 20 to 30 °C, all samples showed a significant decrease in G'. This phenomenon can be attributed to the melting of coconut oil, which has a melting point of 24–25 °C (Michel et al., 2022).

For MPC and RC-based PCAs, there was a further decrease in G′ **Figure 3-3A**) and G" (**Figure 3-3B**) but an increase in tan δ (**Figure 3-3C**) as the temperature beyond 30 °C, due to a more rapid decrease in the total number and strength of casein-casein bonds in the cheese matrix and a change

to a more liquid-like character. Further softening was observed when the PCAs containing MPC and RC reached crossover points (tan δ = 1, G' = G") at around 46–50°C, indicating that the cheese had transformed from solid to viscous. The difference in melting point can be attributed to protein composition differences. MPC contains a mix of whey proteins and caseins, with whey proteins cross-linking among themselves and with caseins during heating, weakening the casein network. In contrast, the RC cheese analogue forms a stronger protein network. These findings align with Salunke & Metzger (2022), who reported higher melting points for MCC (micellar casein) than MPC in processed cheese. After reaching a peak at 73 °C and 80 °C for MPC and RC cheeses, respectively, tan δ decreased. This reduction can be attributed to the denaturation of whey protein (70-80 °C), which enhanced protein cross-linking, including the formation of structures between whey protein and caseins (Considine et al., 2007). Additionally there was an increase in hydrophobic-induced casein interaction, which further enhanced elastic behaviour, resulting in the decrease of tan δ values (Atik & Huppertz, 2023; Grasso et al., 2021).

Plant-protein-based PCAs did not exhibit softening and viscous behaviour with increasing temperature beyond 30 °C, indicated by the low tan δ value (between 0.2–0.4). This observation was in agreement with Dobson (2023) who compared the commercial plant-based cheese alternative with commercial dairy cheese. One possible explanation is hydrogen bonds played an important role in milk cheese samples, making them more sensitive to temperature changes, while hydrophobic interactions were more dominant in plant protein gels and exhibited greater resistance to temperature changes (Paula Vilela et al., 2020; Zhu et al., 2021). Hemp protein-based PCAs have a slightly higher tan δ than other plant protein-based PCAs, despite showing no melting properties. This could be due to factors such as protein structure and molecular interactions, which would be interesting to investigate further in the future.

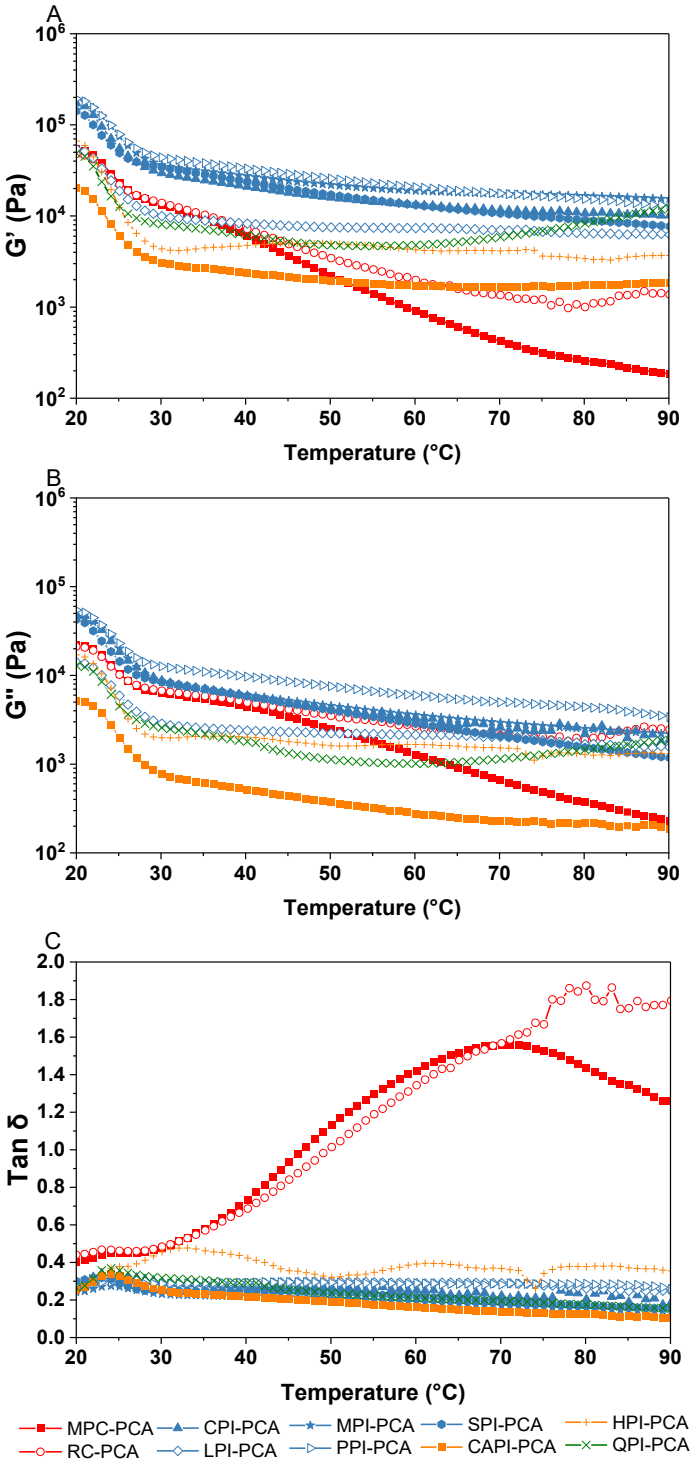


Figure 3-3. Storage modulus (G′) (A), Loss modulus (G") (B), and tan δ (C) as a function of temperature of processed cheese analogues (ω = 1 Hz, γ = 0.5%). PCA: processed cheese analogue; MPC: milk protein concentrate; RC: rennet casein; CPI: chickpea protein isolate; LPI: lentil

protein isolate; MPI: mung bean protein isolate; PPI: pea protein isolate; SPI: soy protein isolate; CAPI: canola protein isolate; HPI: hemp protein isolate; QPI: quinoa protein isolate. Proteins of the same category are labelled with the same colour.

3.3.3. Texture profile

The texture parameters of PCAs are presented in **Figure 3-4**. The cheese samples containing quinoa protein and canola protein were not measured, as they were too soft and had a sandy texture and, thus, could not be cut into a cylindrical shape like the other samples. Cheese samples containing 18% zein showed the highest hardness (35,616 g) and chewiness (5,055 g), with results that were significantly different from those for other samples (**Figure 3-4A**). It has been reported that zein can form a protein network only at temperatures higher than its glass transition temperature (Tg = 28 °C at 20% moisture content) (Salgado et al., 2023). At room temperature, the zein–water network will harden quickly and lose viscoelasticity (X. Zhang et al., 2022), forming a tough and hard texture. It was suggested that the presence of other proteins (e.g., casein, soy, or pea proteins) or hydrocolloids, or the addition of alkaline agents (calcium hydroxide) could improve the structural functionality of the zein network. This can result in the formation of a viscoelastic network that provides cohesion and imparts a softer texture, as opposed to using zein alone or simply adding it to an ingredient-based mix (Ozturk et al., 2023; Salgado et al., 2023).

Apart from zein-based PCA, cheeses containing milk proteins, chickpea, mung bean, and pea proteins exhibited similar hardness, while lentil and soybean proteins showed lower hardness. The hemp protein PCA had the lowest hardness. Springiness indicates how well a cheese sample springs back after it has been deformed during the first compression. PCAs containing MPC, RC, mung bean, soy, pea, zein, and hemp proteins had higher springiness than chickpea and lentil samples. Zein-based PCA had the highest chewiness due to its highest hardness, which was not

desirable for cheese products. MPC and RC cheese samples exhibited moderate chewiness, higher than plant protein-based PCAs. Cheeses containing pea, soy and hemp proteins also had moderate chewiness, with no significant differences from milk-protein-based PCAs. Resilience shows how well a product resists to regain its original height. It was found that PCA samples containing MPC or RC had higher resilience. Not all samples showed a clear fracture: only PCA samples containing soy protein and pea protein showed fracturability, with the pea protein sample showing higher fracturability (Data not shown).

The moderate hardness (821–826 g) and chewiness (296–370 g), and good springiness and resilience of milk-protein-based (RC and MPC) PCAs were possibly due to the formation of a highly uniform and compact protein network (observed in microstructure), which is in agreement with other studies (Mazinani et al., 2021; Salunke & Metzger, 2022). PCAs containing plant proteins showed similar hardness but poor chewiness, springiness and resilience to milk-based PCAs. This may be due to the formation of large protein aggregates at pH near the isoelectric point or at high ionic strength, making them less resistant to rupture, and less capable of holding water (Andoyo et al., 2018; Rinaldoni et al., 2014; Yang, 2017). As observed, legume proteins provide higher hardness, closer to casein cheeses, while hemp protein offers greater resilience, chewiness and springiness. The combination of different plant proteins may yield a better texture profile.

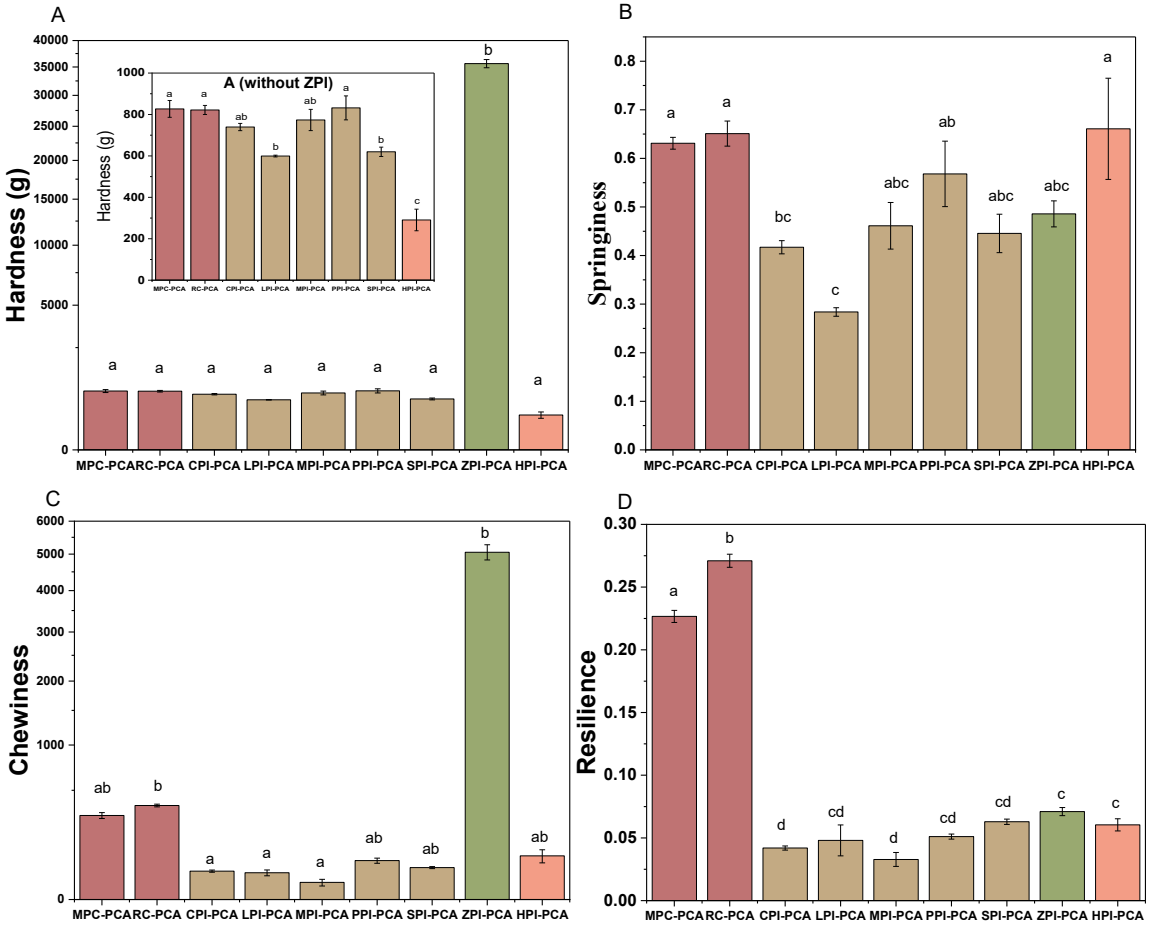


Figure 3-4. Texture profile of processed cheese analogues containing different proteins: (A) hardness (with and without zein protein isolate), (B) springiness, (C) chewiness, and (D) resilience. No textural properties for canola and quinoa protein-based cheese samples were obtained due to softness. Values with the same letter are not significantly different ($p < .05$). PCA = processed cheese analogue; MPC = milk protein concentrate; RC = rennet casein; CPI = chickpea protein isolate; LPI = lentil protein isolate; MPI = mung bean protein isolate; PPI = pea protein isolate; SPI = soy protein isolate; ZPI = zein protein isolate; HPI = hemp protein isolate. Proteins of the same category are labelled with the same colour.

3.3.4. Meltability

Meltability is a critical functional characteristic for processed cheese products, defined as the ability of cheese to flow and spread upon heating, accompanied by a visual loss of integrity of

individual cheese shreds (Guinee, 2011). It is primarily influenced by the number and strength of casein–casein interactions (Park et al., 1984). Table 2 presents the melting properties of all the samples. Only the samples containing milk proteins (i.e., MPC or RC) demonstrated meltability, with melt areas of 34.2% and 84.3%, respectively. Furthermore, the RC sample exhibited the greatest extent of diameter expansion, compared to MPC. These results align with those reported by Salunke (2022), who indicated that increasing whey protein content in processed cheese led to textural defects and decreased meltability in cheese products. This is because whey protein can cross-link among themselves as well as with caseins at high temperatures, weakening the casein–casein interactions. The presence of intact casein micelles in RC results in extensive protein–protein and protein–fat globule interactions, forming a fibrous casein network. None of the plant protein samples exhibited any melting behaviour (**Figure S 3-2**), consistent with the observations made by Grasso et al. (2021). The authors noted that cheddar cheese exhibited superior meltability, while plant-based products displayed poor meltability due to the lack of a continuous protein network. Although cheese meltability is affected by several factors, including the protein network, moisture-to-protein ratio, moisture-in-non-fat solids, starch content, and the addition of emulsifying salts in the formulation, among these, the protein network has a greater impact than others (Grasso et al., 2021; Zhang, Jiang, et al., 2024).

3.3.5. Stretchability

Stretchability is an important quality attribute of melted cheese. A stretchability test was conducted on the milk-protein-based PCA samples with melting properties ($\tan \delta > 1$) and zein-based samples (based on Mattice & Marangoni (2020b)). Furthermore, soy protein (without melting properties) was added for comparison. PCAs were prepared using the method described in Section 3.2.6. The stretchability results, including the maximum pull force, total work done (the area from the initial

pull to the stable point), and stable stretch distance, were used as parameters to compare the stretching of the samples (**Table 3-2** and **Figure 3-5**). Due to the limited sensitivity of the texture analyzer, it was unable to detect the stretch breaking point of the samples. In this context, the relatively stable point (gradient ~ 0) was employed as an indicative measure of the stretch distance. In cheese, stretchability refers to the ability of the casein network to maintain its integrity without breaking when it is pulled. This depends on intact casein to maintain the strength of the strands with enough calcium and phosphorus (Lucey & Fox, 1993; Lucey et al., 2003). It is also affected by how the casein molecules stick together and handle energy (Lucey et al., 2003). The stretch test requires casein molecules to be close, yet flexible enough to quickly change shape (Lucey & Fox, 1993).

Table 3-2. Mean values (n = 3) of the functional properties obtained from the cheese stretchability rig of processed cheese analogues containing MPC, RC, SPI, and ZPI.

	MPC-PCA	RC-PCA	SPI-PCA	ZPI-PCA
Max pull force, g	725.24±149.61[a]	548.74±111.45[a]	244.33±18.78[b]	274.54±46.97[b]
Stable point, mm	65.68±11.44[a]	74.52±5.29[a]	35.95±13.44[b]	57.05±3.02[a]
Total work done, g.mm (0-stable point)	11991.31±5127.51[a b]	14875.56±2192.18[a]	5454.19±2943.53[b]	10243.07±1038.12[a b]

Note. Values with the same superscript letter are not significantly different ($P < 0.05$). PCA: processed cheese analogue; MPC: milk protein concentrate; RC: rennet casein; SPI: soy protein isolate; ZPI: zein protein isolate.

In comparison, PCA containing milk proteins (i.e., RC or MPC) exhibited higher stretchability than plant proteins, characterized by higher maximum pull force, total work done, and stretch distance. MPC showed slightly lower stretch distance and total work done than RC, possibly due to the presence of whey proteins interacting with casein, which may disrupt the casein-casein

network. This result aligns with Salunke's study (2022), where cheese samples containing micellar casein (MCC) exhibited greater stretch than the MPC sample. The study explained that the strands in MPC cheese samples proved to be fragile, breaking shortly upon fork lifting, whereas the MCC cheese samples displayed longer strands, indicating that the presence of whey proteins negatively influenced the cheese's stretchability.

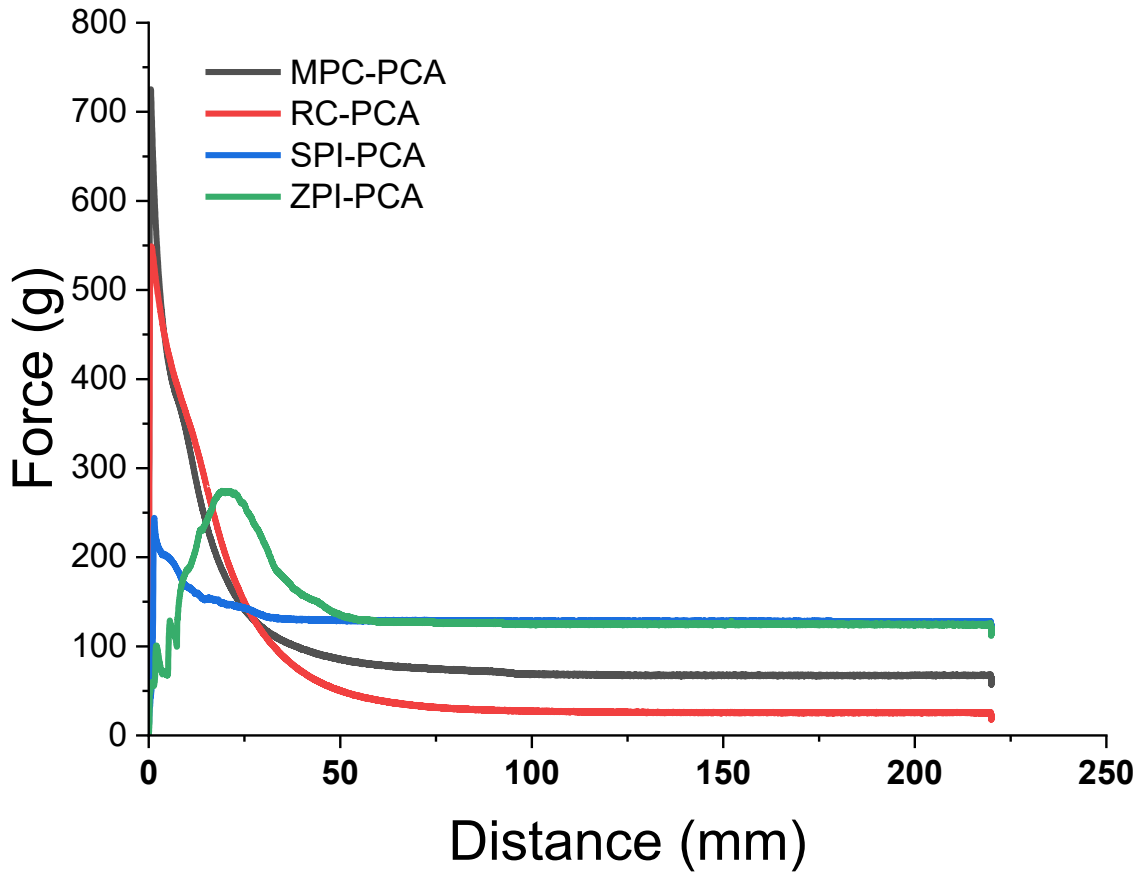


Figure 3-5. Stretchability derived from texture profile analysis of processed cheese analogues (PCA) containing rennet casein (RC), milk protein concentrate (MPC), soy protein isolate (SPI), and zein protein isolate (ZPI).

Previous studies have indicated that cheese made with zein demonstrated stretchiness (Grasso et al., 2023; Mattice & Marangoni, 2020b). This is because the zein networks become softer at higher

temperatures due to weakened non-covalent interactions, resulting in improved stretchiness. Processed cheese analogues containing zein exhibited some level of stretchability, although it was lower than that of cheese samples formulated with milk protein, as evidenced by lower maximum pull force ($P < 0.05$), total work done, and stretch distance. The PCA formulated with soy protein exhibited the lowest maximum pull force, total work done, and shortest stretching distance, which was significantly lower than that of the RC sample. The absence of melting behaviour in soy protein (represent all other plant proteins) limited its ability to stretch. The samples could not form a molten mass, which is necessary for the subsequent stretching process, as evidenced by the accompanying photographs (**Figure S 3-3**). It is reasonable to speculate that other PCAs containing various plant proteins (e.g., pea, chickpea, and mung bean) lacking melting properties would similarly lack stretchability. The comparative analysis of PCAs containing zein, rennet casein, milk protein concentrate, and soy protein highlights the role of melting properties in determining their stretchability.

3.3.6. Microstructure

The CLSM visualized the distribution of coconut oil and different proteins in PCAs (**Figure 3-6A**). A homogeneous casein network and uniform distribution of spherical fat droplets (<20 μm) throughout the casein network were observed in the milk-protein-based PCAs, consistent with the findings of Ye et al. (2009) and Noronha et al. (2008) for imitation cheeses made with rennet casein and commercially processed cheeses by Ramel (2017). However, in most plant-protein-based PCAs, including lentils, mung bean, pea, soy, hemp, and canola proteins, the fat droplets formed non-spherical pools or coalesced, leading to fat and protein phase separation. This suggests

that plant proteins generally have poorer emulsifying properties than milk proteins. In contrast, chickpea-based and quinoa-based PCAs exhibited smaller, spherical fat droplets similar to those in MPC and RC, indicating that different plant proteins have varying emulsifying properties. Interestingly, the microstructure of the cheese sample containing quinoa protein revealed that some fat globules were stabilized by quinoa protein (white arrow in **Figure 3-6A**) (Cui et al., 2023; Lingiardi et al., 2022). Moreover, plant-protein-based cheeses tended to form larger protein aggregates with a non-continuous network, with legume proteins forming larger aggregates than hemp, canola, and quinoa proteins. Among these, canola protein aggregates appeared even more diminutive and denser, similar to those in the milk-protein-based PCAs.

The SEM analysis revealed uniform and smooth microstructures with an open and fibrous protein matrix in cheese samples made with MPC and RC (**Figure 3-6B**). Mounsey and O'Riordan (2001) has reported the similar observation for processed cheese. However, the whey protein present in MPC samples adhered to the surface of the casein, resulting in rough and irregular protein aggregates, leading to a coarser structure (Atia et al., 2004). However, larger protein aggregates and a more irregular microstructure were observed in the plant-protein-based PCAs, with legumes forming large clusters (> 50 μm), while hemp protein formed fragmented structures with large, loosely packed aggregates. Additionally, larger pores and gaps were observed in PCAs containing chickpea, lentil and mung bean proteins, which could be attributed to their being less resilient to deformation.

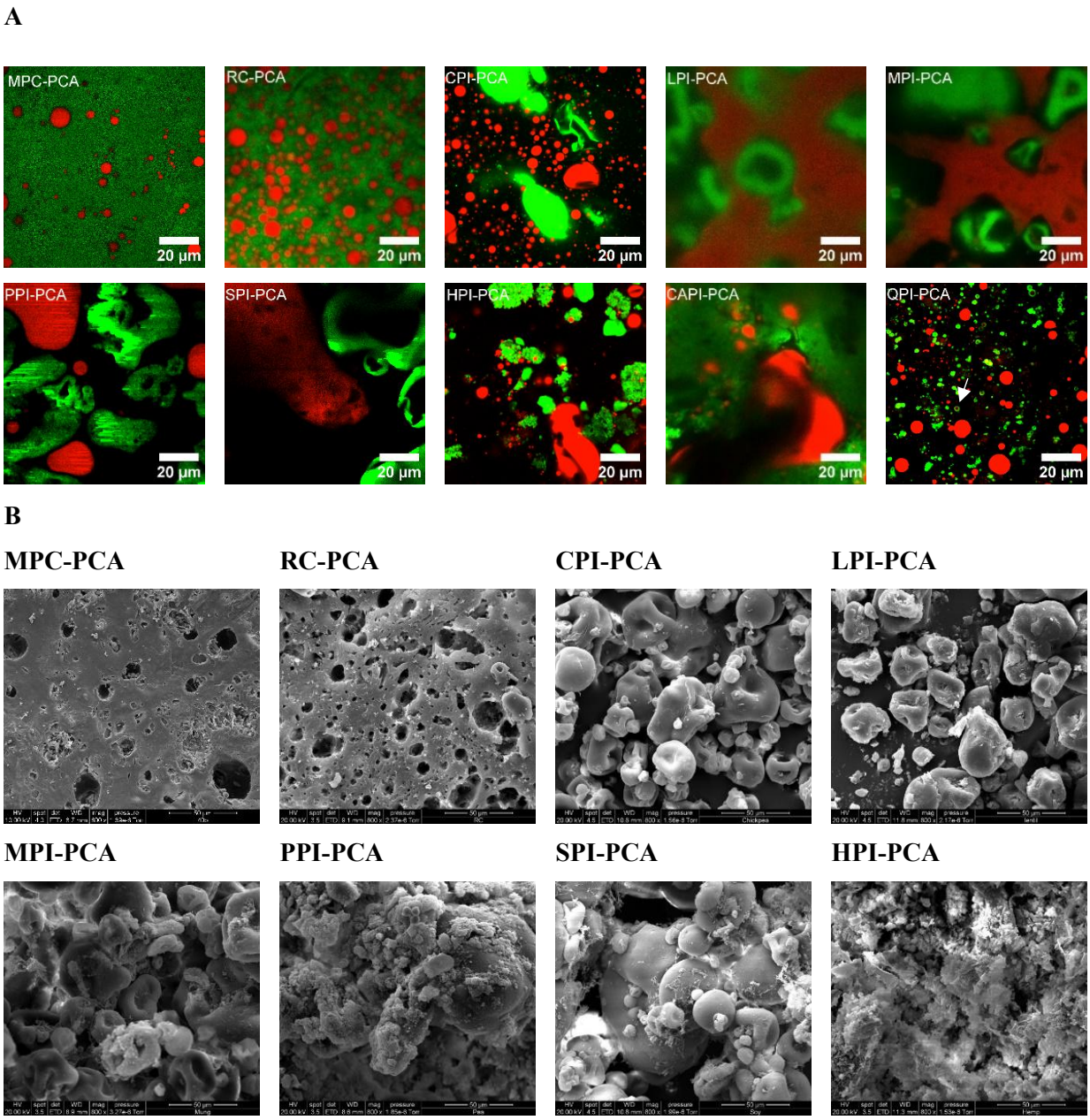


Figure 3-6. Confocal micrographs (CLSM) (A, top) with a scale bar of 20 µm and scanning electron microscope (SEM) (B, bottom) with a scale bar of 50 µm and magnification of 800 of processed cheese analogues containing different protein sources. Fat was stained in red, and protein was stained in green for CLSM analysis. No SEM for canola and quinoa protein-based samples. PCA = processed cheese analogue; MPC = milk protein concentrate; RC = rennet casein; CPI = chickpea protein isolate; LPI = lentil protein isolate; MPI = mung bean protein isolate; PPI

= pea protein isolate; SPI = soy protein isolate; HPI = hemp protein isolate, CAPI = canola protein isolate; QPI = quinoa protein isolate.

In summary, both CLSM and SEM evidenced that the milk-protein-based PCAs showed the most uniform distribution of fat droplets within the protein matrix, resulting in better textural and physical properties. In contrast, most plant-protein-based PCAs exhibited larger protein aggregates with a non-continuous network, and irregular fat droplets were separated from the protein network, resulting in poor emulsifying properties. They did not form as cohesive a network as milk proteins, resulting in a rougher, coarser, and more uneven structure, similar to observations in other studies (Grasso et al., 2021; Li et al., 2013). Larger plant protein aggregates may contribute to relatively higher viscosity during mixing and increased rigidity and stiffness in PCAs, as observed in legume protein-based PCAs. Conversely, smaller aggregates may result in lower viscosity during mixing and softer, sandier textures in PCAs, as seen in canola and quinoa protein-based PCAs.

3.3.7. Comparison of plant proteins in processed cheese analogues using principal component analysis and TOPSIS

The datasets from the apparent viscosity and dynamic rheological measurements were subjected to principal component analysis for data visualization and dimension reduction. As shown in **Figure 3-7**, the scatter plots represent the first two components, with 98.3% of the variance explained by the first component (PC1) and 1% by the second component (PC2). A distinct separation and clustering among proteins were observed. MPC and RC are closely grouped, while CAPI, QPI, LPI, and HPI form another group, and SPI, CPI, PPI, and MPI form a third group. This suggests that proteins within the same group have similar rheological and viscosity properties, but they are significantly different from those in other groups.

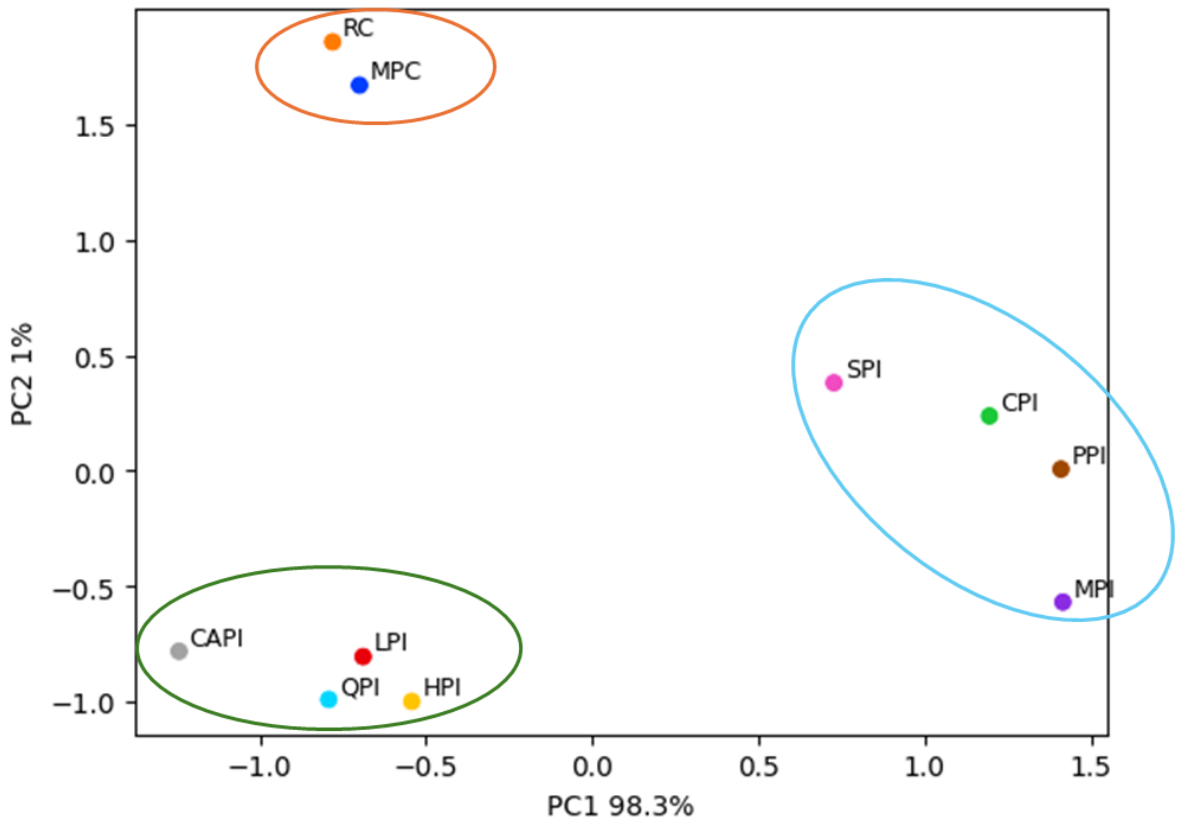


Figure 3-7. Principal component analysis of processed cheese analogues containing different proteins was conducted using apparent viscosity and dynamic rheological results. MPC = milk protein concentrate; RC = rennet casein; CPI = chickpea protein isolate; LPI = lentil protein isolate; MPI = mung bean protein isolate; PPI = pea protein isolate; SPI = soy protein isolate; HPI = hemp protein isolate, CAPI = canola protein isolate; QPI = quinoa protein isolate.

Table 3-3 ranks the processed cheese analogues containing different proteins using TOPSIS, based on the apparent viscosity, dynamic rheological measurements, and textural profile analysis results (excluding zein). RC was set as the ideal solution, receiving a score of 1. As expected, milk protein concentrate (MPC) closely followed, indicating its similarity to the ideal solution. PCAs formulated with LPI, HPI and QPI exhibited moderate performance, with scores ranging from 0.662 to 0.612. Conversely, PCAs containing SPI, CPI, PPI, and MPI scored between 0.565 and 0.546, indicating less optimal performance. However, CAPI cheese demonstrated the lowest score,

indicating the least favorable similarity to the ideal solution. These findings are consistent with the principal component analysis results and provide valuable insights into identifying plant proteins that are most suitable for producing processed cheese analogues with desirable textural and rheological properties to RC.

Table 3-3. The scores of processed cheese analogues containing different proteins were evaluated using apparent viscosity, dynamic rheological measurements, and textural profile analysis results (without zein).

PCAs	RC	MPC	LPI	HPI	QPI	SPI	CPI	PPI	MPI	CAPI
Score	1	0.812	0.662	0.645	0.612	0.565	0.552	0.547	0.546	0.040

Notes. PCAs = processed cheese analogues; RC: rennet casein; MPC: milk protein concentrate; CPI: chickpea protein isolate; LPI: lentil protein isolate; MPI: mung bean protein isolate; PPI: pea protein isolate; SPI: soy protein isolate; HPI: hemp protein isolate, CAPI: canola protein isolate; QPI: quinoa protein isolate.

Consequently, MPI and HPI were selected for further hybrid-cheese studies as contrasting protein systems rather than solely on the basis of their similarity to casein. MPI represented the rigid, large-aggregate behaviour observed among the tested legume proteins, whereas HPI exhibited a softer and more heterogeneous structure with relatively greater springiness and resilience.

Additionally, the differences observed among the PCAs cannot be attributed exclusively to protein source. Although all formulations were standardised to 18% protein and processed under identical conditions, the commercial protein ingredients differed in stated purity and may also have differed in initial solubility, particle size, mineral composition, denaturation history and residual carbohydrate composition. As different quantities of powder were required to achieve the target protein content, the amounts of non-protein components, including possible starch or fibre, also varied and may have influenced protein aggregation, water distribution and rheological behaviour. Furthermore, the constant trisodium citrate concentration controlled the amount added but may not have produced an equivalent ionic environment or functional response in every formulation. These

unmeasured ingredient properties limit the attribution of the observed differences solely to protein source.

3.4. Conclusion

This chapter brought together new information on the differences in the microstructure and physical properties of PCAs formulated with different plant proteins. Plant-protein-based PCAs lacked melting and stretching behaviour, mainly due to the lack of a continuous protein network like casein. Legume protein-based cheeses exhibited similar hardness to RC-based cheeses but displayed inferior springiness, cohesiveness and resilience, likely due to the formation of larger protein aggregates and poor oil-emulsifying ability. In contrast, hemp protein formed aggregates of varying sizes, canola and quinoa proteins tended to create smaller and more uniform aggregates, leading to a softer texture with lower elasticity in cheeses. Based on TOPSIS, lentil protein ranked the highest scores in PCAs compared to other plant proteins, showing performance most similar to milk proteins. PCA containing zein, on the other hand, exhibited distinct characteristics; in particular, they displayed softening properties when heated and had the hardest texture at room temperature. This information provides insight into the differences in physical properties and microstructure between various plant protein ingredients in processed cheese analogues. It guides the selection of plant proteins for developing high-protein plant-based cheeses.

3.5. Acknowledgements

This research work was supported by the Riddet Institute Centre of Research Excellence (CoRE), funded by the New Zealand Tertiary Education Commission. The authors thank the Manawatu Microscopy and Imaging Centre, Massey University, Palmerston North, New Zealand, for supporting the microscopy studies. We would like to thank Yi Zheng for his assistance with data analysis in this chapter.

3.6. Supplementary material

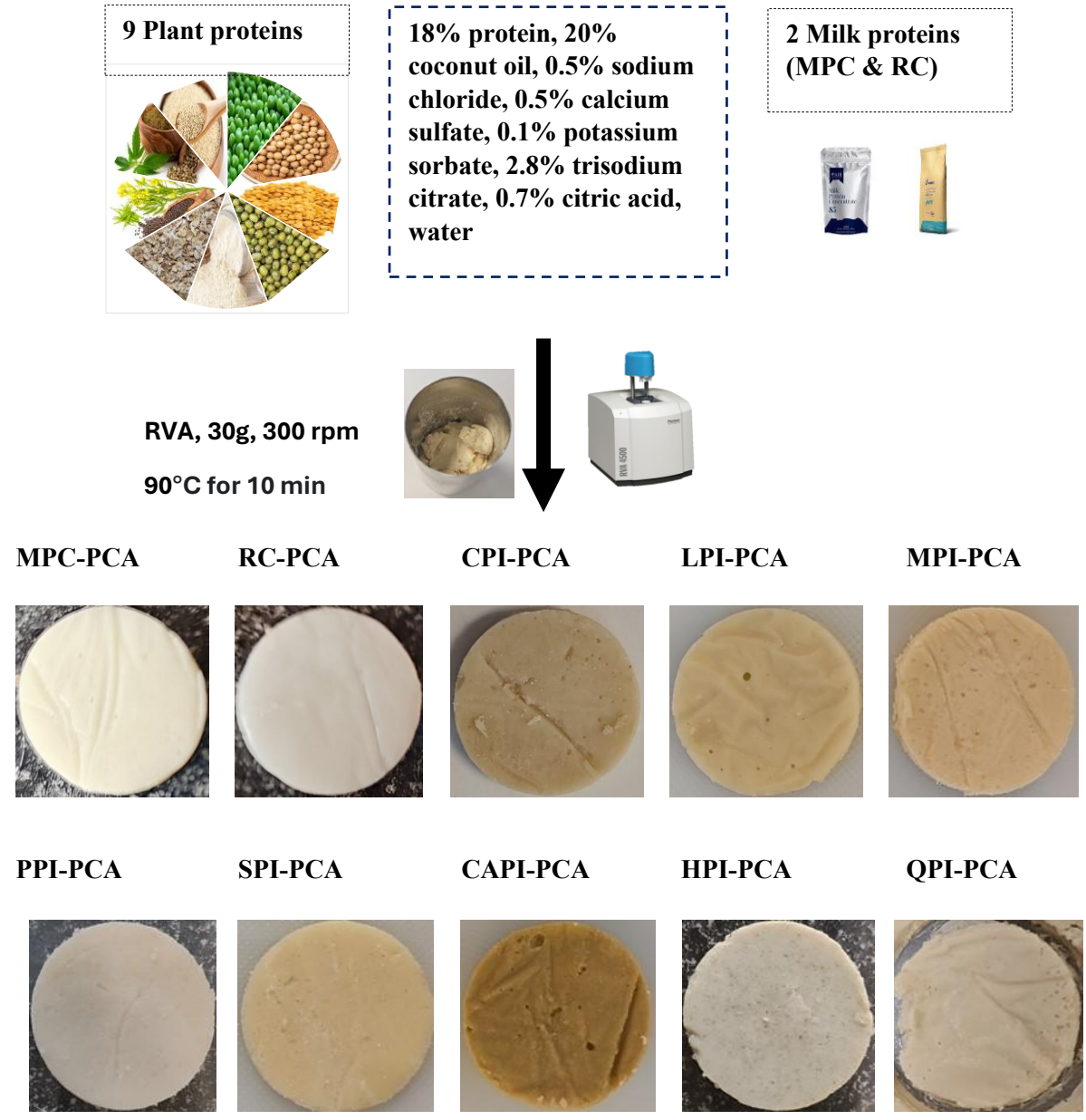


Figure S 3-1. Schematic illustration of the process and visual appearance of processed cheese analogues containing different protein sources. PCA stands for processed cheese analogues. MPC: milk protein concentrate; RC: rennet casein; CPI: chickpea protein isolate; LPI: lentil protein isolate; MPI: mung bean protein isolate; PPI: pea protein isolate; SPI: soy protein isolate; CAPI: canola protein isolate; HPI: hemp protein isolate; QPI: quinoa protein isolate. (Zein-based PCA

was excluded due to failure to prepare in RVA)

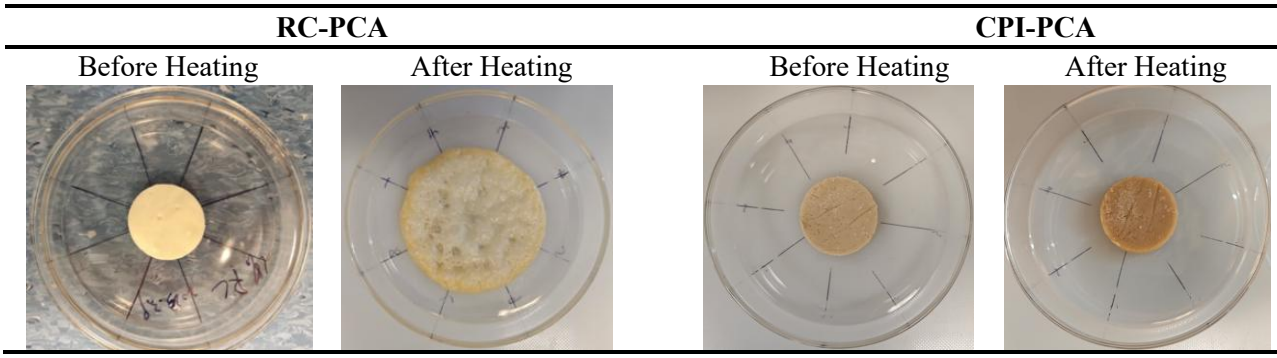


Figure S 3-2. Example photographs of the meltability comparison between RC-based and chickpea-protein-based processed cheese analogues.

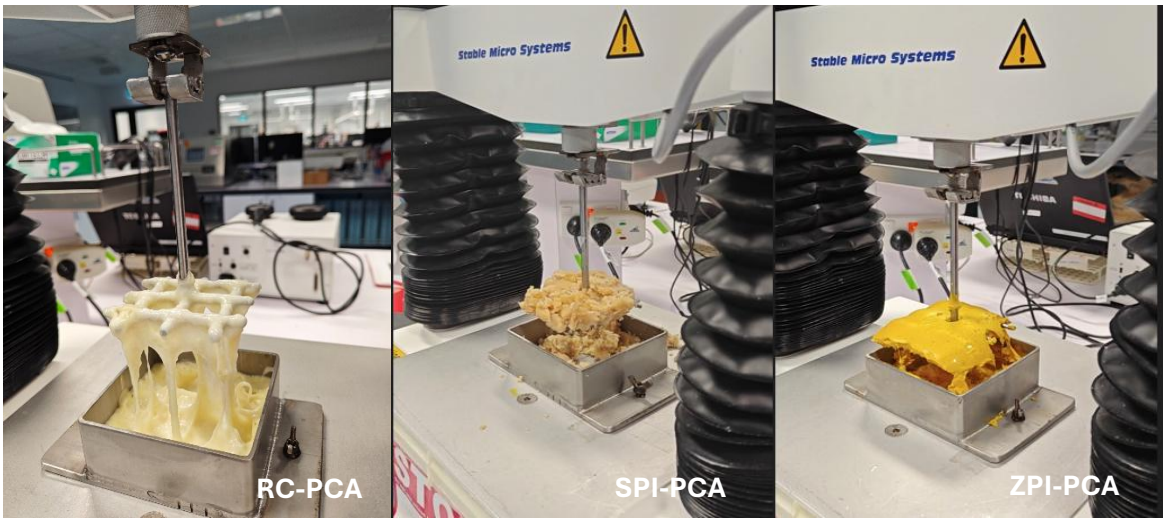


Figure S 3-3. Photographs of melted processed cheese analogues (PCA) containing rennet casein (left), soy protein (middle), zein (right) during the stretchability test.

MASSEY UNIVERSITY TE KUNENGA KI PŪREHUROA UNIVERSITY OF NEW ZEALAND | GRADUATE RESEARCH SCHOOL

STATEMENT OF CONTRIBUTION DOCTORATE WITH PUBLICATIONS/MANUSCRIPTS

We, the student and the student's main supervisor, certify that all co-authors have consented to their work being included in the thesis and they have accepted the student's contribution as indicated below in the Statement of Originality.

Student name:	Di Lu
Name and title of main supervisor:	Aiqian Ye
In which chapter is the manuscript/published work?	Chapter 4

Describe the contribution that the student and members of the supervisory team have made to the manuscript/published work:[1]

Di Lu: Conceptualization, Data curation, Formal analysis, Investigation, Methodology, Writing—original draft.
Debashree Roy: Supervision, Writing—review & editing.
Alejandra Acevedo-Fani: Supervision, Writing—review & editing.
Harjinder Singh: Supervision, Writing—review & editing.
Mark Waterland: Methodology, Writing – review & editing.
Ye Aiqian: Conceptualization, Funding acquisition, Project administration, Supervision, Writing—review & editing.

Please select one of the following three options:

- (●) The manuscript/published work is published or in press

  Please provide the full reference of the research output:

  Lu, D., Roy, D., Acevedo-Fani, A., Singh, H., Waterland, M., & Ye, A. (2026). Physical properties and microstructure of hybrid processed cheeses formulated with plant protein and milk protein ingredients. Food Hydrocolloids, 170, 111688. https://doi.org/https://doi.org/10.1016/j.foodhyd.2025.111688

- ( ) The manuscript is currently under review for publication

  Please provide the name of the journal:

- ( ) It is intended that the manuscript will be published, but it has not yet been submitted to a journal

Student's signature:	Di LU Digitally signed by Di LU DN: cn=Di LU, o=Massey University, email=d.lu@massey.ac.nz Date: 2026.02.04 14:30:02 +13'00'	Main supervisor's signature:	Aiqian Ye Digitally signed by Aiqian Ye DN: cn=Aiqian Ye, o=Massey University, ou=Riddet Institute, email=A.M.YE@massey.ac.nz Reason: I am approving this document Date: 2026.02.27 11:38:48 +13'00'

This form should be placed at the beginning of each relevant thesis chapter.

[1] Refer to the Massey University Publishing and Authorship guidelines (OneMassey for staff, Stream for students) and/ or Contributor Roles Taxonomy (CRediT) guidelines for guidance.

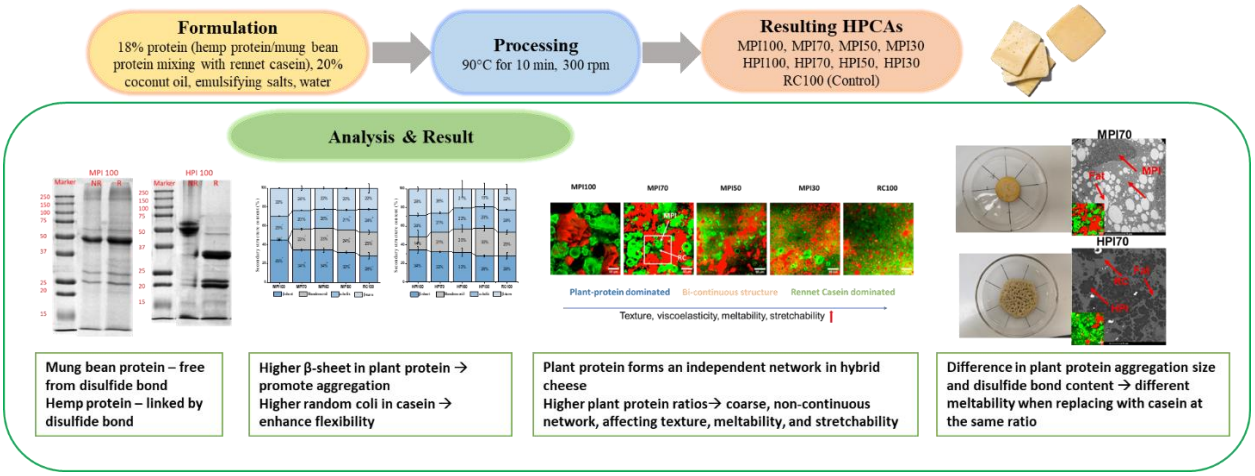
Chapter 4 Physical properties and microstructure of hybrid processed cheeses formulated with plant protein and milk protein ingredients[3]

Abstract

Hybrid processed cheese analogues (HPCAs) containing either mung bean (MPI) or hemp protein (HPI) with rennet casein (RC) at various ratios were prepared and analysed to understand their spatial and microstructural distribution and related physical properties, such as rheological properties, texture profile, meltability, and stretchability. In addition, protein composition and secondary protein structure were studied using SDS–PAGE and FTIR spectroscopy, while CLSM and TEM were employed to visualise the microstructure of the cheese matrix. Results indicated that plant protein types and concentration significantly affected the physical properties and microstructure of HPCAs. The addition of 30 % or more plant protein altered the physical and textural properties as well as the microstructure of the cheese analogues, with a decrease in β-sheet content and an increase in random coil structures. Mung bean protein–based HPCAs exhibit greater stretchability (e.g. 93.8 mm in 30 % MPI vs 41.53 mm in 30 % HPI), rheological, and textural properties, but not meltability (e.g. 1 % in 70 % MPI vs 48 % in 70 % HPI), compared with the hemp protein system at the same mixing ratios. This difference can be attributed to the size of the plant protein aggregation. All data were analysed by one-way ANOVA with Tukey's test ($p < 0.05$). These findings deepen our understanding of plant protein-based and hybrid cheeses, paving the way for optimised plant-based dairy alternatives.

[3]This chapter has been published as Lu, D., Roy, D., Acevedo-Fani, A., Singh, H., & Ye, A. (2026). Physical properties and microstructure of hybrid processed cheeses formulated with plant protein and milk protein ingredients. *Food Hydrocolloid*, Vol. 170 Pages 111688

Graphic Abstract



4.1. Introduction

Processed cheese is a type of cheese manufactured by blending natural cheeses with emulsifying salts and other ingredients to enhance its melting properties, shelf life and flavour (McSweeney et al., 2017). They are extensively used in various culinary applications such as pizza, sauces and grilled cheese sandwiches (Dobson & Marangoni, 2023; Grasso et al., 2021). Recently, plant proteins have garnered considerable attention as consumers seek alternatives to dairy products. However, designing plant-based cheese products that match traditional milk-based cheeses presents substantial challenges (Grossmann & McClements, 2021), particularly in achieving the desired texture, meltability and flavour.

Processed plant-based cheese analogues in the market are made from non-dairy ingredients and primarily produced from polysaccharides (especially starches), vegetable oil (e.g. coconut, coca, and palm oils), minor fractions of plant protein (e.g. legume, nut, and seed proteins), salt (e.g. sodium citrate), texturiser (e.g. xanthan gum, agar, and alginic acid), and acidulant (e.g. acetic acid, citric acid, and lactic acid) (Grossmann & McClements, 2021; Kovačević et al., 2024). Commercially, numerous plant-based cheese formulations considerably rely on non-protein ingredients, such as starch and coconut oil, to provide structure and functionality to the final product, rather than protein, sacrificing the nutritional value (Grasso et al., 2022; Grasso et al., 2021).

Blending plant proteins with dairy proteins offers a potential solution to maintain functional attributes and provide diverse nutritional values. In addition, interest in research on plant proteins and their functional contributions to hybrid cheeses and cheese analogues have significantly increased in recent years (Zhang, Jiang, et al., 2024). Soy and pea proteins are the most commonly

used ingredients for developing plant-milk protein hybrid cheeses analogues (Farahmandfar et al., 2011; Mazinani et al., 2020; Omrani Khiabanian et al., 2020; Rinaldoni et al., 2014). Recently, researchers have also explored the use of other plant proteins, such as faba, chickpea, lentil and mung bean proteins, as alternatives owing to their commercial availability and nutritional and functional properties (Garcia-Fontanals et al., 2023; Moradi et al., 2021; Rodrigues et al., 2021; Seleet et al., 2014; Tojan, 2021; Tojan et al., 2024). For instance, Tojan et al. (2024) reported that replacing 30% of cow milk with mung bean protein isolate in acid–heat-coagulated paneer reduced several textural properties and disrupted the compact casein matrix. In contrast, the present study examines mung bean–casein and hemp–casein processed cheese analogues across multiple blending ratios and relates their microstructural and secondary-structure differences to meltability, stretchability and rheological behaviour. In addition, Rodrigues et al. (2021) concluded that up to 25% of milk proteins in cream cheese can be replaced with pulse proteins without significantly altering the overall composition and characteristics of the final product. A higher proportion of plant protein in hybrid cheese resulted in a weaker structure, poorer texture and a more open network than milk-based cheeses (Mazinani et al., 2020; Mazinani et al., 2021; Moradi et al., 2021). Although these studies highlight the effects of plant protein substitution on the final cheese properties, they do not provide insight into the underlying structural and physicochemical changes occurring within the cheese matrix at the microscopic level.

In this chapter, mung bean protein and hemp protein were selected to mix with rennet casein (RC) at various ratios to development hybrid processed cheese analogues (HPCAS), based on prior trial evaluating various plant proteins in processed cheese analogues (Chapter 3) (Lu et al., 2025). Results demonstrated differences in rheological, microstructural, and textural properties, with hemp protein showing higher scores (closer to rennet casein cheese, which scored 1) than mung

bean protein. A separate pre-trial also confirmed differences in disulphide bond content and particle sizes between mung bean and hemp proteins (Supplementary **Table S 4-1** and **Figure S 4-1**), making it interesting to explore how these differences influence their interactions with caseins in the cheese matrix.

Mung beans contain about 25%-28% protein, and major proteins are globulins, which constitute 60% of total protein (Li et al., 2023). The functional properties of mung bean protein are comparable to soybean protein, indicating similar surface hydrophobicity (Itoh et al., 2006; Mendoza et al., 2001; Tang & Sun, 2010; Yi-Shen et al., 2018). In addition, mung bean proteins are rich in vicilin-type proteins, which lack sulphur-containing amino acids. This affects their functional properties, such as gelation and protein network stability, by limiting disulphide bond formation (S. Shrestha et al., 2023). Hemp seeds contain around 25% protein, comprising about 20%-30% albumin and 60%-80% globulins (edestin) (Chen et al., 2023; Xu et al., 2021). RC is commonly used in processed cheese (Noronha, Duggan, Ziegler, O'Riordan, et al., 2008; Noronha, Duggan, Ziegler, Stapleton, et al., 2008; Ye & Hewitt, 2009a; Ye et al., 2009), which forms a continuous hydrated matrix, stabilising the oil-in-water interface by acting as an emulsifier. Emulsifying salts are added to the mixture to ensure adequate casein hydration and allow casein to emulsify the fat. Replacing RC with plant protein may change texture, rheological, and melting properties (Ørskov et al., 2021). A previous study explored replacing 30% of milk with mung bean protein to develop cottage cheese (Tojan et al., 2024), finding that it reduced texture properties such as hardness and cohesiveness while increasing elasticity. However, it did not investigate the effects of varying substitution ratios on texture, microstructure and key functionality, particularly meltability and stretchability.

This Chapter aimed to understand the spatial and microstructural distribution of mung bean and hemp proteins in hybrid cheese systems to gain insights into their interactions with RC and how microstructure affects cheese functionality. We hypothesize that the structure and functionality of these hybrid cheese systems differ due to the distinct properties and interactions of mung bean and hemp proteins with RC. To achieve this, we compared the protein composition and structure, rheological properties, microstructure, texture, meltability and stretchability between mung bean protein-based and hemp protein-based hybrid cheese systems. This will allow the optimisation of plant protein blends and have implications for modifying plant proteins to enhance their texture and physicochemical properties, tailoring them for specific applications in cheese products.

4.2. Materials and methods

4.2.1. Materials

Rennet casein (RC; SureProteinTM 779) containing 82% protein was applied as milk protein and was obtained from Fonterra Co-operative Group Ltd., New Zealand. Mung bean protein isolate (85%; MPI) were purchased from Bulk Powders New Zealand. Hemp protein isolate (70%; HPI) and virgin coconut oil were purchased from Davis Trading Company, New Zealand. All chemicals used were of analytical grade and were obtained from Sigma Chemical Co., unless otherwise specified.

4.2.2. Preparation of HPCAs

HPCAs were made by mixing mung bean protein or hemp protein with RC at different mass ratios, namely, 100:0, 70:30, 50:50, 30:70, and 0:100, based on the total protein content. Each formulation was adjusted to a total sample mass of 30 g, with a final protein concentration of 18% (w/w) on a wet basis. The formulation used was previously described by Ye et al.'s (2009) study, with some

modifications. Specifically, the formulation contained 18% protein, 20% coconut oil, 0.5% sodium chloride, 0.5% calcium sulphate, 0.1% potassium sorbate, 2.8% trisodium citrate, and water on a weight ratio basis. Subsequently, citric acid was added to control the pH of all samples around 5.4. To achieve an 18% protein concentration, the protein powder amount was adjusted to accommodate variations in protein content among different sources. HPCAs were prepared using a Rapid Visco Analyser (RVA-4; Newport Scientific Pty Ltd, Warriewood, NSW, Australia). HPCAs samples of 30 g were prepared in an aluminium cell fit with a polycarbonate paddle (Lu et al., 2025). All dry ingredients and oil were manually blended with water for 5 min and then hydrated for 1 h at room temperature in an aluminium cell. The mixture was loaded onto the RVA instrument and processed as follows: equilibration at 50 °C, followed by heating to 90 over 4 min, maintaining at 90 °C for 10 min. The sample was then cooled to 50 °C at a rate of 0.2°C /s, mixing at 300 rpm from heating to cooling stages. The HPCAs developed were named as HPI100, HPI70, HPI50, HPI30, MPI100, MPI70, MPI50, MPI30, and RC100. For example, HPI100 contains only hemp protein, while HPI70 contains 70% hemp protein and 30% RC, and so on. All samples with protein, fat, and moisture ratios are shown in **Table 4-1Table 4-1**. All samples were prepared in different sizes for various types of analysis and stored at 4 °C for further use.

Table 4-1. Protein, fat, and moisture contents of processed hybrid cheese analogues.

	MPI100	MPI70	MPI50	MPI30	HPI100	HPI70	HPI50	HPI30	RC100
Protein (%, w/w)	18	18	18	18	18	18	18	18	18
Mung bean	18	12.6	9	5.4	0	0	0	0	0

protein (%)									
Hemp protein (%)	0	0	0	0	18	12.6	9	5.4	0
Rennet casein (%)	0	5.4	9	12.6	0	5.4	9	12.6	18
Fat (%, w/w)	20	20	20	20	20	20	20	20	20
Moisture (%)	42.8^{ad}	42.9^{ad}	42.2^{acd}	43.4^{a}	39.7^{b}	40.7^{bd}	40.7^{bd}	42.6^{ade}	40.3^{bce}

Values within a row not sharing a common superscript differ significantly ($p < 0.05$). The standard deviation of moisture values are less than 0.01. Ratios: MPI/HPI100 (100% plant protein), MPI/HPI70 (70% plant protein, 30% rennet casein), MPI/HPI50 (50% plant protein, 50% rennet casein), MPI/HPI30 (30% plant protein, 70% rennet casein), RC100 (100% rennet casein).

4.2.3. Sodium dodecyl sulphate–polyacrylamide gel electrophoresis (SDS–PAGE)

SDS–PAGE was used to characterise the protein profiles of the HPCAs, under reducing and non-reducing conditions. HPCAs include samples containing plant protein and rennet casein in the following ratios: 100:0, 90:10, 80:20, 70:30, 50:50, 30:70, 20:80, 10:90, and 0:100. Each cheese sample was prepared in a sample buffer (5.55 mg / mL) containing 0.5 M Tris-HCl, pH 6.8, 2% (w/v) SDS, 150 mL/L glycerol, 0.0025% (w/v) bromophenol blue, and 5% (v/v) 2-mercaptoethanol only in the case of reducing conditions. Subsequently, the sample was boiled for 10 min and cooled at room temperature. Each well of the gel with a 16% resolving gel and 4% stacking gel was loaded with 5 μL of the sample containing 0.1% (w/w) of proteins or molecular

weight markers (Catalog # 161–0377, Bio-Rad, USA). A PowerPac Basic (Bio-Rad, USA) was used to conduct electrophoresis at a constant voltage of 150 V in a tris-glycine running buffer (0.025 M Tris, 0.192 M glycine and0.1 % (w/v) SDS). After electrophoresis, the gels were stained with Coomassie Brilliant Blue R-250 staining solution (Bio-Rad, USA) for 3 h, followed by destaining with a 10% isopropanol/glacial acetic acid solution overnight using a shaker (OM6, RATEK, Australia) (Beghdadi et al., 2022; Hu et al., 2023).

4.2.4. Dynamic rheological analysis

Rheological properties were measured using a stress-controlled rheometer (Physica MCR 302, Anton Paar, Austria) equipped with a 20 mm diameter parallel plate with a 2.0 mm gap. HPCAs were removed from the aluminium cell and then rolled into a slice (cheese slice) with a uniform thickness of approximately 2.2 mm. Cheese slices were carefully cut into 20 mm diameter discs using a cylindrical cutter and equilibrated at room temperature in a plastic bag for 1 h before the experiment. The cheese discs were placed on the surface of the lower plate. The upper serrated plate (parallel plate) was lowered until it reached a 2 mm gap distance, and the sample was trimmed and left to rest for 15 min in the rheometer. Meanwhile, the exposed edge of the samples was coated with a thin layer of mineral oil to minimize moisture loss during the measurement. The linear viscoelastic range was obtained by conducting an amplitude sweep at 1 Hz as the percentage of strain values varied from 0.01% to 100%. Subsequently, the linear region was selected (0.5% of strain amplitude), and a frequency sweep was conducted at 20 °C with the frequency varying from 0.01 to 10 Hz. This was followed by a temperature sweep at a constant frequency of 1 Hz and a constant strain amplitude of 0.5%. In addition, the temperature was increased from 20 °C to

90 °C at 3 °C/min using a Peltier heating element. Moreover, the storage modulus (G'), loss modulus (G"), and loss tangent (tan δ) were determined.

4.2.5. Microstructure

Confocal laser scanning microscopy (CLSM) and transmission electron microscopy (TEM) analyses were conducted at the Manawatu Microscopy and Imaging Centre (Massey University, Palmerston North, New Zealand).

4.2.5.1. CLSM

Microstructural analysis of HPCAs prepared using RVA was conducted using a Confocal Laser Scanning Microscope (ZEISS LSM 900, Germany). Fresh cheese samples prepared using RVA were cut into thin layers and stained with a fluorescent dye solution containing 1% Nile Red (1 mg/ml in acetone), which stains the fat phase, and 1% Fast Green FCF (1 mg/ml in Milli-Q water), which stains the protein phase, for 10 min before imaging. Fast Green FCF and Nile Red were excited with He–Ne laser at 633 nm and argon laser at 488 nm, respectively (Auty et al., 2001; Gallier et al., 2012). Representative images are reported, which were captured using a 20× objective lens.

4.2.5.2. TEM

HPCAs were examined using TEM. The samples were first sliced into small cubes (1 mm × 1 mm × 1 mm) and embedded in 3% agarose. According to Li et al. (2021), the samples were placed in 3% glutaraldehyde in 0.1 M sodium cacodylate (pH 7.2) for at least 24 h. Subsequently, the samples were washed in buffer and dehydrated using a graded acetone series. Finally, the samples were embedded in moulds with fresh resin and cured in a 60 °C oven for 48 h. Light microscope

sections (1 mm) were cut using a glass knife on an ultramicrotome (Leica EM UC7, Germany) and heat-fixed onto glass slides. These sections were stained with 0.05% toluidine blue and viewed under a light microscope. Thin sections (around 100 nm) were cut using a diamond knife, stretched with chloroform, and mounted on grids using a Coat-Quick 'G' pen (Daido Sangyo, Japan). Afterwards, the grids were stained and washed and then stained with lead citrate, followed by another wash using Milli-Q water. The samples were imaged with a Tecnai G2 Spirit BioTWIN (FEI Company, Czech Republic) paired with a Veleta TEM camera (Olympus SIS, Germany).

4.2.6. Texture profile analysis (TPA)

TPA was conducted using TAXT .plus (Stable Micro Systems Ltd., Godalming, Surrey, UK). Cheese samples prepared using the RVA (section 3.2.2) were transferred to moulds and stored at 4 °C. Afterward, the cheese samples were cut into cylinders with a height of 20 mm and a diameter of 15 mm for the analysis. A 50 mm compression cylinder probe (P/50) attached to a 50 kg load cell was utilised for all TPA measurements. Two compression-decompression cycles were conducted with a pre-test speed of 1.00 mm/s, test speed of 5.00 mm/s, and post-test speed of 5.00 mm/s to compress the cheese sample to 75% of its initial height. TPA parameters were measured as hardness, springiness, cohesiveness, chewiness, and resilience. The standard deviation of the results was calculated.

4.2.7. Meltability and Stretchability

The meltability of HPCAs prepared with RVA was measured using a modified Schreiber melt test (Kosikowski, 1977). Cheese samples were rolled into slices with a uniform thickness of approximately 5 mm and 30 mm in diameter, placed on glass Petri dishes, and heated in an oven

at 170 °C for 10 min. Radius of expansion in four directions (0°, 90°, 180°, and 270°) was measured after cooling to 20 °C. The melt index was the average value of the four radius readings.

A stretchability test was conducted using a TA-HD plus Texture analyser (Stable Micro Systems Ltd., Godalming, Surrey, UK) with a modified cheese stretchability rig, which included an in-house built post hook and a base pot (Supplementary **Figure S 4-2**). HPCAs were prepared using the formulation discussed in section 4.2.2 but heated in a water bath at 90 °C for 10 min at 300 rpm, allowing for the production of a large sample size. The samples (150 g) were weighed and evenly distributed in the pot. Subsequently, the base pot and post hook with the cheese sample were heated in the oven at 95 °C for 15 min. To minimise drying during heating, the cheese was covered with aluminium foil. Moreover, the hook–sample–pot assembly was placed on TA, and a thermometer (temperature probe) was inserted into the cheese. Once the temperature reached 60 °C, the test was initiated by pulling the hook out of the melted sample. The test speed and distance were set to 10 mm/s and 200 mm, respectively.

4.2.8. Analysing protein structure with Fourier transform infrared (FTIR) spectroscopy

Protein structure changes in HPCAs with different plant protein to rennet casein ratios were evaluated via FTIR spectroscopy(Gawat et al., 2024; Salgado et al., 2023). Cheese samples were cut into thin layers before being placed directly on the crystal and pressed down onto it. The analysis was conducted using a Nicolet™ iS™ 5 FTIR Spectrometer (Thermo Fisher Scientific Inc., Waltham, MA, USA) with an iD7 ATR accessory (Thermo Fisher Scientific Inc., Waltham, MA, USA). The scan was conducted between 4000 and 450 cm−1 with a resolution of 2 cm^{-1}. The background spectrum was initially obtained and automatically subtracted from every acquisition

and was reset after scanning for 1 h. For each sample spectrum, 32 scans were accumulated and averaged.

The deconvolution of the amide I region (1600 and 1700 cm^{-1}) was done for further quantitative analysis. First, each spectrum was processed for baseline correction and smoothed using a 25-point Savitzky-Golay filter with a second-order polynomial to improve the signal-to-noise ratio in Origin® software (2021b). Next, automatic peak fitting was conducted using the second derivative, and subsequent peak fitting was done using the Gaussian assumption implemented in the Peakfit 4.12 software (Systat Software, Inc., CA, USA). The resulting peaks after deconvolution were identified based on known IR spectral data for protein secondary structures. Several iterations were conducted until the fit converged with a final fitting curve that achieved a corrected $R^2 \geq 0.99$. Finally, the area under each peak was evaluated against the total area and expressed as a percentage. Reported values for β-sheet and β-turns are accumulated values of more than one peak.

4.2.9. Statistical analysis

All experiments were performed in triplicate (unless otherwise specified). Results are reported as mean values and standard deviations. To identify differences between HPCAs formulations, the data were subjected to one-way ANOVA analysis using SPSS, followed by Tukey's comparison difference. Differences were considered significant at a level of $p < 0.05$.

4.3. Results and discussion

4.3.1. Protein composition

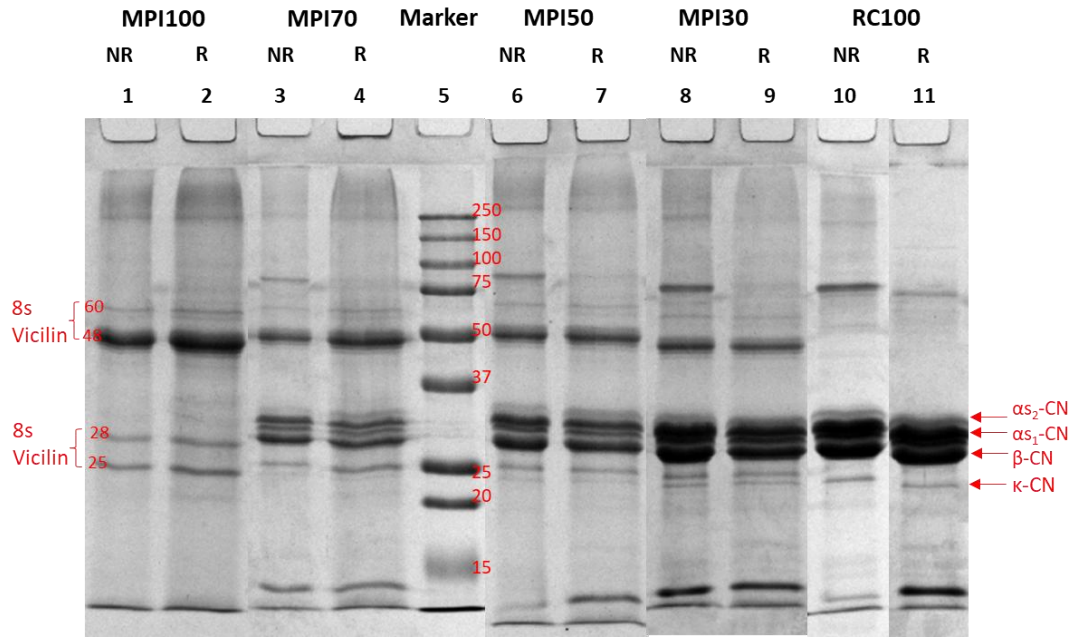
The major protein constituents of HPCAs were identified using SDS–PAGE. The mung bean protein-based cheese sample (MPI100) exhibited SDS–PAGE bands with molecular weights

ranging from 80 to 26 kDa, with no major distinctions between PAGEs under reducing and non-reducing conditions (**Figure 4-1A**). Bands at ~ 60, 48, 28 and 25 kDa, corresponding to sub-units of vicilin-like globulin, remained unchanged under reducing conditions (lane 1 & 2, **Figure 4-1A**). This is consistent with reports indicating that 8S vicilin, which lacks disulphide bonds, contains 89% protein and no sulphur-containing amino acids (Smriti Shrestha et al., 2023; Yi-Shen et al., 2018). However, this study did not observe the 7S (~16 and ~28 kDa) and 11S (~24 and ~40 kDa) subunits, likely owing to differences in mung bean protein variety and isolation methods compared to previous reports. For casein cheese (RC100, lane 10 & 11), α_{s1}- and β-caseins were observed as the two most predominant protein bands in both non-reducing and reducing conditions, while α_{s1}- and κ-caseins presented as two faint bands. For cheese samples made by blending MPI and RC, all proteins from both MPI and RC were observed in both the PAGEs under reducing and non-reducing conditions, indicating no complexation between the caseins and mung bean protein. This is consistent with the study results of Beghdadi et al. (2022), who found that co-heating casein with pea proteins (7.5:2.5) did not result in interaction between the two, because no new complexes were observed in SDS–PAGE. Instead, the pea protein formed its own gel at a low pH, acting as a 'space-filling gel' within the casein gel.

Hemp protein comprises ~20%-30% albumin and 60%-80% edestin (globulin) (Chen et al., 2023; Xu et al., 2021). Edestin is further divided into 7s and 11s protein fractions (**Figure 4-1B**). In non-reducing SDS–PAGE, a band around 54 kDa was attributed to the edestin monomer, which disappeared under reducing conditions owing to the cleavage of disulphide bonds, resulting in three distinct bands at ~34, ~21, and ~18 kDa for the acidic and the basic sub-units (Do et al., 2024). Meanwhile, a band around 48 kDa was associated with the 7s globulin sub-unit, with little effects under reducing conditions. In cheese samples made by mixing HPI with RC, for instance,

under non-reducing conditions, a thick band at 54 kDa was observed in HPI50 (lane 6, **Figure 4-1B**), and both β-casein and α_{s1}-casein were also observed. However, the band intensities of α_{s1}-casein and α_{s2}-casein were weaker than that in reducing PAGE. The observed decrease in α_{s1}-casein and α_{s2}-casein band intensities in non-reducing conditions may indicate potential interactions between α_{s2}-casein and HPI proteins. In addition, the reduction of the α_{s1}-casein and α_{s2}-casein band intensities was not observed in case of MPI-based hybrid cheese samples under non-reducing conditions (**Figure 4-1**) further suggested the potential interactions between αs2-casein and HPI proteins. Given that α_{s2}-casein contains two disulphide bonds, it is hypothesized that disulphide linkages could form between α_{s2}-casein and HPI. However, under reducing conditions, the α_{s2}-casein band became less distinguishable, likely due to overlap with the acidic subunit of HPI. Preliminary results suggest a potential interaction between α_{s1}-casein, α_{s2}-casein, and HPI, the exact nature of these interactions via disulphide bond exchange or non-covalent association requires further investigation.

A



B

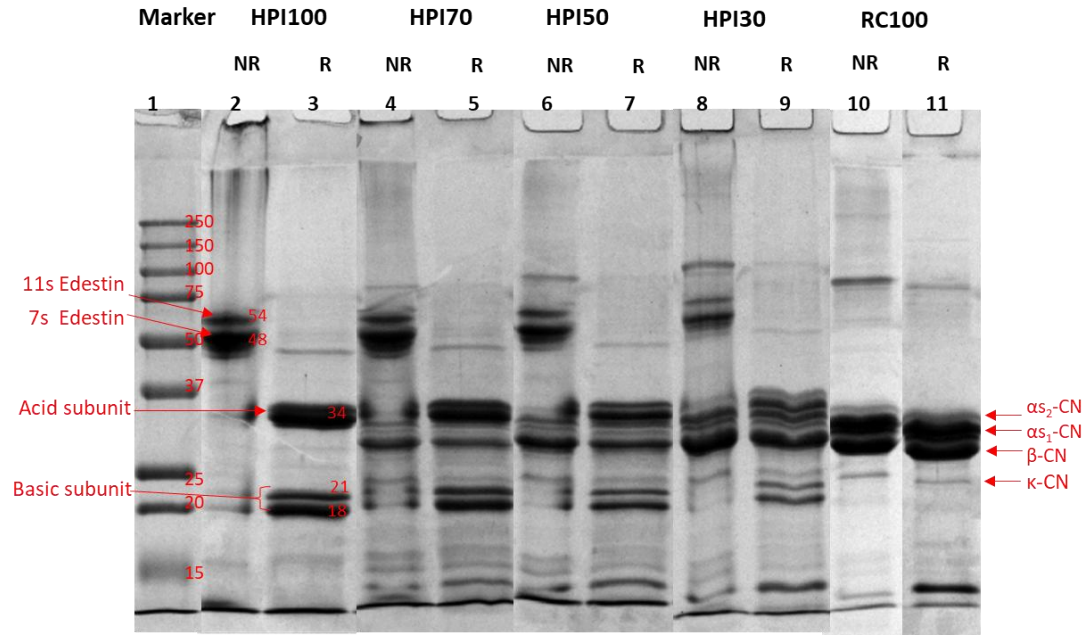


Figure 4-1. SDS-PAGE profile of hybrid processed cheese analogues (HPCAs) made with mung bean protein (MPI) (A) or hemp protein (HPI) (B) and rennet casein (RC) at varying ratios. Ratios: MPI/HPI100 (100% plant protein), MPI/HPI70 (70% plant protein, 30% rennet casein), MPI/HPI50 (50% plant protein, 50 % rennet casein), MPI/HPI30 (30% plant protein, 70% rennet casein), RC100 (100% rennet casein). The samples were prepared under reducing (R) and non-

reducing (NR) conditions. Molecular weight marker in kDa; αs1-CN: αs1-casein; αs2-CN: αs2-casein; β-CN: β-Casein; κ-CN: κ-Casein.

4.3.2. Rheological properties of HPCAs

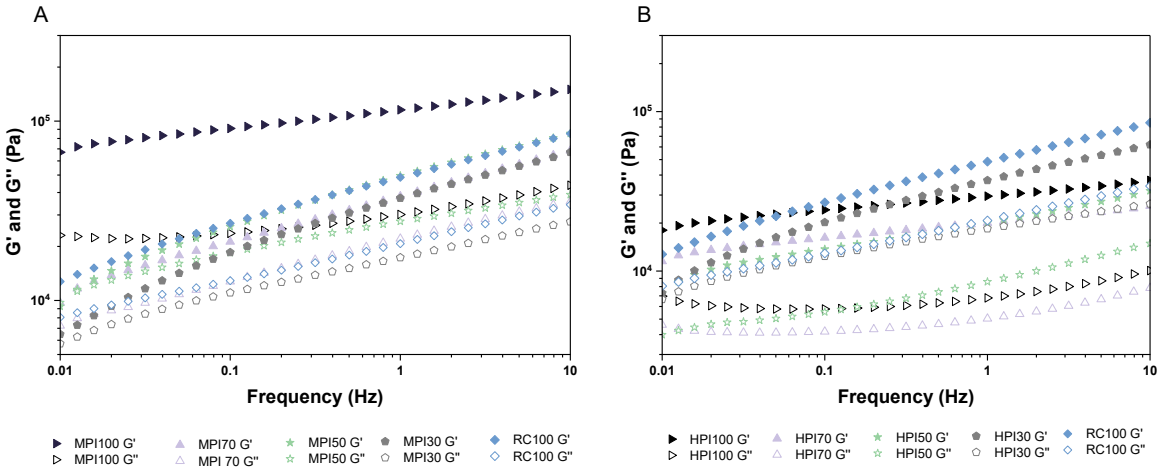
4.3.2.1. Frequency sweep

A frequency sweep test was performed on HPCAs over a range of angular frequencies (0.01 to 10 Hz) within the linear viscoelastic region (0.5% strain level). Parameters of interest are the storage modulus (G') and loss modulus (G''), which respectively characterise the elastic (solid-like) and viscous (liquid-like) components of cheese response to deformation. **Figure 4-2A** and **B** demonstrate that all cheese samples exhibited more elastic-like behaviour, as G' was higher than G'' throughout the tested frequency range.

In the mung bean protein-based HPCAs (**Figure 4-2A**), MPI exhibited the highest G' values and was relatively independent of frequency changes, indicating superior elastic properties and a more rigid structure. In addition, the lower frequency dependence suggests that non-covalent bonds, such as hydrophobic interactions and hydrogen bonds, might control the gel network (Zhu et al., 2021). By contrast, RC100 cheese had lower G' and G'' values and tended to be more frequency-dependent, indicating a more dynamic protein network. Mixing mung bean protein with casein at different ratios resulted in a weaker gel with a less integrated network, as observed by the lower G' values at 0.01 Hz compared with MPI100 and RC100. With increasing frequency, the G' and G'' values of MPI70, MPI50, and MPI30 increased, likely owing to the re-organisation of protein networks under stress. Similar observations were found in hemp protein-based hybrid cheese samples (**Figure 4-2B**). HPI100 cheese was less frequency-dependent than RC100 cheese, and mixtures of hemp protein and RC exhibited weaker networks, likely owing to the incomplete

integration of the two proteins. In addition, HPI100 cheese was less stiff than MPI100 owing to significantly lower G' values. The G' and G" values of HPI70 were more similar to HPI100 than RC100, indicating that hemp protein more strongly influences the structure of the hybrid cheese at a 70% concentration, whereas MPI70 showed a similar trend to RC100. This observation indicates that hemp protein is more disruptive to the casein-casein interactions than mung bean protein.

Rheological results of the present study are consistent with those of several previous studies on the effects of plant proteins on rheological properties of plant protein hybrid cheeses or plant protein–casein mixtures (Beghdadi et al., 2022; Beliciu & Moraru, 2011; K. Li et al., 2018; Silva et al., 2019a; Zhang, Jiang, et al., 2024). These studies concluded that casein and plant proteins did not co-aggregate in the mixtures during heating, and that each type of protein formed its own independent network with G' and G" decrease, indicating a weaker structure in mixed system.



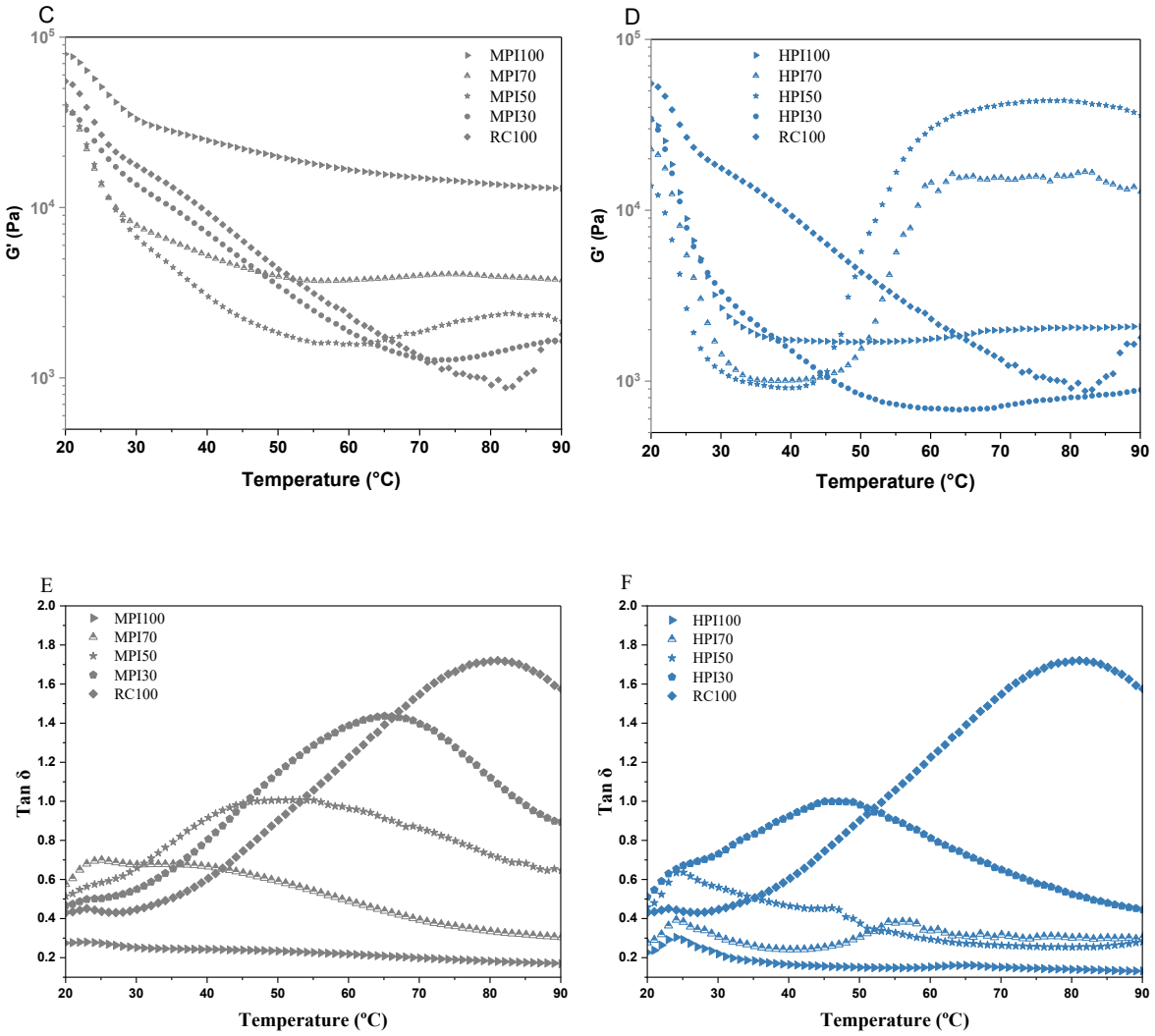


Figure 4-2. Rheological properties of hybrid cheese analogues made with mung bean protein (MPI) or hemp protein (HPI) and rennet casein at varying ratios. Storage modulus (G′) and loss modulus (G″) vs. frequency at 20 °C, γ = 0.5% (A, B). G′ (C, D) and tan δ (E, F) vs. temperature (ω = 1 Hz, γ = 0.5%). Ratios: MPI/HPI100 (100% plant protein), MPI/HPI70 (70% plant protein, 30% rennet casein), MPI/HPI50 (50 % plant protein, 50% rennet casein), MPI/HPI30 (30% plant protein, 70% rennet casein), RC100 (100% rennet casein).

4.3.2.2 Temperature sweep

When cheese is heated, there is a dramatic decrease in the total number and strength of bonds in the cheese matrix owing to the shrinkage of the para-casein network (Fox, 2017a). This is indicated by the decrease in G' and G" (**Figure 4-2C** and **D**) and the increase in tan δ (G"/G') (**Figure 4-2E**

and **F**). Cheese samples with a tan δ < 1 exhibit solid behaviour, while those with a tan δ > 1 exhibit more liquid-like behaviour. The transition of cheese from solid to liquid (tan δ = 1) occurs at a specific temperature, known as the transition temperature. In the initial heating segment, all samples exhibit an increase in tan δ to ~25 °C, which is consistent with the melting of coconut oil (Dobson & Marangoni, 2023) (**Figure 4-2E** and **F**). Neither mung bean nor hemp protein-based cheeses (MPI100, MPI70, HPI100, HPI70 and HPI50) exhibited significant softening as the temperature increased to 90 °C, maintaining tan δ values at <1 (G' > G"). This indicates that plant protein did not exhibit softening and viscous behaviour with increasing temperature. Moreover, the addition of plant protein to cheese reduced tan δ, suggesting that plant proteins disrupted casein-casein interactions. The transition temperature and tan δ values increased with increasing levels of RC. For instance, MPI50 and MPI30 had transition temperatures at 45 °C, and RC100 transitioned at 55 °C. In addition, tan δ values peaked at 50, 65 and 82 °C with values of 1, 1.4 and 1.7, respectively, indicating enhanced formation of the casein-casein network, which corresponds with other findings in the literature for commercially processed cheese (Dobson & Marangoni, 2023; Noronha, Duggan, Ziegler, O'Riordan, et al., 2008). After reaching the peak temperature, tan δ decreased, likely owing to increased hydrophobic-induced protein interactions (Bryant & McClements, 1998).

When the same amount of hemp or mung bean protein was mixed with casein protein (i.e., MPI50 *vs.* HPI50, MPI30 *vs.* HPI30), the tan δ values were higher in the mung bean protein-based hybrid cheese. This indicates that a stronger casein-casein network was formed in the mung bean protein system. In other words, hemp protein disrupted the casein-casein interactions more significantly than mung bean protein. Interestingly, G' values of HPI70 and HPI50 exhibited different behaviour than other cheese samples (**Figure 4-2D**). These samples indicate a distinct decrease in G' and G"

(data not shown) from 20 °C to ~40 °C, followed by an increase in both moduli up to ~60 °C, suggesting network restructuring or protein-protein interactions, and the formation of a more structured yet flexible network. After 60 °C, the moduli plateaued, indicating the formation of a stable structure. However, in the case of HPI30, the low concentration of hemp protein limits its ability to interact with casein. As a result, casein had a more dominant influence, contributing to the gradual decrease in G' with increasing temperature, without the same network re-structuring observed at high hemp protein concentrations. The hypothesis suggests that the presence of disulphide bonds in hemp protein, rather than in mung bean protein, may facilitate interactions with casein as the temperature increases. This is supported by evidence that heating above a critical unfolding temperature enhances the accessibility of buried thiol (-SH) groups, thereby promoting the formation of intermolecular disulphide bonds (Dapčević-Hadnađev et al., 2018). These results aligned with SDS-PAGE results of a possible interaction between HPI with αs2-casein.

4.3.3. Microstructure

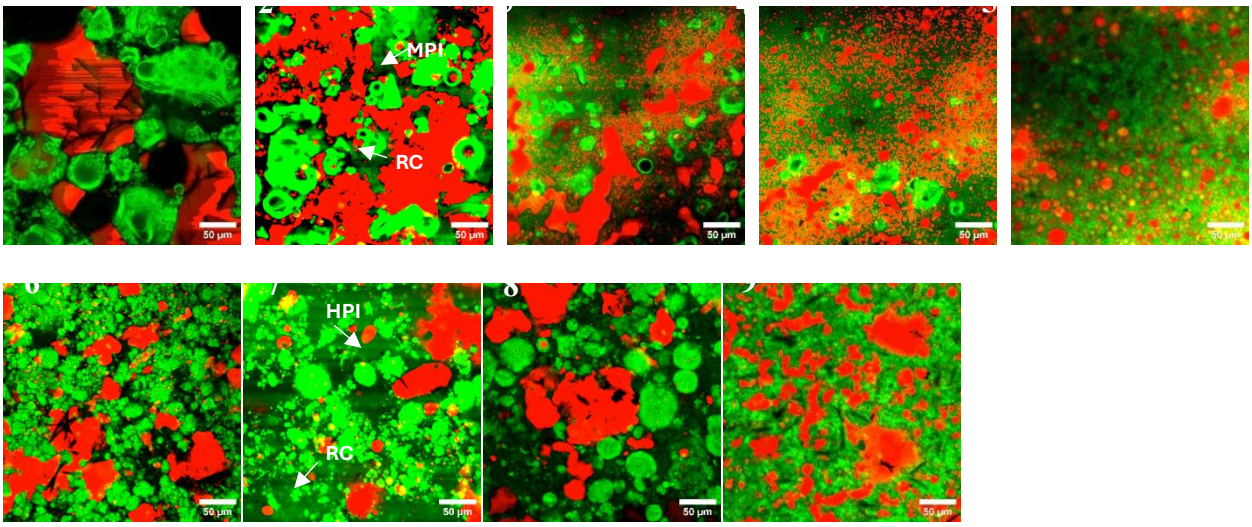
CLSM analysis was applied to understand protein and lipid distributions within the microstructure of HPCAs (**Figure 4-3A**). In general, the addition of plant proteins to the cheese formulation led to a heterogeneous microstructure, wherein the proteins formed aggregates with a non-continuous network (e.g., MPI100, HPI100) with large pools of fat separated from the protein, suggesting that plant proteins may contribute to weaker fat-protein interactions compared to casein. The microstructure differed from the commercial starch-dominated plant-based cheeses observed by Grasso et al. (2021), wherein the distribution of fat globules had a generally spherical shape, stabilised by other hydrocolloids. Similarly, the addition of plant protein to starch-based cheese presented protein aggregates/clusters that were non-homogeneously distributed within the cheese

network. With the increasing ratio of RC in the cheese matrix, more fat pools broke down into spherical fat droplets and were trapped in the casein network, resulting in a more continuous cheese network, in agreement with the observation of commercially processed cheeses (Grasso et al., 2021; Ramel & Marangoni, 2017).

Mung bean protein tended to form large, deflated sphere particles ranging from 10 to 100 μm, resulting in a coarse, rough, and granular structure (**Figure 4-3A** (1)). When combined with casein, mung bean protein disrupted the formation of the casein network, especially at high protein levels (e.g. **Figure 4-3A** (2)). This disruption resulted in a non-continuous casein structure and a cheese matrix predominantly composed of mung bean protein. Consequently, fragmented sections of the casein network filled the gaps where the mung bean protein was not interconnected. When HPCAs comprised >50% RC, the cheese network shifted from being dominated by mung bean protein to casein. Casein prevented the mung bean protein particles from clustering, with mung bean protein particles acting as a filler.

Hemp protein tended to form smaller, denser, and more evenly distributed particles ranging from 1 to 50 μm (**Figure 4-3A** (6)). Similar to mung bean protein, HPCAs at high levels of hemp protein, the cheese matrix primarily comprised hemp protein (e.g. **Figure 4-3A** (7)). A more continuous and smooth casein network was formed with 70% RC in HPCAs (**Figure 4-3A** (9)). Notably, hemp protein disrupted the casein network more than mung bean protein owing to more hemp protein particles being dispersed in the cheese matrix.

A



B

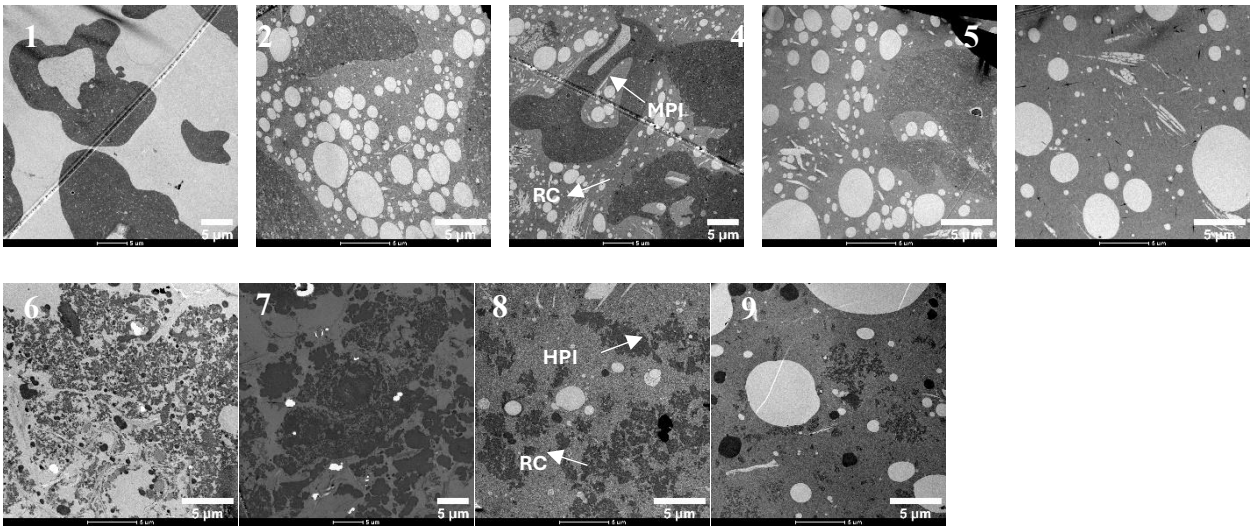


Figure 4-3. Representative CLSM (A) and TEM (B) images of mung bean protein (MPI) and hemp protein-based (HPI) hybrid processed cheese analogues. Fat in red and protein in green in CLSM. MPI100: 100% mung bean protein in cheese (1); MPI70: 70% mung bean protein, 30% rennet casein (2); MPI50: 50% mung bean protein, 50% rennet casein (3); MPI30: 30% mung bean protein, 70% rennet casein (4); RC100: 100% rennet casein (5); HPI100: 100% hemp protein in cheese (6); HPI70: 70% hemp protein, 30% rennet casein (7); HPI50: 50% hemp protein, 50% rennet casein (8); HPI30: 30% hemp protein, 70% rennet casein (9). CLSM images scale bars = 50 µm and TEM images scale bars = 5 µm.

TEM was also applied to provide high-resolution imaging for observing cheese microstructure (**Figure 4-3B**). The micrograph of MPI100 demonstrated a large circular structure (around 30 μm), which is also seen by CLSM (**Figure 4-3B** (1)). The particles were present as individual particles and merged into larger agglomerates (Loveday & Halim, 2024). After adding RC, a distinct boundary was observed between MPI (darker grey) and RC (lighter grey), indicating little or no interaction with casein. In addition, numerous fat droplets with a more homogenous distribution were observed in the casein network rather than in MPI100. Moreover, casein and fat droplets were observed in the hollow part of the MPI aggregation (e.g. MPI30).

TEM micrograph of HPI100 appeared to have a more fragmented and heterogeneous structure. As RC increased, this non-protein inclusion became less noticeable. In addition, TEM confirmed that hemp protein aggregates appeared as small irregular flakes and smaller in size than mung bean aggregates and were dispersed in the cheese matrices. In the mixed system, they were darker in colour than RC (e.g. **Figure 4-3B** (4) and (8)). In fact, the protein aggregation size and shape formed are closely related to the production process, and commercial plant protein isolates often form particulate structures with large protein aggregation and partial or extensive denaturation before heat treatment (Beghdadi et al., 2022; Hadnađev et al., 2018; Loveday & Halim, 2024; Lyu et al., 2023).

4.3.4. Texture profile of HPCAs

Texture parameters of the HPCAs were examined using a texture analyser (**Table 4-2**). Cheese samples of MPI100, MPI70 and RC100 exhibited higher hardness than the other samples. Hardness decreased as the mung bean protein concentration decreased, likely because the network was disrupted by the presence of different protein types in the cheese matrix. Although the total

protein content remained at 18%, the dual-protein system formed independent networks, reducing the effective protein concentration and overall structural strength. In contrast, RC100 formed a smooth and strong network without interference from plant proteins, resulting in higher hardness. In addition, cheese with hemp protein had lower hardness than those with mung bean protein (i.e. HPI100 *vs* MPI100), suggesting a denser network with stronger interactions in the mung bean protein, as observed at the microstructure level. By contrast, hemp protein forms smaller, more uniformly dispersed aggregates, creating a more flexible structure and resulting in lower hardness. As the hemp protein concentration increased, the hardness further decreased accordingly. Moreover, HPI50 and HPI30 were too soft to be tested, therefore, there were no results for these samples.

In addition, springiness indicates how well a cheese sample springs back after deforming during the first compression. It was found that only the RC100 samples showed the highest springiness and chewiness, whereas samples containing plant proteins significantly affected their springiness and chewiness. Cohesiveness is the strength of the internal bonds that make up the cheese structure and how well the cheese can be deformed before it breaks (Rosenthal & Thompson, 2021). Resilience indicates how well a cheese sample resists regaining its original height. With an increasing ratio of casein in the cheese samples, cohesiveness and resilience increased. Moreover, the addition of over 50% RC to the hybrid cheeses showed similar resilience to RC100. HPI100 cheese showed higher cohesiveness and resilience than MPI100, likely owing to the more uniform distribution of hemp protein in the cheese matrix, allowing for better recovery after deformation. By contrast, mung bean protein forms large aggregates, leading to a denser and more rigid structure in the cheese (Tojan, 2021). This denser structure typically increases the hardness because the larger aggregates create a more compact and less flexible network. However, this rigidity can also

reduce resilience because the cheese is less likely to bounce back after being compressed or deformed.

These findings are consistent with those of previous studies (Khiabanian et al., 2022; Mazinani et al., 2020; Omrani Khiabanian et al., 2020) that evaluated the textural properties of feta cheese manufactured from MPC with the addition of plant proteins. The findings indicate that cheese hardness, cohesiveness, springiness, and chewiness decreased with increasing levels of pea or soy proteins. For instance, H. Li et al. (2018) stated that the addition of soymilk hindered the aggregation of skim milk, decreasing gel strength. A similar observation was reported by Monga et al. (2022), in that the presence of globular proteins decreases the compactness of protein structure, which manifested as a decrease in cohesiveness of hybrid cheese than dairy cheese. Briefly, although hybrid cheeses with plant proteins typically have inferior texture to milk-based cheeses, varying plant proteins and ratios can help match milk protein texture.

Table 4-2. Textural profile of processed hybrid cheese analogues

	MPI100	MPI70	MPI50	MPI30	HPI100	HPI70	HPI50	HPI30	RC100
Hardness	806.68^{ab} ± 53.87	649.72^{b} ± 51.49	396.98^{c} ± 21.62	371.69^{c} ± 30.90	297.71^{c} ± 27.7	89.64^{d} ± 9.02	n/a	n/a	821.79^{a} ± 22.00
Springiness	0.38^{a} ± 0.04	0.27^{a} ± 0.12	0.28 ^{a} ± 0.02	0.30^{a} ± 0.03	0.28^{a} ± 0.02	0.35^{a} ± 0.05	n/a	n/a	0.65^{b} ± 0.03
Cohesiveness	0.05^{a} ± 0.01	0.32^{b} ± 0.05	0.63^{c} ± 0.03	0.75^{c} ± 0.02	0.53^{bc} ± 0.10	0.73^{c} ± 0.02	n/a	n/a	0.69^{c} ± 0.01
Chewiness	14.38^{a} ± 3.45	54.92^{ab} ± 10.33	68.79^{b} ± 5.21	83.91^{b} ± 14.50	41.67^{a} ± 6.30	23.46^{a} ± 4.93	n/a	n/a	370.58^{c} ± 10.60
Resilience	0.03^{a}	0.09^{ac} ± 0.02	0.22^{b} ± 0.01	0.27^{b} ± 0.01	0.18^{bc} ± 0.05	0.19^{bc} ± 0.02	n/a	n/a	0.27^{b}

Values within a row not sharing a common superscript differ significantly ($p < 0.05$). Ratios: MPI/HPI100 (100% plant protein), MPI/HPI70 (70% plant protein, 30% rennet casein), MPI/HPI50 (50% plant protein, 50% rennet casein), MPI/HPI30 (30% plant prtein, 70% rennet casein), RC100 (100% rennet casein).

4.3.5. Meltability and Stretchability

Meltability is a crucial functional characteristic of processed cheese, defined as its ability to flow and spread when heated, resulting in the visual loss of individual cheese shreds (Guinee, 2011). This property is mainly influenced by the strength of casein–casein interactions (Park et al., 1984). Upon heating, the cheese network softens as milk fat melts > ~40 °C. Moreover, continued heating causes the casein network to contract owing to increased hydrophobic interactions. This contraction reduces contact between casein molecules, weakening the overall network and leading to further softening or melting of the cheese (Lamichhane et al., 2018; Lucey et al., 2003).

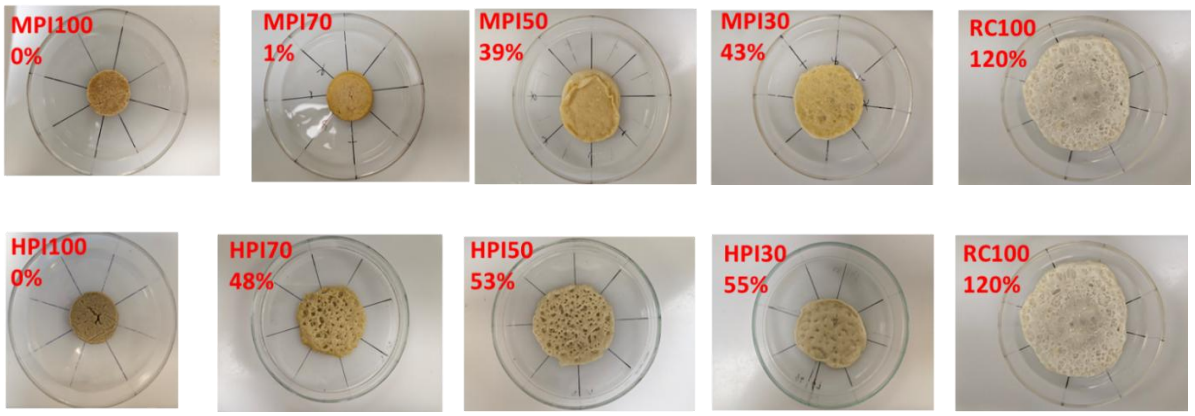
Figure 4-4A presents melting properties of the samples. Notably, increasing casein content in the hybrid system increased the expansion area. The presence of casein micelles in RC results in extensive protein–protein and protein–fat globule interactions, forming a fibrous casein network. At high temperatures, there is a more rapid relaxation of casein protein-protein bonds and a change to a more liquid-like character. The addition of plant protein can lead to cross-linking among themselves as well as with caseins at high temperatures, weakening the casein-casein interactions. The pure plant protein-based cheese samples, HPI100 and MPI100, exhibited no melting behaviour, consistent with the previous observations (Grasso et al., 2021), owing to the lack of a continuous protein network.

Hemp protein-based hybrid cheeses (e.g. 48% in HPI70 and 53% in HPI50) tend to have higher meltability than those prepared with mung bean protein at the same ratios (e.g. 1% in MPI70 and 39% in MPI50). This is more significant at higher plant protein ratios. This may be attributed to the formation of smaller and more uniformly dispersed hemp protein aggregates, as observed in CLSM and TEM micrographs. These structural differences likely disrupted casein-casein

interactions more extensively than mung bean protein. Rheological results indicated that this disruption led to weaker casein-casein interactions, facilitating melting. Moreover, the surface of HPI70 and HPI50 exhibited a more porous, honeycombed structure, suggesting that hemp protein in hybrid cheese releases water more effectively, promoting larger expansion during heating. However, as the casein proportion increased in the HPI and MPI hybrid cheese systems, the difference became smaller as casein became dominant.

Stretchability is an important quality attribute of melted cheese. A stretchability test was conducted on the HPCA samples with melting properties from the results mentioned above, excluding MPI100 and HPI100. Owing to the limited sensitivity of the texture analyser, it cannot detect the stretch breaking point of the samples. Thus, the stretch processes were video recorded, and the stretch distance was checked using the texture analyser software and then compared among samples (**Figure 4-4B**). In cheese, stretchability is the ability of the casein network to maintain its integrity without breaking when it is pulled. This depends on intact casein to maintain the strength of the strands with enough calcium and phosphorus (Lucey & Fox, 1993; Lucey et al., 2003). In addition, it is affected by how the casein molecules stick together and handle energy. The stretch test requires casein molecules to be close yet flexible enough to quickly change shape.

A



B

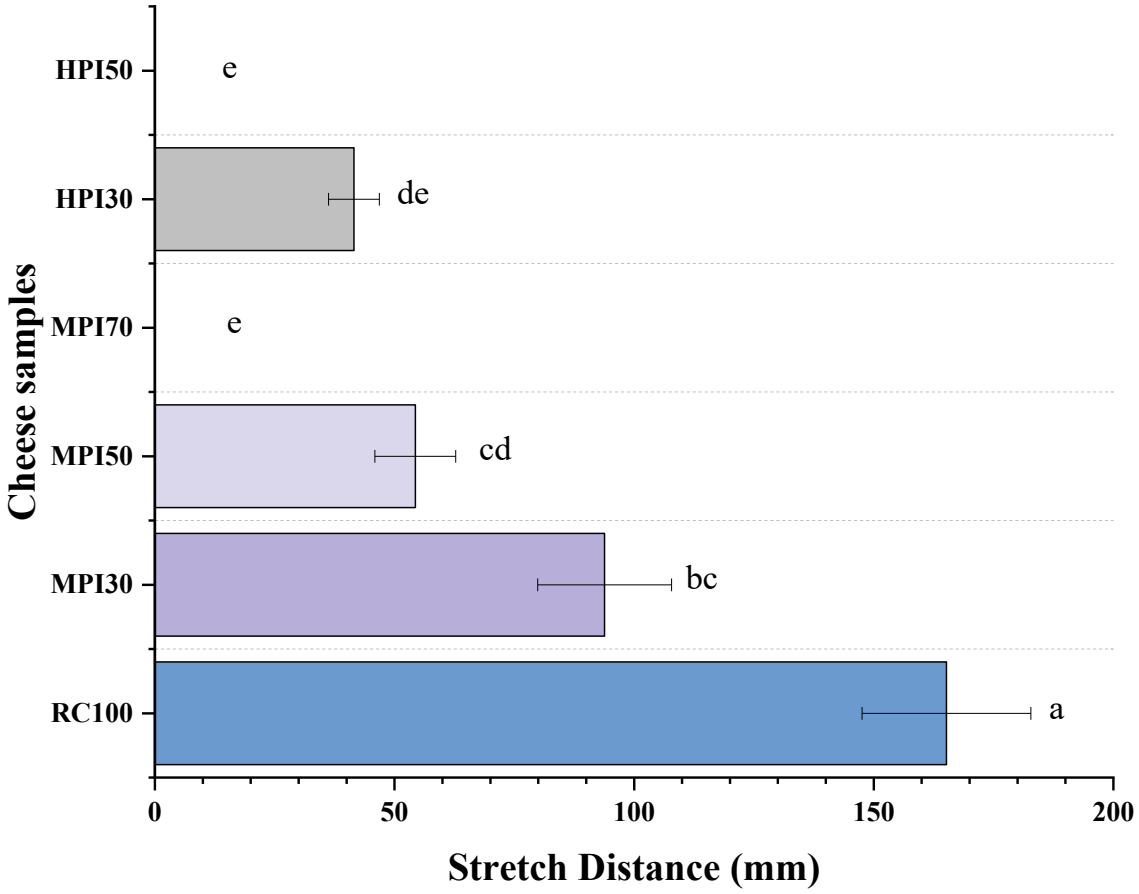


Figure 4-4. Representative images (A) of hybrid processed cheese analogues (HPCAs) made with mung bean protein (MPI) or hemp protein (HPI) and rennet casein at varying ratios, after heating at 170 °C for 10 min, with melting index. Stretch distance of hybrid cheeses (B). Values within a row not having common superscripts differ significantly ($p < 0.05$). Ratios: MPI/HPI100 (100%

plant protein), MPI/HPI70 (70% plant protein, 30% rennet casein), MPI/HPI50 (50% plant protein, 50% rennet casein), MPI/HPI30 (30% plant protein, 70% rennet casein), RC100 (100% rennet).

In comparison, cheese samples containing only RC exhibited the highest stretchability, characterised by the longest stretch distance. The addition of 30% or more plant protein in the hybrid system significantly affected the stretchability of HPCAs by interrupting the casein network, changing it from a continuous network to a non-continuous network. Unlike melting properties, hybrid cheeses with mung bean protein exhibited greater stretchability than those with hemp protein at the same ratios (e.g. 93.8 mm in MPI30 *vs* 41.53 mm in HPI30). As discussed in melting behaviour, mung bean protein formed larger aggregates, which interrupt the cheese matrix less frequently but hinder casein flow during melting, thereby reducing meltability but improving stretchability. In other words, the fewer interactions between casein–casein in HPI hybrid cheese samples compared with MPI hybrid cheese samples further decreased stretchability while enhancing meltability. When the cheese is heated, these small hemp protein aggregates in the casein network have less impact on the relaxation of the casein network, allowing it to flow more freely and thereby improving melting properties. However, these small aggregates interrupt the casein network more uniformly, which negatively impacts the cheese stretchability. This results in more points of disruption within the casein network, decreasing stretchability. Another proposed reason may relate to the presence of disulphide bond in hemp protein, which could promote cross-linking with casein at high temperatures, further interrupting the casein network.

4.3.6. Analysing protein structure with FTIR

FTIR spectroscopy measures the vibrational movements of molecules caused by the absorption of infrared radiation by chemical bonds in functional groups. FTIR spectra for HPCAs were recorded

in the 450–4000 cm^{-1} range. In protein, the amide I (1600–1700 cm^{-1}) bands are commonly analysed, primarily associated with C=O and N–H stretching, reflecting protein secondary structure depending on hydrogen bonding and conformation of the polypeptide: such as α-helix (1650–1660 cm^{-1}), β-sheet (1610–1642 cm^{-1}), β-turn (1660–1699 cm^{-1}), and random coil (unordered, 1640–1650 cm^{-1}) structures. The amide II band (1480–1580 cm^{-1}), which originates mainly from N–H bending and C–N stretching vibrations, is less commonly used for secondary structure determination due to its lower sensitivity and overlap with other signals (Saji, Ramani, Gandhi, Seth, & Sharma, 2024). Thus the amide I bands were analysed and deconvoluted to examine protein structure changes in the hybrid cheese samples (**Figure 4-5** and supplementary **Figure S 4-3**). MPI and HPI promoted the formation of β-sheet structures, which gradually decreased as the RC content increased (43% in MPI100, 39% in HPI100, and 32% in RC100). This observation is consistent with Sim et al.'s (2021) study, which found that plant proteins tend to have more β-sheet structures, leading to protein aggregation. In particular, MPI had a high β-sheet content, suggesting increased exposure of hydrophobic regions, which may contribute to a firmer and more rigid cheese structure (Jadhav et al., 2024). As RC content increases, more disordered structures were promoted, making the hybrid cheeses more flexible—an important factor for functional properties such as meltability and stretchability. MPI100 indicated no random coil structures, whereas HPI100 exhibited a higher proportion, indicating that HPI may provide greater flexibility in cheese structure than MPI. Adding RC to mung bean protein blends (30:70, 50:50, and 70:30) reduced the helical structures in hybrid cheeses. However, the helical structure content did not significantly differ between pure mung bean cheese and pure RC cheese, indicating that the interaction between casein and mung bean protein primarily influences the helical structure in mixed formulations rather than in their pure forms. For hemp protein blends, a similar

decreasing trend in the helical structure was observed with the addition of RC, though the changes were not statistically significant. In addition, while the β-turn content showed a reduction in mung bean and hemp protein blends upon the addition of RC, these decreases were not statistically significant. These results suggest that although α-helices and β-turns contribute to the structural properties of the protein networks, they may not be the primary factors influencing the functional characteristics of these hybrid cheeses.

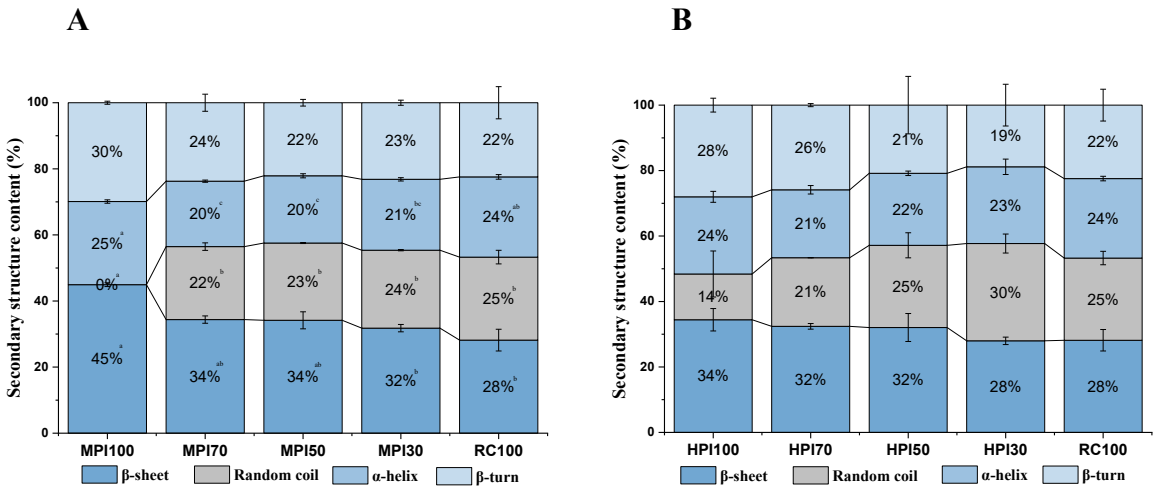


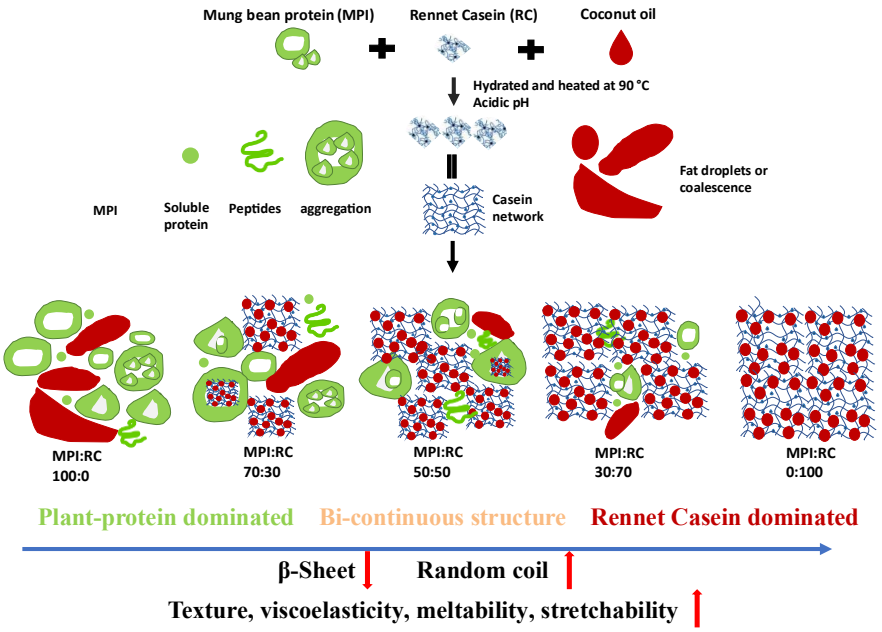
Figure 4-5. Secondary structure content of mung bean protein-based hybrid cheeses (A) and hemp protein-based hybrid cheeses (B) by FTIR. Referenced location of secondary structures: β-sheet (1610–1642 cm^{-1}), Random coil (1640–1650 cm^{-1}), α-helix (1650–1660 cm^{-1}) and β-turn (1660–1699 cm^{-1}) (Gawat et al., 2024; Sadat & Joye, 2020). All values are reported as the mean ± SEM, where N = 3 (3 replicates with 3 measurements). Values within a row not having common superscripts differ significantly ($p < 0.05$). Ratios: MPI/HPI100 (100% plant protein), MPI/HPI70 (70% plant protein, 30% rennet casein), MPI/HPI50 (50% plant protein, 50% rennet casein), MPI/HPI30 (30% plant protein, 70% rennet casein), RC100 (100% rennet casein).

4.3.7. Structure–functionality relationship proposed in plant protein-casein HPCAs

Figure 4-6 presents the development of the microstructure of HPCAs at different plant protein-to-RC ratios and the relationship between structure and functionality. After mixing and heating

ingredients, namely, plant protein, RC, coconut oil, emulsifying salts and water, the proteins undergo hydration, interaction with emulsifying salts, denaturation, and gelation. Particularly, plant proteins exist in various forms after hydration, with a small amount as soluble protein and peptides, but primarily as aggregates. By contrast, casein interacts with itself, solubilizes through emulsifying salts, sequesters calcium ions, and forms a gel-like network. In the absence of casein, the coconut oil does not evenly disperse, forming fat coalescence, whereas, with casein present, coconut oil droplets are evenly dispersed throughout the casein network. At high plant protein ratios, the network is mainly dominated by plant proteins. However, as the proportion of casein increases, a bicontinuous structure develops, wherein plant proteins and casein form independent networks. This transition is accompanied by decreased β-sheet content and increased random coil structures, resulting in a smooth and homogeneous matrix. As casein levels continue to rise, they become the primary structural component, improving viscoelastic and functional properties, whereas plant proteins function as fillers within the matrix. Mung bean protein (**Figure 4-6A**) tends to form larger aggregates than hemp protein (**Figure 4-6B**), which blocks the melting of the casein network during heating. By contrast, hemp protein integrates more into the casein network, leading to greater disruption of its structure. The presence of disulphide bonds in hemp protein may also promote interactions with casein during heating, further contributing to this disruption. This possibly contributes to increased meltability but reduced stretchability compared with mung bean protein.

A



B

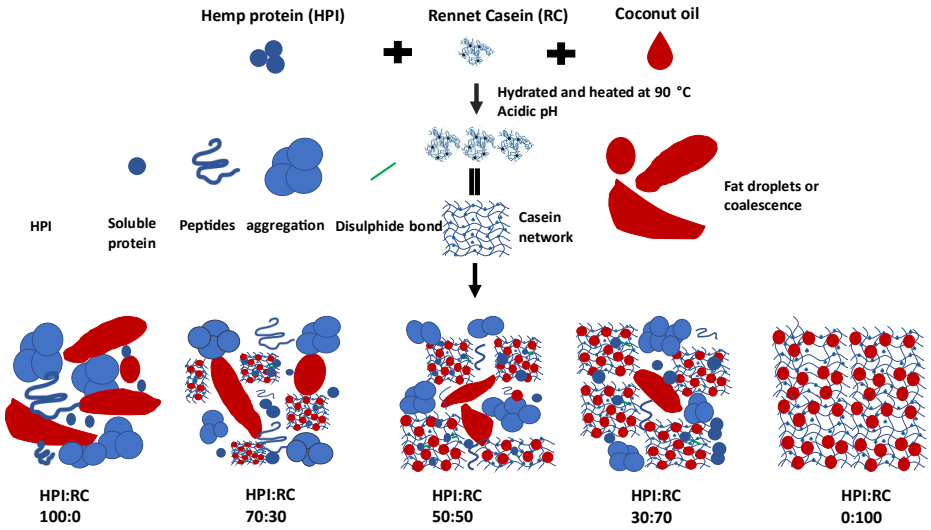


Figure 4-6. A schematic diagram summarizing the development of the microstructure of mung bean protein (A) and hemp protein-based hybrid cheeses (B) at different plant protein-to-rennet casein ratios and the relationship between structure and functionality. Ratios: MPI/HPI100 (100% plant protein), MPI/HPI70 (70% plant protein, 30% rennet casein), MPI/HPI50 (50% plant protein,

50% rennet casein), MPI/HPI30 (30% plant protein, 70% rennet casein), RC100 (100% rennet casein).

4.4. Conclusions

This chapter provided insights into changes in protein structure and microstructure in hybrid processed cheese (HPCAs) formulated with mung bean protein and RC, as well as hemp protein and RC. Incorporating plant protein into cheese affected its microstructural, textural and functional properties because the formation of an independent protein network was observed and one may affect the other in the cheese matrix. Among the tested formulations, mung bean protein–based HPCAs exhibited greater stretchability, rheological and textural attributes than those containing hemp protein at the same ratios, despite exhibiting low meltability. These differences may be attributed to variations in the size of plant protein aggregates. In addition, the presence of disulphide bonds in hemp protein may enhance interactions with casein at rising temperatures. Overall, blending plant proteins with milk proteins to create hybrid cheese analogues offers promising potential for achieving desired textures and functionalities, depending on incorporation ratios and specific plant proteins used. This study contributes to understanding the structure–functionality relationship in hybrid cheeses and their potential applications in the growing plant-based food industry. In future, other techniques such as confocal Raman microscopy will be used to gain deeper structural insights and distinguish between plant and milk proteins in hybrid cheeses. Additionally, amino acid profiling (e.g., via RP-HPLC) and targeted analyses of disulphide bonding and intermolecular forces will be undertaken to provide more direct evidence of the molecular interactions governing cheese functionality.

4.5. Acknowledgments

The authors thank the Manawatu Microscopy and Imaging Centre, Massey University, Palmerston North, New Zealand, for supporting the microscopy studies.

4.6. Supplementary material

Table S 4-1. Particle size of mung bean protein and hemp protein dispersions (1% v/w)

	Mung bean protein	Hemp protein
D [4, 3] (µm)	118.527 ± 5.654	33.324 ± 1.360
D (0.5) (µm)	100.502 ± 3.885	18.832 ± 1.138

A **B**

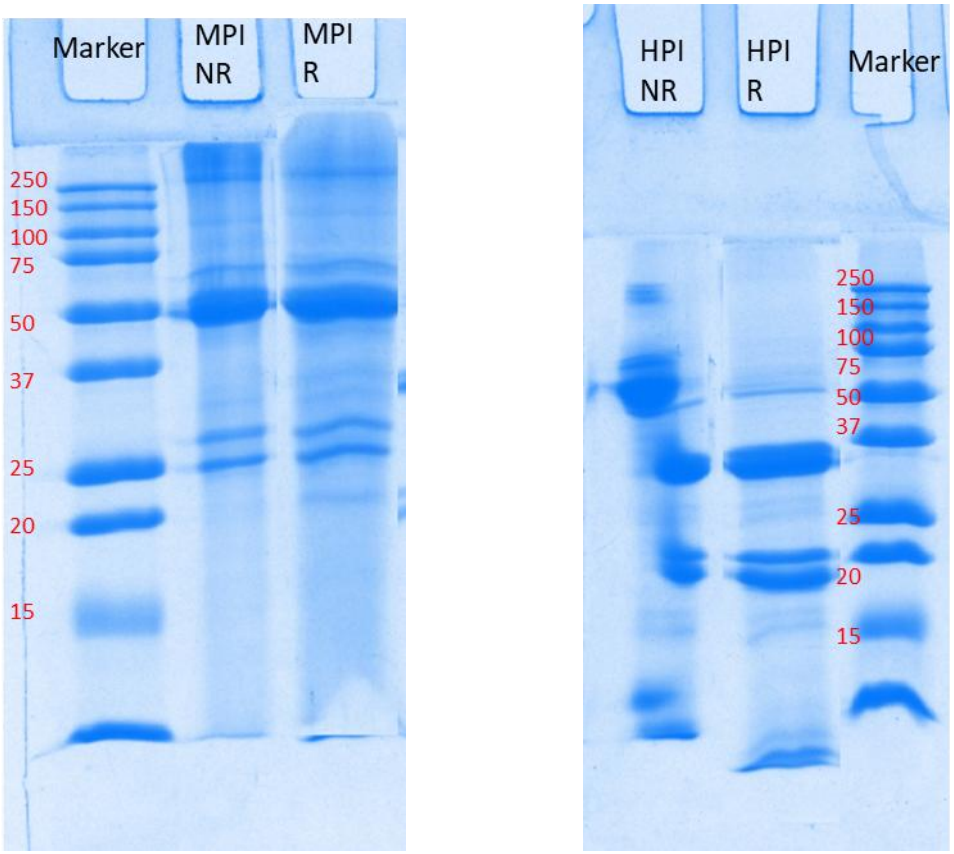
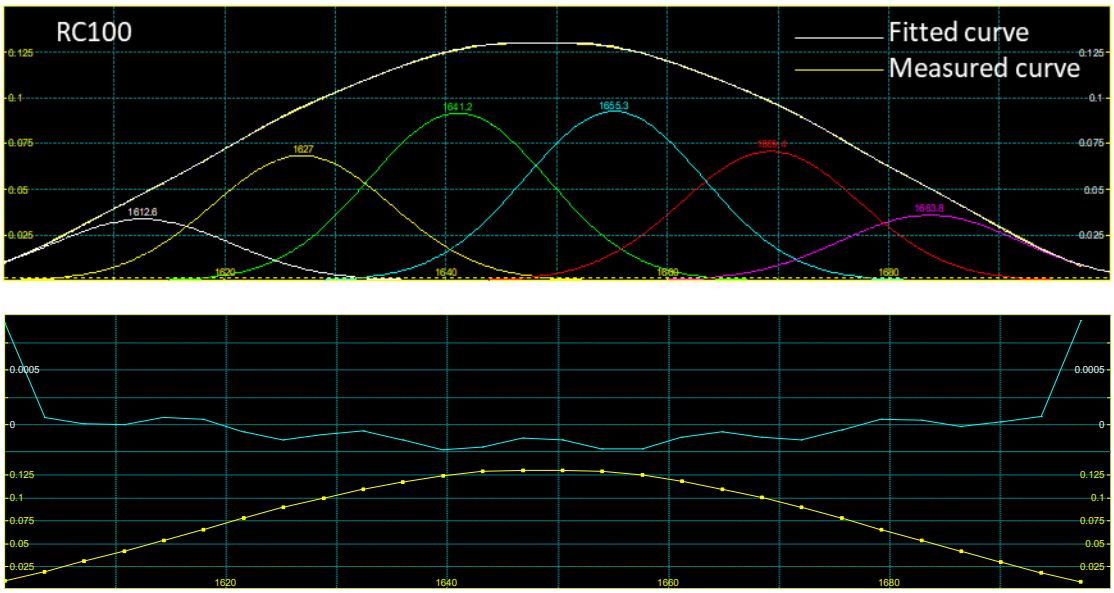


Figure S 4-1. SDS-PAGE profile of mung bean protein powder (A) and hemp protein powder (B). The samples were prepared in reducing (R) and non-reducing (NR) conditions.



Figure S 4-2. Photo of the cheese stretchability rig, including in-house built post hooks and a base pot with dimensions.

A



B

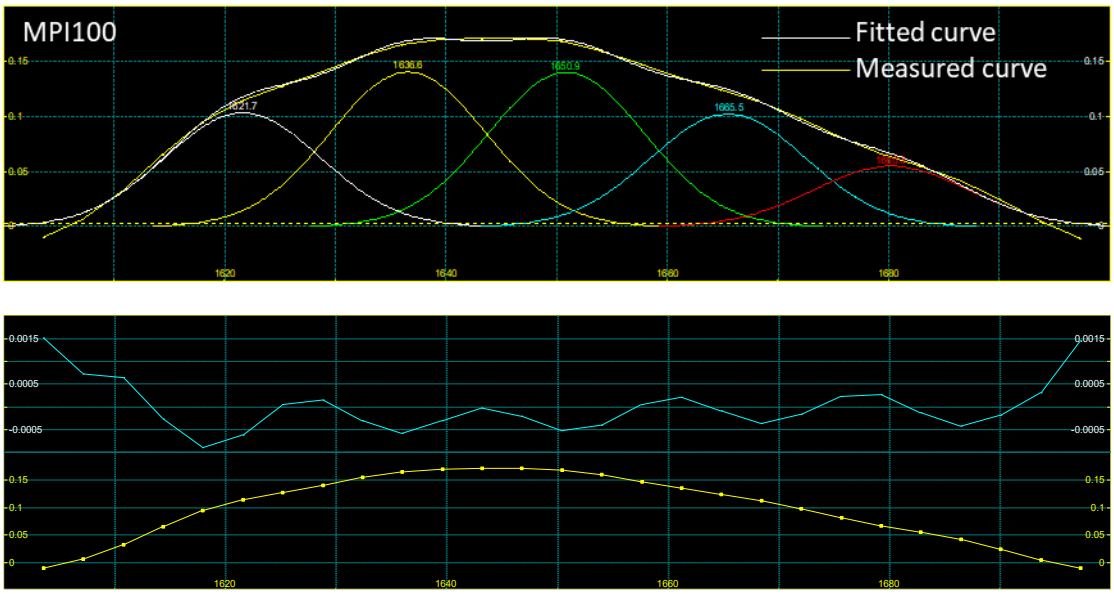


Figure S 4-3. Example of FTIR Peak Fitting (top) and Second Derivative Analysis (bottom) of RC100 (A) and MPI100 cheese (B).

MASSEY UNIVERSITY
TE KUNENGA KI PŪREHUROA
UNIVERSITY OF NEW ZEALAND

GRADUATE RESEARCH SCHOOL

STATEMENT OF CONTRIBUTION
DOCTORATE WITH PUBLICATIONS/MANUSCRIPTS

We, the student and the student's main supervisor, certify that all co-authors have consented to their work being included in the thesis and they have accepted the student's contribution as indicated below in the Statement of Originality.

Student name:	Di Lu
Name and title of main supervisor:	Aiqian Ye
In which chapter is the manuscript/published work?	Chapter 5

Describe the contribution that the student and members of the supervisory team have made to the manuscript/published work:[1]

Di Lu: Conceptualization, Data curation, Formal analysis, Investigation, Methodology, Writing—original draft.
Cushla McGoverin: Formal analysis, Investigation, Methodology, Writing—reviewing & editing.
Yi Zheng: Formal analysis, Methodology, Writing—original draft.
Debashree Roy: Supervision, Writing—review & editing. Alejandra Acevedo-Fani: Supervision, Writing—review & editing. Harjinder Singh: Supervision, Writing—review & editing. Mark Waterland: Writing—review & editing. Ye Aiqian: Conceptualization, Funding acquisition, Project administration, Supervision, Writing—review & editing.

Please select one of the following three options:

- (●) The manuscript/published work is published or in press

  Please provide the full reference of the research output:

  Lu, D., McGoverin, C., Roy, D., Acevedo-Fani, A., Singh, H., Waterland, M., Zheng, Y., & Ye, A. (2026). Distinguishing plant and milk proteins and their interactions in hybrid cheese using confocal Raman microscopy with machine learning. Food Chemistry, 498, 147102. https://doi.org/https://doi.org/10.1016/j.foodchem.2025.14

- ( ) The manuscript is currently under review for publication

  Please provide the name of the journal:

- ( ) It is intended that the manuscript will be published, but it has not yet been submitted to a journal

Student's signature:	Di LU Digitally signed by Di LU DN: cn=Di LU, o=Massey University, email=d.lu@massey.ac.nz Date: 2026.02.04 15:31:19 +13'00'	Main supervisor's signature:	Aiqian Ye Digitally signed by Aiqian Ye DN: cn=Aiqian Ye, o=Massey University, ou=Riddet Institute, email=A.M.YE@massey.ac.nz Reason: I am approving this document Date: 2026.02.27 11:39:12 +13'00'

This form should be placed at the beginning of each relevant thesis chapter.

[1] Refer to the Massey University Publishing and Authorship guidelines (OneMassey for staff, Stream for students) and/ or Contributor Roles Taxonomy (CRediT) guidelines for guidance.

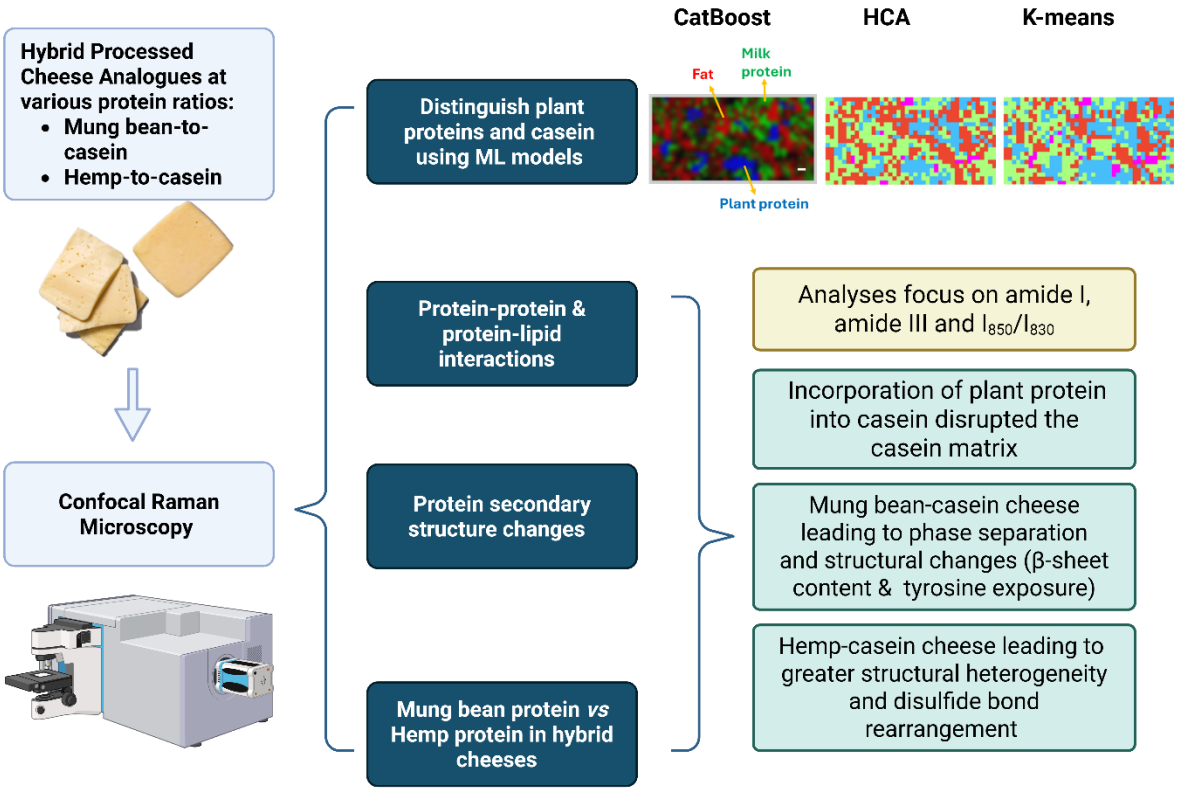
Chapter 5 Distinguishing plant and milk proteins and their interactions in hybrid cheese using confocal Raman microscopy with machine learning[4]

Abstract

The increasing demand for plant-based alternatives to milk protein has led to the development of hybrid processed cheese analogues (HPCAs) combining plant proteins and casein. However, their complex microstructure and molecular interactions remain poorly understood. This chapter integrated confocal Raman spectroscopy with advanced machine learning for high-resolution spatial mapping and molecular characterization of HPCAs containing mung bean protein isolate (MPI) or hemp protein isolate (HPI) with casein. This integration helped distinguish between protein sources and elucidate structural changes. The addition of casein changed the HPI structure, promoting structural disorder, disulfide bond rearrangement, and a sharp decrease in the tyrosine doublet ratio from 4.5 in HPI100 to 1.2 in HPI50. Conversely, casein interaction with MPI led to microstructural segregation and changes of β-sheet content (from 53% in MPI100 to 20% in MPI30). This integrated method represents a powerful tool for analysing protein structure and interactions in complex food systems.

[4]This chapter has been published as Lu, D., McGoverin, C., Roy, D., Acevedo-Fani, A., Singh, H., Waterland, M., Zheng, Y., & Ye, A. (2026). Distinguishing plant and milk proteins and their interactions in hybrid cheese using confocal Raman microscopy with machine learning. Food Chemistry, 498, 147102.

Graphic Abstract



5.1. Introduction

The growing shift towards plant-based proteins as a sustainable alternative to animal proteins has attracted substantial interest in the food industry. Despite their potential, plant proteins often face challenges in matching the functional properties of animal proteins, such as solubility, foaming and emulsification (Zhang, Jiang, et al., 2024). These limitations hinder their ability to fully replace animal proteins in many food applications. To address these limitations, hybrid cheeses combining plant and milk proteins have been developed to explore new possibilities in food formulation. In our previous study, we compared various plant proteins in plant-based processed analogues, and among these, MPI and HPI showed the most distinct differences in structural and functional characteristics (Chapter 3) (Lu et al., 2025). Further, we combined MPI or HPI with rennet casein (RC) at varying ratios to produce hybrid processed cheese analogues (HPCAs) (Chapter 4). We found that the addition of plant proteins significantly altered the physical, textural and microstructural properties of the cheese analogues. Notably, the mechanisms underlying these changes differed between MPI/RC–based and HPI/RC–based cheeses, likely owing to differences in the size of protein aggregates and the presence of disulfide bonds, which influenced the structural and functional properties of the final product (Lu, Roy, et al., 2026). However, the underlying molecular interactions between plant and milk proteins remain insufficiently understood. Therefore, building on our previous study, this study aimed to further investigate the structural and functional modifications in hybrid cheese systems through Raman spectroscopy.

Raman spectroscopy, an analytical technique based on the inelastic scattering of light, provides molecular insights into the composition and structure of materials. Although this technique has been used to analyse various food matrices, its application in cheese research has been relatively limited. Studies have investigated its use in detecting starch in spreadable cheese (Oliveira et al.,

2016), monitoring protein and chemical changes during Cheddar cheese ageing (Dewantier et al., 2023; Holroyd et al., 2023), and predicting cheese quality traits (Stocco et al., 2024). Raman imaging, which integrates spectroscopy with spatial mapping, can be used to visualise the microstructure and distribution of cheese components (Chawanji et al., 2022; Holroyd & Nickless, 2024; Smith, 2013). In addition, Nickless and Holroyd (2020) used Raman imaging and multivariate analysis to distinguish whey protein from casein. These studies highlight the advantages of multivariate techniques in differentiating components with similar Raman spectra, as computational algorithms can detect subtle spectral variations to distinguish microscopic domains.

However, the application of Raman imaging in complex cheeses, particularly those incorporating dairy and plant proteins, remains largely unexplored. No studies have specifically focused on identifying milk and plant proteins in hybrid cheese. The complexity of hybrid cheeses, along with their varying protein structures, fat contents and emulsifying agents, complicates the identification of individual components. A major obstacle is the spectral overlap between milk and plant proteins, which limits the effectiveness of conventional peak analysis. Moreover, the presence of emulsifying salts, water and fluorescence from plant proteins further complicates spectral interpretation.

This chapter aimed to investigate the interactions between casein and plant proteins in HPCAs through confocal Raman microscopy combined with machine learning (ML). We specifically focused on mapping the spatial distribution of components in both single-protein and dual-protein cheeses. In dual-protein cheeses, we distinguished casein from plant proteins, examined protein–protein and protein–lipid interactions, assessed changes in secondary protein structures in response to an increasing plant protein ratio and compared the effects of HPI and MPI when combined with

casein. We hypothesised that 1) protein and lipid distributions in dual-protein cheeses might vary with the plant protein to casein ratio, influencing fat dispersion and protein–lipid interactions. 2) Casein and plant proteins may form large independent networks depending on the protein types. 3) Increasing the plant protein content in the hybrid cheese may alter secondary protein structures of both proteins, impacting cheese functionality. To verify our hypothesis, we used chemometric and ML techniques, including multivariate analysis and CatBoost models, to enhance spectral interpretation. This chapter highlights the potential of Raman spectroscopy in characterising the microstructure and protein interactions of hybrid cheeses, offering insights into the structural dynamics of mixed-protein systems.

5.2. Materials and Methods

5.2.1. Materials

Rennet casein (RC; SureProteinTM 779) containing 82% protein was obtained from Fonterra Co-operative Group Ltd., New Zealand. Mung bean protein isolate (85%; MPI) was purchased from Bulk Powders New Zealand. Hemp protein isolate (70%; HPI) and virgin coconut oil were purchased from Davis Trading Company, New Zealand. All chemicals used were of analytical grade and obtained from Sigma Chemical Co., unless otherwise specified.

5.2.2. Preparation of HPCAs

HPCAs were prepared by mixing MPI or HPI with RC at ratios of 100:0, 70:30, 50:50, 30:70 and 0:100 to achieve a total protein content of 18% (wet weight). As reported by Lu et al. (2025), the formulation for HPCAs included 18% protein, 20% coconut oil, 0.5% sodium chloride, 0.5% calcium sulfate, 0.1% potassium sorbate, 2.8% trisodium citrate and water on a weight ratio basis, with pH adjusted to 5.4 using citric acid. HPCAs were prepared using a Rapid Visco Analyser

(RVA-4; Newport Scientific Pty Ltd, Warriewood, NSW, Australia). HPCAs samples of 30 g were prepared in an aluminium cell fitted with a polycarbonate paddle. All dry ingredients and coconut oil were manually blended with water for 5 min and then hydrated for 1 h at room temperature in an aluminium cell. The mixture was processed using the following RVA profile: equilibration at 50 °C, followed by heating to 90 °C over 4 min, maintaining at 90 °C for 10 min. The sample was then cooled to 50 °C at a rate of 0.2 °C/s, mixing at 300 rpm from heating to cooling stages. The resulting samples were labelled MPI100, MPI70, MPI50, MPI30, HPI100, HPI50 and RC100, with the numbers indicating the plant protein ratios. Individually packed samples were stored at 4 °C and analysed using Raman spectroscopy within 1 week.

5.2.3. Instrumentation and parameters

A LabRAM HR Evolution Raman confocal microscope (HORIBA France SAS) was used to generate Raman images for HPCAs. This microscope is equipped with 532 and 785 nm excitation lasers and a thermoelectrically cooled charge-coupled device detector. Cheese samples were scanned using a 532 nm excitation wavelength with adjusted laser power to minimize fluorescence. For example, a laser power of 37.5 mW was used, corresponding to an estimated power density of approximately 190 mW/μm² for MPI–RC samples, while half of this power was applied to HPI–RC samples. A 100× oil immersion objective and a T1: 600 gr mm^{-1} BLZ = 500 nm grating were used, giving a spectral resolution of 2–3 cm^{-1}.

The 532 nm excitation was selected to provide strong Raman scattering and high spatial resolution. Preliminary tests confirmed that the fluorescence background was manageable, and multiple spectra were collected from the same area to ensure that no significant spectral changes occurred during measurement.

5.2.4. Raman imaging

Cheese samples were stored at 4°C and cut into thin layers (1–2 mm) using a razor blade was covered with a cover glass. Images were immediately acquired at 4°C using a heating and cooling stage (THMS600 Linkam) with a 100× (1.30 NA) oil immersion lens and a 50 μm pinhole aperture. The images were acquired at 10–15 μm below the cut surface of the samples, and random regions in each sample were scanned. For low-resolution imaging, spectra were recorded in the range of 200–1800 cm^{-1} with a 0.5 s integration time and a 5 μm step with 41 and 21 increments in the x- and y-directions, respectively, to sample an area of 200 × 100 μm. For high-resolution imaging, spectra were recorded in the range of 200–1800 cm^{-1} with a 0.5 s integration time over a grid measuring 1.5 × 1.5 μm and 34 increments in both directions to sample an area of 50 × 50 μm. The same formulation was imaged with low-resolution mapping in three technical replicates and high-resolution mapping in two technical replicates. For each replicate, a single field of view was scanned, with an acquisition time of 0.5 s per point and a total imaging time of ~10 min.

5.2.5. Reference spectra of cheese ingredients

The reference Raman spectra of individual cheese ingredients, including hydrated RC, HPI, MPI, coconut oil, trisodium citrate (TSC), calcium sulfate and citric acid, were acquired using glass slides covered with aluminium foil. Spectra were collected with a 532 nm excitation laser (37.5 mW), a 50× objective lens, a 50 μm pinhole aperture and an acquisition time of 10 s. The presented reference spectra represent the average of at least three replicates ($n \geq 3$).

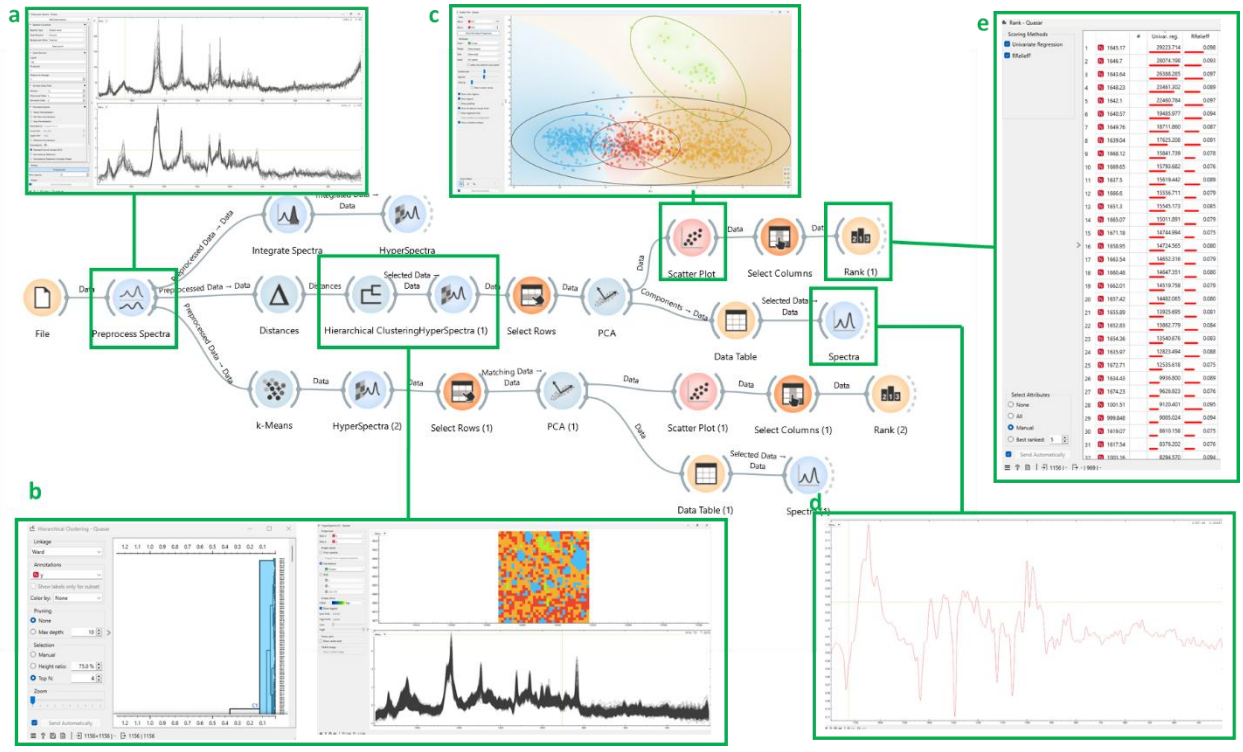
5.2.6. Raman imaging data processing using Quasar

Raman imaging data were analysed using Quasar, an open-source Python library designed for ML and spectral data visualisation (Toplak et al., 2021). A representative workflow with a few

examples of hierarchical clustering is shown in **Figure 5-1A**. Raw data were pre-processed using rubber band correction (with the peak direction set to positive and the background action set to subtract), spike removal and Savitzky–Golay smoothing (window size, 13; polynomial order, 3) and normalised using a standard normal variate to enhance spectral quality and address fluorescence interference (**Figure 5-1A**_a). Multiple analytical approaches were used to map the chemical composition of samples. To visualise key chemical components, integrated peak mapping was performed using specific spectral regions: 1730–1750 cm^{-1} for lipids, 1600–1700 cm^{-1} for amide I, and 1200–1300 cm^{-1} for amide III, peak height of 1001 cm^{-1} for phenylalanine (Phe) and 834 cm^{-1} for TSC. In addition, two unsupervised clustering algorithms, hierarchical and k-means clustering, were used to classify spectral features and distinguish proteins in mixed systems. Hierarchical clustering using Ward's linkage generated a dendrogram (**Figure 5-1A**_b), iteratively grouping similar data points, whereas k-means clustering divided data into a predefined number of clusters (K), iteratively adjusting cluster centroids until convergence. These approaches were applied to the spectral range of 200–1800 cm^{-1}, with 3–6 clusters being selected to efficiently differentiate between lipids, protein types and other cheese components. After initial clustering, the spectra in each cluster were carefully examined, and the number of clusters was adjusted if necessary to ensure that lipids, protein types, and other cheese components were properly differentiated. Principal component analysis (PCA) was used to reduce dimensionality and visualise clusters on scatter plots (**Figure 5-1A**_c). Loading plots were examined to identify Raman shifts contributing to spectral variance and interpret key spectral features differentiating the chemical compositions of samples (**Figure 5-1A**_d). The first principal component (PC1) was used to capture protein-related variance. Subsequently, Raman shifts were ranked based on the

absolute values of their PC1 loadings, highlighting the spectral regions most strongly associated with protein differentiation in the absence of class labels (**Figure 5-1A**_e).

A



B

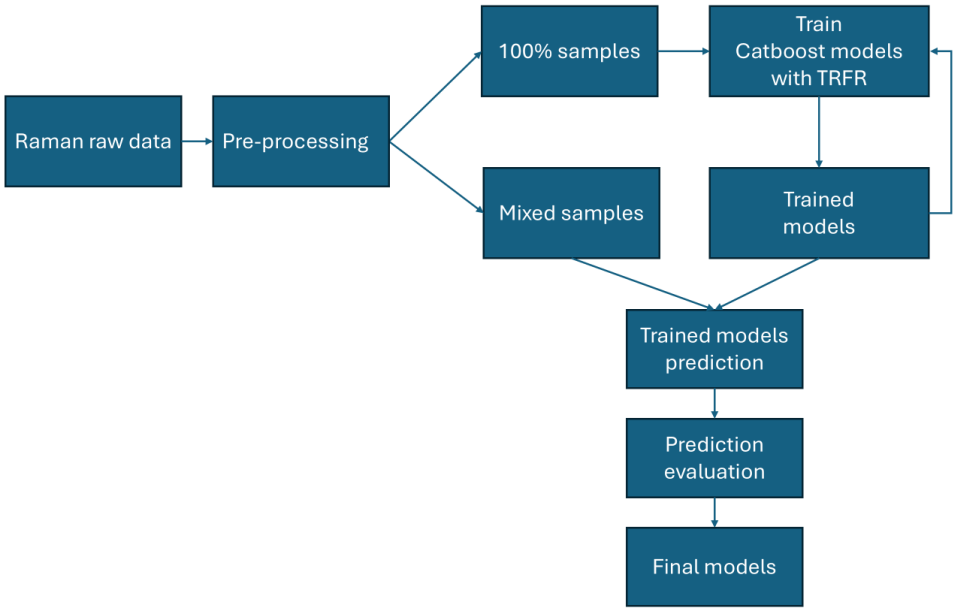


Figure 5-1. Workflow for unsupervised analysis in Quasar (A). The 200–1800 cm−1 data were pre-processed with baseline correction, spike removal, Savitzky-Golay smoothing, and normalization (Box a). Hierarchical clustering grouped spectra into four clusters, with corresponding hyperspectral images (Box b). Principal Component Analysis (PCA) of PC1 and PC2 visualized cluster separation: PC1 separates the blue, red, and yellow clusters, while PC2 separates the green cluster (Box c). Loading plots from PC1 identified Raman shifts contributing to spectral variance (Box d), which were ranked by significance for feature selection (Box e). Workflow for supervised classification using CatBoost with Top-Ranked Feature Removal (TRFR) (B): pre-processed single-protein cheese samples trained the models, which were used to predict protein type in mixed cheese samples. Two prediction evaluations were used to determine whether additional training cycles were required.

Tyrosine doublet ratio (I_{850}/I_{830}) was analysed after being pre-processed in Quasar described above, including baseline correction and normalization. Spectral clusters corresponding to different proteins were identified using k-means clustering. The spectra within each cluster were then averaged, and the tyrosine doublet ratio was determined from the mean spectrum of each cluster. Results are presented as mean values (in triplicate) with standard deviations.

5.2.7. Raman imaging data processing using CatBoost and transfer learning

The data processed using Quasar were analysed using Python on the Google Colab platform. CatBoost ML models were trained using MPI100, HPI100 and RC100 datasets to classify protein types. Data related to fat content were removed based on their values at a Raman shift of 1744 cm^{-1}, with the threshold set at 60% of the value range at 1744 cm^{-1}. The datasets were randomised and validated through 5-fold cross-validation before training with the whole dataset. Accuracy was used as the primary performance metric to evaluate the model. The CatBoost classifier was trained for 100 iterations with a tree depth of 4 and a learning rate of 0.1. The Logloss function was employed as the optimization objective. A fixed random seed (42) was applied to ensure model reproducibility. The trained models demonstrated the ability to distinguish MPI and HPI from RC.

To extend the applicability of the trained models, a transfer learning approach was implemented to enable the transfer of learned knowledge from models trained on single-protein cheese samples to mixed-protein cheese samples. This approach allowed the models to predict protein types in mixed-protein cheese samples, leveraging prior knowledge from pure protein systems. In addition, a feature selection method, top-ranked feature removal (TRFR), was integrated into the training process. TRFR iteratively removed the highest-ranked features identified by the models, compelling the models to learn from lower-ranked spectral features. This strategy aimed to enhance model robustness and improve generalisability in predicting protein composition in complex systems. The trained models were used to predict protein types in mixed-protein cheese samples, and the prediction results were used to evaluate the performance of the TRFR-trained models. The prediction evaluation was determined by two criteria: the similarity between the predicted and actual protein ratios and the similarity between the predicted plots and previous confocal laser scanning microscopy (CLSM) observation analysis (Lu, Roy, et al., 2026).

CatBoost was chosen in this study for its efficiency and robustness in handling complex datasets. Unlike traditional gradient boosting algorithms, CatBoost employs ordered boosting, which reduces overfitting and target leakage. Moreover, its default parameters generally provide strong performance with little or no hyperparameter tuning. The workflow of the training process is shown in **Figure 5-1B**.

5.2.8. Deconvolution of the amide I region

Deconvolution of the amide I region (1600–1700 cm^{-1}) was performed for quantitative analysis. The average spectrum from the protein cluster identified using k-means clustering was extracted using Quasar. The spectrum was subjected to baseline correction using a linear method between two selected points in the spectrum and smoothed using a 5-point Savitzky–Golay filter with a polynomial order of 2 to enhance the signal-to-noise ratio in Origin® (2021b). Peak fitting was performed using the second derivative method, followed by iterative Gaussian peak fitting. Peak assignment was performed using known Raman spectral data for secondary protein structures. Several iterations were performed until the fit converged, ensuring a final fitting curve with a corrected R^2 value of ≥0.99. The area under each peak was calculated relative to the total area and expressed as a percentage.

All results were expressed as the mean and standard deviation, as calculated from the three average spectra collected from three different images. Data were subjected to one-way analysis of variance using SPSS, followed by Tukey's comparison test. Differences were considered significant at a p-value of <0.05. The reported values for β-sheets and β-turns represent the cumulative contributions of multiple peaks.

5.3. Results and Discussion

5.3.1 Overview of Raman spectra of components in HPCAs

This section briefly summarises the Raman spectra of protein and lipid components. Cheese exhibits several characteristic bands suitable for Raman imaging, particularly within the 200–1800 cm^{-1} region (Smith et al., 2017). Studies have identified Raman bands associated with proteins and lipids (Wang, 2016; Nickless, 2020; Smith, 2017) (**Table 5-1Table 5-1**).

In the 200–1800 cm^{-1} region, key protein-related bands provide insights into the identification and secondary structures of proteins. For instance, the phenylalanine ring breathing mode at 1001–1003 cm^{-1} serves as a marker for protein presence. The amide I band (1600–1700 cm^{-1}), primarily associated with C=O and N–H stretching vibrations, reflects protein secondary structures depending on hydrogen bonding and the conformation of polypeptides: α-helices at 1645–1657 cm^{-1}, random coil structures at 1650–1660 cm^{-1}, β-sheets at 1665–1680 cm^{-1} and β-turns at 1670–1699 cm^{-1}. The amide III band (1200–1300 cm^{-1}), which corresponds to C–N stretching and H–N–C bending vibrations, further distinguished protein secondary structures as follows: β-sheets at 1238–1245 cm^{-1}, random coils near 1250 cm^{-1} and α-helices at 1260–1300 cm^{-1}, which often overlapped with β-turns (Smith, 1994; Wang et al., 2016; Zhao et al., 2004). These spectral features are essential for differentiating plant proteins from casein in complex food matrices. Herein, the reference Raman spectra of RC and HPI exhibited differences in respective amide I and amide III bands, with RC showing bands at 1663, 1257 and 1238 cm^{-1} and HPI showing bands at 1665, 1260 and 1240 cm^{-1} (Supplementary **Figure S 5-1**). These slight shifts suggest differences in the contents of secondary structures, particularly β-sheets and random coils, which may influence protein conformation and hydrogen interactions. In addition, the Raman spectrum of HPI showed bands at 528 and 542 cm^{-1}, indicating the presence of disulfide bonds. Similar findings have been reported in our previous study (Lu, Roy, et al., 2026).

The reference Raman spectrum of coconut oil exhibited bands at 1746, 1655, 1440, 1298, 1125, 1082, 1062, 890 and 871 cm^{-1} (Supplementary **Figure S 5-1**). These bands correspond to specific molecular vibrations, including C=O stretching vibrations in triacylglycerol esters (1746 cm^{-1}); C=C stretching vibrations (1655 cm^{-1}); CH_2 scissoring associated (1440 cm^{-1}); CH_2 twisting attributed to phospholipids such as phosphatidylcholine (PC), phosphatidylinositol (PI) and phosphatidylserine (PS) (1298 cm^{-1}); C–C stretching vibrations in fatty acids, specifically saturated fatty acids (1082, 1062 and 1125 cm^{-1}); and phospholipid headgroup vibrations (890 and 871 cm^{-1}).

Table 5-1. Typical Raman shifts of Raman bands and general assignments in protein and lipid structure in the range of 200–1800 cm^{-1}.

Origin	Raman shifts (cm^{-1})	Assignment and Structural information
Cystine	496–513	S-S stretch
	514–525	*gauche−gauche−gauche* conformation, *gauche−gauche−trans* conformation
	527–548	*trans−gauche−trans* conformation
	630–670	*gauche* C-S of Met, Cys, Cys/2
	700–745	*trans* C-S of Met, Cys, Cys/2
Tyrosine	850/830	Fermi resonance between ring fundamental and overtone State of phenolic OH group (exposed or buried, hydrogen-bond donor or acceptor)
Tryptophan	760, 880, 1360	Indole ring Sharp intense band indicates buried residues; sensitive to environment polarity
Phenylalanine/tyrosine	622/644	Ring breathe I622/I644 indicates the ratio of Phe and Tyr
Phenylalanine	1003	Ring breathe Conformation insensitive; useful as an internal intensity standard
Aspartic and glutamic acids	1400−1430	C=O stretch of COO^- Ionized carboxyl groups
Aliphatic residues	1450, 1465	C−H bending Microenvironment, polarity

Tyrosine, tryptophan, phenylalanine residues	1610−1616	C=C stretch, aromatic ring vibrations
amide I	1650−1685	Amide C=O stretch, N–H wag
amide III	1235–1300	N–H in-plane bend, C–N stretch
Phospholipids	890, 871	phospholipid headgroup vibrations
	1298	CH_2 twisting attributed to phospholipids such as phosphatidylcholine (PC), phosphatidylinositol (PI), and phosphatidylserine (PS)
Fatty acids	1082, 1062	C–C stretching from fatty acids
	1125	C–C stretching from saturated fatty acids
	1440	CH_2 scissoring
Unsaturated fatty acids	1655	C=C stretching
Ester groups of lipids	1744	C=O carbonyl fats

Adapted from Nickless and Holroyd (2020), Smith (1994), Smith et al. (2017),Wang et al. (2016), and Zhao et al. (2004)

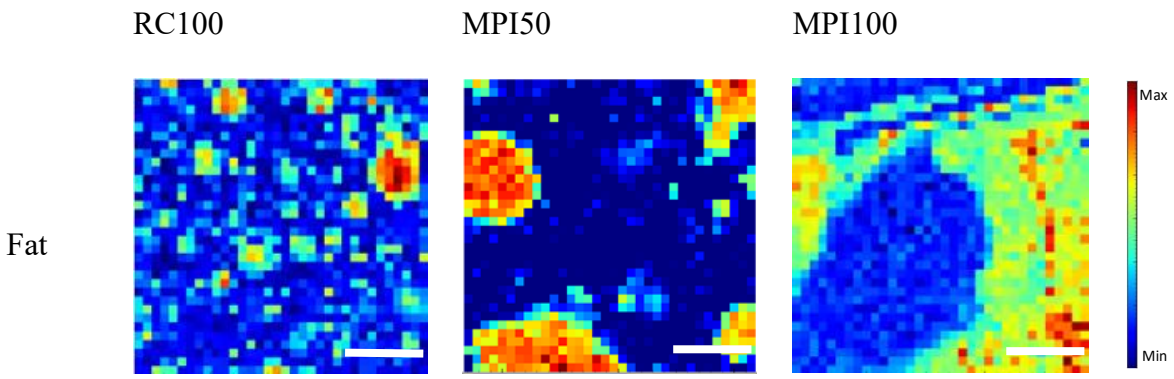
5.3.2 Spatial distribution of components in both single- and dual-protein cheese systems

Initially, Raman images were generated using higher-spatial-resolution datasets, with a 1.5 μm step to cover an area of 50 × 50 μm. The spectral intensity at specific wavenumber ranges corresponding to key chemical components, such as fat (1730–1750 cm^{-1}), protein-related bands, including Phe ring breath (1001 cm^{-1}), the amide I (1600–1700 cm^{-1}), the amide III (1200–1300 cm^{-1}), and TSC (834 cm^{-1}). Integrated peak maps enabled the analysis of the spatial distribution and concentration of various chemical bonds, facilitating structural interpretation and interface characterisation (Nickless & Holroyd, 2020). **Figure 5-2** presents representative Raman images of RC100, MPI50 and MPI100, demonstrating structural differences among these formulations. In RC100, fats were present as small, uniformly distributed droplets (approximately 1.5–5 μm), whereas proteins, observed from the Phe, amide I, and amide III peaks, formed a continuous and

homogeneous network. All three spectral regions showed similar spatial distributions of protein, confirming consistent identification of protein-rich domains. Differences in color intensity arise from variations in Raman scattering efficiency and vibrational origin. Thus, the observed intensity differences represent complementary contrast rather than inconsistency in protein mapping. After the incorporation of MPI into RC (MPI50), the fat droplet size increased to approximately 5–25 μm; however, in MPI100, fats coalesced into larger pools. Concurrently, plant protein formed aggregates, disrupting the continuous casein network in MPI50. These findings are consistent with those of CLSM reported in the previous study (Lu, Roy, et al., 2026), demonstrating the structural modifications induced by plant protein addition. As the plant protein content increased, fat–protein interactions weakened, leading to greater microstructural segregation and larger fat droplet formation. Although casein in RC100 effectively stabilised fat droplets, the introduction of MPI disrupted the protein network, reducing the emulsification capacity of casein. This disruption is likely attributed to the higher molecular weight of plant proteins and the limited exposure of hydrophobic sites, which tend to remain buried within the compact molecular structures of plant proteins (Kim et al., 2020). The Raman images of other HPCAs formulated with different plant protein ratios (MPI30 and MPI70) and protein types (HPI50) are provided in Supplementary **Figure S 5-2**. These images confirmed that the selected feature peaks can effectively distinguish different components and reveal microstructural changes across formulations. In terms of protein type, the Phe-rich component in HPI exhibited smaller, more fragmented pixels, whereas MPI appeared as larger patches and aggregated regions (HPI50 vs MPI50).

Furthermore, Raman imaging enabled the identification and spatial mapping of TSC, which was detected within the casein matrix in RC100 but not within the MPI matrix in MPI100. This difference may occur because mung bean protein lacks the strong calcium-binding sites found in

casein, which limits its interaction with TSC. Incorporating TSC resulted in a shift in its characteristic bands from 844 and 955 cm^{-1} (as observed in the reference spectrum of TSC, Supplementary **Figure S 5-1**) to 834 cm^{-1} and 969 cm^{-1}, respectively, in all cheese matrix. This shift is likely indicative of calcium citrate formation, as citrate molecules sequester Ca^{2+} ions to inhibit the formation of large casein-coated fat globules, thereby enhancing cheese stability through an emulsifying effect. The other spectral shifts observed in MPI–RC formulations, in which calcium sulfate was included, further support the likelihood of calcium citrate formation. These findings are consistent with those of previous studies, as pure calcium citrate exhibits characteristic bands at 836 and 970 cm^{-1}, which are similar to those detected in the hybrid cheese matrix (Campos et al., 2022; Smith et al., 2017). Other ingredients present at concentrations below 1% in the cheese formulations were not detected on Raman images. This phenomenon may be attributed to subsampling, that is, these ingredients were absent in the analysed regions, or their concentrations were too low to be detected using the selected instrument parameters (Smith et al., 2017).



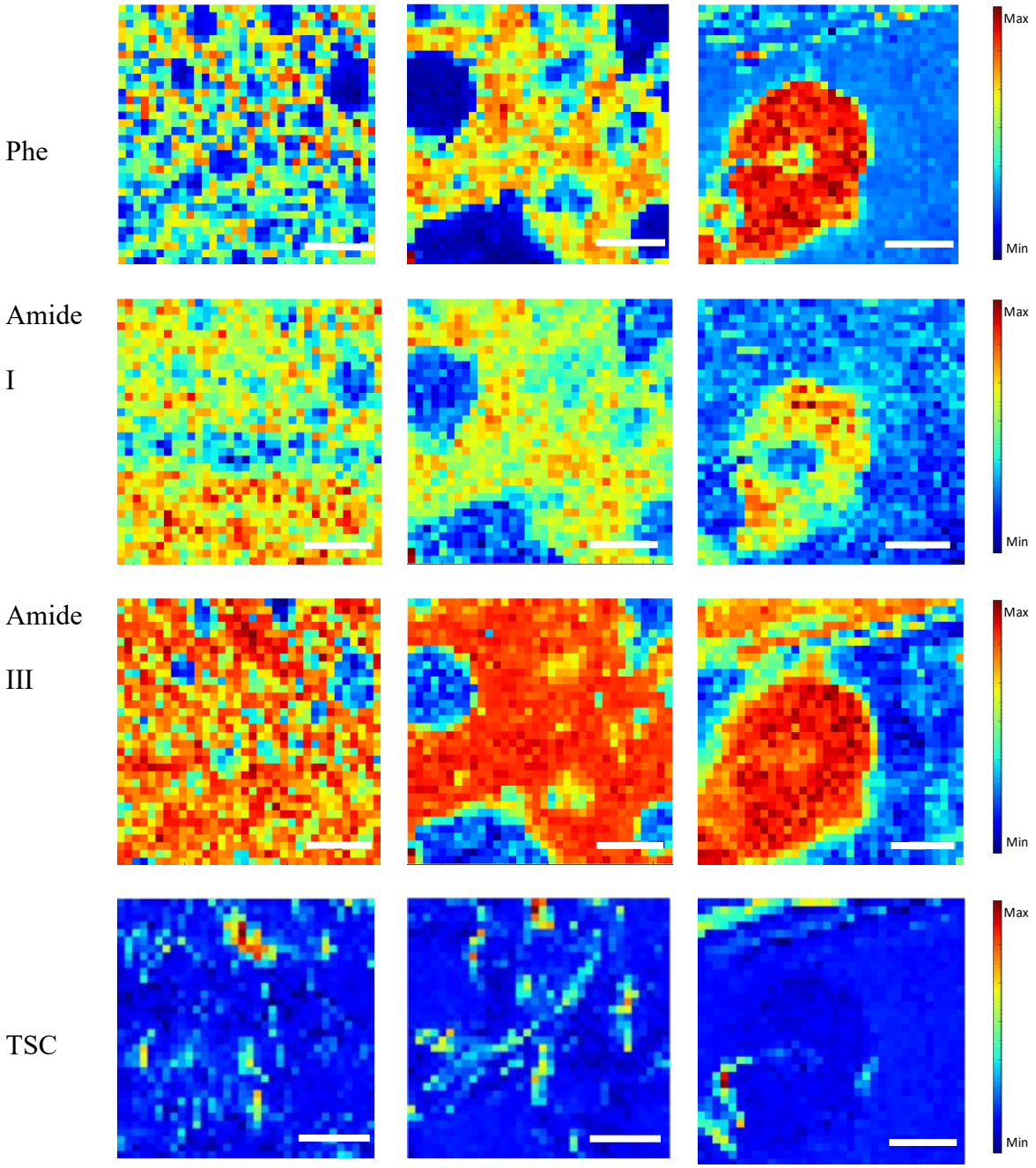


Figure 5-2. Raman images of processed cheeses formulated with 100% rennet casein (RC100), 50% rennet casein and 50% mung bean protein (MPI50), and 100% mung bean protein (MPI100). Distribution of fat (1730–1750 cm^{-1}), phenylalanine (Phe, 1001 cm^{-1}), amide I (1600–1700 cm^{-1}), amide III (1200–1300 cm^{-1}), and trisodium citrate (TSC, 834 cm^{-1}) is shown, with red indicating high and dark blue low concentration. The scale bars are each 15 μm in length.

5.3.3. Distinguish plant proteins and caseins in dual-protein cheese systems

To distinguish plant proteins from casein in mixed-protein cheese formulations, the Raman spectra of MPI, HPI and RC were initially recorded in single-protein cheese systems. Briefly, the average spectra of MPI, HPI, RC and coconut oil were extracted from MPI100, HPI100 and RC100 samples, respectively, by selecting the lipid and amide I regions with high intensity (**Figure 5-3**). As the Raman spectrum of coconut oil showed no significant differences among RC100, MPI100 and HPI100, the spectrum of coconut oil in RC100 was used as a representative. This spectrum provides insights into protein structures in a single-protein cheese system and differences between these structures. Although changes in spectral regions corresponding to proteins and fats were observed before and after processing (compared with their reference spectra), discussing the effects of processing on structural changes in proteins and fats is beyond the scope of this study.

The Raman spectrum of RC100 (**Figure 5-3A**, green) exhibited lipid-related peaks at 1738, 1440, 1297, 1123 and 1060 cm^{-1} and protein-related peaks at 1648, 1614, 1251, 1001, 850 and 830 cm^{-1}. These findings indicate co-localization of protein and lipid signals, suggesting possible protein-lipid interactions via the hydrophobic effect within the matrix. However, these co-localizations were not detected in HPI100 and MPI100, as there were no peaks at 1738 cm^{-1} for C=O stretching vibrations in triacylglycerols and 1297 cm^{-1} for CH_2 twisting in phospholipids.

Several protein-related Raman peaks provide valuable insights for comparing different proteins in cheese. In the amide I region (**Figure 5-3B**), HPI exhibited a peak at 1649 cm^{-1}, which is primarily attributed to α-helical structures. In the amide III region (**Figure 5-3C**), HPI showed distinct peaks at 1264 (α-helices), 1250 (random coils) and 1233 (β-sheets) cm^{-1}, suggesting a mixed secondary structure composition. In the amide I region, RC showed a peak at 1648 cm^{-1}, which is also indicative of α-helical structures; however, this peak may be influenced by coconut oil, given its proximity to the 1651 cm^{-1} band associated with lipids (Smith et al., 2017). In addition, RC showed

a small shoulder at 1670 cm^{-1}, which is typically attributed to β-sheet formation, and a broad peak at 1251 cm^{-1} in the amide III region, which is associated with random coils. On the contrary, MPI exhibited a dominant α-helical signature with peaks at 1650 and 1265 cm^{-1} alongside β-sheet–related peaks at 1666 and 1243 cm^{-1}. These spectral differences suggest variations in protein structures and potential interactions within the cheese matrix. The presence of both α-helices and β-sheets in MPI indicates a more structured protein conformation than that in HPI or RC, whereas the broad peak at 1251 cm^{-1} in RC suggests increased protein unfolding, a more unordered structure or reduced secondary structure stability.

The tyrosine (Tyr) doublet bands at 830 and 850 cm^{-1} result from the Fermi resonance and ring vibrations of the para-substituted benzene ring (Smith, 1994). The intensity ratio, I_{850}/I_{830} monitors the hydrogen bonding and accessibility of the phenolic hydroxyl (OH) groups, indicating whether the Tyr residues are exposed or buried. If the I_{850}/I_{830} ratio is >1, Tyr residues are most likely located on the protein network surface. The phenolic OH groups are involved in moderate-to-weak hydrogen interactions (acting as both proton acceptors and donors). If the I_{850}/I_{830} ratio is <1, Tyr residues are likely to be fully or partially buried inside the protein structure. The phenolic OH groups function as proton donors in strong hydrogen interactions (Sadat et al., 2022).

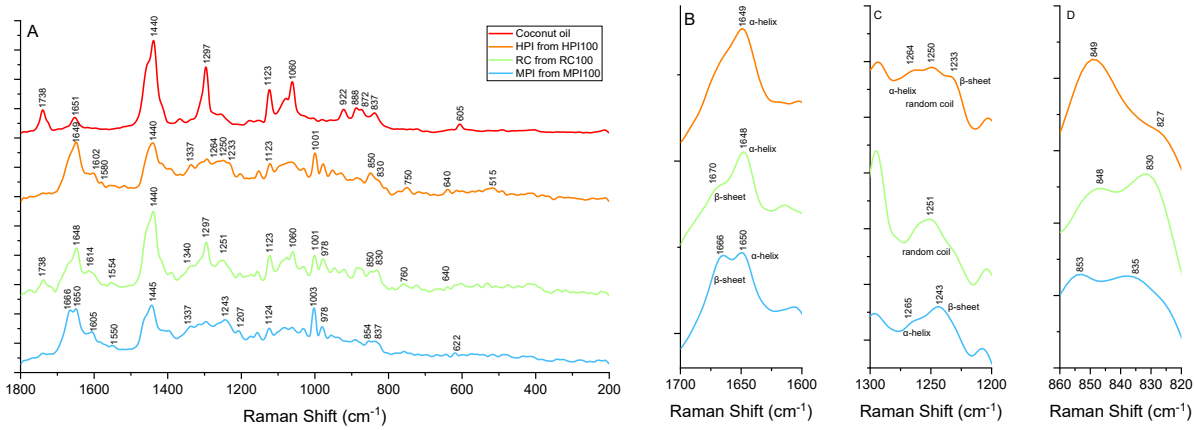
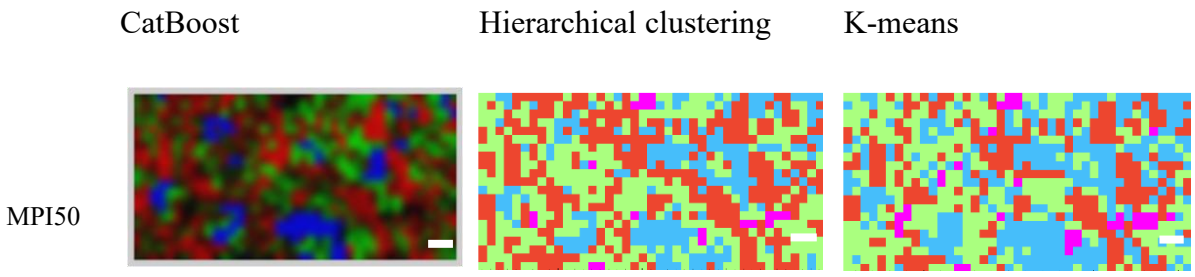


Figure 5-3. Average Raman spectra of mung bean protein, hemp protein, casein protein, and coconut oil extracted from cheese formulated with 100% mung bean protein (MPI100), 100% hemp protein (HPI100), and 100% rennet casein (RC100) by selecting the lipid and amide I regions with high intensity in the range of 200–1800 cm^{-1} (A), amide I region (1600–1700 cm^{-1}) (B), amide III region (1200–1300 cm^{-1}) (C), and tyrosine residues region (820–850 cm^{-1}) (D).

As shown in **Figure 5-3D**, RC had an I_{850}/I_{830} ratio of <1 (0.76) (data in Supplementary **Table S 5-1**), which suggests that Tyr residues are buried within the protein network. This finding may be attributed to the strong casein–casein interactions forming a dense, cross-linked matrix in the cheese. This matrix buries many Tyr residues and promotes strong hydrogen interactions, potentially influencing the firmness and elasticity of the cheese. On the contrary, the I_{850}/I_{830} ratio of HPI was >1 (4.5), which indicates that Tyr residues are mostly exposed in HPI. This finding suggests weaker protein–protein interactions, which allow Tyr residues to be more accessible for forming hydrogen bonds with water. These interactions contribute to a softer texture in cheese, a finding consistent with those reported by Lu, Roy, et al. (2026). The I_{850}/I_{830} ratio of MPI (1.15) was between those of RC and HPI, indicating the exposure of some Tyr residues. The reported ratios were derived from pre-processed, averaged spectra and should be interpreted cautiously, as they mainly illustrate relative trends in Tyr residue exposure among protein systems.

Given the large dataset, both supervised (CatBoost) and unsupervised (hierarchical clustering and k-means) models were used to differentiate mung bean protein and hemp protein from casein in dual-protein cheese systems. **Figure 5-4** presents the Raman images of MPI50 and HPI50 along with their corresponding average spectral data. The CatBoost model was trained using labelled data from RC100, MPI100 and HPI100, with predictions displayed as follows: RC in green, MPI

or HPI in blue and lipids in red in MPI50 and HPI50 samples. Results showed that the model effectively applied learned patterns to predict protein distribution in mixed-protein cheese systems, even as spectral characteristics changed. CatBoost provides the advantage of feature ranking using its tree-based algorithm, which identifies the relative importance of each Raman shift in the predictive performance of the model (Supplementary **Figure S 5-3**). This ranking helps understand the key spectral regions that contribute most to the differentiation of protein sources, offering insights into the underlying chemical differences. The model revealed that the wavenumber region near 1440–1460 cm^{-1} was most significant for distinguishing RC from MPI, whereas the regions at 1440–1460, 1280 and 1367 cm^{-1} were most significant for differentiating RC from HPI. These Raman shifts correspond to vibrational modes associated with CH_2/CH_3 bending (1440–1460 cm^{-1}), amide III and C–N stretching (near 1280 cm^{-1}) and CH deformation or bending (near 1367 cm^{-1}), which reflect differences in the protein backbone structure, side-chain composition and lipid or hydrophobic group interactions between RC and plant proteins (Shoko et al., 2024; Smith et al., 2017; Smith, 1994; Z. Y. Zhang et al., 2023). In particular, casein, rich in hydrophobic residues, exhibits a side-chain environment and protein–lipid association distinct from those of globular plant proteins, leading to stronger CH_2/CH_3 and amide III band intensities. The 1440–1460 cm^{-1} region likely serves as a proxy for lipid-associated domains, consistent with the stronger lipid co-localization observed in RC-containing systems.



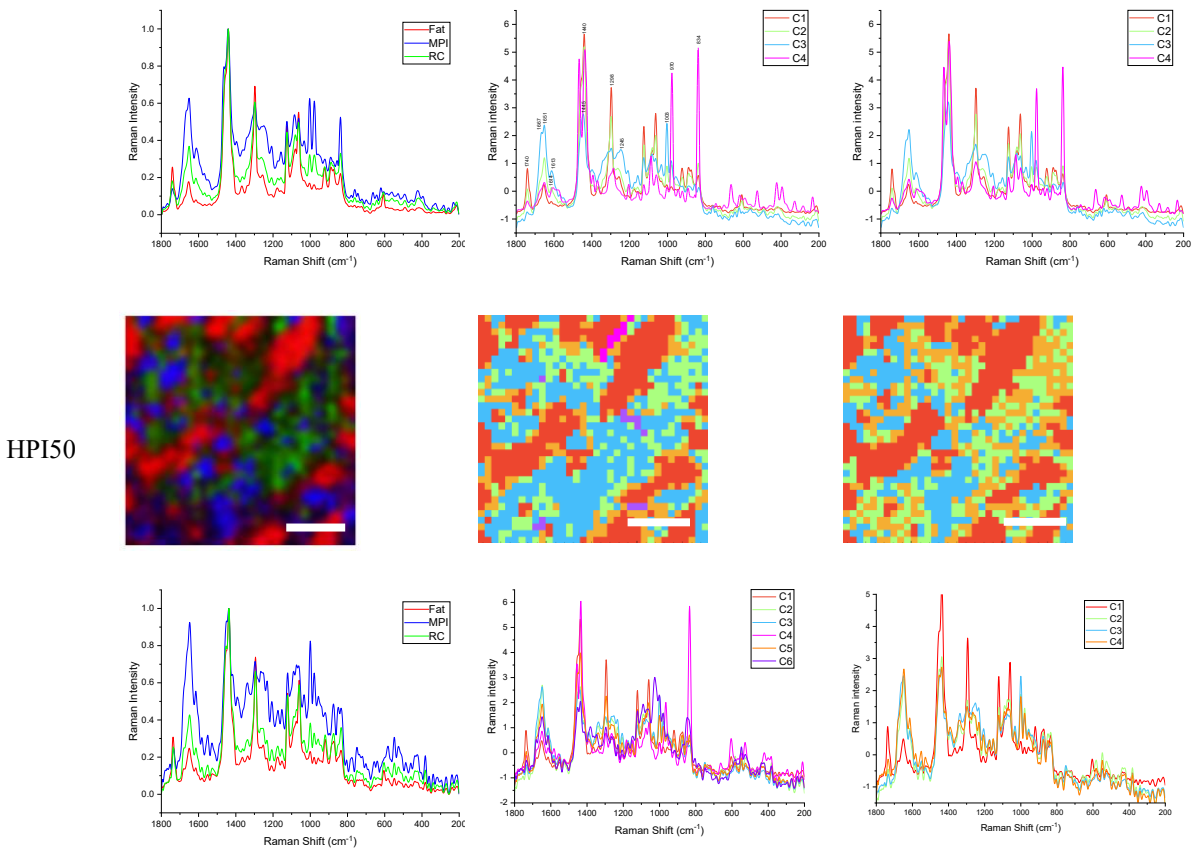


Figure 5-4. Raman images of MPI50 and HPI50 cheeses (top) and their average spectra data (bottom) using the CatBoost (left), hierarchical clustering (middle), and k-means models (right). The CatBoost model was trained using single-protein cheese samples – RC100, MPI100, and HPI100 – with predicted RC shown in green, mung bean/hemp protein in blue, and fat in red in MPI50 and HPI50. MPI50 was imaged at low resolution (5 × 5 µm grid, 200 × 100 µm area) and HPI50 at high resolution (1.5 × 1.5 µm grid, 50 × 50 µm area). Colors indicate clusters from hierarchical clustering or k-means. Scale bars are 15 µm in length. MPI50: cheese formulated with 50% mung bean protein and 50% rennet casein. HPI50: cheese formulated with 50% hemp protein and 50% rennet casein.

The Raman images generated using the CatBoost model served as a reference for comparing with those obtained from hierarchical and k-means clustering. For simplicity, the clustering results are interpreted as follows: red represents fats, green represents RC-dominated regions, blue represents MPI/HPI-dominated regions, pink represents TSC and orange represents the interface between fats and proteins. Of both unsupervised methods, k-means clustering identified plant proteins in a manner more consistent with CatBoost predictions. These findings align with previously reported

CLSM and transmission electron microscopy findings (Lu, Roy, et al., 2026), such as the circular structures observed in MPI particles. Supplementary **Figure S 5-4** provides additional Raman images of HPCAs. The results show that these analysis models are consistent and can distinguish components in hybrid cheese with different formulations. Notably, in HPI50, hierarchical clustering required six clusters to distinguish HPI from RC, whereas k-means clustering achieved this differentiation using only four clusters. Both unsupervised models detected additional components, such as TSC. In addition, they successfully identified interfaces between fats and proteins in the high-resolution images of HPI50.

PCA was performed to the protein-specific clusters in MPI50 identified using k-means clustering (i.e. fats, TSC and interface clusters were removed) to distinguish RC from MPI. PC1 successfully mapped their spatial distribution (**Figure 5-5A**). The PC1 loadings plot showed that positive loadings were dominated by lipid-associated bands, including 1741, 1440, 1297, 1123 and 1063 cm^{-1}, whereas negative loadings were dominated by protein-associated bands, including 1668, 1650, 1606,1400, 1240, 1003, 956 and 855 cm^{-1} (**Figure 5-5C**). Ranking variables by their absolute values confirmed that the amide I region (1667–1674 cm^{-1}), which is associated with β-sheets, was most influential in differentiating MPI from RC. Additional contributors included lipid-related peaks, Phe bands and amide III differences (**Figure 5-5E**). These findings are consistent with the spectral characteristics observed in single-protein cheese systems (RC100 and MPI100), highlights that the higher content of β-sheets content in MPI than in RC is a key factor influencing the structural and functional properties of the hybrid cheese matrix.

A similar trend was observed in the case of HPI50 (**Figure 5-5B**), wherein both PC1 loadings and importance ranking scores highlighted amide I as a key spectral region contributing to the differentiation between RC and HPI. In this region, spectral variations were observed near 1660

(random coils) and 1664–1672 cm^{-1} (β-sheets) (**Figure 5-5D** and **F**). Additional contributors identified from PC1 loadings included peaks at 1603 (Phe), 1542 (amide II), 1334 (possibly CH bending or side-chain vibrations) (Shoko et al., 2024), 933 (β-sheet stretching), 900 (tentatively assigned to C–C stretching or ring vibrations) (Freire et al., 2017), and 754 cm^{-1} (possibly Cystine C-S stretching) (Smith, 1994). These spectral differences effectively reflected the spatial distributions of HPI and RC in HPI50.

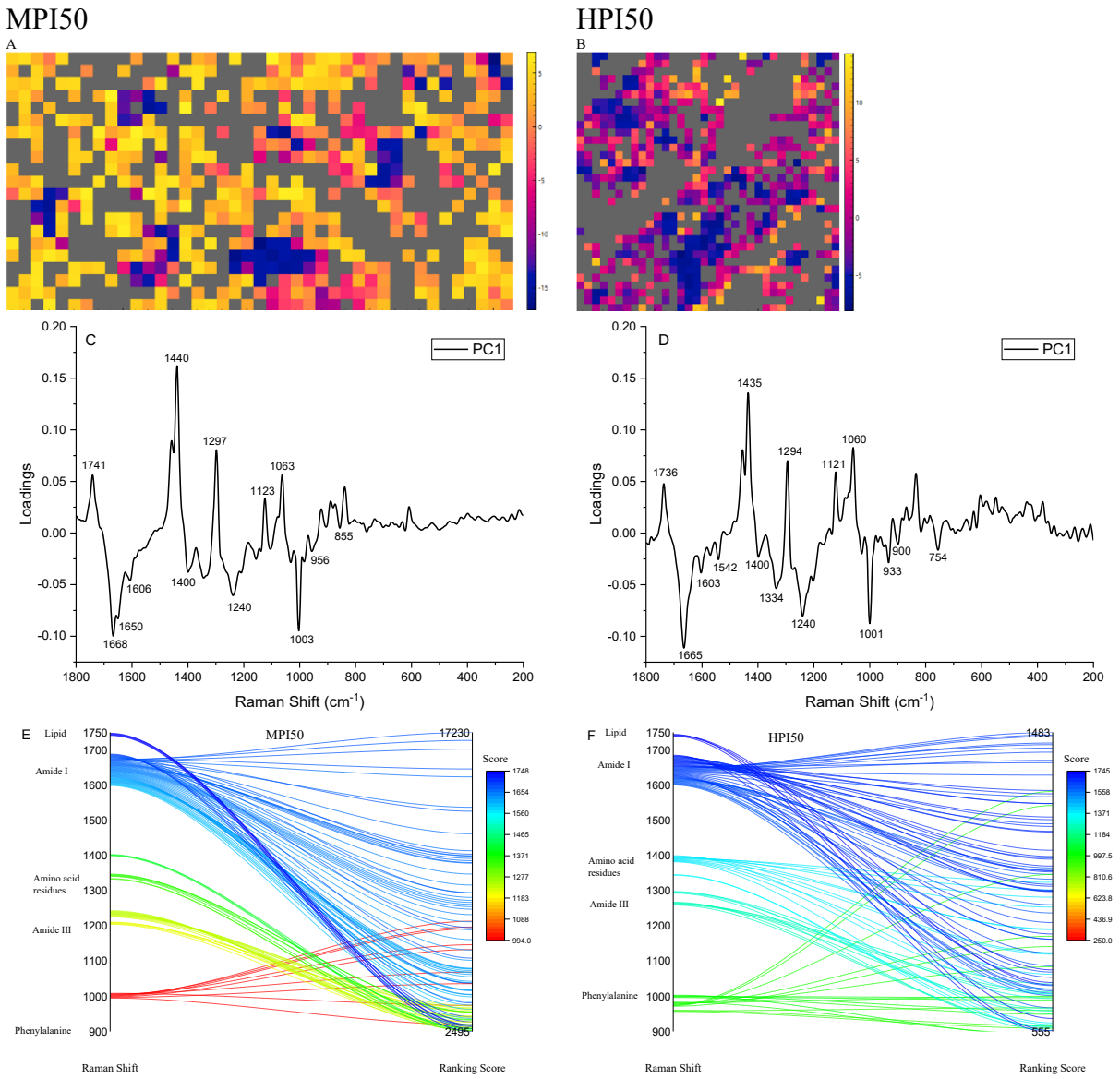


Figure 5-5. Raman images of MPI50 and HPI50 based on PC1 scores for the 200–1800 cm^{-1} region (A & B, yellow = high, dark blue = low plant protein concentration), with corresponding

loadings plots (C & D). Top 100 Raman shifts distinguishing RC from MPI or HPI are ranked (E & F), with lines connecting each shift (left axis) to its importance score (right axis, colour-coded). MPI50 was imaged at low resolution (5 × 5 μm grid, 200 × 100 μm), HPI50 at high resolution (1.5 × 1.5 μm grid, 50 × 50 μm). Key bands include Amide I (1600–1700 cm^{-1}), Amide III (~1250–1300 cm^{-1}), and bands associated with lipid (1745 cm^{-1}). MPI50: cheese formulated with 50 % mung bean protein and 50 % rennet casein. HPI50: cheese formulated with 50 % hemp protein and 50 % rennet casein.

β-sheets (1664–1672 cm^{-1}) were prominent in both HPI50 and MPI50, indicating that both plant proteins influenced the secondary structure of casein, but the extent of β-sheet contribution varied. The amide II peak (1542 cm^{-1}) appeared significant in HPI50 but was less pronounced in MPI50, suggesting differences in hydrogen bonding and backbone flexibility between the two plant proteins. The presence of additional peaks in HPI50 (932, 900 and 755 cm^{-1}) indicated that interactions between HPI and RC led to more structural heterogeneity than those between MPI and RC, with distinct RC and MPI regions showing clearer spectral separation. By comparing the spectral features of mixed-protein cheeses with those of single-protein cheeses, the models successfully differentiated between plant and milk proteins while providing valuable structural insights.

5.3.4. Protein–protein and protein–lipid interactions

To examine protein–protein and protein–lipid interactions in dual-protein cheese systems, the average Raman spectra of RC, HPI and MPI in single-protein cheeses (RC100, HPI100 and MPI100, respectively) were compared with their counterparts in dual-protein cheeses (HPI50 and MPI50). The spectra were extracted using k-means clustering to assess structural changes upon mixing.

As shown in **Figure 5-6A**, the Raman spectrum of RC in MPI50 exhibited slight shifts in amide I and amide III bands (from 1670, 1648 and 1251 cm^{-1} in RC100 to 1678, 1651 and 1260 cm^{-1} in

MPI50, respectively). These spectral shifts suggest an increase in β-sheet content and potential α-helix stabilisation. On the contrary, the spectrum of RC in HPI50 showed multiple peaks in the amide III region (1265, 1251 and 1230 cm^{-1}), indicating a more heterogeneous secondary structure. These findings suggest that compared with mung bean protein, hemp protein induces greater structural heterogeneity in casein. The subsequent analysis of Tyr residues supported these structural differences. In RC100, Tyr residues were largely buried owing to strong casein–casein interactions indicated by an I_{850}/I_{830} ratio of <1 (0.76). Conversely, RC in HPI50 exhibited a slightly higher I_{850}/I_{830} ratio (~0.95) (Supplementary Table S1), suggesting higher exposure of Tyr residues owing to weakened casein–casein interactions following the incorporation of HPI. Notably, the spectrum of RC in MPI50 lacked the peak at 850 cm^{-1} but showed a sharp peak at 837 cm^{-1}. These changes indicated that more Tyr residues were buried after the incorporation of MPI, likely reflecting reduced interactions between RC and MPI. These findings are consistent with earlier observations that mung bean protein forms larger aggregates (Lu, Roy, et al., 2026; Lu et al., 2025). These aggregates create gaps between casein micelles and modify the Tyr environment in RC. The spectrum of RC in RC100 exhibited a peak at 530 cm^{-1}, which is attributed to the disulfide bonds in α_{S2}-casein. However, in MPI50, no distinct disulfide peak was observed, suggesting reduced cross-linking in the presence of MPI. Conversely, in HPI50, RC showed peaks at 526 and 549 cm^{-1}, indicating potential disulfide bond rearrangements.

On comparing the Raman spectra of MPI in MPI100 and MPI50 (**Figure 5-6B**), we found that the amide I region exhibited no significant peak shifts; however, a decrease in β-sheet intensity was observed after the incorporation of RC. No significant differences were observed in the amide III region of MPI between MPI100 and MPI50, indicating the predominance of β-sheet structures. These findings suggest that MPI retains its aggregated structure and that its interaction with casein

may lead to microstructural segregation instead of conformational changes. The I_{850}/I_{830} ratio slightly increased from 1.15 in MPI100 to 1.43 in MPI50. This change suggests that the incorporation of RC increases the exposure of Tyr residues in MPI, slightly weakening protein–protein interactions. An increase in lipid intensity was observed in the spectrum of MPI in MPI50, indicating an increase in MPI–lipid co-localizations.

The Raman spectra of HPI in HPI100 and HPI50 (**Figure 5-6C**) exhibited a peak at 1649 cm^{-1} (α-helix). In HPI50, an additional shoulder was observed at 1661 cm^{-1}, which indicated an increase in the content of random coils upon the incorporation of RC. These findings were further supported by the spectral changes in the amide III region of HPI50, wherein higher intensity at 1251 cm^{-1} (random coil) suggested structural destabilisation. These findings indicate that casein disrupts the structural integrity of hemp protein, promoting structural disorder. The I_{850}/I_{830} ratio decreased from 4.5 in HPI100 to 1.20 in HPI50, suggesting a significant reduction in Tyr residue exposure in the presence of casein. These findings indicate that casein–HPI interactions lead to structural rearrangements, increasing intramolecular interactions and reducing the accessibility of water to Tyr residues. Furthermore, shifts in disulfide bond–related peaks in HPI50 (from 515 and 535 cm^{-1} in HPI100 to 507, 526 and 549 cm^{-1} in HPI50) suggested disulfide bond rearrangements, likely influenced by casein–HPI interactions. An increase in lipid intensity was observed in the spectrum of HPI in HPI50, indicating increased HPI–lipid co-localizations.

Altogether, Raman spectroscopy revealed distinct structural interactions between RC and MPI as well as RC and HPI in dual-protein cheese systems. The incorporation of RC does not significantly alter the structure of MPI but rather promotes its microstructural segregation. In contrast, RC disrupts the structural integrity of HPI, inducing structural disorder and disulfide bond

rearrangements while reducing the exposure of Tyr residues. For both plant proteins, the inclusion of RC increases their co-localization with lipids.

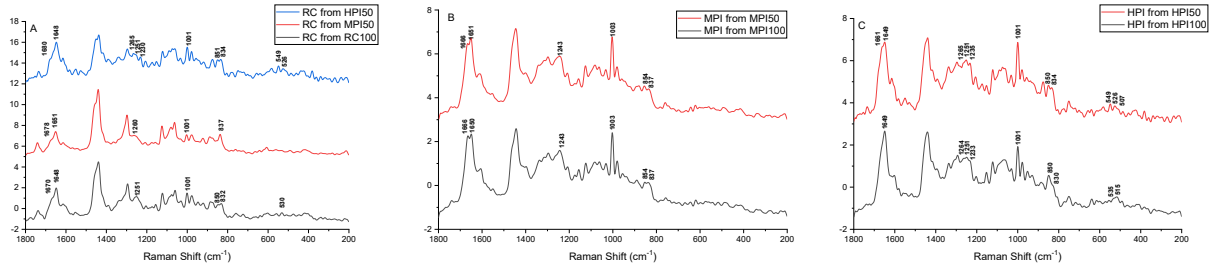


Figure 5-6. Average spectra of RC from RC100, MPI50, and HPI50 (A), MPI from MPI100 and MPI50 (B), and HPI from HPI100 and HPI50 (C). Spectra were extracted using k-means clustering to evaluate structural changes upon mixing. RC100: cheese formulated with 100% rennet casein. MPI100: cheese formulated with 100% mung bean protein. MPI50: cheese formulated with 50% mung bean protein and 50% rennet casein. HPI100: cheese formulated with 100% hemp protein. HPI50: cheese formulated with 50% hemp protein and 50% rennet casein.

5.3.5. Changes in protein secondary structures in MPI–RC cheese systems

Given that the amide I region was identified as an important spectral feature for distinguishing MPI and HPI from RC and relevant spectral changes were observed in dual-protein cheese systems, quantitative analysis was performed to elucidate changes in protein secondary structures in this region through deconvolution.

Table 5-2 shows the quantitative analysis of protein secondary structure changes in HPCAs containing MPI and RC at various ratios. **Figure S 5-5** presents the peak fitting of the amide I band, providing additional information for the quantification. In MPI100, α-helix (38%) and β-sheet (53%) structures were predominant. However, as the proportion of casein increased, a shift from β-sheet (20% in MPI30) to β-turn (9% in MPI100 and 41% in MPI30) was detected, suggesting alterations in hydrogen interactions (Sim et al., 2021). An increase in the proportion of MPI influenced the structural conformation of RC. A higher proportion of MPI was associated

with higher contents of α-helices and β-sheets and a lower content of random coils. These structural shifts suggest stabilisation of the protein network, which may contribute to enhanced rigidity and impact textural attributes such as firmness and elasticity. In addition, the aggregated intermolecular β-sheet structures near 1620 cm^{-1} in both MPI100 and RC100 (Supplementary **Figure S 5-5**) indicated a denser microstructure and higher firmness (Ong et al., 2020), which aligns with the findings of our previous study. However, it is important to consider the differences between MPI–lipid and RC–lipid interactions. RC exhibits more frequent co-localizations with coconut oil, which likely obscures the amide band at approximately 1670 cm^{-1} (Smith et al., 2015). Consequently, the observed secondary structure of RC is more influenced by the intensity of co-localized lipid features in the Raman spectra than that of MPI. As cheese samples are a complex food matrix, the results are intended to highlight relative trends and indicative structural differences.

Table 5-2. Relative amount of protein secondary structures in MPI–RC cheese samples determined by peak fitting of the amide I in Raman Spectra

	MPI secondary structure change (%)				RC secondary structure change (%)			
	α-helix	Random coil	β-sheet	β-turn	α-helix	Random coil	β-sheet	β-turn
MPI100	38 ± 10	0	53 ± 8^{a}	9 ± 3^{a}	–	–	–	–
MPI70	41 ± 12	0	50 ± 14^{a}	8 ± 3^{a}	54 ± 9	0^{a}	37 ± 5^{a}	8 ± 4
MPI50	49 ± 5	0	19 ± 8^{b}	32 ± 6^{a}	45 ± 16	22 ± 12^{b}	28 ± 10^{ab}	5 ± 4
MPI30	38 ± 17	0	20 ± 9^{b}	41 ± 16^{b}	36 ± 13	37 ± 8^{b}	16 ± 6^{b}	11 ± 10
RC100	–	–	–	–	35 ± 8	44 ± 1^{b}	11 ± 4^{b}	10 ± 4

Values within a column not having common superscripts differ significantly ($p < 0.05$). RC100: cheese formulated with 100% rennet casein. MPI100: cheese formulated with 100% mung bean protein. MPI70: cheese formulated with 70% mung bean protein and 30% rennet casein. MPI50: cheese formulated with 50% mung bean protein and 50% rennet casein. MPI30: cheese formulated with 30% mung bean protein and 70% rennet casein.

5.3.6. Comparison of RC–MPI and RC–HPI interactions in dual-protein cheese systems

Raman spectroscopy highlighted distinct structural interactions between RC and MPI and between RC and HPI in hybrid cheese systems. These interactions may influence the texture and functionality of cheese. As reported previously (Lu, Roy, et al., 2026), MPI–based HPCAs exhibited greater stretchability and higher G' values and hardness, but lower resilience, cohesiveness and meltability compared to HPI-based counterparts. The Raman spectra provide a possible explanation for these behaviours, indicating that MPI promotes pronounced protein domain separation and higher β-sheet content, consistent with stronger protein aggregation. Consequently, MPI tends to form a more segregated and rigid protein microstructure. This interpretation is in line with the rheological results, where elevated G′ values and lower tan δ reflect a more elastic and less deformable network, ultimately leading to reduced meltability and stretchability. Furthermore, the altered Tyr interactions and weakened disulfide cross-linking in MPI–RC cheese samples indicated reduced interconnectivity between casein and MPI. In contrast, HPI–RC mixtures displayed indication of disulfide bond rearrangement and random coil enrichment, implying a more flexible and heterogeneous network. These structural features are consistent with the SDS-PAGE and rheological behaviour observed in our earlier study (Lu, Roy, et al., 2026), where under non-reducing conditions, a decrease in α_{s1}-casein and α_{s2}-casein band intensities was observed in HPI–RC systems but not in MPI–RC systems, implying potential disulfide-mediated interactions between α_{s2}-casein and HPI. The HPI–RC systems also showed thermally responsive network reorganization in rheological tests, supporting the presence of a dynamic protein network that likely contributes to enhanced meltability compared with the more rigid MPI–RC systems. Overall, the effects of RC–HPI interactions on cheese functionality may differ from those of MPI–RC interactions.

5.4. Conclusions

This study shows that integrating confocal Raman microscopy with both supervised and unsupervised ML models can effectively map the distribution of key components and differentiate between plant proteins and casein in hybrid cheese systems. PCA showed that variations in the amide I and lipid-associated bands were key spectral features for distinguishing casein from plant proteins. Protein–protein and protein–lipid interactions were investigated by comparing the structures of single- and dual-protein cheese systems. In single-protein cheese systems, RC showed more frequent interactions with lipids than MPI and HPI. In hybrid cheeses, an increase in RC content slightly reduced β-sheet content in MPI–RC cheeses and increased random coil content in HPI–RC cheeses as evidenced by changes in both amide I and amide III bands. Deconvolution of the amide I region in MPI–RC cheeses prepared at various ratios validated these findings quantitatively, showing a decrease in β-sheet content but an increase in β-turn content in MPI. Moreover, MPI–RC and HPI–RC interactions had different effects. In particular, the incorporation of HPI induced greater structural disorder and disulfide bond rearrangements. By contrast, the incorporation of MPI enhanced protein domain separation owing to its strong aggregation tendency and high β-sheet content. Although these findings are specific to MPI and HPI in hybrid cheese matrices, the methodology—confocal Raman microscopy combined with ML analysis—can be applied to other plant proteins and food systems. The spatial mapping and spectral analysis approach provides high-resolution insights into protein and lipid distribution, but the specific structural effects and interpretations are expected to vary depending on the protein type and food matrix. This technique offers high-resolution insights that can be validated and complemented by infrared (IR) spectroscopy–based techniques in future research.

5.5. Acknowledgements

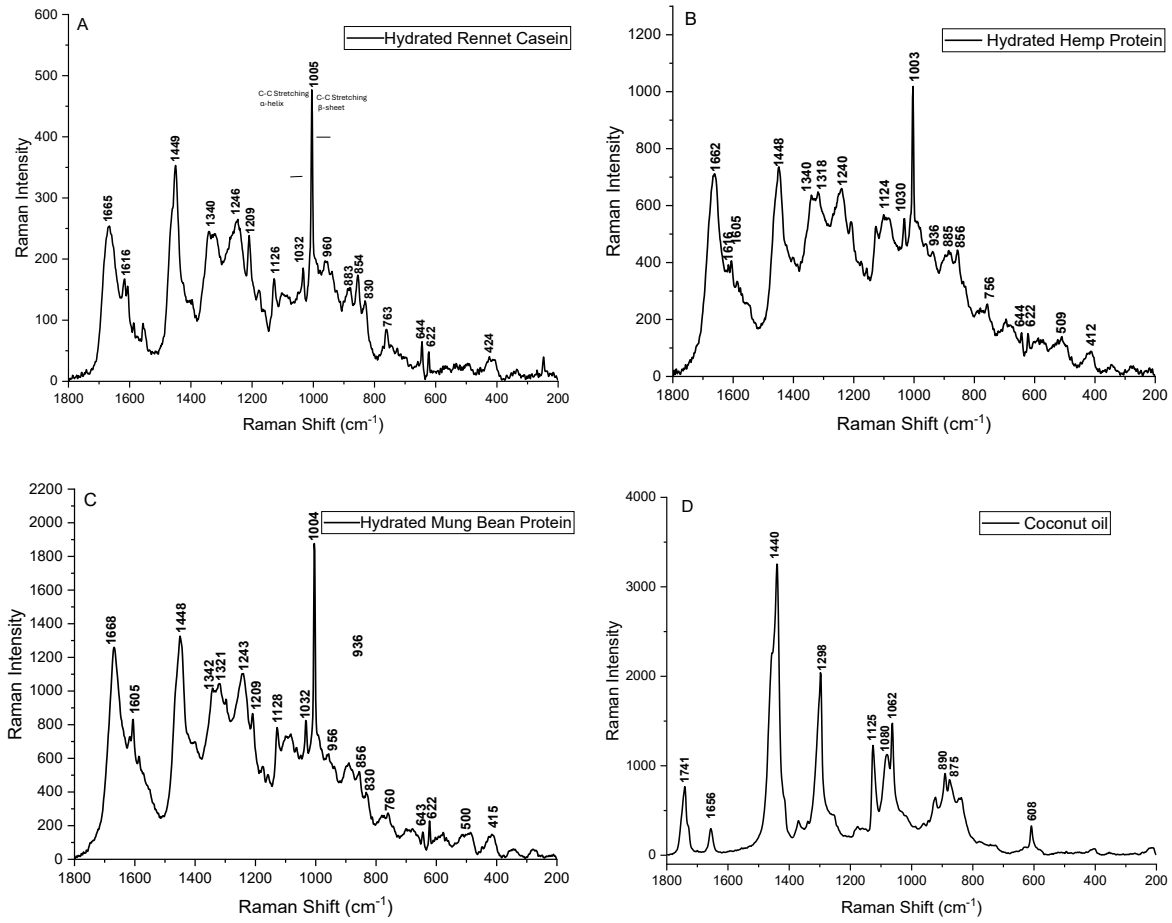
The authors thank Dr. Matthew Perrott for facilitating the sample preparation.

5.6. Supplementary material

Table S 5-1. Analysis of aromatic amino acid environment - Tyr (I_{850}/I_{830}) of the Raman spectra for HPCAs.

	I_{850}/I_{830} (mean ± SD)	I_{850}/I_{830} (mean ± 95%CI)
RC from RC100	0.76 ± 0.18	0.76 ± 0.63
RC from HPI50	0.95 ± 0.04	0.95 ± 0.40
RC from MPI50	0.67 ± 0.01	0.67 ± 0.06
MPI from MPI100	1.15 ± 0.02	1.15 ± 0.06
MPI from MPI50	1.43 ± 0.39	1.43 ± 1.37
HPI from HPI100	4.56 ± 0.89	4.56 ± 3.10
HPI from HPI50	1.20 ± 0.18	1.20 ± 1.61

RC100: cheese formulated with 100% rennet casein. MPI100: cheese formulated with 100% mung bean protein. MPI50: cheese formulated with 50% mung bean protein and 50% rennet casein. HPI100: cheese formulated with 100% hemp protein. HPI50: cheese formulated with 50% hemp protein and 50% rennet casein.



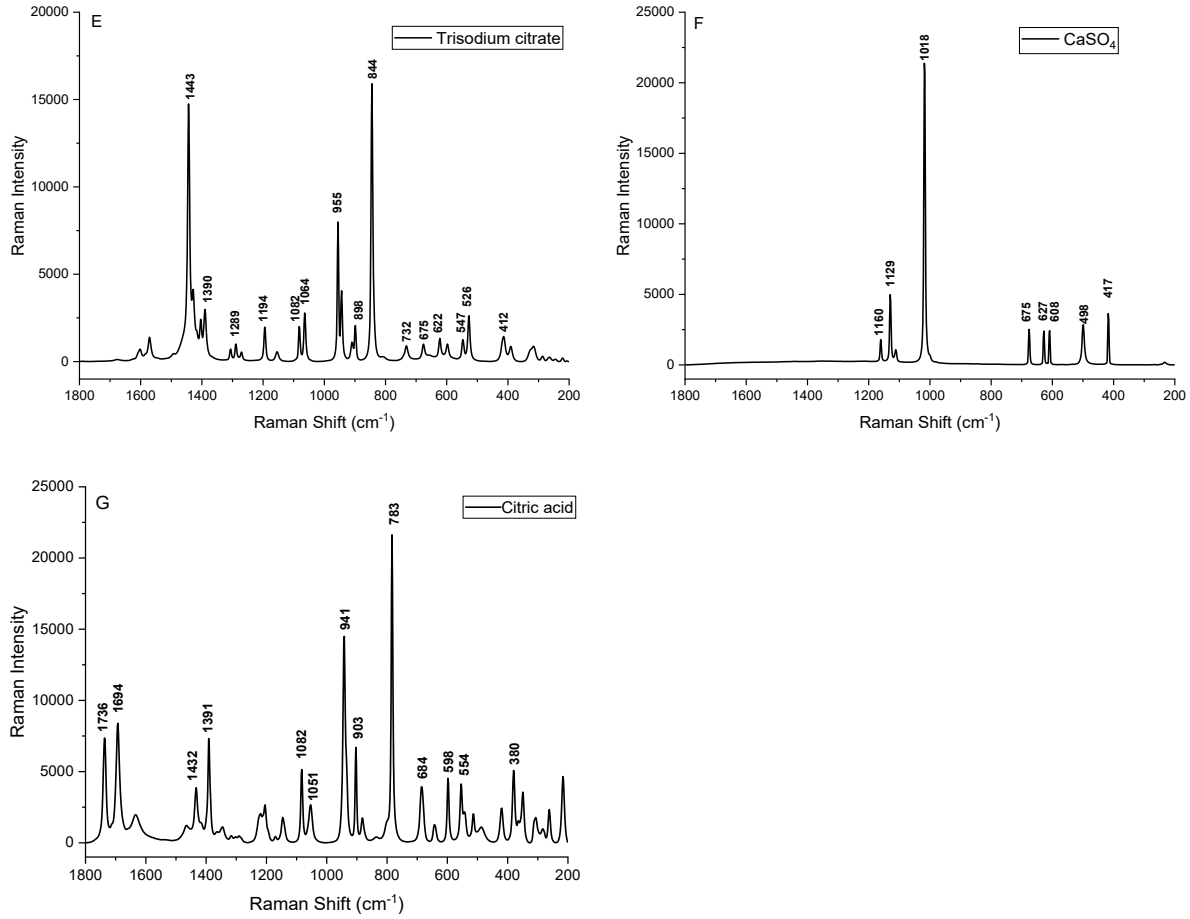
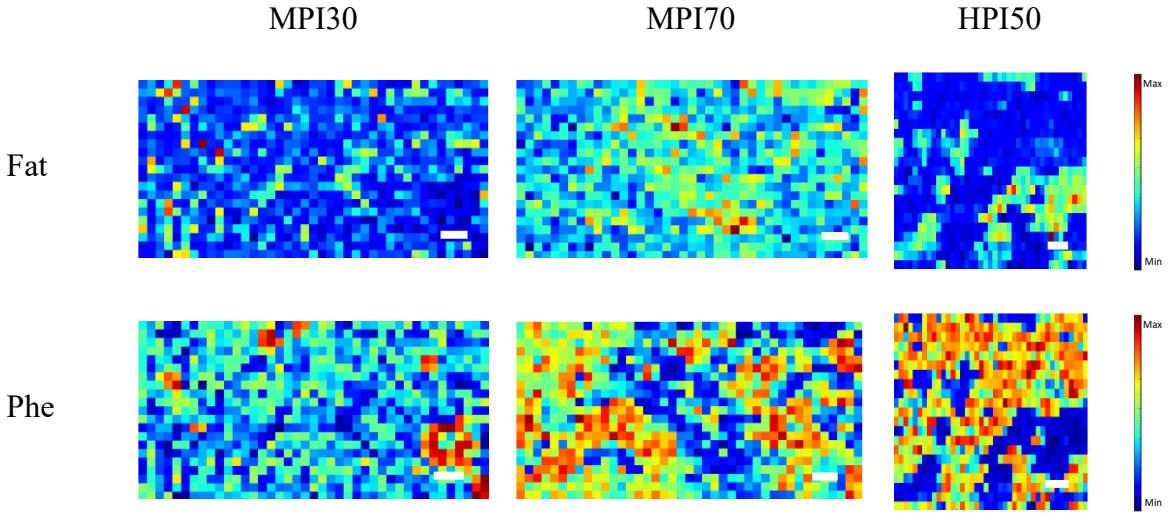


Figure S 5-1. Reference Raman spectra of ingredients used for making hybrid processed cheese analogues, including hydrated rennet casein (A), hemp protein isolate (B), mung bean protein isolate (C), coconut oil (D), trisodium citrate (E), calcium sulphate (F), and citric acid (G).



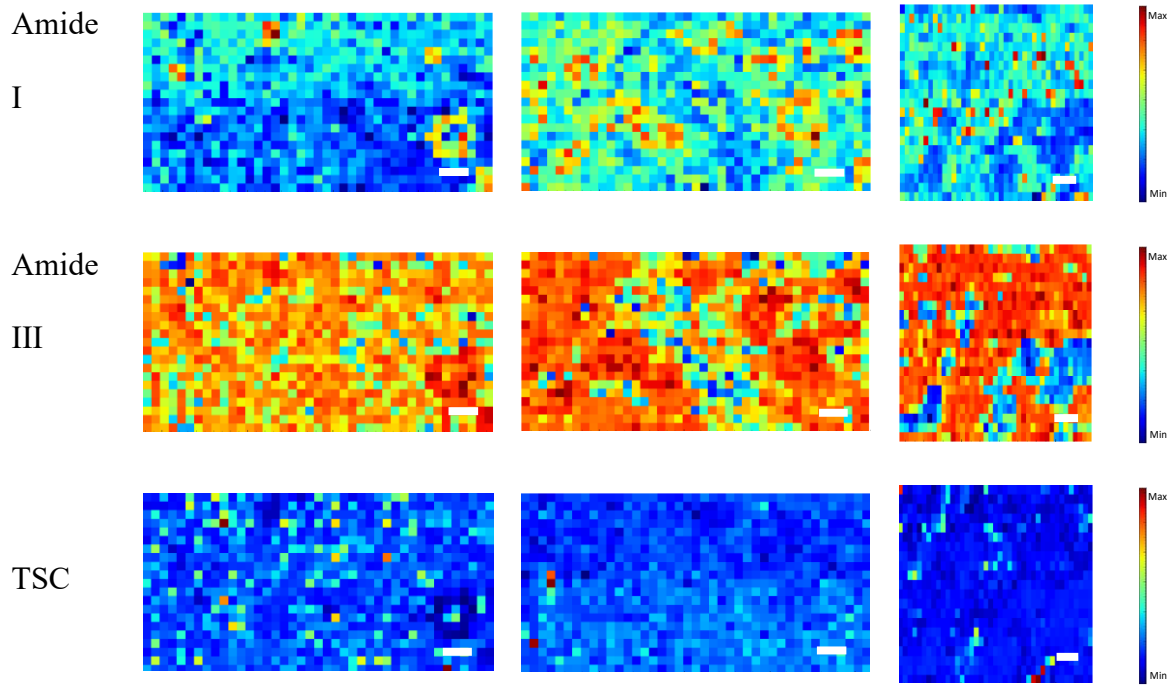


Figure S 5-2. Additional Raman images of processed cheeses formulated with 70% rennet casein and 30% mung bean protein (MPI30), 30% rennet casein and 70% mung bean protein (MPI70), and 50% rennet casein and 50% hemp protein (HPI50). The distribution of fat, amide I, amide III, phenylalanine (Phe), and trisodium citrate (TSC) was mapped using integrated spectral intensities at 1730–1750 cm^{-1}, 1600–1700 cm^{-1}, 1200–1300 cm^{-1} , and peak height of 1001 cm^{-1} and 834 cm^{-1}, respectively. MPI30 and MPI70 images were collected at low resolution with a 5 × 5 µm grid, covering a 200 × 100 µm area, while HPI50 images were collected at low resolution with a 5 × 2.5 µm grid, covering a 100 × 100 µm area. Red indicates a high concentration, while dark blue represents a low concentration, as shown by the colour intensity scale on the right. The scale bars are each 15 µm in length.

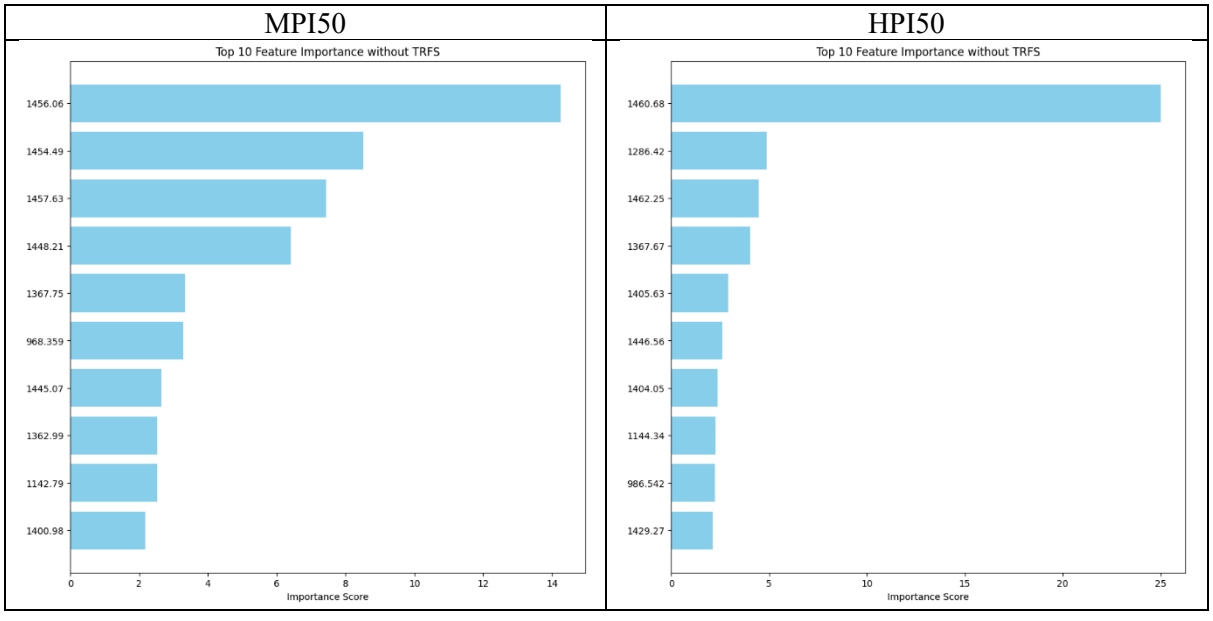


Figure S 5-3. Top 10 Raman features ranking using Catboost model with top-ranked feature removal (TRFR) for cheese samples formulated with 50% rennet casein and 50% mung bean protein (MPI50) and 50% rennet casein and 50% hemp protein (HPI50)

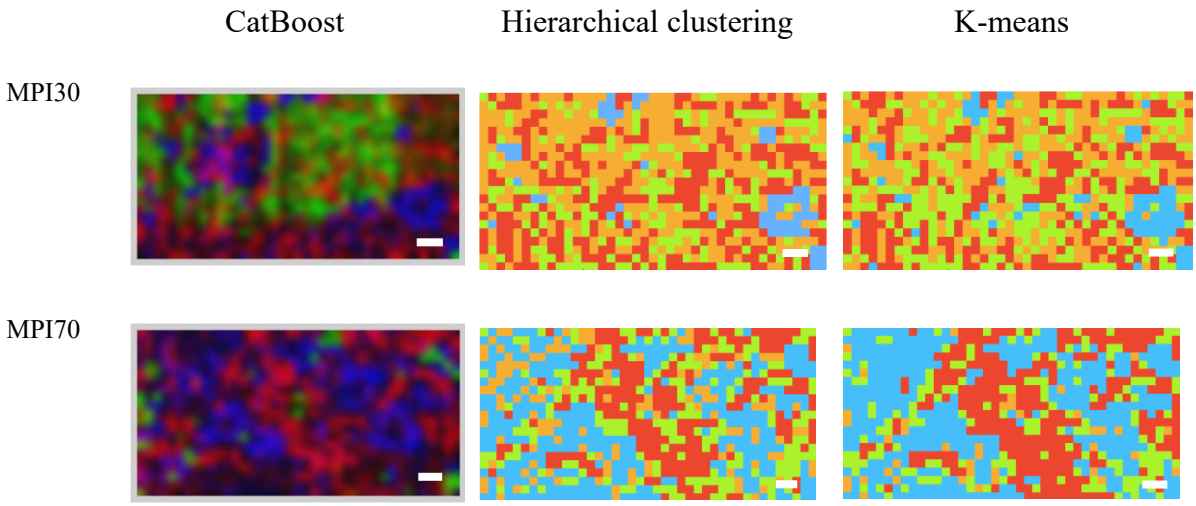
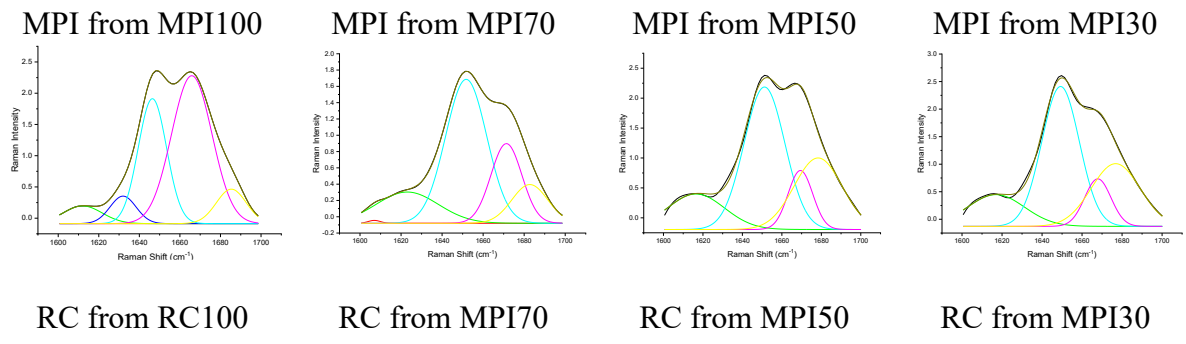
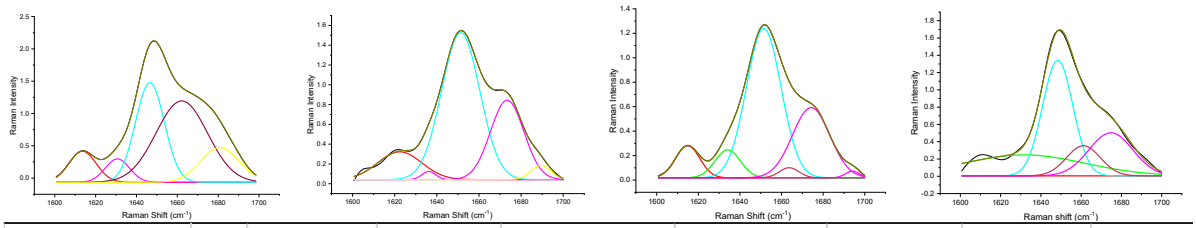


Figure S 5-4. Additional Raman images of MPI30 and MPI70 cheeses using the CatBoost (left), hierarchical clustering (middle), and k-means models (right). The CatBoost model was trained using RC100, MPI100, and HPI100, with predicted RC shown in green, mung bean protein in blue, and fat in red in MPI30 and MPI70. MPI images were collected at low resolution with a 5 x 5 µm grid, covering a 200 x 100 µm area. Different colors represent clusters identified through hierarchical clustering or k-means. Scale bars are 15 µm in length. RC100: cheese formulated with 100% rennet casein. MPI100: cheese formulated with 100% mung bean protein. MPI70: cheese formulated with 70% mung bean protein and 30% rennet casein. MPI50: cheese formulated with 50% mung bean protein and 50% rennet casein. MPI30: cheese formulated with 30% mung bean protein and 70% rennet casein. HPI100: cheese formulated with 100% hemp protein.





		P1	P2	P3	P4	P5	P6	P7
MPI from MPI100	Area	6.8 ± 0.3	7.1 ± 0.4	35.1 ± 0.9	59.1 ± 1.0	10.2 ± 0.7		
	Reduced Chi-Sqr: 0.00000513846							
	R-Square: 0.99999							
	RSS: 0.000778035							
MPI from MPI70	Area	0.3 ± 0.1	14.6 ± 2.1	44.3 ± 1.0	18.5 ± 5.9	10.4 ± 6.4		
	Reduced Chi-Sqr: 0.0000210727							
	R-Square: 0.99995							
	RSS: 0.00103							
MPI from MPI50	Area	21.5 ± 19.5	61.6 ± 20.3	21.6 ± 15.4	59.4 ± 36.4			
	Reduced Chi-Sqr: 0.00133							
	R-Square: 0.99836							
	RSS: 0.07024							
MPI from MPI30	Area	20.5± 16.0	59.7 ± 18.6	30.8 ± 14.2	63.6 ± 34.5			
	Reduced Chi-Sqr: 0.00134							
	R-Square: 0.99833							
	RSSL: 0.07091							
RC from RC100	Area	8.1 ± 0.4	5.4 ± 3.6	27.2 ± 22.5	65.2 ± 39.7	39.2 ± 12.7		
	Reduced Chi-Sqr: 0.0000157589							
	R-Square: 0.99997							
	RSS: 0.000742905							
RC from MPI70	Area	7.3 ± 0.9	0.7 ± 0.3	33.8 ± 1.3	16.0 ± 1.2	1.7 ± 0.5		
	Reduced Chi-Sqr: 0.0001695							
	R-Square: 0.99938							
	RSS: 0.00848							
RC from MPI50	Area	3.8 ± 0.1	3.5 ± 0.4	25.6 ± 1.0	12.9 ± 0.5	0.5 ± 0.1	1.0 ± 0.7	
	Reduced Chi-Sqr: 0.0000081294							
	R-Square: 0.99996							
	RSS: 0.000382082							
RC from MPI30	Area	32.2 ± 18.3	31.7 ± 3.1	7.3 ± 3.1	13.6 ± 6			
	Reduced Chi-Sqr: 0.000839006							
	R-Square: 0.99735							
	RSS: 0.04195							

Figure S 5-5. Representative Raman spectra showing the deconvoluted amide I bands (1600–1700 cm−1) of mung bean/rennet casein mixed cheese samples. For each peak fitting, the area under each peak is presented as mean ± standard error, along with the corresponding Residual Sum of Squares (RSS), reduced chi-square, and R^2 values. RC100: cheese formulated with 100% rennet casein. MPI100: cheese formulated with 100% mung bean protein. MPI70: cheese formulated with 70% mung bean protein and 30% rennet casein. MPI50: cheese formulated with 50% mung bean protein and 50% rennet casein. MPI30: cheese formulated with 30% mung bean protein and 70% rennet casein.

MASSEY UNIVERSITY
TE KUNENGA KI PŪREHUROA
UNIVERSITY OF NEW ZEALAND

GRADUATE RESEARCH SCHOOL

STATEMENT OF CONTRIBUTION
DOCTORATE WITH PUBLICATIONS/MANUSCRIPTS

We, the student and the student's main supervisor, certify that all co-authors have consented to their work being included in the thesis and they have accepted the student's contribution as indicated below in the Statement of Originality.

Student name:	Di Lu
Name and title of main supervisor:	Aiqian Ye
In which chapter is the manuscript/published work?	Chapter 6

Describe the contribution that the student and members of the supervisory team have made to the manuscript/published work:[1]

Di Lu: Conceptualization, Data curation, Formal analysis, Investigation, Methodology, Writing—original draft;Jitraporn Vongsvivut:Investigation, Methodology, Writing—reviewing & editing;Annaleise R. Klein:Investigation, Methodology, Writing—reviewing & editing; Cushla McGoverin:Investigation, Methodology, Writing—reviewing & editing;Mark Waterland:Writing—review & editing; Yi Zheng: Formal analysis, Methodology;Alejandra Acevedo-Fani:Supervision, Writing—review & editing; Debashree Roy:Supervision, Writing—review & editing;Harjinder Singh:Supervision, Writing—review & editing;Aiqian Ye:Conceptualization, Funding acquisition, Project administration, Supervision, Writing—revie

Please select one of the following three options:

- (●) The manuscript/published work is published or in press

  Please provide the full reference of the research output:

  Di, L., Vongsvivut, J., Klein, A. R., McGoverin, C., Waterland, M., Zheng, Y., Acevedo–Fani, A., Roy, D., Singh, H., & Ye, A. (2026). Elucidating Protein–Lipid Microstructure and Interactions in Hybrid Processed Cheeses Using Synchrotron Macro ATR-FTIR Microspectroscopy. Food Structure, 100511. https://doi.org/https://doi.org/1

- ( ) The manuscript is currently under review for publication

  Please provide the name of the journal:

- ( ) It is intended that the manuscript will be published, but it has not yet been submitted to a journal

Student's signature:	Di LU Digitally signed by Di LU DN: cn=Di LU, o=Massey University, email=d.lu@massey.ac.nz Date: 2026.02.25 11:11:31 +13'00'	Main supervisor's signature:	Aiqian Ye Digitally signed by Aiqian Ye DN: cn=Aiqian Ye, o=Massey University, ou=Riddet Institute, email=A.M.YE@massey.ac.nz Reason: I am approving this document Date: 2026.02.27 11:39:36 +13'00'

This form should be placed at the beginning of each relevant thesis chapter.

[1] Refer to the Massey University Publishing and Authorship guidelines (OneMassey for staff, Stream for students) and/ or Contributor Roles Taxonomy (CRediT) guidelines for guidance.

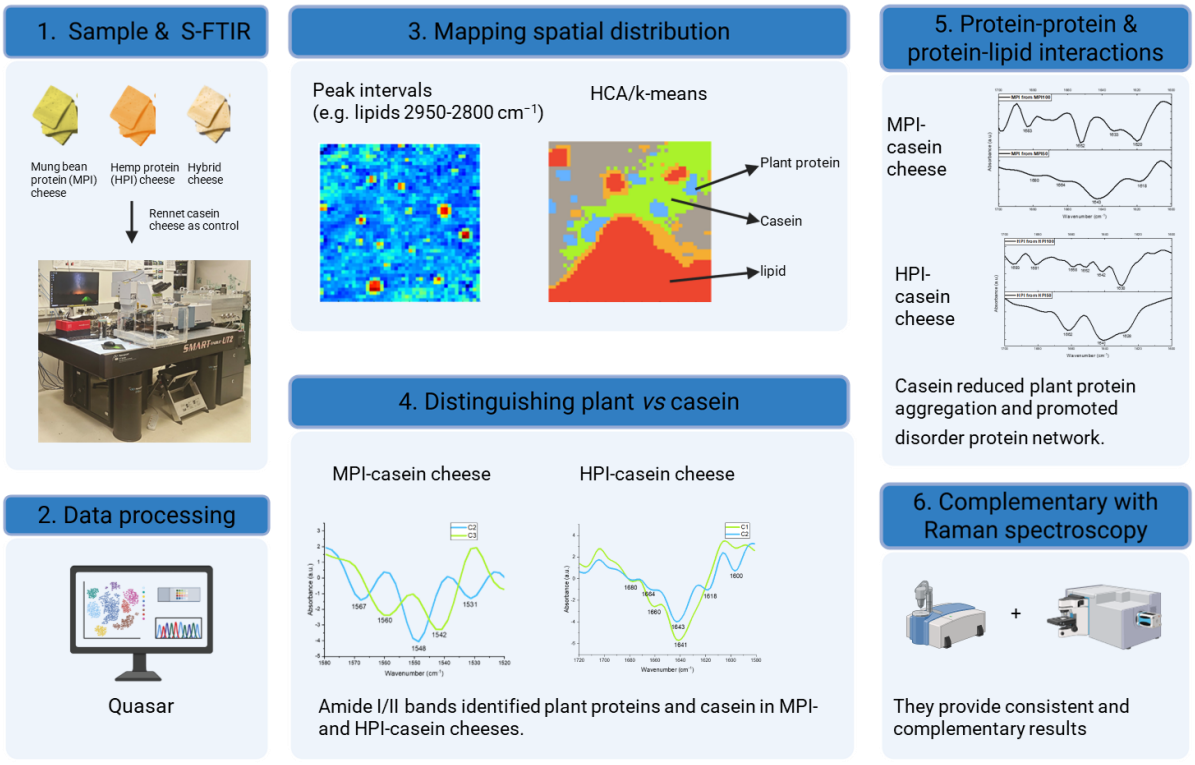
Chapter 6 Elucidating Protein–Lipid Microstructure and Interactions in Hybrid Processed Cheeses Using Synchrotron Macro ATR-FTIR Microspectroscopy[5]

Abstract

Herein, synchrotron-based Fourier-transform infrared (S-FTIR) microspectroscopy was used to investigate the spatial distribution and molecular interactions within hybrid processed cheeses (HPCs) that contain casein and plant proteins. Unsupervised hierarchical cluster analysis (HCA) and k-means clustering provided consistent spatial differentiation, effectively separating the regions that were dominated by plant protein from those dominated by casein. Spectral analysis revealed protein–protein and protein–lipid interactions based on the type of plant protein used across plant-based cheeses and hybrid formulations. Cheese samples that contained only hemp protein isolate (HPI) were dominated by β-sheets (50%) and β-turns (21%), while mung bean protein isolate (MPI)-based cheeses exhibited considerable α-helix (35%) and β-sheet (48%) contents. In HPI–casein hybrid cheeses, hydrogen bonds predominated, with the amide II mode of proteins as the key discriminating component. By contrast, the amide I secondary protein structure was the primary marker that distinguished MPI from casein in MPI–casein cheeses. Increasing the casein content reduced plant protein aggregation and created a more heterogeneous environment, thereby supporting a flexible and disordered protein network. Furthermore, the S-FTIR map of lipids indicated that coconut oil was preferentially associated with casein rather than with plant proteins. Overall, these results highlight the role of S-FTIR microspectroscopy in resolving compositional and molecular-level interactions in hybrid cheese matrices.

[5]This chapter will be published as Lu, D., Vongsvivut, J., Klein,m A.R., McGoverin, C., Waterland, M., Zheng, Y., Acevedo-Fani, A., Roy, D., Singh, H., & Ye, A. (2026). Elucidating Protein–Lipid Microstructure and Interactions in Hybrid Processed Cheeses Using Synchrotron Macro ATR-FTIR Microspectroscopy. Food Structure (under review)

Graphical abstract



6.1. Introduction

Hybrid processed cheese (HPCs), produced by partially replacing milk proteins with plant proteins, are emerging as more sustainable alternatives to conventional cheeses (Zhang, Jiang, et al., 2024). However, incorporating plant proteins, such as hemp protein isolate (HPI) and mung bean protein isolate (MPI), can alter their rheology, texture, functionality, and sensory properties, as reported in Chapter 4 (Lu, Roy, et al., 2026). Fundamentally, incorporating plant proteins introduces new molecular and microstructural challenges. In Chapter 5, we used confocal Raman microscopy to map the distribution of the main components in HPCs formulated with rennet casein (RC) and either MPI or HPI, clearly distinguishing between the dairy and plant protein networks. This analysis revealed complex microstructural segregation and notable molecular changes, showing that the presence of casein altered the secondary structure and tyrosine environment of plant proteins, while the inclusion of plant protein disrupted casein–casein interactions (Lu, McGoverin, et al., 2026). These findings suggest that the internal organisation of HPCs is heterogeneous, and this molecular complexity highlights the need for complementary spectroscopic approaches with higher spatial and structural sensitivity to verify the molecular organisation within such complex matrices.

Fourier-transform infrared (FTIR) spectroscopy has emerged as a powerful analytical tool for probing the molecular composition and structure of materials. By measuring the absorption of infrared (IR) radiation, the technique can provide detailed information on functional groups and intermolecular interactions (Jurowski et al., 2024). In particular, vibrational absorption spectra in the mid-IR spectral range (4000–400 cm^{-1}) contain characteristic fingerprints of the key biomacromolecules that serve as the fundamental building blocks of food systems (i.e. proteins, lipids, carbohydrates, and water), making it useful for both qualitative and quantitative analysis of

food items (Saji et al., 2024). Furthermore, FTIR microspectroscopy, when combined with a microscope, enables spatially resolved chemical imaging at micron scales, and can be used in combination with multivariate analysis as a label-free, non-destructive tool for characterising complex biological and food systems (Saji et al., 2024).

The development of synchrotron-based FTIR microspectroscopy has considerably advanced these capabilities. Unlike an internal IR source (Globar™) used in most laboratory-based FTIR instruments, the synchrotron-IR source provides a highly collimated and intense IR radiation that substantially enhances spatial resolution and signal-to-noise ratio, enabling the acquisition of high-quality spectra in much shorter scanning times. A macro ATR-FTIR microspectroscopy platform has been developed at the Australian Synchrotron, in which the synchrotron-IR beam is coupled with a high-index germanium (Ge) ATR hemispherical crystal (nGe = 4.0). This optical configuration allows the acquisition of FTIR chemical maps at a resolution four times higher than that of standard transmission and reflectance setups. It allows for a step interval (pixel resolution) of as less as 250 nm, making it ideal for resolving microstructures in complex heterogeneous systems at a few microns, such as single cells and biological tissues (Vongsvivut et al., 2019), as well as drug and nutrient microcapsules (REFs), among others (Kim et al., 2023; Silva et al., 2021; Timilsena et al., 2019).

FTIR techniques have been increasingly applied to cheese and dairy products to monitor their composition, microstructure and structural changes during processing and ripening. For example, FTIR has been used to quantify the key compositions of cheese, such as lipid, protein, salt and moisture contents (Koca et al., 2007; Margolies & Barbano, 2018), and to visualise the spatial distribution of lipid and protein microstructures within cheese matrices (Pax et al., 2019). At molecular level, FTIR combined with Raman microspectroscopy enables the assessment of the

secondary structure of proteins by tracking changes in the amide I (ν(C=O) stretching mode of protein backbone) and amide II (mainly δ(N–H) bending and ν(C–N) stretching) regions that reflect maturation processes in cheddar cheese (Dewantier et al., 2023). Recent studies have further integrated FTIR imaging techniques with multivariate analysis to correlate structural changes with functional properties. For example, Ong et al. (2020) demonstrated that pH-dependent alterations in the secondary structure of proteins and microstructural organisation influence the textural properties of cream cheese. Their study reported that low pH conditions were associated with higher β-sheet aggregation, a denser protein matrix and a firmer texture. Furthermore, Pax et al. (2023) showed that synchrotron macro ATR-FTIR microspectroscopy could monitor structural changes in the secondary structure of proteins and alterations in the chemical distribution within mozzarella cheese during freezing and tempering, which could directly affect the performance of thawed cheese. Despite these advances, most FTIR applications have focused on conventional dairy cheeses. More recently, Yiu et al. (2026) used S-FTIR imaging to map structural changes in a pea-protein cheese analogue, showing improved meltability and texture with a dual-polysaccharide system. To date, no studies have reported such advanced analysis of HPCs containing both dairy and plant proteins, leaving a gap for understanding the way mixed-protein systems affect cheese structure and functionality.

Herein, synchrotron macro ATR-FTIR microspectroscopy was used to analyse HPCs formulated with RC and either MPI or HPI, using the same formulations that were previously examined by confocal Raman microspectroscopy (Lu, McGoverin, et al., 2026). The objectives of this chapter were (i) to map the spatial distribution of lipid, protein and water in single-protein cheese systems, (ii) to distinguish plant proteins from milk proteins in dual-protein systems (plant protein: casein = 50:50) using unsupervised multivariate analysis, (iii) to investigate protein–protein and protein–

lipid interactions within HPCs and (iv) to correlate these observations with our previous Raman microscopy findings to highlight complementary molecular insights between the two techniques. By integrating the synchrotron macro ATR-FTIR technique with multivariate analysis, this study provided an enhanced understanding of the molecular organisation and interactions of plant and dairy proteins in hybrid cheese matrices.

6.2. Materials and Methods

6.2.1. Materials

RC (SureProteinTM 779) containing 82% protein was obtained from Fonterra Co-operative Group Ltd. (New Zealand). MPI; 85%) was purchased from Bulk Powders New Zealand. HPI; 70%) and virgin coconut oil were purchased from Davis Trading Company (New Zealand). All chemicals used were of analytical grade and were obtained from Sigma Chemical Co., unless otherwise specified.

6.2.2. Preparation of HPCs

HPCs were prepared by mixing MPI or HPI with RC at ratios of 100:0, 50:50 and 0:100 to obtain a total protein content of 18% (wet weight). The formulation, based on the study by Lu et al. (2025), comprised 18% protein, 20% coconut oil, 0.5% sodium chloride, 0.5% calcium sulfate, 0.1% potassium sorbate, 2.8% trisodium citrate and water on a weight ratio basis, with pH adjusted to ~5.4 using citric acid. HPCs were prepared using a Rapid Visco Analyser (RVA-4; Newport Scientific Pty Ltd, Warriewood, NSW, Australia). The HPC samples (30 g) were prepared in an aluminium cell fitted with a polycarbonate paddle. All dry ingredients and coconut oil were manually blended with water for 5 min and then hydrated in an aluminium cell for 1 h at room temperature (20 °C). The mixture was processed using the following RVA profile: equilibration at

50 °C, heating to 90 °C for 4 min and holding at 90 °C for 10 min. Thereafter, the sample was cooled to 50 °C at a rate of 0.2 °C/s while mixing at 300 rpm throughout the heating and cooling stages. The resulting samples were labelled as MPI100, MPI50, HPI100, HPI50 and RC100, with the numbers indicating the protein ratios within them. Individually packed samples were stored at 4 °C and analysed using synchrotron macro ATR-FTIR microspectroscopy within 1 week.

6.2.3. Synchrotron macro ATR-FTIR microspectroscopic measurements

Synchrotron FTIR (S-FTIR) microspectroscopic analysis was performed at the infrared microspectroscopy (IRM) beamline of the Australian Synchrotron using a Bruker Vertex V80v spectrometer coupled with a Hyperion 3000 FTIR microscope (Bruker Optik GmbH, Ettlingen, Germany), which was equipped with a liquid nitrogen–cooled narrow-band MCT detector. Spatially resolved chemical mapping was performed using a custom macro-attenuated total reflection (macro ATR) device fitted with a 250-μm diameter facet Ge ATR crystal, as previously described (Ong et al., 2020; Pax et al., 2019; Vongsvivut et al., 2019). Spectra were acquired in the 3800–700-cm^{-1} range at 4 cm^{-1} resolution using the OPUS 8.0 software (Bruker). A background spectrum was first recorded in air (128 co-added scans).

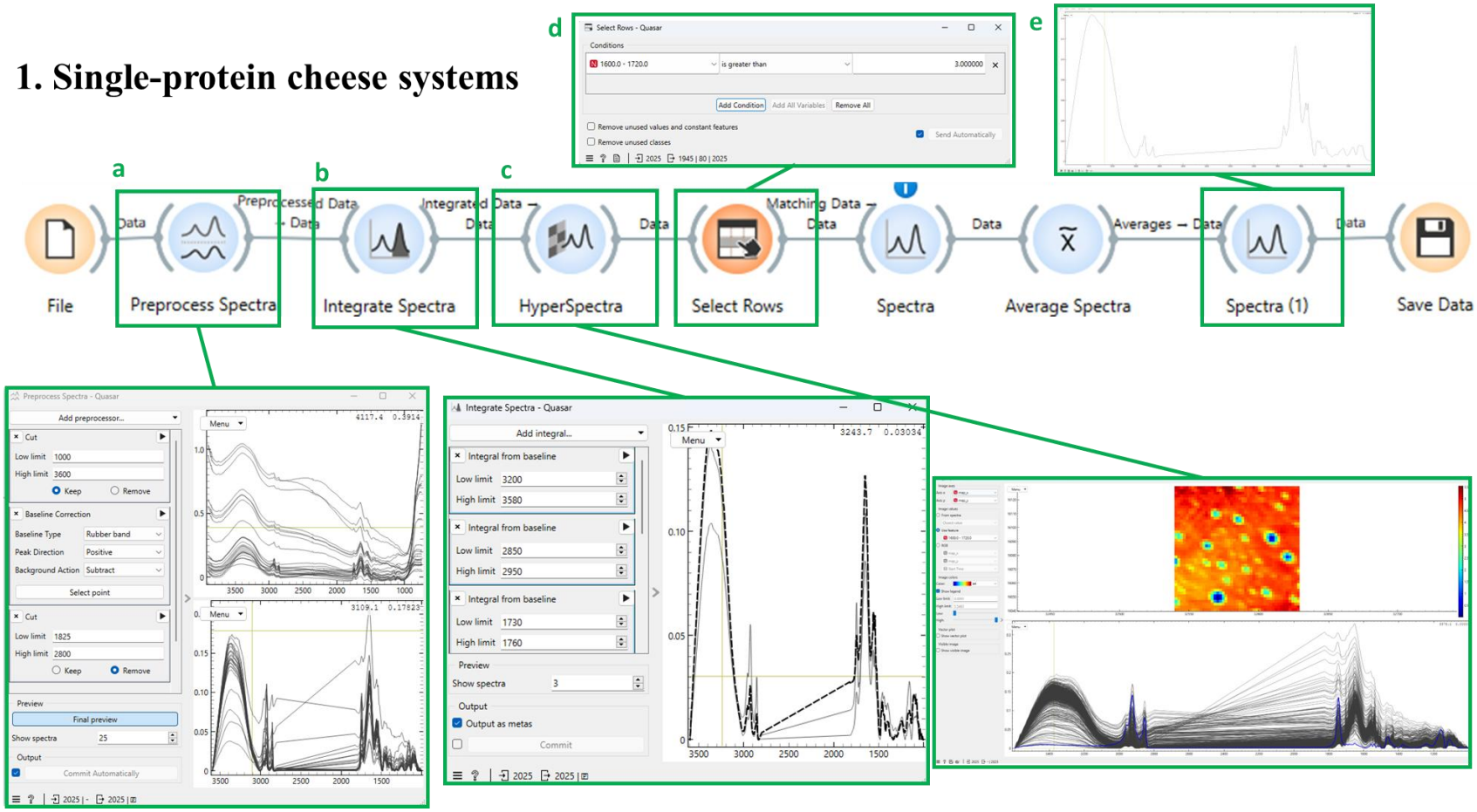
The cheese samples were sliced into ~1–2-mm thickness and pressed against the Ge ATR crystal. The contact quality was monitored via live ATR-FTIR absorbance spectra, with light pressure adjustments as needed. Once good contact with the crystal was established, high-resolution ATR-FTIR maps were collected over areas measuring 90 × 90 μm^2 with a step size of 2 μm. Each spectrum was acquired with 16 co-added scans using a beam-defining projected aperture with a diameter of ~3.1 μm. The default acquisition parameters included three-term Blackman–Harris apodisation, power spectrum phase correction and a zero-filling factor of 2. Atmospheric

compensation was applied to every spectral map using the OPUS 8.0 software suite (Bruker) to remove the effects of atmospheric water vapour and carbon dioxide from the spectra. Each formulation was imaged in duplicate.

6.2.4. Synchrotron FTIR analysis using Quasar

The spectral data were analysed using Quasar, an open-source Python library designed for machine learning and spectral data visualisation (Toplak et al., 2021). A representative workflow with examples of the single-protein cheese systems (RC100, MPI100 and HPI100) and the dual-protein cheese systems (MPI50 and HPI50) is shown in **Figure 6-1**.

For the single-protein cheese systems, the raw data were preprocessed via a rubber-band baseline correction method, retaining the spectra in the ranges of 3600–2800 and 1825–1000 cm^{-1} (**Figure 6-1** box a). Chemical maps were generated by integrating areas under the peaks within specific spectral regions to visualise the spatial distribution of the key chemical components: 3580–3200 (water), 2950–2850 and 1760–1730 (lipids), 1700–1600 (amide I) and 1580–1500 cm^{-1} (amide II) for protein and peptide structures (**Figure 6-1** box b and c). By filtering the rows for specific integrated peaks that meet defined value conditions, group spectra could be selected (**Figure 6-1** box d) and averaged (**Figure 6-1** box e) for further comparison and analysis.


1. Single-protein cheese systems
a
b
c
d
e
File
Preprocess Spectra
Integrate Spectra
HyperSpectra
Select Rows
Spectra
Average Spectra
Spectra (1)
Save Data
Data
Averages
Select Rows - Quasar
Conditions
1600.0 - 1720.0
is greater than
3.000000
Add Condition
Add All Variables
Remove All
Remove unused values and constant features
Remove unused classes
Send Automatically
Preprocess Spectra - Quasar
Add preprocessor...
Cut
Low limit 1000
High limit 3600
Keep
Remove
Baseline Correction
Baseline Type
Rubber band
Peak Direction
Positive
Background Action
Subtract
Select point
Low limit 1825
High limit 2800
Preview
Final preview
Show spectra 25
Output
Commit Automatically
Integrate Spectra - Quasar
Add integral...
Integral from baseline
Low limit 3200
High limit 3580
Low limit 2850
High limit 2950
Low limit 1730
High limit 1760
Show spectra 3
Output as metas
Commit

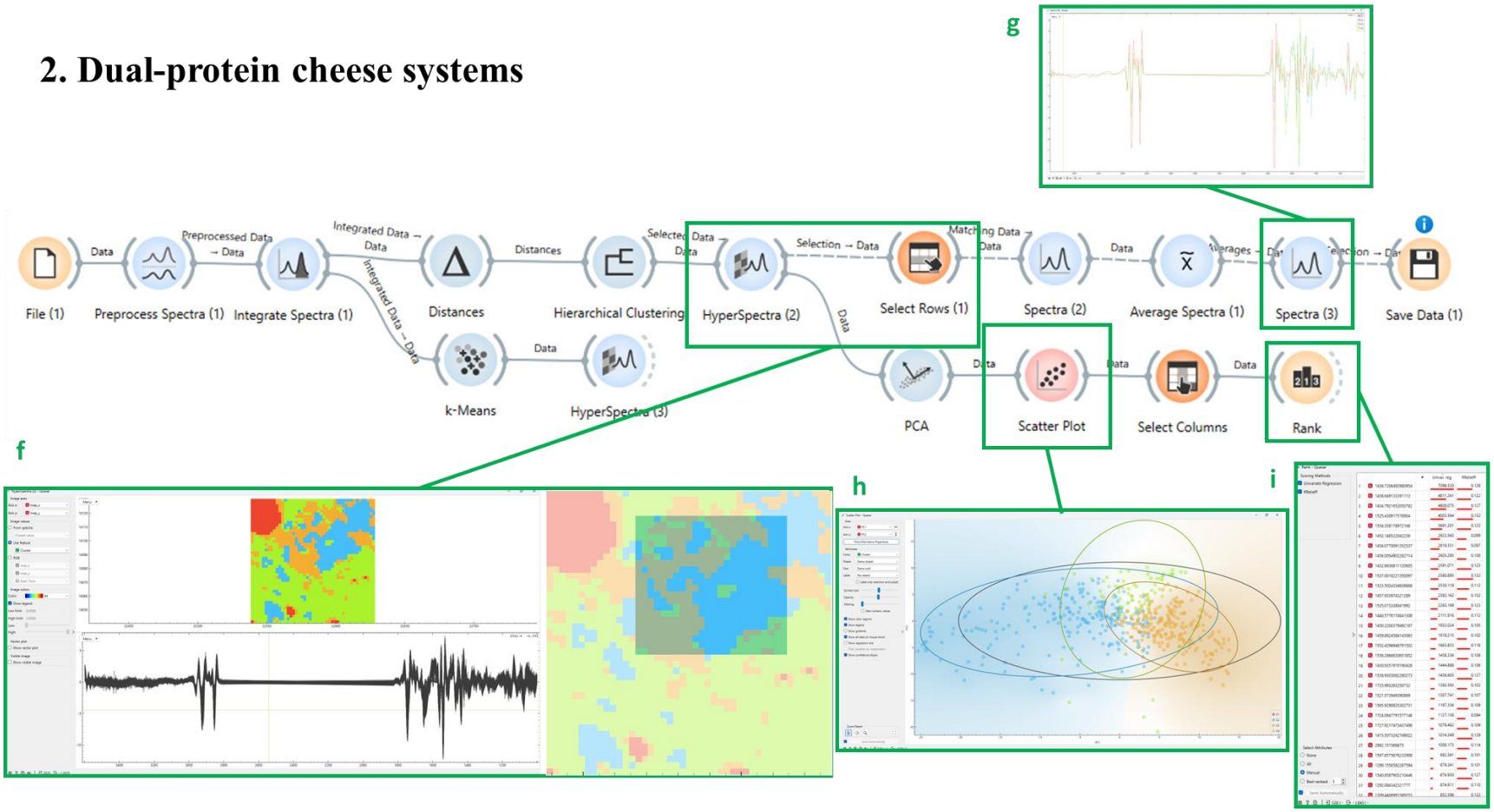


Figure 6-1. Workflow for S-FTIR map image data processing in Quasar, including single-protein (top) and dual-protein cheese systems (bottom). The pre–processed data with baseline correction retained spectra in the ranges of 3600–2800 and 1825–1000 cm^{-1} (Box a). Integrated peak mapping was performed using specific spectral regions (Box b), and hyperspectral images were generated after integration (Box c). Spectra were selected based on defined value conditions (Box d), and their average spectra were calculated (Box e). Hierarchical clustering was applied to group the spectra, and the corresponding hyperspectral images were generated after clustering

(Box f), and the average spectra of selected regions were extracted (Box g). A scatter plot visualizing cluster separation was obtained after Principal Component Analysis (PCA) (Box h). PC2 was applied to rank protein-related variance (Box i).

For the dual-protein cheese systems, the raw data were preprocessed via rubber-band baseline correction method, second derivatisation with the Savitzky–Golay algorithm (polynomial order 3 and 13 smoothing points) and normalisation via standard normal variate to enhance spectral quality, retaining the spectra in the ranges of 3600–2800 and 1825–1000 cm^{-1}. In addition, two unsupervised clustering algorithms, namely, hierarchical clustering and k-means clustering, were employed to distinguish proteins in the mixed systems. Hierarchical cluster analysis (HCA) was performed using an agglomerative approach, which iteratively grouped similar data points to generate a dendrogram. The Pearson distance was used as the distance measure, with a maximum depth of 10. By contrast, k-means clustering was used to partition the data into a predefined number of clusters, with the cluster centroids iteratively adjusted until convergence. Based on the known composition of the cheese samples and after initial clustering and adjustment, four to five clusters were used to efficiently differentiate lipid and protein types. However, we observed that the two corners (top left and bottom right) of the 90 × 90-μm^2 area lay outside the focused synchrotron-IR beam. To reduce noise, only a small, well-focused central area was selected for detailed analysis (**Figure 6-1** box f). The average spectra from the selected area were extracted, and principal component analysis (PCA) was conducted to reduce dimensionality and visualise cluster separation through scatter plots (**Figure 6-1** box h). The second principal component (PC2) was used to rank the variance associated with proteins. Wavenumbers were ranked based on the absolute values of their regression coefficients, highlighting the spectral regions that were highly associated with protein differentiation in the absence of class labels (**Figure 6-1** box i).

6.2.5. Deconvolution of the amide I region

The amide I region (1700–1600 cm^{-1}) was deconvoluted for quantitative analysis. First, the average spectrum from the protein-rich cluster, identified using k-means clustering, was extracted

from Quasar. Thereafter, the spectra were baseline-corrected using a linear method between two selected points corresponding to the lowest-intensity regions in each spectrum and smoothed using a 5-point Savitzky–Golay filter with a polynomial order of 2 in the Origin® software (2021b) to enhance the signal-to-noise ratio. Subsequently, peak fitting was performed using the second derivative method, followed by an iterative Gaussian peak fitting. Peak assignment was performed using known infrared spectral data for protein secondary structures (Fellows et al., 2020; Sadat & Joye, 2020; Tang et al., 2023). Several iterations were performed until the fit converged, ensuring a final fitting curve with a corrected $R^2 \geq 0.99$. Subsequently, the area under each peak was calculated relative to the total area and expressed in percentage. The results were reported as mean values (performed in triplicate) and standard deviations. The data were subjected to one-way ANOVA analysis using SPSS, followed by Tukey's comparison test. Differences were considered statistically significant at a level of $p < 0.05$. The reported values for β-sheets and β-turns represented the cumulative contributions of multiple peaks.

6.3. Results and discussion

6.3.1. Overview of the FTIR spectra of HPCs components

HPCs demonstrated characteristic absorption peaks in the synchrotron ATR-FTIR spectrum, typically within the range of 4000–1000 cm^{-1}. Each peak corresponded to specific vibrational modes of functional groups, enabling the identification of molecular components. These bands could be attributed to specific biomacromolecules, particularly proteins (amide I and II bands), lipids (ν(C–H) and ν(C=O) stretching vibrations) and water (ν(O–H) stretching and δ(H–O–H) bending vibrations), providing valuable molecular insights into the key components and their interactions within HPCs. **Table 6-1** summarises the key FTIR peaks and their corresponding

vibrational modes, identified based on characteristic assignments reported in the literature (Barth, 2007; Du et al., 2018).

For coconut oil, the characteristic absorption bands observed within the 2950–2800-cm^{-1} spectral range could be attributed to the asymmetric and symmetric stretching vibrations of methyl ($–CH_3$) and methylene ($–CH_2$) groups. A strong peak at 1744 cm^{-1} corresponded to the ν(C=O) stretching mode in ester functional groups, which was characteristic of triglycerides in lipids and represented total lipids. The bending vibrations of $–CH_2$ groups produced a peak at ~1465 cm^{-1}, while the band at 1160 cm^{-1} could be attributed to the ν(C–O–C) stretching in the –HC–O–(C=O) ester linkage (Gandhi et al., 2022). These key features helped analysing the lipid component in the HPC samples used in the present study at a molecular level.

Protein-associated absorption bands considerably helped identifying and characterising their secondary structures. The amide I band (1600–1700 cm^{-1}), which predominantly arose from the ν(C=O) stretching vibration, was highly sensitive to protein secondary structure owing to its dependence on the surrounding hydrogen bonding and polypeptide backbone conformation. Characteristic wavenumber ranges for specific protein conformers included α-helices (1660–1650 cm^{-1}), random coil structures (1650–1640 cm^{-1}), β-sheets (1642–1610 cm^{-1}) and β-turns (1699–1660 cm^{-1}) (Hossain Brishti et al., 2021; Sadat & Joye, 2020). The amide II band (1550–1500 cm^{-1}), mainly attributed to δ(N–H) in-plane bending coupled with ν(C–N) stretching modes, contributed to protein structural analysis. These amide features played an important role in distinguishing plant-derived proteins from casein within complex food matrices.

Table 6-1. Band assignment of FTIR absorption peaks typically found in most biological samples containing protein and lipid components (Barth, 2007; Bittante et al., 2022; Ørskov et al., 2023).

Wavenumber values (cm^{-1})	Functional groups	Component
3600-3200	ν(O–H)	Water/Hydroxyl groups
2950–2800	ν(C–H) from methyl ($–CH_3$) and methyl ($–CH_2$) groups of lipids	Lipids
1740[a]	ν(C=O) of esters from lipid triglycerides and fatty acids	Total lipids
1465[b]	$\delta_{scissor}(CH_2)$ from methylene ($–CH_2$) groups	Lipids
1700-1600	Amide I (ν(C=O) in peptide bonds)	Protein
1642-1610	β-sheet	
1650-1640	random coil	
1660-1650	α-helix	
1699-1660	β-turn	
1650-1640	δ(H–O–H)	Water
1570-1500	Amide II (δ(N–H) coupled with ν(C–N))	Proteins
1450	BNQ1$\delta_{as}(CH_3)$	Lipids
1400-1200	Amide III (δ(N–H) coupled with ν(C–N))	Protein
1160	ν_s(C–O–C) from esters	Lipids

Symbols used for vibrational modes: ν_{as} = asymmetric stretch; ν_s = symmetric stretch; δ_s = symmetric in-plane deformation (bend); δ_{as} = asymmetric in-plane deformation (bend); [a] Representative band for total lipids. [b] Sensitive to the orthorhombic-like to hexagonal packing transition of the $–CH_2$ groups in the phospholipid bilayers.

Water exhibited strong characteristic absorption bands owing to its broad range of hydrogen interactions with other surrounding molecules within the food matrix. The broad ν(O–H) stretching band observed in the 3600–3200-cm^{-1} spectral range was associated with hydrogen bonding in water molecules and was highly sensitive to the physical state of water (e.g. free vs. bound water) and the surrounding molecular environment. A weaker δ(H–O–H) bending (scissoring) vibrational mode at ~1640 cm^{-1} often overlapped with the amide I band of proteins, potentially complicating spectral interpretation. These characteristic FTIR bands were the reference framework for analysing the single- and dual-protein hybrid cheese systems.

6.3.2. Spatial distribution of components and protein structure in single-protein systems

The FTIR chemical image of HPCs was generated by integrating specific absorption peaks corresponding to key chemical components, as outlined in the previous section. These included lipid-associated bands (2950–2800 and 1745 cm^{-1}), amide I (1700–1600 cm^{-1}) and water bands (3600–3200 cm^{-1}). **Figure 6-2** shows a representative chemical image of the RC100 sample. RC100 exhibited a homogeneous microstructure, with lipid droplets uniformly distributed within the casein network. The water signal overlapped within the casein matrix, suggesting a close spatial association between water and the casein matrix. This confirmed the amphipathic nature of casein, which possessed both hydrophilic and hydrophobic regions. The hydrophilic domains were capable of binding water, while the hydrophobic regions contributed to the stable incorporation of lipids into the protein matrix (Holt et al., 2013). This result is consistent with that of our previous confocal laser scanning microscopy (CLSM) study (Lu, Roy, et al., 2026).

Lipids	Lipids	Proteins (amide I)	Water
ν(C-H) of CH_2/CH_3	ν(C=O)	ν(C=O)	ν(O–H)
2950-2800 cm^{-1}	1745 cm^{-1}	1700-1600 cm^{-1}	3600-3200 cm^{-1}

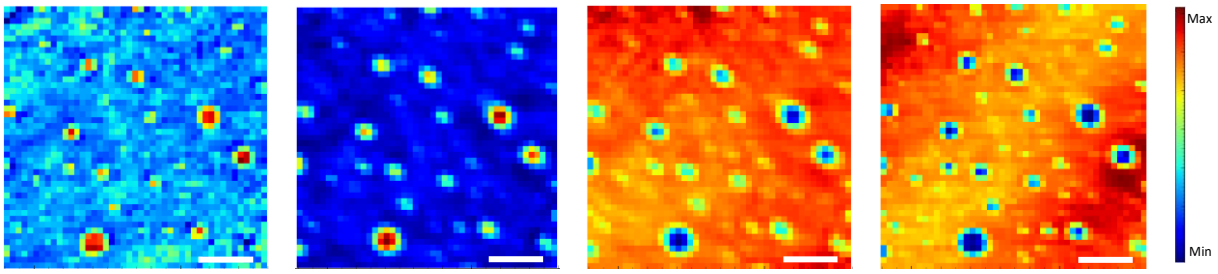


Figure 6-2. A representative FTIR chemical image of the processed cheese formulated with 100% rennet casein (RC100). The distribution of lipids, proteins, and water was mapped using integrated areas under the peaks at 2950-2800 and 1745 cm^{-1}, 1700-1600 cm^{-1} and 3600-3200 cm^{-1}, respectively. Red and blue indicate high and low concentration, respectively, as shown by the colour intensity scale on the right. The scale bars are each 20 µm in length.

However, the plant protein–based cheeses, such as MPI100 and HPI100, presented challenges for synchrotron macro ATR-FTIR measurements owing to their lower springiness and cohesiveness compared with the casein-based cheeses (Lu, Roy, et al., 2026). These physical limitations hindered optimal contact with the Ge ATR crystal, leading to partial loss of spectral information, a low signal-to-noise ratio and occasional sample movements during mapping. Representative images are provided in the Supplementary **Figure S 6-1**.

As obtaining a complete image of the plant-based cheese sample was challenging, protein and lipid spectra were successfully extracted based on peak intensities. These spectral data provided valuable insights into the chemical and functional group differences between plant proteins and casein. **Figure 6-3A** shows the protein spectra generated for the RC100, MPI100 and HPI100 cheese samples, based on their integrated areas under the peaks as described in Section 6.2.4. The primary differences were observed in the amide I region; therefore, a second derivative analysis (**Figure 6-3**) and peak fitting were performed to further investigate the protein secondary structures of MPI (**Figure 6-3C**), HPI (**Figure 6-3D**) and RC (**Figure 6-3E**) in the respective cheese samples.

Notably, the water band at ~1640 cm^{-1} substantially overlapped with the protein random coil component in the amide I region and therefore could not be reliably separated during peak fitting.

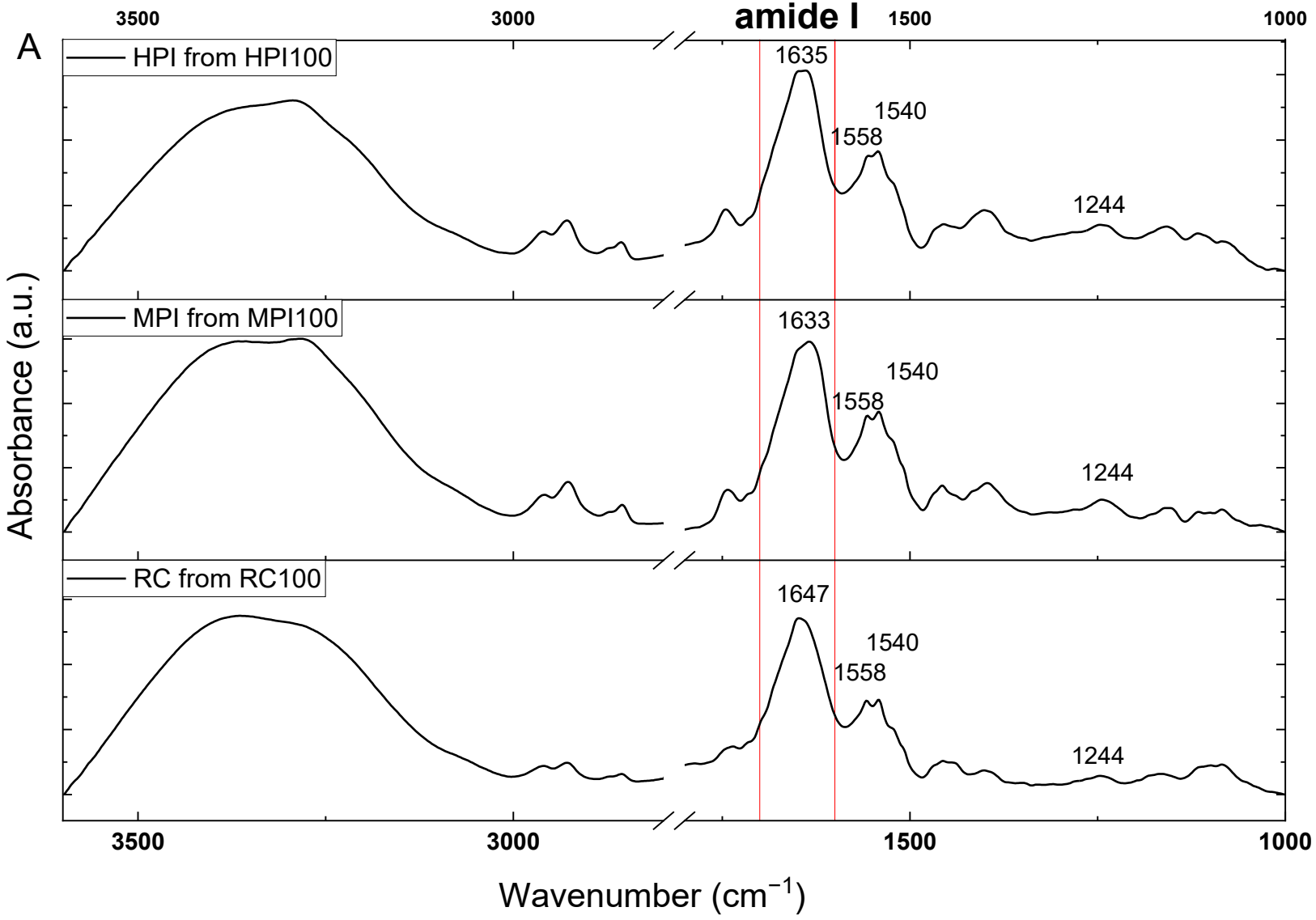
The secondary structure analysis revealed distinct differences among the proteins. The β-sheet structures were observed to be the major protein conformer in the plant protein (1620 cm^{-1} in MPI100 and 1630 cm^{-1} in HPI100), while casein was predominated by random coil structures (1647 cm^{-1}). This finding was consistent with that of previous studies and suggested that plant proteins were more prone to aggregation, contributing to a more rigid cheese structure, while casein exhibited more disordered structures that could facilitate flexibility (Lu, Roy, et al., 2026).

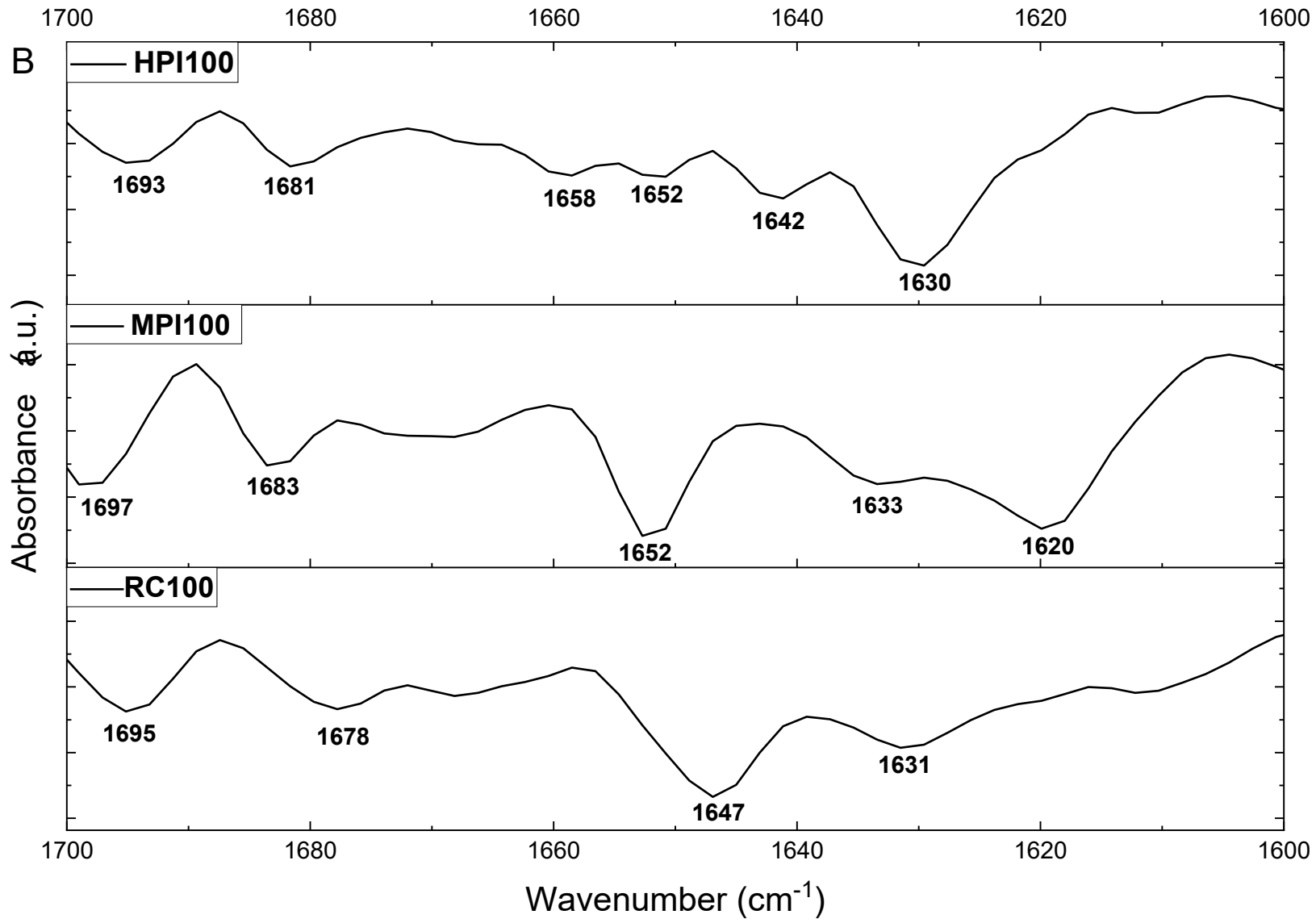
Specifically, MPI exhibited a mixed secondary structure, consisting of α-helix (35%), β-sheet (48%), and β-turn structures (16%) (**Figure 6-3D**). In comparison, HPI contained a lower proportion of α-helix (28%) but a higher content of β-sheets (50%) and β-turns (21%) (**Figure 6-3C**). The increased β-turn content and reduced α-helical structure in HPI suggest a relatively less ordered secondary structure compared with MPI, which may influence its molecular conformational behaviour. RC was predominated by random coils (48%), along with the presence of a few β-sheets (23%) and β-turns (28%) (**Figure 6-3E**). Notably, the β-sheet peak in MPI appeared at 1620 cm^{-1}, which was typically associated with intermolecular β-sheet formation involving stronger hydrogen bonding, suggesting a higher degree of protein aggregation (Sadat & Joye, 2020; Schestkowa et al., 2020). Comparatively, the β-sheet peak in HPI was more prominent at 1630 cm^{-1}, which was indicative of the association between intramolecular β-sheets and protein folding as well as stability, possibly reflecting a more compact and less aggregated structure (Eckhardt et al., 2024). The spectra of coconut oil were generated based on peak intensities obtained for RC100, MPI100 and HPI100. No marked differences were observed among them (Supplementary **Figure S 6-2**).

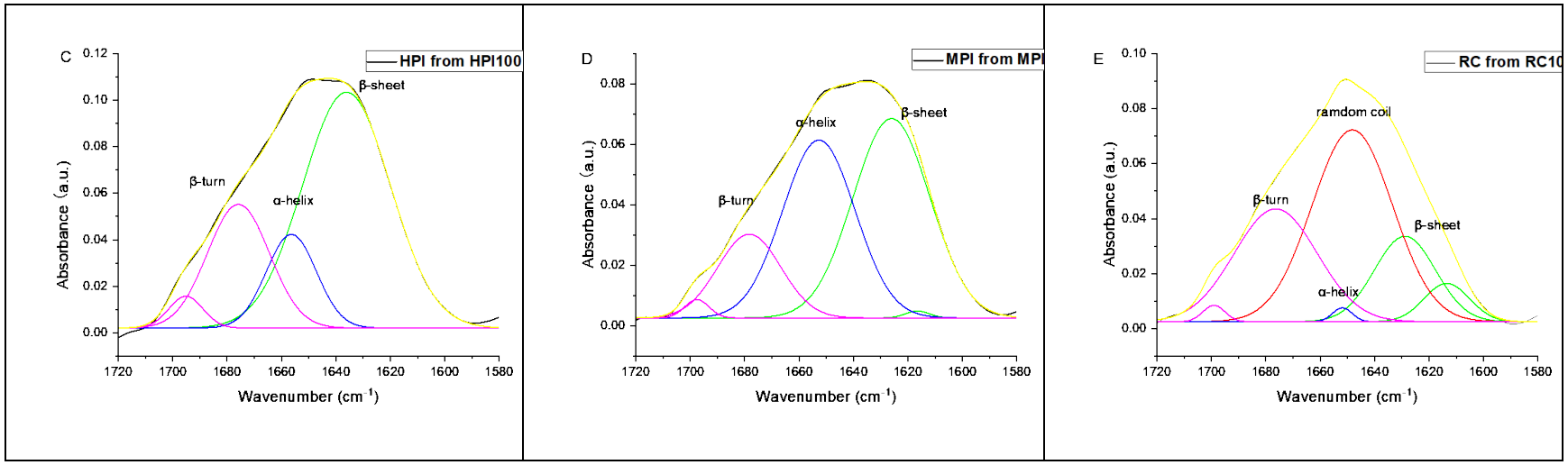
6.3.3. Distinguish plant proteins and caseins in dual-protein cheese systems

Building on the identification of spectral features for individual components in single-protein systems, this section focuses on distinguishing plant proteins from casein within dual-protein hybrid cheeses. The analysis was performed to compare the performances of the two unsupervised classification approaches: HCA and k-means clustering. HCA group spectra were generated based on similarity without prior knowledge of sample composition, allowing for an exploratory assessment of the way different regions clustered together. Similarly, k-means clustering partitions spectra into distinct groups but uses an iterative centroid-based approach, which often produces more balanced cluster sizes.

Accordingly, the cluster maps of MPI50 and HPI50 were generated using HCA and k-means clustering (**Figure 6-4**), respectively. Five clusters were identified in both HCA and k-means analyses, and the results were consistent between these two unsupervised methods. Notably, the edge regions consistently showed loss of spectral information owing to the highly collimated nature of the synchrotron-IR beam, highlighting the influence of imaging artefacts on the results. To further investigate the compositions of different clusters, small areas were selected for detailed analysis using HCA as an example (**Figure 6-5A** and **Figure 6-5B**).


A
amide I
HPI from HPI100
1635
1540
1558
1244
MPI from MPI100
1633
1540
1558
1244
RC from RC100
1647
1540
1558
1244
Absorbance (a.u.)
3500
3000
1500
1000
Wavenumber (cm^{-1})


B
HPI100
1693
1681
1658
1652
1642
1630
MPI100
1697
1683
1652
1633
1620
RC100
1695
1678
1647
1631
Absorbance (a.u.)
1700
1680
1660
1640
1620
1600
Wavenumber (cm-1)



	α-helix (%)	Random coil (%)	β-sheet (%)	β-turn (%)
MPI100	35 ± 28	1 ± 2	48 ± 17	16 ± 12
HPI100	28 ± 10	1 ± 1	50 ± 6	21 ± 16
RC100	1	48 ± 15	23 ± 13	28 ± 2

Figure 6-3. Average protein spectra of RC100, MPI100, and HPI100 cheese samples (A); corresponding second derivative spectra of the amide I region (B); and representative peak fitting of the amide I band for HPI (C), MPI (D), and RC (E). In the peak fitting, the black and yellow lines represent the experimental and final fitted spectra, respectively. The green, blue, red, and pink lines correspond to β-sheet, α-helix, random coil, and β-turn structures, respectively. RC100: cheese with 100% rennet casein; MPI100: cheese with 100% mung bean protein; HPI100: cheese with 100% hemp protein.

The average second derivative spectra of MPI50 were extracted from the selected area of 23 × 23 μm^2 (**Figure 6-5A** (1 and 4)). Clusters 1 (C1; green) and 2 (C2; blue) corresponded to protein-rich regions, which exhibited pronounced amide I bands, while cluster 4 (red) represented lipid-rich regions, which were characterised by strong ν(C–H) stretching vibrations and the ν(C=O) stretching mode of total lipids. Cluster 5 (orange) contained both proteins and lipids, forming a boundary surrounding the lipid-rich regions (**Figure 6-5A** (4)). The PCA scatter plot, used for visualising cluster separation (**Figure 6-5A** (2)), indicated that PC2 primarily distinguished C1 and C2, corresponding to the two protein types. Based on PC2 for ranking, the most discriminative features between mung bean protein and casein were observed to be the amide I band (particularly β-sheet structures), amide II band, lipid-related peaks and the absorption at ~1400 cm^{-1}. This absorption could be attributed to $\nu_s(COO^-)$ stretching modes associated with $\delta_s(CH_3)$ of fatty acids and amino acids (Dewantier et al., 2023; Movasaghi et al., 2008) (**Figure 6-5A** (3)). The amide I and II regions, which are the key features that distinguish mung bean protein and casein, are presented in **Figure 6-5A** (5) and (6), highlighting subtle differences in their peak positions and intensities. In the amide I region, C2 (blue) exhibited a more pronounced β-sheet signal (≈1618 cm^{-1}), while C1 (green) presented higher contributions from the random coil structures (≈1641 cm^{-1}). The amide II region displayed peaks at similar wavenumbers for both the clusters, with C2 exhibiting slightly higher intensity in the second derivative spectrum. Overall, these spectral patterns suggest that C1 is predominantly casein, while C2 is enriched with mung bean protein. Previous CLSM analysis further demonstrated that mung bean protein formed deflated spherical particles, while casein established the continuous network, with mung bean protein being a filler in MPI50 (Lu, Roy, et al., 2026), supporting this interpretation.

HCA K-means

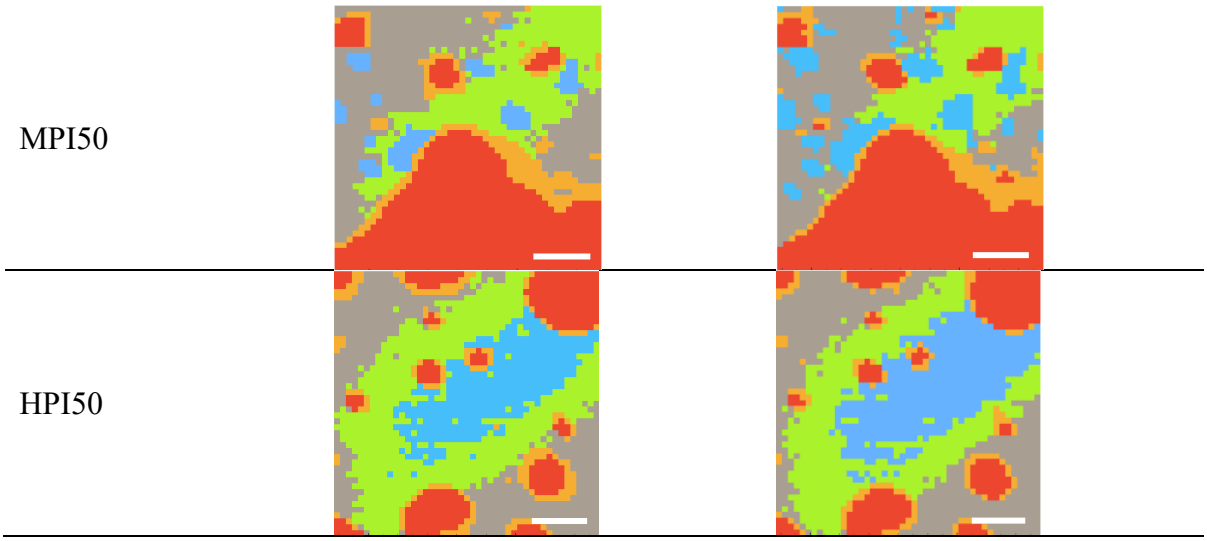
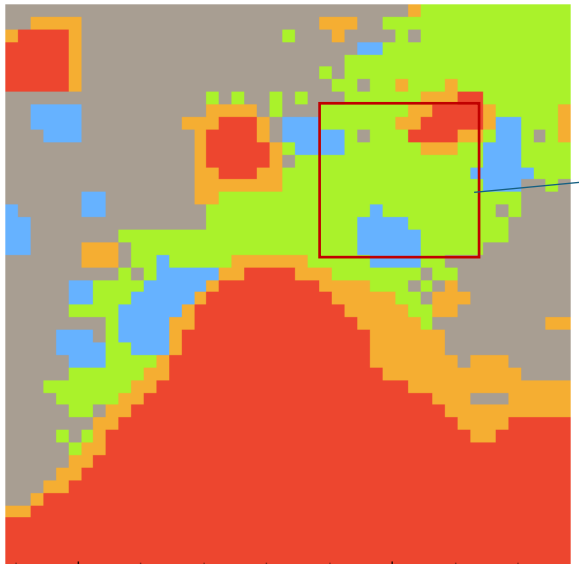


Figure 6-4. Representative FTIR chemical images of MPI50 (top) and HPI50 (bottom) using hierarchical clustering (left) and k-means models (right). Rennet casein is shown in green, mung bean/hemp protein in blue, and lipid in red in MPI50 and HPI50. Different colors represent clusters identified through hierarchical clustering or K-means. Scale bars are 20 μm in length. MPI50: cheese formulated with 50% mung bean protein and 50% rennet casein. HPI50: cheese formulated with 50% hemp protein and 50% rennet casein.

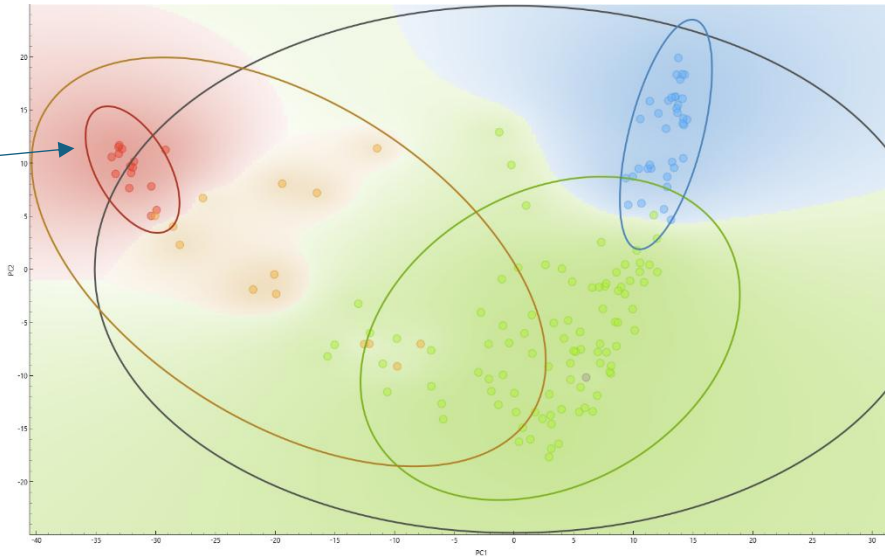
Similarly, the average second derivative spectra were extracted from a selected region of 38 × 42 μm^2 for HPI50 (**Figure 6-5B**). Based on the spectral characteristics, it could be concluded that C1 (red) corresponds to lipid-rich domains, C2 (blue) and C3 (green) represent protein-rich regions and C5 (orange) exhibits mixed contributions from both protein and lipid (**Figure 6-5B** (4)). PC2 indicated that the most discriminative features between hemp protein and casein were primarily associated with the amide II band, followed by the amide I band and lipid-related absorptions (**Figure 6-5B** (3)). Within the amide I region, C2 and C3 displayed subtle differences in their secondary structure, particularly in the relative contributions of the α-helix (~1658 cm^{-1}) and β-turn (~1662 cm^{-1}) components. More pronounced distinctions were observed in the amide II region, where C2 was characterised by spectral features at ~1531, ~1548 and ~1567 cm^{-1}, while C3 was defined by peaks at ~1542 and ~1560 cm^{-1}. These variations reflect differences in backbone δ(N–H) bending and ν(C–N) stretching vibrations, which are known to be sensitive to hydrogen bonding

and the electrostatic environment (Barth, 2007). Overall, the observed spectral patterns suggest that C2 was more consistent with hemp protein, while C3 aligned with casein. The increase in β-structure–associated signals in C2 was consistent with the aggregation tendency of hemp protein, while the spectral profile of C3 corresponded more closely to the flexible and random coil–rich structure of casein. These molecular-level distinctions provided direct evidence for the coexistence and differentiation of hemp protein and casein domains within the hybrid cheese matrix.

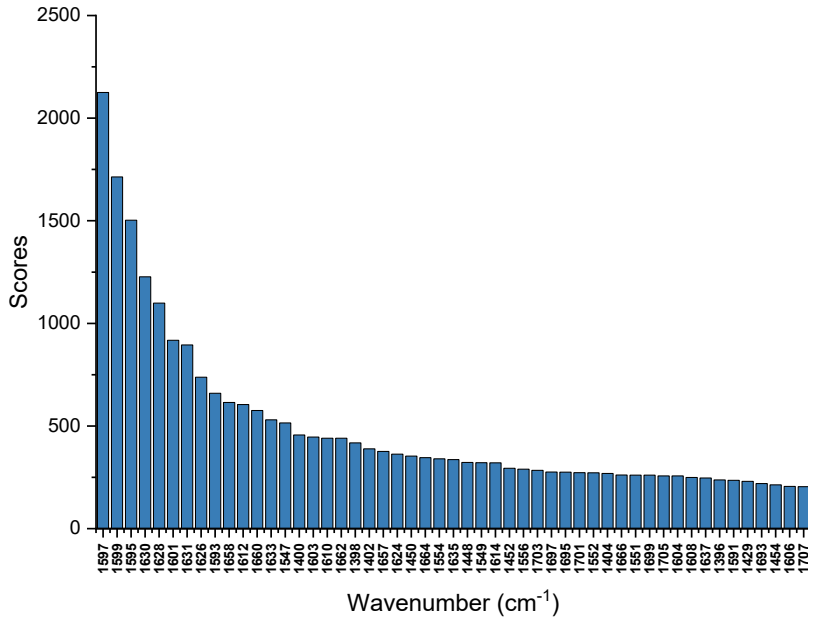
A1



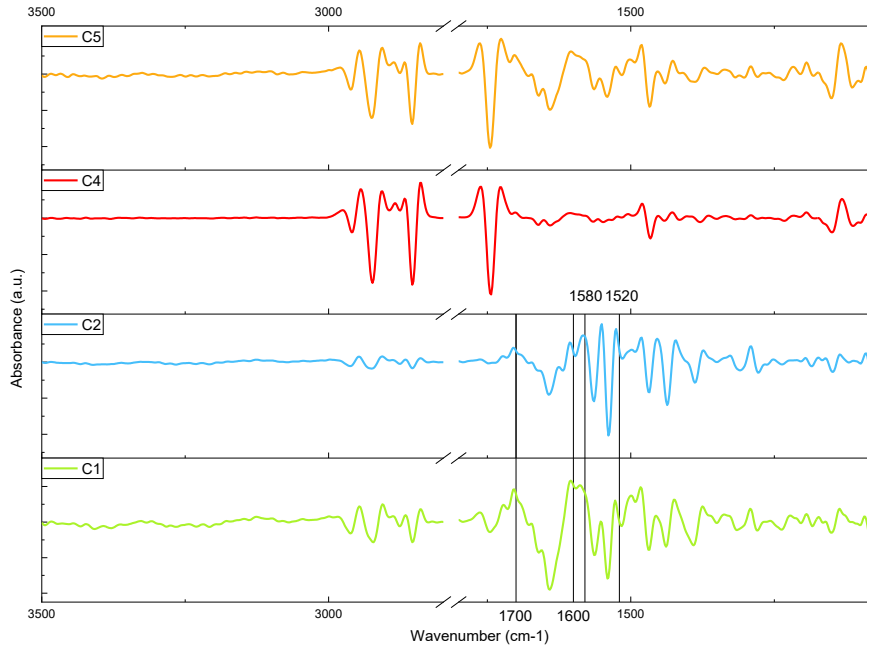
A2



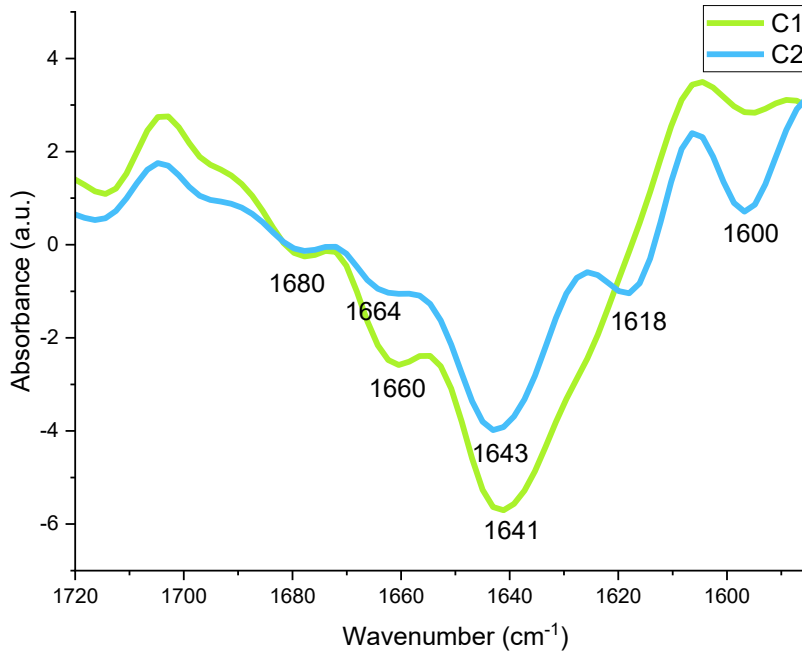
A3


Scores
Wavenumber (cm-1)

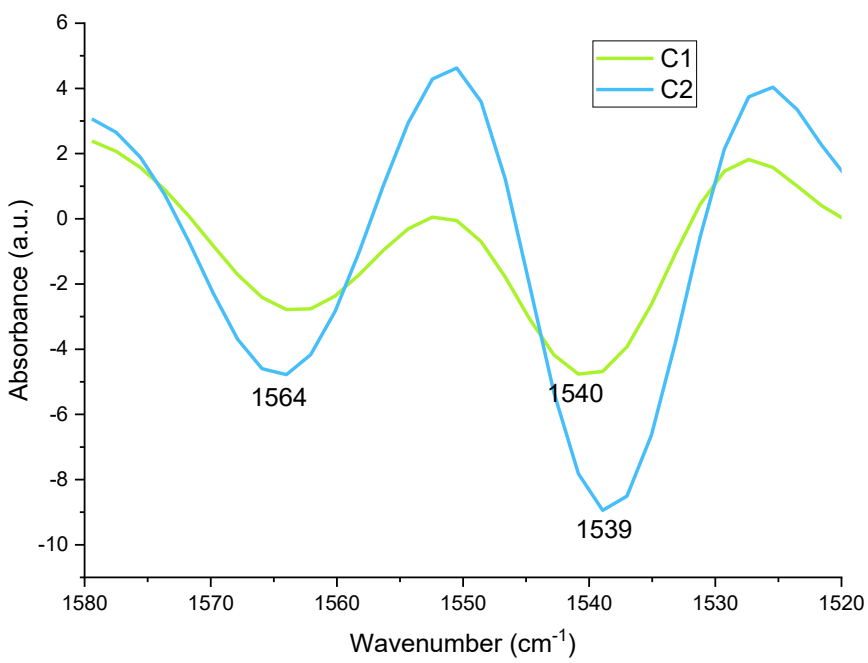
A4


C5
C4
C2
C1
1580 1520
Absorbance (a.u.)
Wavenumber (cm-1)

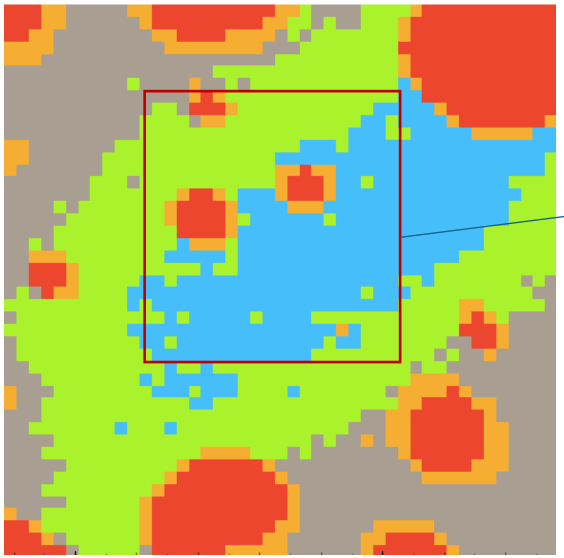
A5


C1
C2
Absorbance (a.u.)
Wavenumber (cm-1)
1680
1664
1660
1643
1641
1618
1600

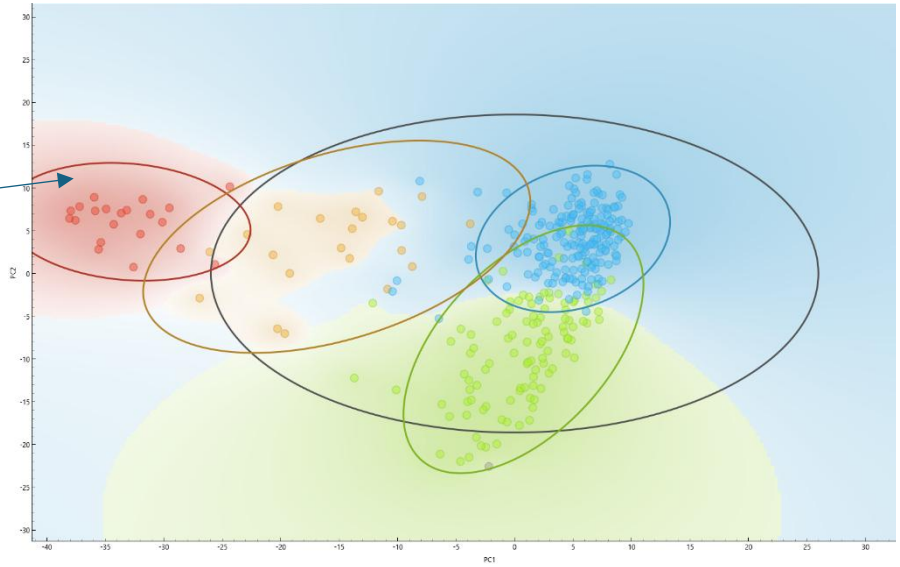
A6


C1
C2
Absorbance (a.u.)
Wavenumber (cm-1)
1564
1540
1539

B1

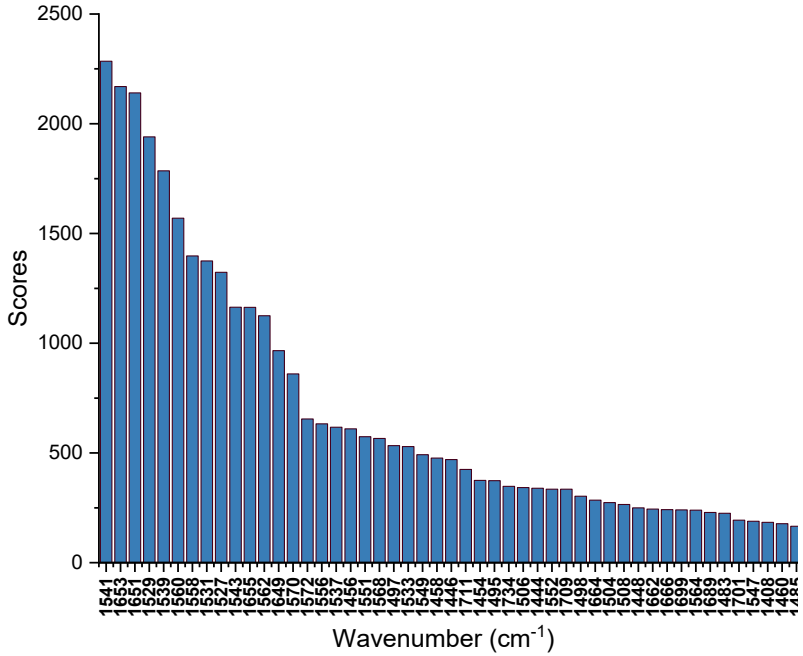


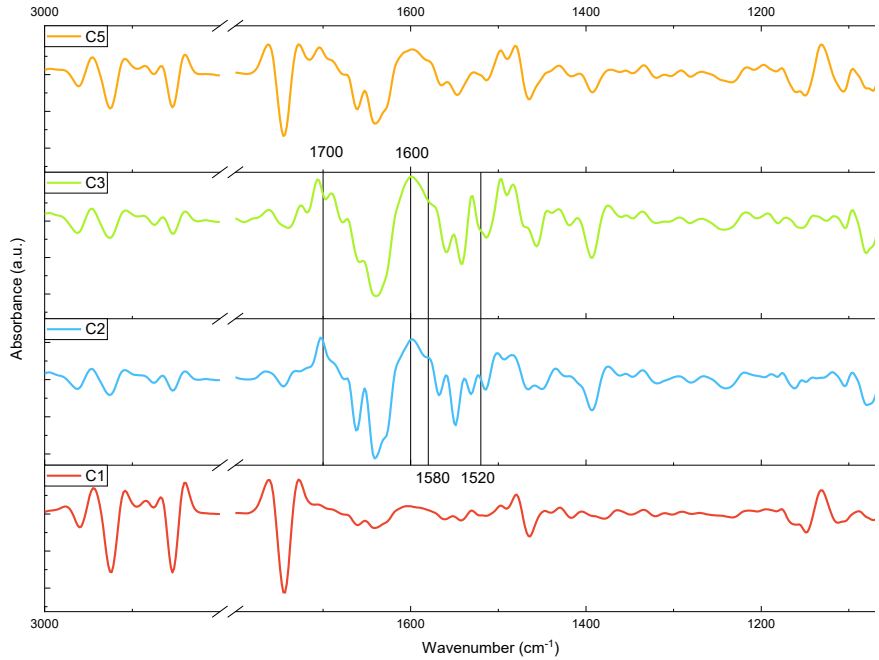
B2



B3

B4


2500
2000
1500
1000
500
0
Scores
Wavenumber (cm-1)


3000
1600
1400
1200
C5
1700
1600
C3
C2
C1
1580
1520
Absorbance (a.u.)
Wavenumber (cm-1)

B5

B6

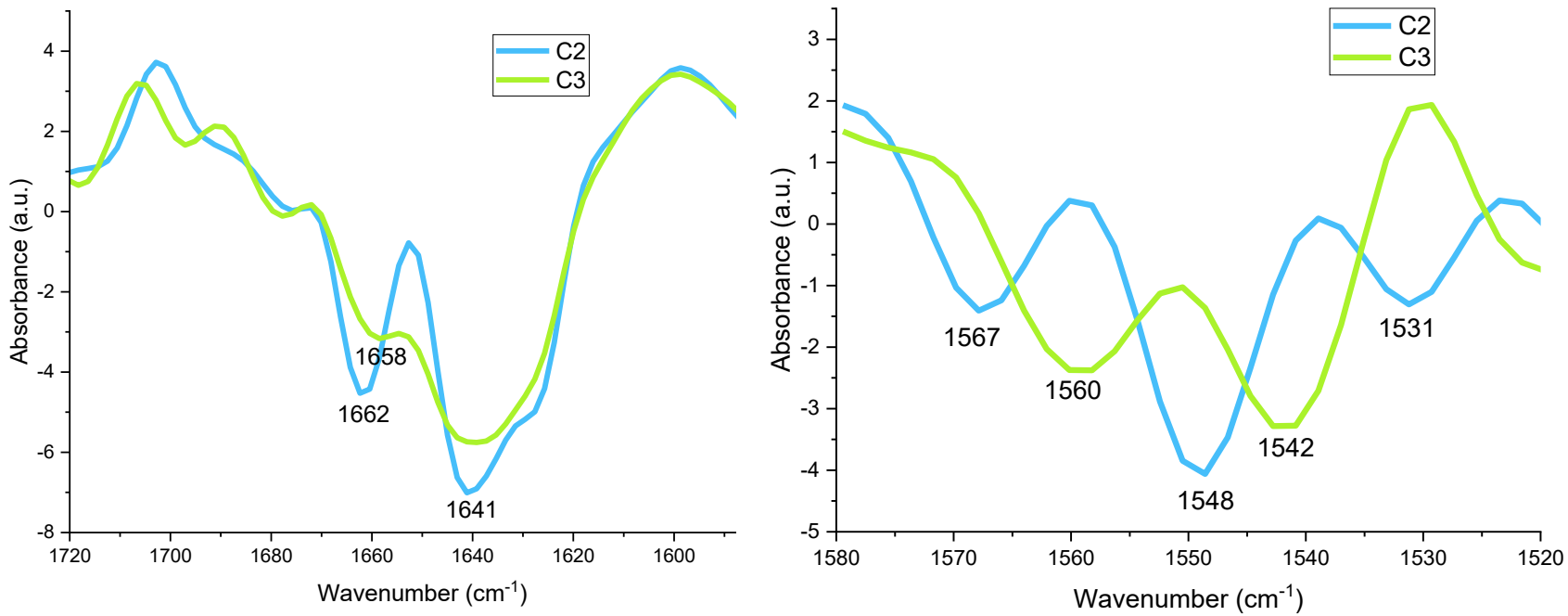


Figure 6-5. FTIR chemical images of MPI50 (A) and HPI50 (B). For MPI50: (A1) hierarchical clustering image, the red box shows region of interest (A2) PCA scatter plot or spectra within region of interest from A1, (A3) ranking based on PC2, (A4) average second derivative spectra of clusters, (A5) amide I region, and (A6) amide II region. For HPI50: (B1) hierarchical clustering image, (B2) PCA scatter plot, (B3) ranking based on PC2, (B4) average second-derivative spectra of clusters, (B5) amide I region, and (B6) amide II region.

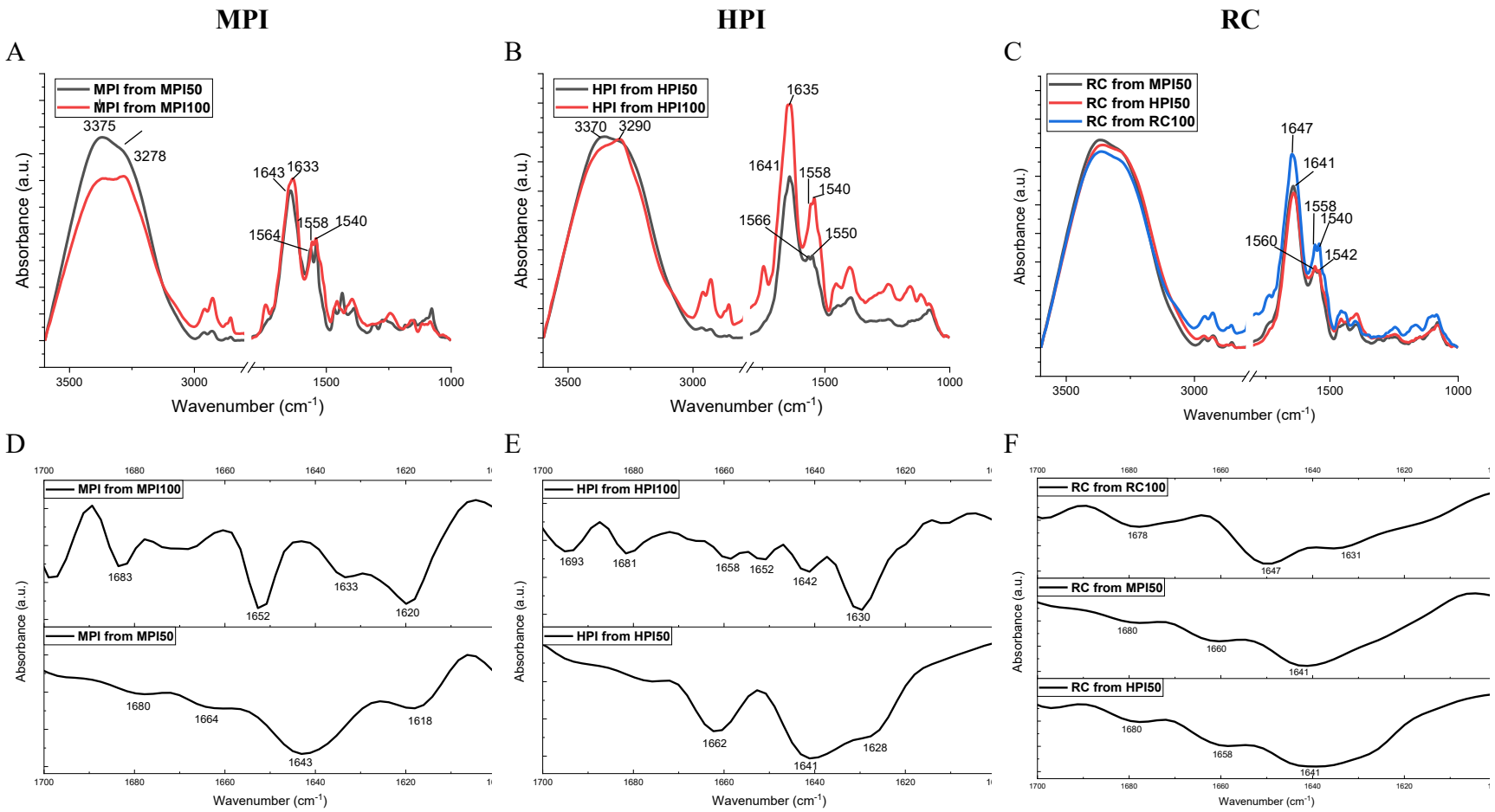


Figure 6-6. FTIR spectra of (A) MPI (from MPI100 and MPI50), (B) HPI (from HPI100 and HPI50), and (C) RC (RC100, MPI50, HPI50) showing protein structural changes in dual-protein systems. Panels (D–F) present the corresponding second-derivative amide I spectra for MPI, HPI, and RC, respectively.

6.3.4. Protein–lipid and protein–protein interactions

Following distinguishing the two protein types within the dual-protein cheese matrix, this section examined the protein–lipid and protein–protein interactions in the mixed systems. C5 contained both protein and lipid peaks and was located adjacent to the lipid regions (**Figure 6-5 A & B**). In the scatter plot of the MPI50 samples (**Figure 6-5A** (2)), C5 (orange) was positioned between C4 (lipid) and C1 (casein) but remained distant from C2 (mung bean protein). This spatial pattern indicated that coconut oil was more strongly co-located with casein than with mung bean protein, which could reflect higher hydrophobic compatibility between casein and lipid. By contrast, the scatter plot of HPI50 presented that C5 encompassed lipids, along with both hemp protein and casein, indicating the association of coconut oil with both types of protein. At the nanoscale, casein exhibits a highly amphiphilic network structure. In particular, β-casein readily adsorbs at the oil–water interface, forming a protective viscoelastic layer that prevents oil droplet coalescence and stabilizes lipid droplets (Zhai et al., 2011). In contrast, plant proteins are generally more rigid, with hydrophobic residues buried within the protein interior, leading to reduced interfacial interactions. They typically contain a higher proportion of β-sheet and fewer α-helix structures, exhibit more fibrillar conformations, and form interfacial films with lower modulus, making emulsions less stable under stress (Kim et al., 2020; X. Zhang et al., 2023). These findings were consistent with the TEM and CLSM observations (Lu, Roy, et al., 2026) and overall suggested that casein exhibited a strongest affinity towards coconut oil, followed by that of hemp protein, whereas mung bean protein exhibited a weaker association.

The spectra of MPI obtained from MPI100 and MPI50, HPI from HPI100 and HPI50 and RC from RC100, MPI50 and HPI50 were extracted to examine protein structural changes in the dual-protein systems (**Figure 6-6**). In the ν(O–H) stretching region (3600–3000 cm^{-1}), the MPI spectrum

obtained from MPI50 exhibited a broader ν(O–H) peak, with a higher wavenumber (~3375 cm^{-1}) than that of MPI100 (~3278 cm^{-1}) (**Figure 6-6A**), indicating weaker hydrogen bonding. This suggests that water in MPI50 was more loosely bound and existed in a less structured hydration environment. The incorporation of casein likely disrupted the compact MPI network through physical interactions and competition for water, resulting in a more open and heterogeneous protein matrix in which water molecules were less constrained. In contrast, MPI100 formed denser aggregates with stronger water binding (Ushkalova et al., 2025). Consistent with this, Nascimento et al. (2024) reported that water-holding capacity is closely related to gel microstructure, with stronger and more compact gels retaining more water. Pure pea protein gels showed higher water-holding capacity than mixed pea–casein systems, which tend to form independent networks. The increased water mobility in the mixed system may be attributed to the presence of larger water-filled cavities of casein, whereas pure plant protein gels form a more compact network that restricts water movement (da Silva et al., 2025).

In the amide I region, the incorporation of casein decreased the β-sheet content of mung bean protein (~1633 cm^{-1}) while increasing the proportion of disordered protein structures (1643 cm^{-1}). Second derivative analysis (**Figure 6-6D**) indicated decreases in α-helix and β-sheet structures with a concomitant increase in random coil contents. This suggested that casein disrupted β-sheet stacking and aggregation within the mung bean protein, resulting in a more disordered peptide environment. Furthermore, in the amide II region, the band at ~1540 cm^{-1} in MPI100 remained unchanged compared with that in MPI50, while the band at ~1558 cm^{-1} shifted to ~1564 cm^{-1}. This shift was indicative of changes in the local hydrogen-bonding environment around the peptide backbone, with higher wavenumbers reflecting weak N–H hydrogen bonding and more disordered local structure (Barth, 2007; Cobb et al., 2020). Although rheological and microstructural analyses

showed that plant protein and casein did not co-aggregate during heating and instead formed independent networks at the micron scale (Lu, Roy, et al., 2026), the introduction of a second protein component nevertheless disrupted the aggregation behaviour and secondary structure of mung bean protein at smaller length scales. This effect can be attributed to structural frustration, whereby steric constraints and competition for water prevent optimal protein–protein packing, forcing local conformational rearrangements within the plant protein. Similar frustration effects have been reported in fibre and mixed gel systems, where local mismatches promote irregular void formation and weaken water retention (Liu et al., 2025). The small-angle X-ray scattering and nuclear magnetic resonance data have shown incorporation of 20% plant protein into casein gels (or vice versa) can induce structural changes, with gel properties governed by large-scale organization and pore size distribution rather than molecular composition alone (da Silva et al., 2025). An additional mechanism may contribute to the observed interactions between plant protein and casein in the mixed systems. Owing to the porous nature of the casein network, attractive interactions and partitioning behaviour may allow plant protein particles to partially penetrate the casein matrix, depending on their size. Smaller plant protein particles can occupy the pores within the casein network, simultaneously displacing water (Peixoto et al., 2015). This redistribution of water may reduce water-holding capacity and weaken protein–water hydrogen bonding, consistent with the higher ν(O–H) wavenumbers and the shifts in amide I and amide II bands observed by FTIR. Such size-dependent partitioning provides a mesoscale mechanism linking network architecture to local hydration and peptide bonding environments.

Similarly, the addition of casein in HPI50 produced a more heterogeneous spectrum, and the dominant ν(O–H) absorption peak shifted to a higher wavenumber (~3370 cm^{-1}) than that observed for HPI100 (~3290 cm^{-1}). This blue shift indicated that the mixed system resulted in a

higher proportion of loosely hydrogen-bonded water, suggesting a less compact network structure than that of the pure hemp protein matrix. This effect occurred owing to the chaperone-like activity of casein, which could inhibit protein self-aggregation (Chuang et al., 2019). In addition, casein could compete with HPI for forming hydrogen bonds with water and protein side chains, further limiting HPI–HPI interactions. This was accompanied by a decrease in β-sheet protein (~1633 cm^{-1}) and an increase in disordered (~1641 cm^{-1}) and β-turn (1662 cm^{-1}) structures (**Figure 6-6 B & E**), consistent with a less aggregated and more flexible protein network. In the amide II region (mainly δ(N–H) and ν(C–N) modes), the bands at ~1540 and ~1558 cm^{-1} in HPI100 shifted to ~1550 and ~ 1566 cm^{-1}, respectively. These blue shifts towards the high energy range reflect alterations in the local hydrogen-bonding environment around the peptide backbone. Similar hydrogen bond–mediated shifts have been reported for starch–casein systems (Sun et al., 2016), highlighting the role of hydrogen bonding in modulating protein–matrix interactions. While comparing the RC spectra from RC100, MPI50 and HPI50, no notable changes were observed (**Figure 6-6C**). However, analysis of the second derivative spectra indicated minor differences in the RC component between MPI50, HPI50 and RC100. Specifically, the peaks at ~1640 cm^{-1} were broader in the mixed-protein systems and exhibited a small shoulder corresponding to α-helical protein structures. These observations suggest that the presence of casein better perturbs the structural organisation of plant proteins than vice versa.

Overall, in the mixed systems, despite the formation of independent protein networks at the micron scale, both networks occupy the same physical space and aggregate simultaneously. Competition for water and local hydrogen-bond rearrangements generate intermediary-scale structural frustration, which disrupts the native folding and aggregation pathways of each protein. These

effects are sufficient to modify the vibrational environments of O–H, amide I, and amide II groups, explaining the observed spectral shifts in the mixed systems.

6.3.5. Complementary insights into Raman and S-FTIR results

FTIR and Raman spectroscopies are complementary techniques, as polar groups produce strong IR absorptions, while nonpolar groups exhibit strong Raman scattering. Raman microspectroscopy was previously employed for characterising HPCs, identifying protein types, lipids and additives in hybrid cheese as well as for distinguishing the interactions between MPI–casein and HPI–casein. HPI increased structural disorder and facilitated disulphide bond rearrangements, while MPI enhanced protein domain separation due to stronger aggregation and higher β-sheet content (Lu, McGoverin, et al., 2026; Lu, Roy, et al., 2026). Herein, the molecular information obtained by conducting S-FTIR and Raman microspectroscopies was observed to be correlated; their complementary insights are summarised in **Table 6-2**.

Table 6-2. Complementary insights of confocal Raman microscopy and S-FTIR for protein structure analysis in HPCs

Spectroscopic Feature	Confocal Raman Microscopy (1800-200 cm^{-1})	Synchrotron FTIR (4000-1000 cm^{-1})
Sample preparation	Simple	Simple
Amide I (1700-1600 cm^{-1})	Good sensitivity; less water interference; suitable for secondary structure deconvolution	Strong sensitivity, but water absorbance overlaps in amide I (1650-1640 cm^{-1}), complicating analysis in HPCs
Amide II (1570-1500 cm^{-1})	Weaker signal	Stronger than Raman spectroscopy
Amide III (1400-1200 cm^{-1})	Detectable, complementary to Amide I	Weak in HPCs
I_{850}/I_{830} ratio, Tyr environment)	Yes – informative on protein–water interactions	No

S–S stretch (550-500 cm^{-1})	Yes – useful for monitoring disulfide bonds and conformational stability	Not accessible
Phospholipids (1001 cm^{-1})	Yes – can detect	Limited – less specific
Water interference	Minimal	Strong δ(H–O–H) bending overlaps with amide I
Spatial resolution	High (~1 μm)	Good with synchrotron-IR beam (3.2 μm)
Suitability for HPCs (~40% moisture)	Highly suitable – less spectral distortion from water, can resolve protein/lipid domains in situ	Challenging – strong water absorbance makes secondary structure analysis less reliable

Protein analysis in high-moisture systems was particularly challenging for FTIR spectroscopy, as the intense δ(H–O–H) bending vibration of water overlapped with the amide I region, complicating analysis of the secondary protein structure (Miller & Dumas, 2010; Sadat & Joye, 2020). Although FTIR spectroscopy is the gold standard for analysing protein secondary structure owing to its strong amide I/II signals and extensive spectral databases, its application in hydrated materials remains limited. Alternatively, Raman spectroscopy is far less affected by water interference, as its scattering intensity depends on the changes in molecular polarizability, with strongly polar water molecules contributing only weak Raman signals (Larkin, 2018). In addition, Raman spectroscopy is particularly sensitive to disulphide bonds and aromatic residues, while confocal mapping correlates structural and microstructural features. As the hybrid cheese examined in this study contained ~40% moisture (Lu, Roy, et al., 2026), Raman spectroscopy became a relatively robust tool for examining protein structural changes. At the same time, FTIR spectroscopy was a valuable method used for cross-validation and providing complementary insights. The FTIR and Raman spectroscopy results were consistent with the previous reports on hemp globulin–casein interactions. For example, Chuang et al. (2019) showed that casein exerted a chaperone-like effect, inhibiting hemp globulin aggregation and improving colloidal stability. Meanwhile, Chuang et al.

(2021) that pH-cycling promoted HG–SC nanoparticle formation mainly via hydrogen bonding and disulfide interactions. Similarly, our FTIR analysis suggested that casein suppressed β-sheet formation in hemp protein (limiting aggregation) through hydrogen bonding, while the Raman analysis results indicated disulphide bond rearrangement and increased structural disorder in hybrid cheese (Lu, McGoverin, et al., 2026). These complementary findings indicate that HPI–casein creates a flexible, dynamic protein network that supports enhanced meltability and aligning with lower G′ values and a more deformable, energy-dissipating network. By contrast, the stronger aggregation and higher β-sheet content of MPI result in a rigid, segmented microstructure with pronounced protein domain separation, elevated G′, and reduced network connectivity, which is consistent with decreased meltability and stretchability (Lu, Roy, et al., 2026). These structural differences highlight how protein secondary structure and molecular interactions are associated with the macroscopic texture and functional properties of hybrid cheeses.

Dewantier et al. (2023) applied FTIR and Raman spectroscopy to classify cheddar cheeses by maturity, with the amide I and II bands driving FTIR classification and lipid-associated bands dominating in Raman spectra. Ørskov et al. (2023) used the same techniques to assess the microstructural composition and interactions in imitation cheese containing casein, lipids and modified starches. Although these methods successfully identified the components, they failed to resolve the specific interaction types, likely owing to limited resolution. This limitation underscored the need for more advanced analytical approaches, such as high-resolution S-FTIR, to unravel the detailed interactions within the complex food matrix.

Sadat and Joye (2020) compared the results of FTIR and FT-Raman spectroscopy for analysing the secondary structure of four globular proteins in aqueous solution and hydrated zein and gluten, demonstrating that water removal was essential for obtaining FTIR spectra. After correction, both

FT-Raman and FTIR spectra were well defined with comparable secondary structure estimations. However, herein, water removal was not performed to preserve the native hydration environment of the proteins. Moreover, as the interaction of protein with water could slightly shift the H_2O bending signal (Zuber et al., 1992), there remained a risk of the development of subtraction artefacts. To leverage the combined strengths of FTIR and Raman spectroscopies, a multimodal approach was developed by combining both the techniques; this integration enabled a more thorough and nuanced exploration of chemical structures (Jurowski et al., 2024). This became a powerful tool for conducting studies on complex food matrices in future.

6.4. Conclusions

This chapter used high-resolution S-FTIR microspectroscopy to map the spatial distribution of the key biomacromolecules in processed hybrid cheeses and to differentiate plant proteins from casein via unsupervised multivariate analysis. Although both HCA and k-means clustering produced broadly similar spatial patterns, HCA generated more stable and structurally meaningful clusters. Therefore, subsequent analyses were based on HCA results. This technique offered insights into intermolecular interactions, such as protein–protein and protein–lipid interactions. Overall, the S-FTIR results were complementary to those obtained from Raman spectroscopy, reinforcing the observations across both the techniques.

In the hemp protein–casein cheeses, the S-FTIR results suggested that the interactions between hemp protein and casein were likely mediated by hydrogen bonding and Raman spectroscopy offered a complementary insight into the arrangement of disulfide bonds. The amide II region emerged as the key spectral feature that distinguished these two protein types. Alternatively, for mung bean protein–casein cheeses, the amide I region played the dominant role in differentiating

casein from mung bean protein. Increasing the proportion of casein in these mixtures reduced both MPI and HPI aggregation and weakened N–H hydrogen bonding, indicating that water was less strongly bound and that the protein network was more flexible.

Regarding lipid distribution, S-FTIR analysis indicated that coconut oil was preferentially associated with casein rather than with plant proteins. Overall, these findings highlighted the complementary nature of S-FTIR and Raman spectroscopies in resolving both compositional differences and molecular interactions within hybrid cheese matrices.

6.5. Acknowledgments

The synchrotron macro ATR-FTIR experiment was undertaken at the Infrared Microspectroscopy (IRM) beamline at the Australian Synchrotron, part of ANSTO, via merit-based beamtime proposal (ID. M22940) in February 2025.

6.6. Supplementary material

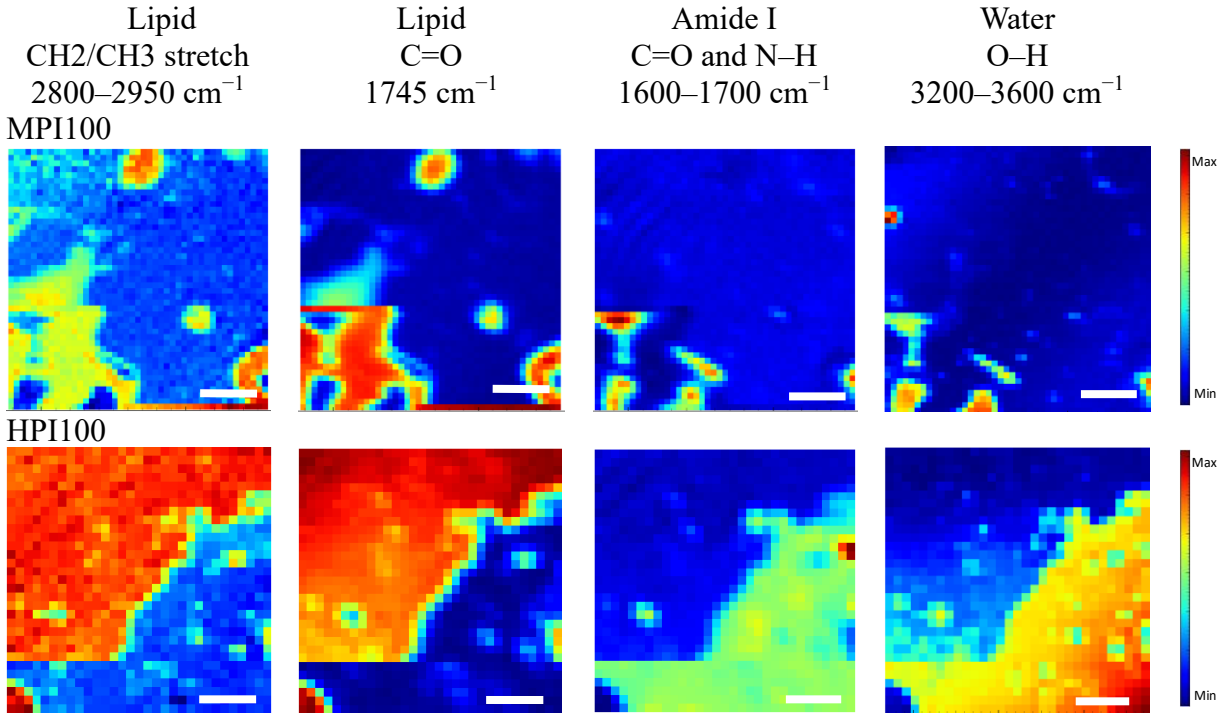


Figure S 6-1. A representative S-FTIR chemical images of the processed cheese formulated with 100% mung bean protein (MPI100) and 100% hemp protein (HPI100). The distribution of lipids, proteins, and water was produced using integrated areas under specific bands at 2950-2800 and 1745 cm−1, 1700-1600 cm−1, and 3600-3200 cm−1, respectively. Red indicates a high concentration, while dark blue represents a low concentration, as shown by the colour intensity scale on the right. The scale bars are each 20 µm in length.

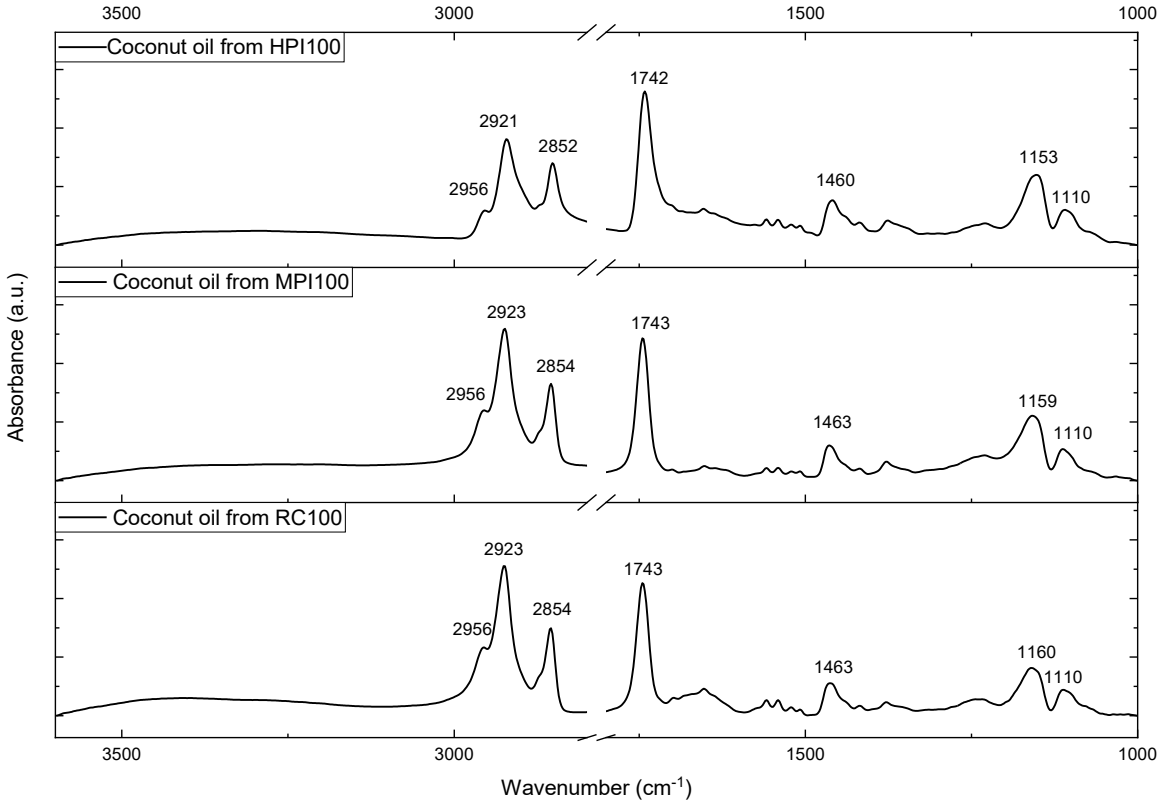


Figure S 6-2. Average coconut oil spectra obtained from HPI100, MPI100, and RC100 cheese samples. RC100: cheese with 100% rennet casein; MPI100: cheese with 100% mung bean protein; HPI100: cheese with 100% hemp protein.

MASSEY UNIVERSITY
TE KUNENGA KI PŪREHUROA
UNIVERSITY OF NEW ZEALAND

GRADUATE RESEARCH SCHOOL

STATEMENT OF CONTRIBUTION
DOCTORATE WITH PUBLICATIONS/MANUSCRIPTS

We, the student and the student's main supervisor, certify that all co-authors have consented to their work being included in the thesis and they have accepted the student's contribution as indicated below in the Statement of Originality.

Student name:	Di Lu
Name and title of main supervisor:	Aiqian Ye
In which chapter is the manuscript/published work?	Chapter 7

Describe the contribution that the student and members of the supervisory team have made to the manuscript/published work:[1]

Di Lu: Conceptualization, Data curation, Formal analysis, Investigation, Methodology, Writing—original draft.
Debashree Roy: Supervision, Writing—review & editing.
Alejandra Acevedo-Fani: Supervision, Writing—review & editing.
Harjinder Singh: Supervision, Writing—review & editing.
Ye Aiqian: Conceptualization, Funding acquisition, Project administration, Supervision, Writing—review & editing.

Please select one of the following three options:

○	The manuscript/published work is published or in press Please provide the full reference of the research output:
○	The manuscript is currently under review for publication Please provide the name of the journal:
◉	It is intended that the manuscript will be published, but it has not yet been submitted to a journal

Student's signature:	Di LU Digitally signed by Di LU DN: cn=Di LU, o=Massey University, email=d.lu@massey.ac.nz Date: 2026.02.25 11:15:04 +13'00'	Main supervisor's signature:	Aiqian Ye Digitally signed by Aiqian Ye DN: cn=Aiqian Ye, o=Massey University, ou=Riddet Institute, email=A.M.YE@massey.ac.nz Reason: I am approving this document Date: 2026.02.27 11:40:06 +13'00'

This form should be placed at the beginning of each relevant thesis chapter.

[1] Refer to the Massey University Publishing and Authorship guidelines (OneMassey for staff, Stream for students) and/ or Contributor Roles Taxonomy (CRediT) guidelines for guidance.

Chapter 7 A Hydrolysis-Based Strategy to Improve Meltability in Processed Cheese Analogues[6]

Abstract

Plant-based cheese analogues often exhibit poor meltability. In this chapter, mung bean protein isolate (MPI) was enzymatically hydrolysed using Alcalase for different durations to improve the meltability of MPI-based and hybrid cheeses, with additional comparison to trypsin-treated proteins. The degree of hydrolysis (DH) increased rapidly with enzymatic treatment (e.g. ~9% after 1 min and ~20% after 120 min). Increasing DH induced pronounced structural modifications, including reductions in molecular weight and particle size, and an increase in surface hydrophobicity. These changes were supported by RP-HPLC and SEC-HPLC analyses, which revealed extensive protein breakdown into low-molecular-weight peptides and altered peptide profiles. The reduced molecular size enhanced protein solubility but decreased water-holding capacity. Consequently, plant-based and hybrid cheeses formulated with MPI hydrolysates exhibited reduced elasticity, a more fragmented and heterogeneous microstructure, and improved melting behaviour with increasing DH. At comparable DH, trypsin-treated MPI showed significantly higher surface hydrophobicity (168.97 *vs* 63.35) and larger particle size (D[4,3], 86.78 *vs* 49.42 μm) than Alcalase-treated MPI, leading to greater aggregation, a more rigid protein network, and poorer meltability. These results demonstrate that enzyme-specific hydrolysis generates peptides with distinct structural characteristics, which play a more critical role than DH alone in determining the functional properties of the final cheese products. This study provides an efficient strategy for improving the meltability of plant-based cheese and enables a deep understanding of the structure-function mechanism induced by enzyme hydrolysis.

[6]This chapter will be published as Lu, D., Acevedo-Fani, A., Roy, D., Singh, H., & Ye, A. (2026). A Hydrolysis-Based Strategy to Improve Meltability in Processed Cheese Analgues, intented to submit to Food Hydrocolloid

7.1. Introduction

The global demand for plant-based and hybrid dairy alternatives has grown rapidly in response to concerns surrounding environmental sustainability, ethical considerations, and changing consumer health and lifestyle preferences (Day, 2013; Mazac et al., 2023; Zhang, Jiang, et al., 2024). Cheese analogues formulated by partially or fully replacing milk proteins with plant-derived proteins represent one of the fastest-growing sectors within this category. While global cheese production and consumption continue to rise, the market for plant-based cheese is also expanding steadily, although it still represents a small but rapidly increasing proportion of the dairy alternatives market (Alehosseini et al., 2025; Grossmann & McClements, 2021).

Despite strong market growth, the development of high-function quality, protein-rich plant-based cheese alternatives presents significant techno-functional challenges. Early generations of commercial plant-based cheeses were predominantly starch- or fat-based with little or no protein, offering poor nutritional value and lacking the crucial functionality provided by dairy proteins – most notably meltability (Grasso et al., 2021). In dairy systems, casein is uniquely capable of melting and flowing upon heating due to its flexible, amphiphilic structure and the formation of a continuous protein network that rearranges during thermal treatment (Atik & Huppertz, 2023; Salunke et al., 2022; Savello et al., 1989). By contrast, most plant proteins do not form comparable heat-responsive networks and instead produce rigid or brittle matrices that soften with heat but do not exhibit true melting or stretching behavior. Consequently, even when plant proteins are incorporated into cheese-like matrices, functional performance remains limited (Braitmaier et al., 2024; Grasso et al., 2021). In Chapter 3, nine plant proteins (lentil, soy, pea, chickpea, mung bean, hemp, canola, zein, and quinoa) were evaluated, showing that none were able to produce a meltable cheese analogue (Lu et al., 2025). Although zein has shown some melting potential (Sutter et al.,

2023), its applications are constrained by requirements for high concentrations, resulting in hard, brittle textures at room temperature and limited nutritional value, making it less desirable for plant-based cheese applications (Lu et al., 2025). Other studies have attempted to enhance meltability and texture by incorporating modified starches or polysaccharides into plant-protein-based systems (Lyu et al., 2023; Noronha, Duggan, Ziegler, O'Riordan, et al., 2008; Sanders et al., 2024b; Yiu et al., 2026). However, in such systems, the improved functionality is largely driven by starch or hydrocolloid behavior rather than by the plant proteins themselves, highlighting the ongoing challenge of achieving protein-driven meltability in plant-based cheese analogues.

Mung beans are a nutritionally dense and sustainable source, containing approximately 25–28% protein, rich in lysine, and offering a balanced amino acid profile (Li et al., 2023). The major storage proteins are globulins, and ~89% of these are 8S vicilins (Yi-Shen et al., 2018). The 8S vicilin fraction has been extensively studied and is known to share structural and functional similarities with soybean 7S β-conglycinin (Itoh et al., 2006; Mendoza et al., 2001; Tang & Sun, 2010). However, mung bean vicilin lacks disulfide bonds due to low levels of sulfur-containing amino acids, which contribute to its limited gelation and network-forming capacity. Previous work in Chapters 3 and 4 has shown that cheeses formulated with mung bean protein develop coarse, aggregated microstructures and show inferior meltability compared to those made with lentil, soy, or hemp proteins (Lu, Roy, et al., 2026; Lu et al., 2025). In Chapters 5 and 6, in hybrid systems combining mung bean protein with casein, phase separation has been observed, and spectroscopic analyses have shown reductions in β-sheet structures with increasing casein ratios, coinciding with improvements in microstructure and functional performance (Lu, McGoverin, et al., 2026; Lu, Vongsvivut, et al., 2026).

To overcome these limitations, enzymatic hydrolysis has emerged as a promising approach to tailor the techno-functional properties of plant proteins. Enzymatic cleavage breaks down the native protein into smaller peptides and amino acids, resulting in reduced molecular weight, increased solubility, greater surface hydrophobicity, and exposure of ionizable groups (Wouters et al., 2016). Controlled enzymatic hydrolysis is known to improve functional behaviors such as emulsification, foaming, gelation, water binding, and thermal responses (Chen & Campanella, 2022; Ganesh et al., 2022; C. Liu et al., 2019; Vogelsang-O'Dwyer et al., 2022; Wang et al., 2022; Xie et al., 2021). However, extensive hydrolysis often disrupts protein structure to an extent that impairs functionality, leading to excessive peptide solubilization, weakened networks, and poor textural integrity (Kanokwan Promjeen et al., 2025; Wouters et al., 2016). Therefore, a controlled or moderate hydrolysis may offer an optimal strategy for improving the meltability and structural performance of plant-protein-based cheese analogues. A limited number of studies have investigated the use of enzymatically modified plant proteins to partially replace fat or casein in cream cheese or Mozzarella cheese analogues (K. Li et al., 2018; Limit et al., 2024; Xie et al., 2021; Zhang, Ling, et al., 2024). These studies reported that partial enzymatic hydrolysis reduced cheese elasticity, disrupted the continuity of the protein network, and improved melting and stretching properties. However, research focusing specifically on plant-based cheeses formulated with protein hydrolysates remains scarce, and the relationship between hydrolysate structural characteristics and cheese functionality is still not well understood.

In this chapter, two widely used commercial proteases, Alcalase and trypsin, were employed to generate MPI hydrolysates. Alcalase, a subtilisin-derived alkaline serine endopeptidase from *Bacillus licheniformis*, cleaves peptide bonds adjacent to hydrophobic and aromatic residues and is known for broad substrate specificity. Trypsin, by contrast, commonly derived from porcine

sources exhibits a highly specific cleavage pattern, primarily acting on the carboxyl side of lysine and arginine residues (Shuai et al., 2022; Vogelsang-O'Dwyer et al., 2022). Comparing the effects of these two enzymes at similar degrees of hydrolysis level will elucidate the role of enzyme specificity in determining protein structure and ultimately on cheese functionality.

The hypothesis of this chapter is that limited enzymatic hydrolysis of MPI will enhance performance (particularly meltability) of plant-based and hybrid cheese analogues, and that the extent of improvement is dependent on both the degree of hydrolysis and the structural characteristics of the resulting peptides. To test these hypotheses, the study established the flowing aims: 1) characterise the enzymatic hydrolysis of MPI using Alcalase, including its physicochemical and structural changes; 2) evaluate the functionality of cheeses formulated with Alcalase-hydrolysed MPI powders of varying degrees of hydrolysis; 3) assess processed hybrid cheeses prepared using MPI hydrolysed for 30 min blended with casein (50:50) to compare the functional properties with non-hydrolysed controls; and 4) compare the functional performance of Alcalase- and trypsin-derived MPI hydrolysates at similar degrees of hydrolysis to elucidate how enzyme specificity influences cheese characteristics.

7.2. Materials and Methods

7.2.1. Materials

Rennet casein (RC; SureProteinTM 779) containing 82% protein was obtained from Fonterra Co-operative Group Ltd., New Zealand. Mung bean protein isolate (85%; MPI) was purchased from Bulk Powders New Zealand. Alcalase® 2.4L (Bagsværd, Denmark) and Trypsin (T0303, Sigma-Aldrich) were purchased. All other chemicals used were of analytical grade and obtained from Sigma Chemical Co., unless otherwise specified.

7.2.2. Sample preparation and enzymatic hydrolysis

MPI was dispersed in distilled water (containing 0.02% sodium azide) to a final concentration of 10% (w/v) protein in a total volume of 100 mL. The suspension was stirred using a magnetic stirrer and allowed to dissolve overnight at room temperature. The protein solution was then transferred into a pH-stat–compatible beaker, which was placed in a water bath set at 50 °C for Alcalase hydrolysis or 37 °C for trypsin hydrolysis. The pH was adjusted to 8.0 and maintained using 0.2 M NaOH. The solution was equilibrated at the target temperature and pH for 30 min prior to enzyme addition.

The pH-stat system was configured with 0.2 M NaOH as the titrant, titration steps of 0.1 mL, and a dosing volume of 5% of the burette volume at 50 mL/min. Data were recorded at 1 s^{-1} for time points 1, 3, 5, 10, and 15 min, and at 1 min^{-1} for 30 and 120 min. Enzymatic hydrolysis was initiated by adding Alcalase at an enzyme-to-substrate ratio of 1:100 (v/w) or trypsin at 1:100 (w/w) (Wang et al., 2022). Samples were collected at 1, 3, 5, 10, 15, 30, and 120 min, with the pH continuously maintained at 8.0 throughout hydrolysis.

At each time point, the hydrolysate was immediately transferred to a larger preheated beaker and placed in a boiling water bath. The temperature of the sample was monitored until it reached 85 °C, then maintained at this temperature for 15 min to ensure complete enzyme inactivation. Aliquots (5 mL) were collected in Eppendorf tubes for particle size analysis and SDS-PAGE, while the remaining hydrolysate was freeze-dried for subsequent cheese analogue development. The freeze-dried hydrolysates were labelled A1, A3, A5, A10, A15, A30, and A120, corresponding to different Alcalase hydrolysis times. Their protein content was determined using a Kjeldahl autoanalyzer

(Foss Tecator, Sweden) according to AOAC method 2001.11, with a nitrogen conversion factor of 6.25 for mung bean protein, yielding approximately 80% protein.

7.2.3. Degree of hydrolysis (DH)

The degree of hydrolysis, representing the percentage of peptide bonds cleaved during enzymatic hydrolysis, was determined using the o-phthaldialdehyde (OPA) method (Nielsen et al., 2001). The OPA reagent was prepared by mixing borate buffer, SDS, OPA, and 2-mercaptoethanol. Standard solutions were prepared using glycine in tetraborate buffer to generate a calibration curve. Protein extracts (25 µL) or standards (100 µL) were mixed with 1 mL of OPA solution or blank (without OPA) in a cuvette, incubated at 20 °C for 2 min, and absorbance was measured at 340 nm using a UV–Vis spectrophotometer (UV-1700, Shimadzu, Japan). To determine the total number of amide groups, MPI was fully hydrolyzed in 6 M HCl at 110 °C for ~18 h. The free amino groups (NH_2) in samples were calculated from the glycine standard curve, and the degree of hydrolysis was expressed relative to a serine standard. OPA reagent with 100 µL Milli-Q water was used as the blank. Measurements were performed on three independent batches of hydrolysates, and for each batch, three replicates were analysed. Results are reported as mean ± standard deviation.

7.2.4. Surface hydrophobicity of protein

The mung bean protein and its hydrolysate powders of 0.15g were dissolved in 15 mL 10 mM phosphate buffer solution (pH=7). The solution was shaken at room temperature for 2 hours, allowing hydration, followed by centrifugation at 10,000 x g for 15 min. Then the solution was diluted with phosphate buffer to obtain six protein concentrations (0.005-0.02%). The addition of 1-anilino-8-naphthalene sulfonate (ANS, 20 µL; 8.0 mM in phosphate buffer) to a 4 mL diluted sample, and left in darkness for 15 min. The fluorescent property of the ANS-protein conjugates

was analyzed at wavelengths 390 nm (excitation) and 470 nm (emission), using a spectrofluorometer device. The results are presented as the slopes ($r^2 > 0.99$) of the absorbance versus protein concentration (Vogelsang-O'Dwyer et al., 2023).

7.2.5. Determination of hydrolysate particle size distribution

The particle size distribution of Alcalase-hydrolysed MPI samples was measured immediately after enzyme inactivation using a Mastersizer 2000 laser diffraction particle size analyser (Malvern Instruments, UK) at 20 °C. Samples were added to the dispersion unit and diluted with water as needed to maintain an obscuration level of 10–15%. Water was used as the dispersant, with a refractive index of 1.33 and a viscosity of 0.89 mPa·s. Each hydrolysate was measured in triplicate. The volume-weighted mean diameter (D[4,3]) and median diameter (d(0.5)) were recorded to characterise particle size differences. Results are reported as mean ± standard deviation.

7.2.6. Sodium dodecyl sulphate–polyacrylamide gel electrophoresis (SDS–PAGE)

SDS–PAGE was used to characterise the MPI and its hydrolysates under non-reducing conditions. 10% mung bean protein solution and its hydrolysates were diluted in a sample buffer containing 0.5 M Tris-HCl, pH 6.8, 2 % (w/v) SDS, 150 mL/L glycerol, 0.0025 % (w/v) bromophenol blue. Each well of the gel with a 16 % resolving gel and 4 % stacking gel was loaded with 10 μL of the sample containing 0.2 % (w/w) of proteins or 5 μL molecular weight markers (Catalog # 161–0377, Bio-Rad, USA). After electrophoresis, the gels were stained with Coomassie Brilliant Blue R-250 staining solution (Bio-Rad, USA) for 3 h, followed by destaining with a 10 % isopropanol/glacial acetic acid solution overnight using a shaker (OM6, RATEK, Australia). (Hu et al., 2023; Lu, Roy, et al., 2026)

Processed hybrid cheese analogues were also prepared using MPI hydrolysates obtained at 10, 15, and 30 min, each blended with rennet casein at a 50:50 protein ratio. These three formulations were analysed by SDS–PAGE under both reducing and non-reducing conditions following the same procedure. For reducing conditions, 5% (v/v) 2-mercaptoethanol was added to the sample buffer.

7.2.7. Characterization of MPI Hydrolysates by Size Exclusion and Reverse-Phase High-Performance Liquid Chromatography (SEC- and RP-HPLC)

SEC analysis was carried out using a BisoSep-SEC-s2000 column (300 × 7.8 mm, Part No. 00H-2145-K0) on a BisoSep system. The column was operated at 25 °C with a flow rate of 1 mL/min. The mobile phase consisted of 45% acetonitrile containing 0.1% trifluoroacetic acid (TFA). Sample solutions were prepared by dissolving hydrolysate powders in water and filtering through a 0.22 μm membrane prior to injection. Detection was performed at 214 nm using a UV detector. Low molecular weight protein and peptide standards were used for calibration. A calibration curve of log molecular weight versus retention time was constructed to estimate the molecular weight distribution of hydrolysate samples (Mession et al., 2017).

RP-HPLC analysis was performed on an Agilent 1200 system equipped with a Jupiter C18 column (250 × 4.6 mm, 300 Å, 5 μm). Hydrolysate powders were dissolved in water (5 mg/mL) and filtered through a 0.45 μm membrane prior to analysis. The column temperature was maintained at 35 °C, and detection was carried out at 214 and 280 nm. The mobile phases were 0.1% TFA in water (A) and 0.1% TFA in 60% acetonitrile (B). The elution program was as follows: 0–10 min, 100% A; 10–90 min, linear gradient from 0 to 50% B; 90–100 min, increase to 75% B; 100–101 min, return to 100% A. The flow rate was 1 mL/min (Vogelsang-O'Dwyer et al., 2023). All sample injections

were performed in duplicate, and peak areas were used for qualitative and quantitative comparison of hydrolysate profiles

7.2.8. Solubility of protein

The mung bean protein and its hydrolysate powders were dissolved in 10 mM phosphate buffer solution (pH=7) to prepare a 2 mg/mL solution. The solution was shaken at room temperature for 2 hours, allowing hydration, followed by centrifugation at 10,000 x g for 15 min. The protein content of the supernatant was measured using the Kjeldahl method. The solubility was calculated as the percentage of the supernatant protein content to the total protein content (Ganesh et al., 2022).

7.2.9. Water-holding (WHC) and oil-holding capacity (OHC) of protein

The water-holding capacity was determined by weighing 0.5 g of the sample (M_0) into a centrifuge tube and weighing it together as M_1. Ten millilitres of Milli-Q water were added, and the mixture was allowed to hydrate for 2 h at room temperature. The slurry was then centrifuged at 10,000 rpm for 15 min at 25 °C. After centrifugation, the supernatant was carefully discarded, and the centrifuge tube containing the pellet was weighed (M_2). The water-holding capacity was calculated using the equation below and expressed as grams of water retained per gram of protein (Wintersohle et al., 2023). The tests were performed in duplicate.

WHC (g water/g protein) = $[M_2-M_1]/M_0$

The oil-holding capacity was determined by weighing 0.5 g of the sample (M_0) into a centrifuge tube and weighing it together as M_1. Ten millilitres of coconut oil were added, and the mixture was allowed to hydrate for 2 h at room temperature. The slurry was then centrifuged at 10,000 rpm for 15 min at 30 °C. After centrifugation, the supernatant was carefully discarded, and the centrifuge

tube containing the pellet was weighed (M_2). The oil-holding capacity was calculated using the equation below and expressed as grams of oil retained per gram of protein. The tests were performed in duplicate.

OHC (g oil/g protein) = $[M_2-M_1]/M_0$

7.2.10. Preparation of processed cheese analogues

Protein cheese analogues (PCAs) were prepared by blending MPI or its freeze-dried Alcalase hydrolysates with rennet casein (RC) at protein ratios of 100:0, 50:50, and 0:100. The formulation used was previously described by (Lu, Roy, et al., 2026; Ye et al., 2009). Briefly, the formulation contained 18 % protein, 20 % coconut oil, 0.5 % sodium chloride, 0.5 % calcium sulphate, 0.1 % potassium sorbate, 2.8 % tri-sodium citrate, and water on a weight ratio basis. Subsequently, citric acid was added to control the pH of all samples to around 5.6. PCAs were prepared using a Rapid Visco Analyser (RVA-4; Newport Scientific Pty Ltd, Warriewood, NSW, Australia). PCAs samples of 30 g were prepared in an aluminium cell fitted with a polycarbonate paddle. All dry ingredients and oil were manually blended with water for 5 min and then hydrated for 1 h at room temperature in an aluminium cell. The mixture was loaded onto the RVA instrument and processed as follows: equilibration at 50 °C, followed by heating to 90 °C over 4 min, maintaining at 90 °C for 10 min. The sample was then cooled to 50 °C at a rate of 0.2 °C/s, mixing at 300 rpm from heating to cooling stages.

PCAs were named according to their composition: MPI100 and its hydrolysed variants (e.g., MPI100_A1, MPI100_A3) contained only MPI or its hydrolysates; MPI50 and its hydrolysed variants (e.g., MPI50_A10, MPI50_A15, MPI50_A30) represented 50:50 blends of MPI (or hydrolysates) with RC; and RC100 consisted solely of RC. The moisture content was determined

by drying the samples in an oven at 105 °C until a constant weight was obtained. The average moisture of PCAs was 42%.

7.2.11. Microstructure of PCAs

Confocal laser scanning microscopy (CLSM) and transmission electron microscopy (TEM) analyses were conducted at the Manawatu Microscopy and Imaging Centre (Massey University, Palmerston North, New Zealand).

Microstructural analysis of RVA-prepared PCAs was performed using a confocal laser scanning microscope (ZEISS LSM 900, Germany). Thin sections of fresh cheese were stained with Nile Red (fat) and Fast Green FCF (protein) following the standard procedures (Auty et al., 2001; Gallier et al., 2012; Lu, Roy, et al., 2026), and imaged using a 20× or 40× objective lens. Laser excitation at 488 nm and 633 nm was used for Nile Red and Fast Green FCF, respectively.

PCAs were examined using TEM following the previously established sample preparation protocol (Li et al., 2021; Lu, Roy, et al., 2026). Briefly, samples were fixed, dehydrated, embedded in resin, and ultrathin sections (~100 nm) were collected and stained with uranyl acetate and lead citrate. The samples were imaged with a Tecnai G2 Spirit BioTWIN (FEI Company, Czech Republic) paired with a Veleta TEM camera (Olympus SIS, Germany).

7.2.12. Rheological analysis

Rheological properties were measured using a stress-controlled rheometer (Physica MCR 302, Anton Paar, Austria) equipped with a 20 mm diameter parallel plate with a 2.0 mm gap. Based on the previous protocol (Lu, Roy, et al., 2026), PCAs were cut into 20 mm diameter discs and equilibrated at room temperature prior to testing. The exposed edge of the samples was coated with a thin layer of mineral oil to minimize moisture loss during the measurement. The linear

viscoelastic region was first identified by amplitude sweeps at 1 Hz, after which a strain of 0.1% was selected for subsequent measurements. Frequency sweeps (0.01–10 Hz at 20 °C) and temperature sweeps (20–90 °C at 3 °C/min, 1 Hz) were conducted to determine the storage modulus (G′), loss modulus (G″), and loss tangent (tan δ).

7.2.13. Meltability

The meltability of PCAs prepared with RVA was measured using a modified Schreiber melt test (Kosikowski, 1977). Cheese samples were rolled into slices with a uniform thickness of approximately 5 mm and 30 mm in diameter, placed on glass Petri dishes, and heated in an oven at 170 °C for 10 min. Radius of expansion in four directions (0°, 90°, 180°, and 270°) was measured after cooling to 20 °C. The melt index was the average value of the four radius readings.

7.2.14. Statistical analysis

All experiments were performed in triplicate (unless otherwise specified). Results are reported as mean values and standard deviations. To identify differences between PCAs formulations, the data were subjected to one-way ANOVA analysis using SPSS, followed by Tukey's comparison of differences. Differences were considered significant at a level of $p < 0.05$.

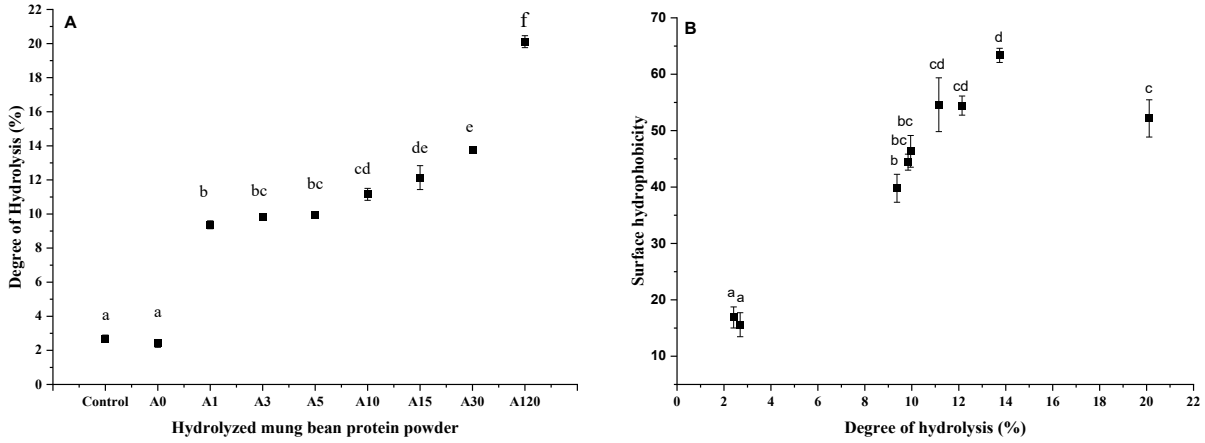
7.3. Results and discussion

7.3.1. MPI hydrolysis using Alcalase

7.3.1.1. Degree of hydrolysis

The DH of MPI treated with Alcalase is presented in **Figure 7-1A**. Upon enzyme addition, the DH rapidly increased to over 9% within the first minute. Only minimal changes occurred during the first 5 min, and no significant differences were observed across the 10–15 min and 15–30 min

intervals, where the DH remained approximately 12–13%. A further increase was observed during extended hydrolysis, reaching a maximum of ~20% at 120 min. The DH is known to depend strongly on protein characteristics, enzyme-to-substrate (E/S) ratios, and hydrolysis conditions such as temperature and pH. For example, K. Promjeen et al. (2025) reported higher DH values (28.58–41.51%) using higher Alcalase concentrations (1–10% v/w) and longer hydrolysis times (3–9 h) at pH 8.5. Liu et al. (2022) also demonstrated that Alcalase yielded the highest DH (23.55%) among several proteases after 4 h at pH 8 and 60 °C with an enzyme activity of 3000 U/g substrate. Under even more intensive conditions (7% E/S, 55 °C, pH 8 for 7 h), Karami et al. (2022) achieved DH values of 53–56%. In contrast, the present study tends to apply limited hydrolysis, where lower E/S ratios and shorter reaction times produce modest but controlled degrees of peptide bond cleavage. Such limited hydrolysis is often sufficient to induce desirable conformational and structural modifications that enhance protein–protein interactions, whereas more extensive hydrolysis can markedly reduce molecular weight and potentially impair functional properties (Vogelsang-O'Dwyer et al., 2022; Wang et al., 2022).



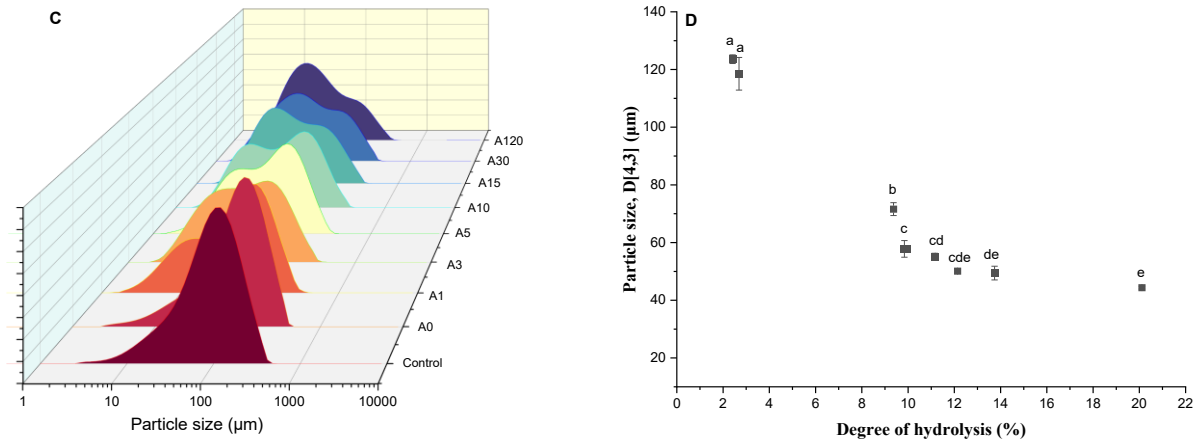


Figure 7-1. Degree of hydrolysis (DH) of mung bean protein isolates as a function of hydrolysis time (A); relationship between surface hydrophobicity and DH of Alcalase-treated hydrolysates (B); particle size distribution profiles (C); and corresponding volume-weighted mean diameters (D[4,3]) (D) of mung bean protein during hydrolysis. Sample numbers indicate hydrolysis time (min).

7.3.1.2. Surface hydrophobicity

Surface hydrophobicity (H_0) is an important structural parameter that reflects protein unfolding and conformational changes. The H_0 of the MPI treated with Alcalase increased with DH (**Figure 7-1B**), from 15.6 for non-hydrolyzed MPI to 63.4 for the 30 min hydrolysate and then decreased to 52.2 for the 120 min hydrolysate, while still remaining higher than the non-hydrolyzed MPI. Partial hydrolysis increased surface hydrophobicity by exposing hydrophobic sites previously buried within the protein molecule as large proteins were cleaved into smaller peptides. However, extended hydrolysis led to a decrease in H_0, likely because newly exposed hydrophobic regions aggregated through hydrophobic interactions, becoming partially re-buried within the resulting structures (Shuai et al., 2022; Vogelsang-O'Dwyer et al., 2023; Wang et al., 2022).

7.3.1.3. Particle size distribution

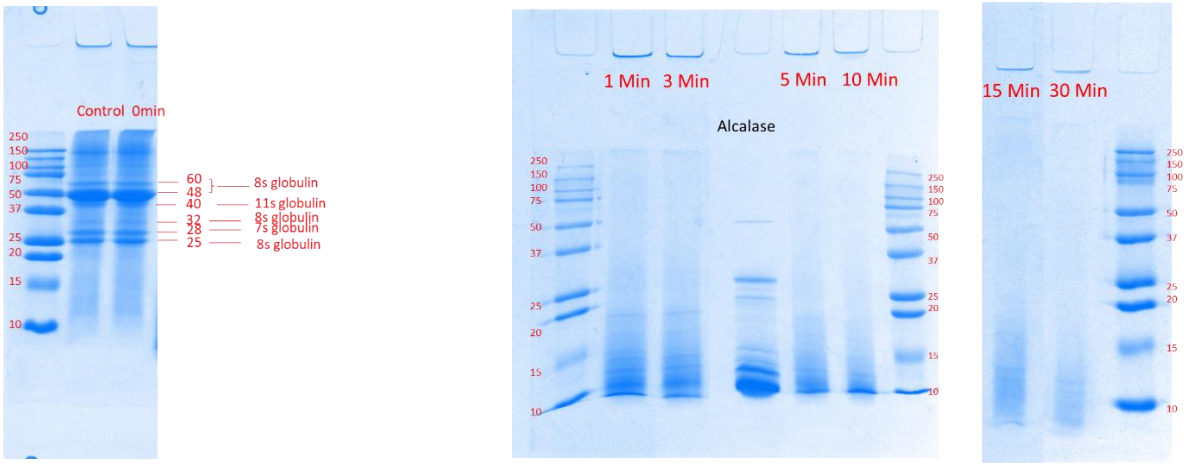
The particle size distributions and corresponding volume-weighted mean diameters (D[4,3]) of MPI and its hydrolysates are presented in **Figure 7-1C** & **D**. Native MPI and the 0-min sample exhibited a single peak with an average particle size of approximately 118–123 μm (D [4,3]). Following Alcalase hydrolysis, the samples displayed a bimodal distribution with reduced particle sizes. At 30 and 120 min, the average particle sizes decreased to 49 μm and 44 μm (D [4,3]), respectively, indicating enzymatic breakdown of protein aggregates and formation of smaller particles. The result is consistent with Liu et al. (2022) and Ganesh et al. (2022), who also reported that the average particle size of Alcalase-hydrolyzed MPI was smaller than that of the native protein, although their hydrolysates exhibited a single peak rather than a bimodal distribution.

7.3.1.4. SDS-PAGE

The protein profiles of MPI and its hydrolysates are presented in **Figure 7-2A**. In the non-hydrolyzed samples (control and 0 min), SDS–PAGE revealed several prominent bands at approximately 60, 48, 40, 32, 28, and 25 kDa, corresponding to the major globulin fractions of mung bean, including the 7S, 8S, and 11S storage proteins (S. Shrestha et al., 2023; Yi-Shen et al., 2018). Previous studies have shown that 8S vicilin lacks disulfide bonds; therefore, reducing and non-reducing SDS–PAGE yield similar banding patterns (Lu, Roy, et al., 2026).

Following Alcalase treatment, extensive degradation of high-molecular-weight proteins was observed even within the first minute of hydrolysis, with most bands above 25 kDa disappearing. After 10 min and beyond, no distinct bands were detected above 20 kDa, and the remaining protein fragments predominantly migrated below 15 kDa. This shift toward low-molecular-weight components indicates substantial peptide generation and confirms the rapid and efficient proteolytic action of Alcalase on MPI.

A



B

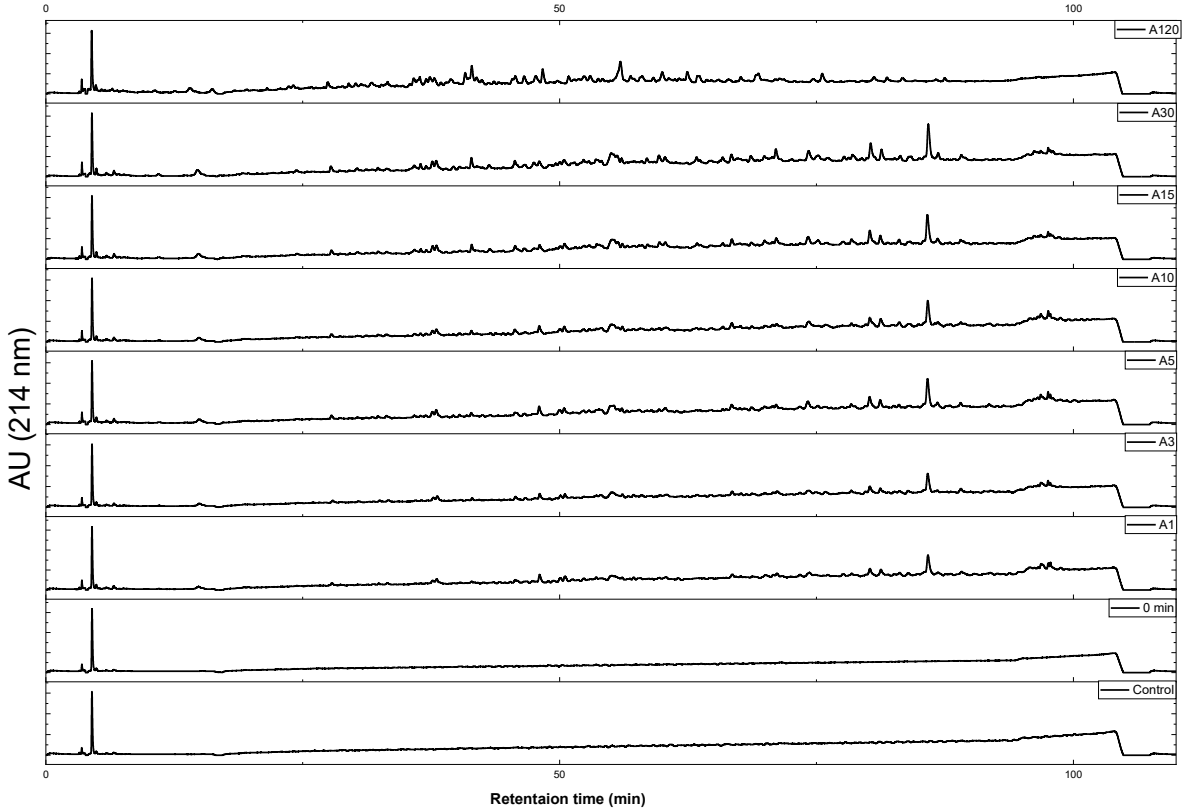


Figure 7-2. SDS-PAGE profiles (A), and RP-HPLC chromatograms (214 nm) (B) of mung bean protein and Alcalase-generated hydrolysates. Sample numbers represent hydrolysis time (min).

7.3.1.5. SEC- and RP-HPLC

The molecular weight distribution of MPI during Alcalase hydrolysis was evaluated using size exclusion chromatography (**Table 7-1**). In the control and 0-min samples, only <5 kDa fragments were detected in the soluble fraction, indicating that the native high-molecular-weight globulins were largely insoluble under the extraction conditions. Upon the onset of hydrolysis, these insoluble proteins became solubilized, resulting in the appearance of 10–50 kDa (5.1%), 5–10 kDa (52.1%), and <5 kDa (39%) peptides within the first minute. With continued hydrolysis, these protein fractions were progressively degraded, leading to a gradual decline in medium-molecular-weight peptides and a dominance of low-molecular-weight species. By 120 min, approximately 89% of the soluble components were <5 kDa, demonstrating extensive hydrolysis and efficient peptide generation by Alcalase. Additionally, higher DH values are generally associated with higher protein solubility, suggesting an enhancement in protein solubility due to increased hydrolysis. This could contribute to the improved functional and bioactive properties of the hydrolysate (K. Promjeen et al., 2025).

Table 7-1. Molecular weight distribution of mung bean protein isolate (MPI) during Alcalase hydrolysis determined by size-exclusion chromatography (SEC)

	10-50K	5-10K	< 5K	< 1K
Control			100%	
A0			100%	
A1	5%	52%	39%	4%
A3	5%	51%	39%	4%
A5	5%	53%	38%	4%
A10	3%	50%	44%	3%
A15	4%	32%	63%	1%
A30	4%	28%	62%	6%
A120	2%	3%	89%	6%

Control: non-hydrolyzed mung bean protein isolate (MPI). A: Alcalase-treated samples; the numbers following A indicate the hydrolysis time (min).

Peptides are separated mainly based on their hydrophobicity as well as molecular mass. RP-HPLC chromatograms at 214 nm are shown in **Figure 7-2B** (280 nm as supplementary Figure S1). Hydrophilic peptides are eluted first, while hydrophobic peptides are eluted later (Vogelsang-O'Dwyer et al., 2023). The non-hydrolysed MPI (control and 0 min) showed only a few small peaks, consistent with insoluble proteins and limited peptide diversity. In contrast, all hydrolysed samples exhibited many more small peaks, and overall peak intensity increased progressively with hydrolysis time, indicating the formation of a broader range of peptide fragments. Across the hydrolysed samples, stronger peaks were consistently observed in the later part of the chromatogram (after ~80 min elution time), which correspond to more hydrophobic peptide species. As hydrolysis time increased, these hydrophobic-associated peaks became more pronounced, reflecting exposure or release of hydrophobic regions during peptide bond cleavage. Interestingly, in the 120-min hydrolysed sample, a greater number of small peaks appeared in the early elution region (before ~50 min), while the dominant hydrophobic peaks after ~80 min decreased. This pattern suggests that prolonged hydrolysis further breaks down hydrophobic peptides into smaller, more hydrophilic fragments, shifting the overall profile toward lower-molecular-weight and more polar peptides. This trend was consistent with the surface hydrophobicity results, which showed a decrease in surface hydrophobicity of the 120 min hydrolysate.

7.3.1.6. Protein solubility

The solubility of protein hydrolysates is often a prerequisite for improving the functional properties of plant-based foods. Alcalase-treated MPI hydrolysates (**Figure 7-3A**) showed increased solubility with higher DH, from 10% for non-hydrolysed MPI to 70% (30 min) and 73% (120 min). Hydrolysis generates smaller peptides and exposes ionizable and hydrophobic groups, thereby

increasing the solubility (Vogelsang-O'Dwyer et al., 2022). It has been reported that Alcalase hydrolysis significantly improved faba bean protein solubility at pH 8, with the highest solubility corresponding to the highest DH (C. Liu et al., 2019). Similarly, Ganesh et al. (2022) observed that the solubility of almond protein isolate increased following Alcalase hydrolysis, whereas solubility decreased when treated with transglutaminase due to the formation of higher molecular weight protein aggregates in solution. Protein solubility is governed by the balance between protein–protein and protein–water interactions and is strongly influenced by pH (Vogelsang-O'Dwyer et al., 2022). It is also affected by the choice of enzyme, peptide size, protein conformation, and surface hydrophobicity (Ganesh et al., 2022; Shuai et al., 2022; Vogelsang-O'Dwyer et al., 2023; Wouters et al., 2016).

7.3.1.7. Water-holding (WHC) and oil-holding capacity (OHC) of protein

WHC and FHC of proteins are critical determinants of texture in plant-based food products. Alcalase-hydrolysed MPI exhibited a reduced WHC (**Figure 7-3B**), which is likely attributable to the breakdown of large protein molecules into smaller peptides that are unable to form a three-dimensional network capable of physically entrapping water (Wouters et al., 2016). In addition, water-soluble peptides remained in the supernatant and were removed during WHC measurement. These soluble proteins, despite having strong protein–water interactions, did not contribute to the measured WHC of the sediment fraction. This observation is consistent with the findings of Yin et al. (2008) who reported a reduction in the WHC of hydrolyzed hemp proteins and attributed this effect to the solubilization of hydrophilic protein groups that originally contributed to water retention in the non-hydrolyzed protein matrix. Promjeen et al. (2025) reported that a low level of Alcalase (1%) decreased the WHC of MPI hydrolysates, which was attributed to a reduced availability of polar functional groups, such as –COOH, $–NH_3$, and –OH, thereby limiting protein–

water interactions. In contrast, a higher enzyme concentration (10%) combined with 6 hours hydrolysis was associated with increased WHC, likely due to the exposure of additional hydrophilic groups that created more water-binding sites. In addition, the higher availability of hydrophobic groups can negatively impact WHC (Wouters et al., 2016); therefore, the overall WHC is affected by the balance between these effects.

The OHC of protein hydrolysates is determined by both the fat bound through hydrophobic interactions between proteins and lipids, and the fat physically entrapped within the protein matrix (Wouters et al., 2016). No significant differences in OHC were observed among the different treatments (**Figure 7-3C**). This may be attributed to a balance between opposing effects: the increased availability of hydrophobic groups following hydrolysis, which can enhance OHC, and the reduction in protein molecular size along with the release of ionizable groups, which may negatively affect the ability of the protein matrix to retain oil. As a result, no pronounced changes in OHC were detected across the enzymatic treatments.

Overall, the DH increased with hydrolysis time and increasing DH was accompanied by an increase in surface hydrophobicity, indicating progressive exposure of hydrophobic regions due to protein unfolding and partial cleavage. This may be partly due to aggregation of newly exposed hydrophobic regions, but RP-HPLC indicates that the main cause is further breakdown of hydrophobic peptides into smaller, more hydrophilic fragments, as shown by the shift from late- to early-eluting peaks with prolonged hydrolysis. In addition, particle size decreased with increasing DH, and both SEC-HPLC and SDS-PAGE confirmed the degradation of high-molecular-weight proteins into predominantly low-molecular-weight peptides. The reduction in molecular size led to increased protein solubility but decreased water-holding capacity, as smaller peptides are less effective at retaining water compared with non-hydrolyzed MPI. In contrast, oil-

holding capacity showed no significant differences among samples. Based on these molecular and functional changes, the protein hydrolysates were applied in a plant-based cheese model system to investigate their effects on rheological properties, microstructure, and meltability.

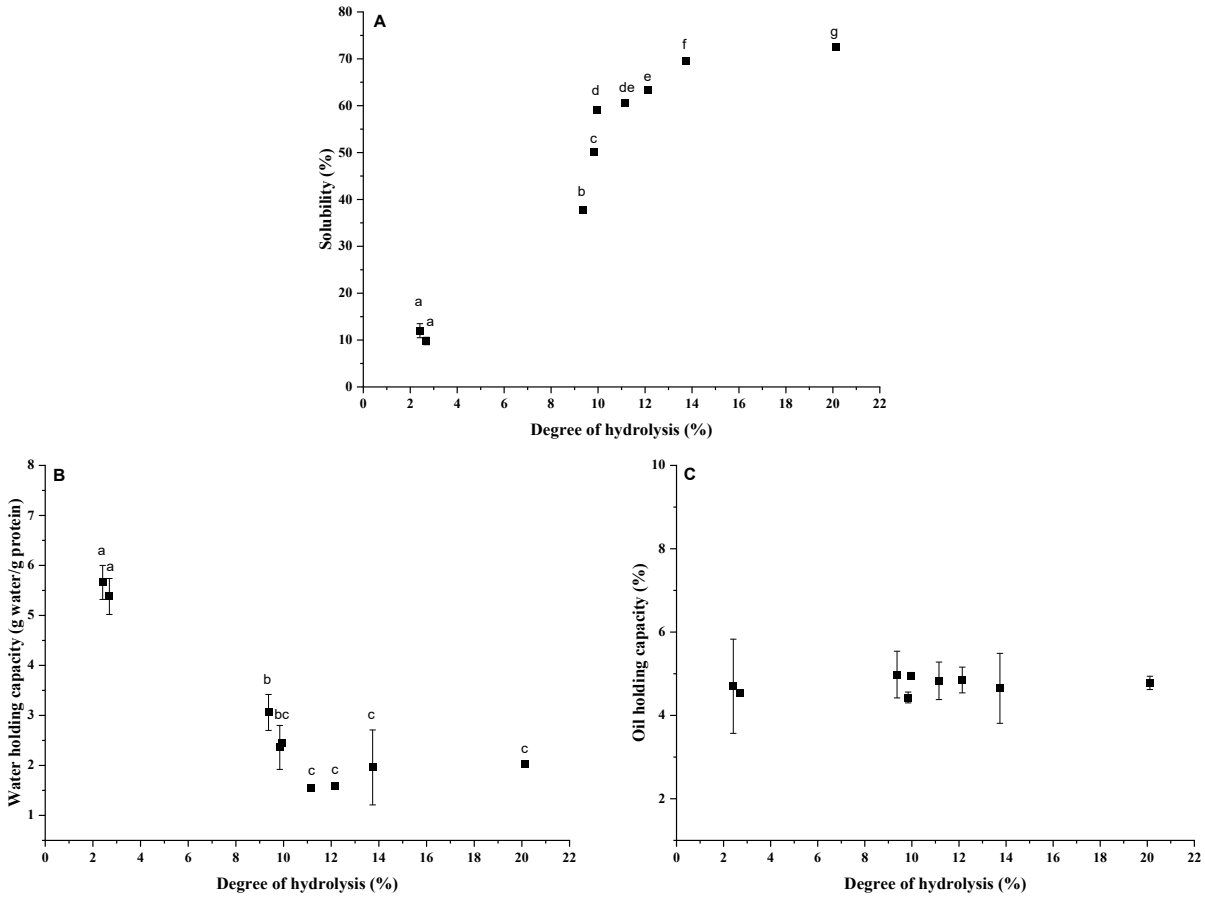


Figure 7-3. Solubility, water-holding capacity, and oil-holding capacity of mung bean protein and its Alcalase-generated hydrolysates as a function of degree of hydrolysis (DH). Sample numbers indicate hydrolysis time (min).

7.3.2. Processed cheese analogues with Alcalase hydrolysed MPI

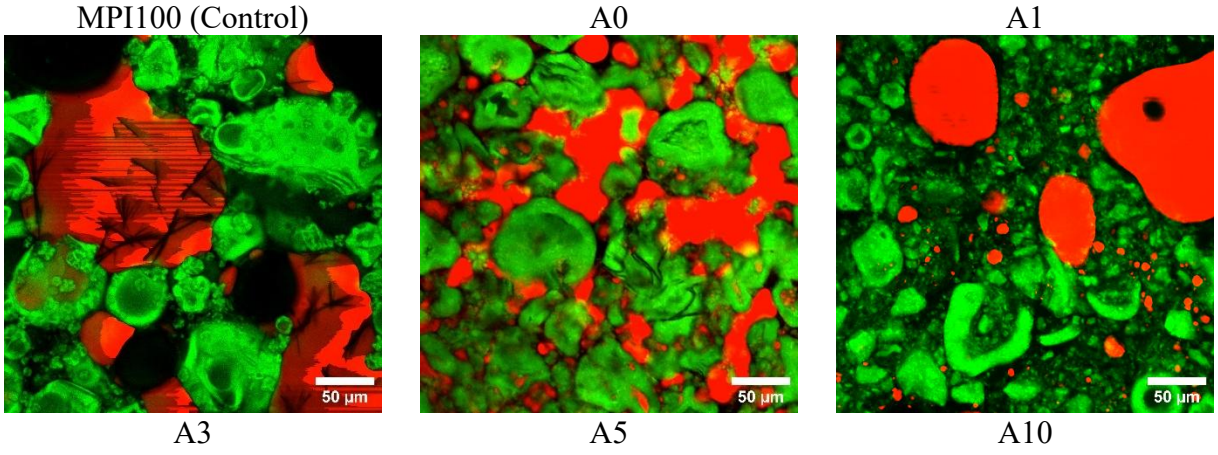
7.3.2.1.Microstructure of PCAs

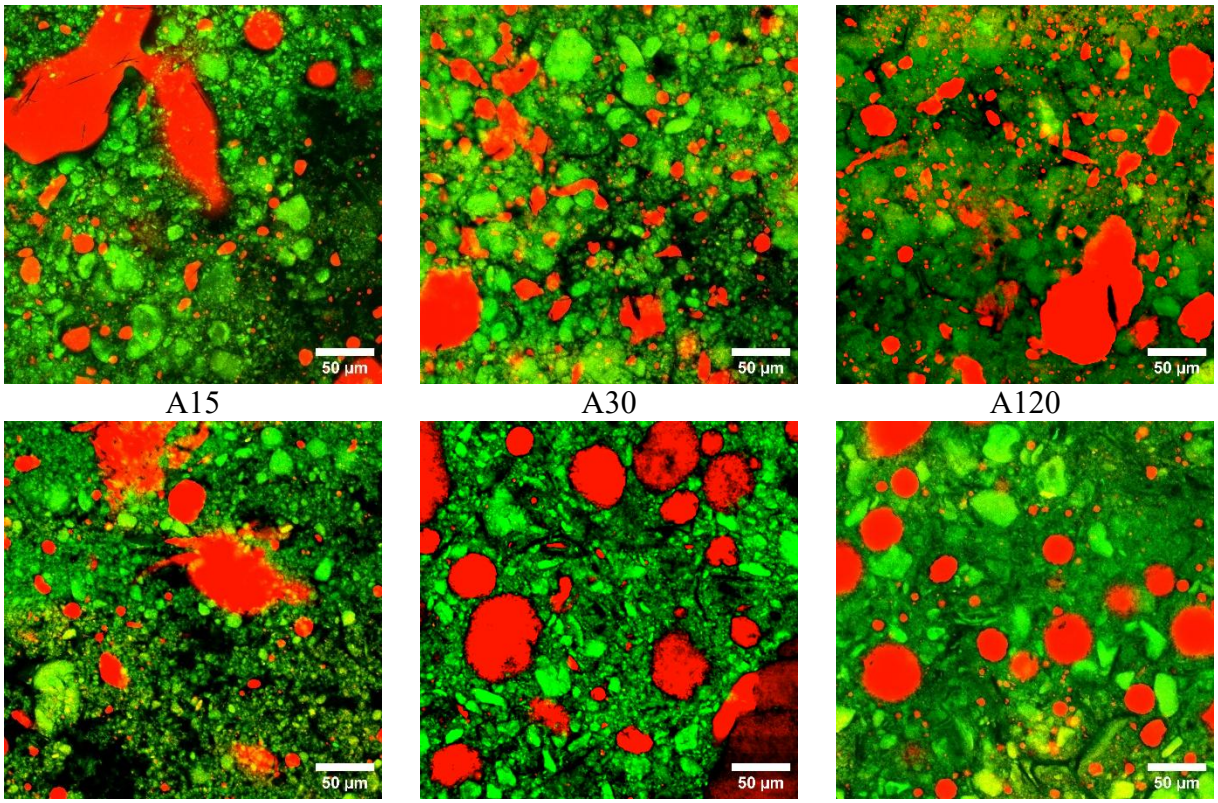
CLSM imaging (**Figure 7-4A**) revealed a clear reduction in protein particle size following hydrolysis, consistent with particle size distribution results. Compared with the control and 0-min samples, which displayed large, dense protein clusters, the hydrolyzed samples showed smaller

and more dispersed protein particles. As hydrolysis time increased, the protein network became progressively fragmented and more uniformly distributed throughout the cheese matrix, which may induce the lower strength of the gel (Chen & Campanella, 2022). Hydrolysis also influenced fat distribution. The control and 0-min samples contained large fat pools, whereas these pools were disrupted into smaller droplets in the hydrolyzed samples, resulting in a more homogeneous dispersion of fat within the matrix. Such redistribution of fat may contribute to changes in melting behaviour (Ørskov et al., 2021). Even after 120 min of hydrolysis, some protein aggregates remained visible, suggesting partial re-aggregation of peptides during cheese formation.

TEM analysis supported the CLSM findings (**Figure 7-4B**). The control sample exhibited large, compact protein particles, while the hydrolyzed samples displayed more fragmented and heterogeneous structures. Slight structural differences were also observed between cheeses made with the control MPI and those prepared with the 0-min hydrolyzed protein. Because the 0-min sample was dissolved at pH 8 prior to freeze-drying, this step slightly improved protein solubility and altered its distribution in the final cheese matrix compared with the untreated control.

A





B

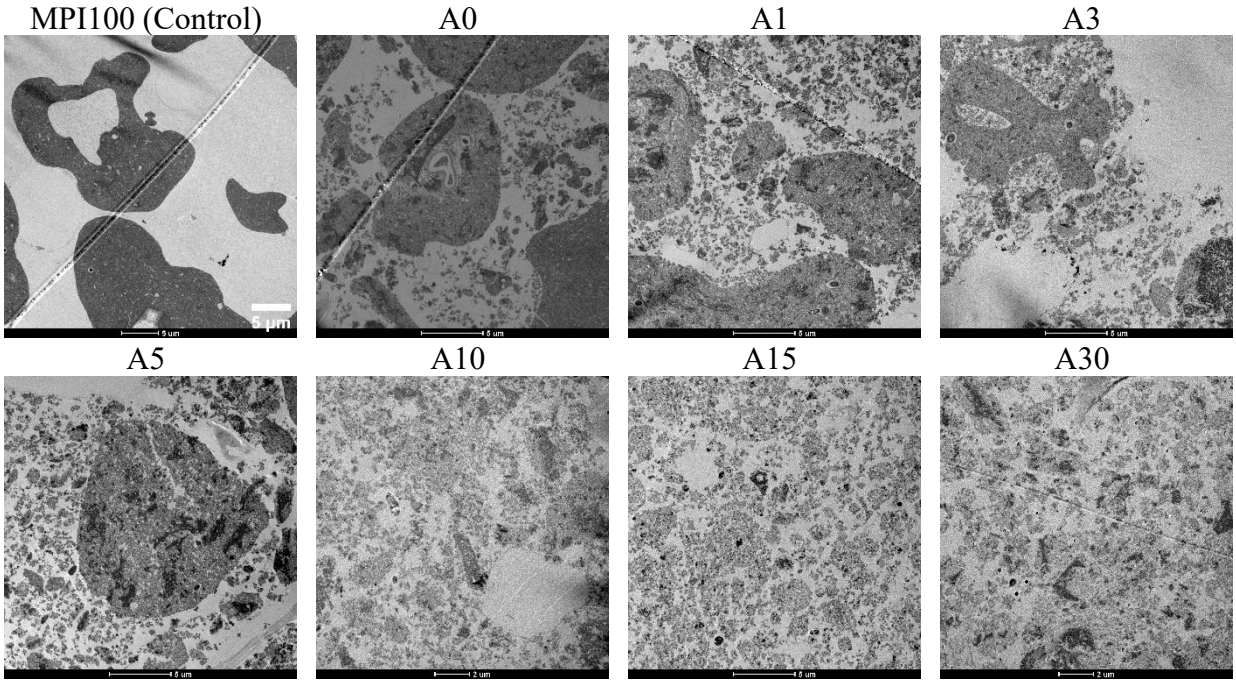


Figure 7-4. Representative CLSM (A) and TEM (B) images of plant-based cheeses formulated with non-hydrolyzed mung bean protein (MPI) and Alcalase-hydrolyzed MPI at different

hydrolysis times. In CLSM images, fat is shown in red and protein in green. Scale bars: 50 μm for CLSM and 5 μm or 2 μm for TEM. Numbers indicate the Alcalase hydrolysis time (min).

7.3.2.2.Rheological properties of PCAs

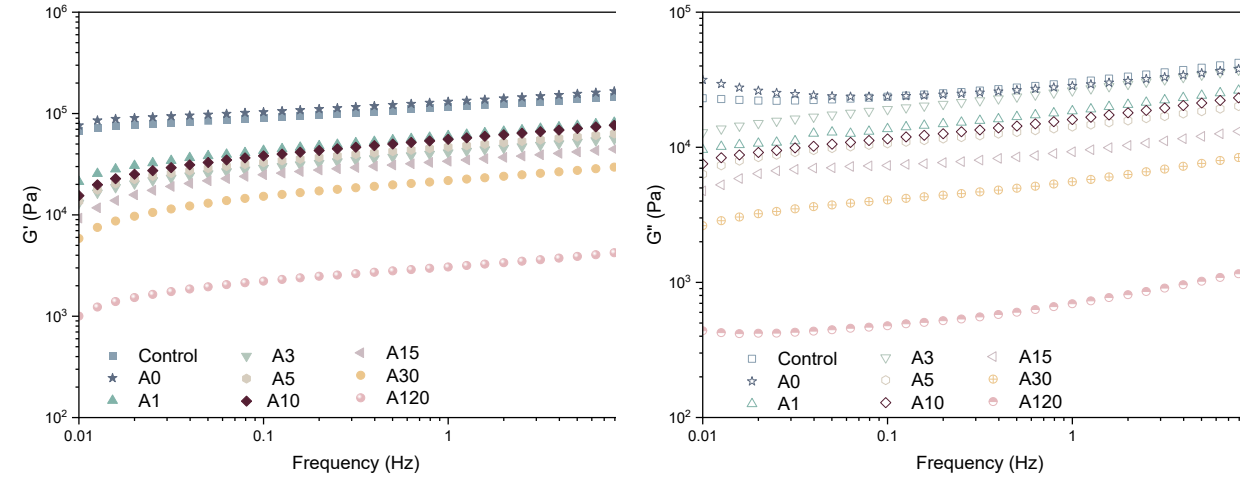
Rheological analysis was conducted to evaluate how different degrees of enzymatic hydrolysis influence the viscoelastic behavior and thermal stability of MPI-based PCAs. Understanding these changes is essential because the functional performance of processed cheese is closely governed by its viscoelastic network.

The frequency sweep analysis showed that cheeses formulated with non-hydrolyzed mung bean proteins (control and 0-min samples) exhibited the highest G′ values, indicating the strongest elastic network among all samples (**Figure 7-5A & B**). As the DH increased, both G′ and G″ decreased, reflecting the weakening of the protein matrix. In the 120-min hydrolyzed samples (paste-like matrix), although G′ remained higher than G″ (G′ > G″), confirming elastic dominance, both values were significantly lower than in all other treatments. Overall, increasing hydrolysis time led to continuous reductions in elasticity (G′) and viscosity (G″), consistent with extensive cleavage of the protein aggregates responsible for network formation. In general, enzymatic hydrolysis limits the ability to form strong networks by decreasing the average molecular mass (Wouters et al., 2016). Klost et al. (2020) reported that peptides smaller than 17 kDa were not incorporated into the gel network, thereby hindering gel network formation. In addition, the prolonged hydrolysis altered the type of interactions, which were insufficient to form a three-dimensional network, thus reducing the elasticity.

Temperature sweep measurements (20–90 °C) revealed a minor peak in tan δ around 25 °C across all samples, corresponding to the melting of coconut oil within the cheese matrix (**Figure 7-5C**).

Beyond this temperature, tan δ decreased (tan δ < 0.3), indicating that the samples maintained predominantly elastic behavior as the fat phase transitioned to liquid. For the control, 0, 1, 3, 5, and 10-min hydrolyzed cheeses, no substantial changes in tan δ were observed throughout the temperature range, suggesting that their networks remained stable upon heating. In contrast, cheeses containing proteins hydrolyzed for 15 min or longer displayed notable changes in their thermal behavior. The 15-min sample showed a slight increase in tan δ above 55 °C, which became more pronounced at longer hydrolysis times. The 30-min sample exhibited a broader tan δ peak between 55–65 °C (≈0.3), while the 120-min hydrolyzed cheese displayed a sharper peak at approximately 60 °C (≈0.4). These peaks indicate thermally induced softening of the protein matrix as the weakened network begins to lose structural integrity. After the peak, tan δ decreased and was accompanied by an increase in G', indicating the development of a more rigid and elastic structure, most likely due to moisture loss and the restructuring and aggregation of the protein network (Grasso et al., 2025). Overall, the emergence and intensification of tan δ peaks with increasing hydrolysis time reflect the progressive weakening of the mung bean protein network. Extensive hydrolysis generates smaller peptides that disrupt network continuity, making the matrix more susceptible to thermal softening. The sharper peak observed in the 120-min sample further suggests that excessive hydrolysis produces a highly fragmented structure with reduced thermal stability.

A B



C

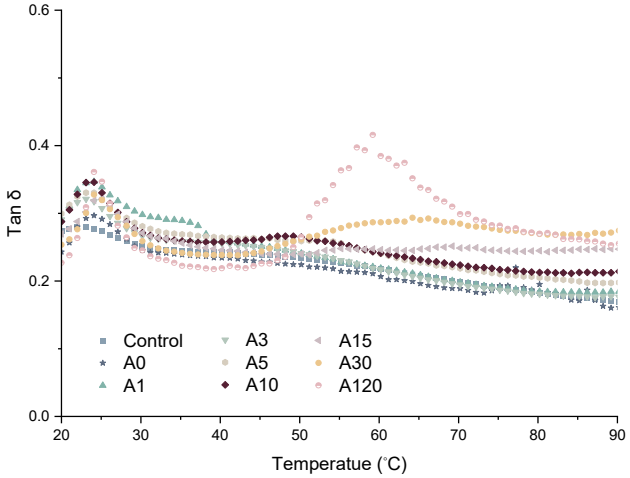


Figure 7-5. Rheological properties of plant-based cheese formulated with non-hydrolyzed MPI and Alcalase-hydrolyzed MPI. Storage modulus (G′) (A) and loss modulus (G″) (B) vs. frequency at 20 °C, γ = 0.1 %. Tan δ vs. temperature (f = 1 Hz, γ = 0.1 %) (C). Numbers indicate the Alcalase hydrolysis time (min).

7.3.2.3.Meltability of PCAs

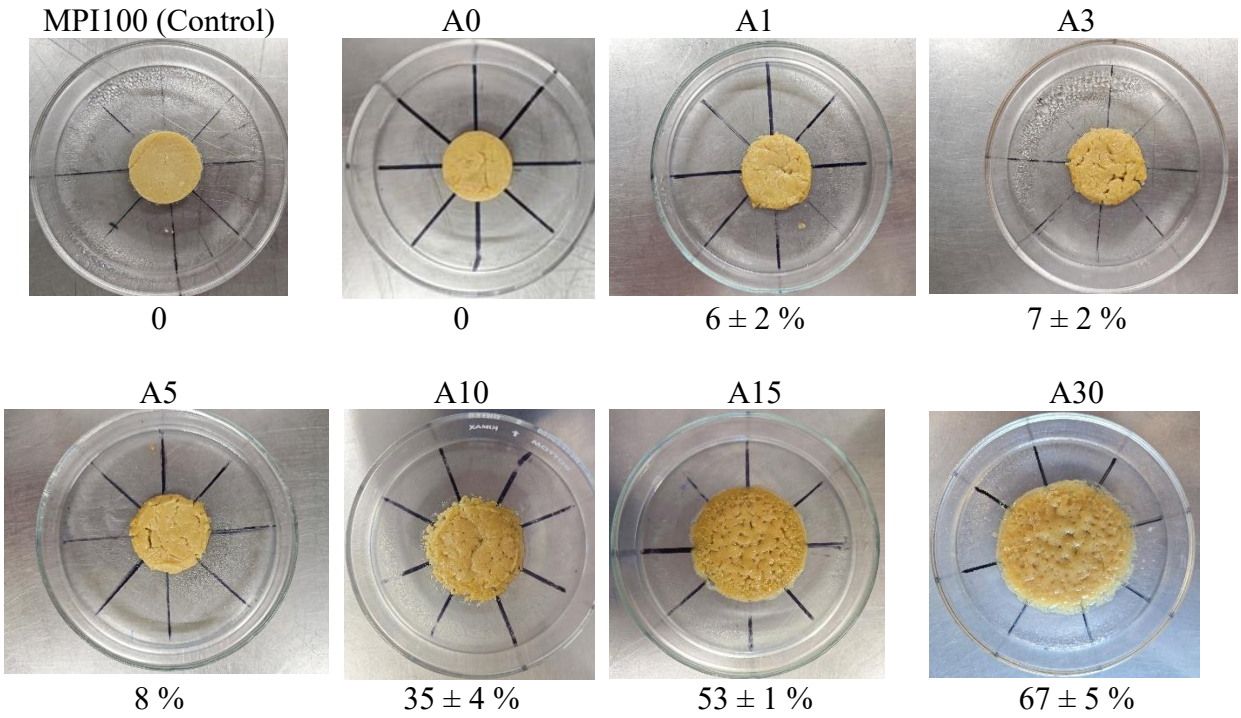
In traditional cheese, meltability is primarily determined by the strength and continuity of casein–casein interactions (Park et al., 1984). Heating induces contraction of the casein network due to increased hydrophobic interactions, which reduces molecular contact and weakens the network, linking with softening and melting (Lamichhane et al., 2018; Lucey et al., 2003). In contrast, plant

protein–based cheeses often exhibit limited meltability because they lack a continuous protein network (Grasso et al., 2021). Previous studies have shown that cheese analogues formulated with various plant proteins do not melt effectively (Lu et al., 2025), as their protein networks tend to aggregate and form rigid structures rather than flowing or stretching/viscoelastic mass like dairy cheese.

Figure 7-6 shows the melting behavior of PCAs prepared with hydrolyzed MPI and the correlation with DH. Overall, meltability increased with the DH. Limited improvement was observed when DH was below 10%. However, once DH exceeded 10%, meltability increased substantially. At 10 min hydrolysis (DH 11%), meltability reached 35%, and at 30 min (DH 13.7%), it further increased to 67%. These results indicate that a moderate extent of hydrolysis substantially enhances the melting performance of the plant-based cheeses.

The improved meltability can be attributed to several structural and functional changes induced by enzymatic hydrolysis. First, hydrolysis generates smaller peptides, and reduces intermolecular crosslinking, and weakens the integrity of the protein matrix. This interpretation is consistent with rheological measurements, which showed a reduction in elasticity and heat stability, indicating a matrix that softens and flows more readily under heat. Second, microstructural observations support these findings. CLSM revealed that hydrolysed PCAs exhibited fewer large protein aggregates and a more fragmented, finely dispersed protein network compared with the non-hydrolysed samples. This more uniform distribution and reduced aggregate size likely facilitate heat transfer and matrix mobility during melting. A fragmented network also reduces structural resistance, allowing the matrix to deform and spread more easily when heated. Additionally, the surfaces of cheeses with DH above 10% displayed a more porous, honeycombed structure, which is consistent with the reduced water-holding capacity caused by hydrolysis. The decreased ability

to retain water facilitates water release and allows greater expansion during heating, thereby promoting improved meltability. However, the PCA prepared with 120 min of hydrolysis resulted in extensive degradation of the protein matrix with more hydrophilic groups, which could not form a solid mass and therefore could not be tested for meltability. This indicates that, beyond a certain point, extensive peptide formation compromises matrix formation altogether.



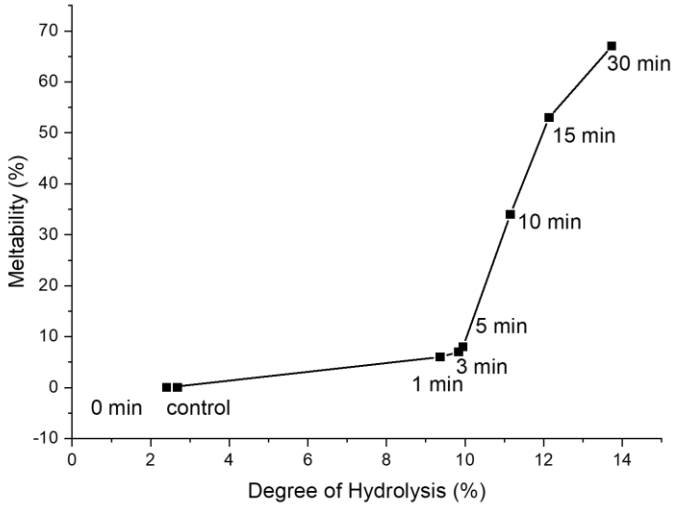


Figure 7-6. Representative images of plant-based cheese formulated with non-hydrolyzed MPI and Alcalase-hydrolyzed MPI, after heating at 170 °C for 10 min, with melting index (top). The relationship between the degree of hydrolysis and meltability (bottom).

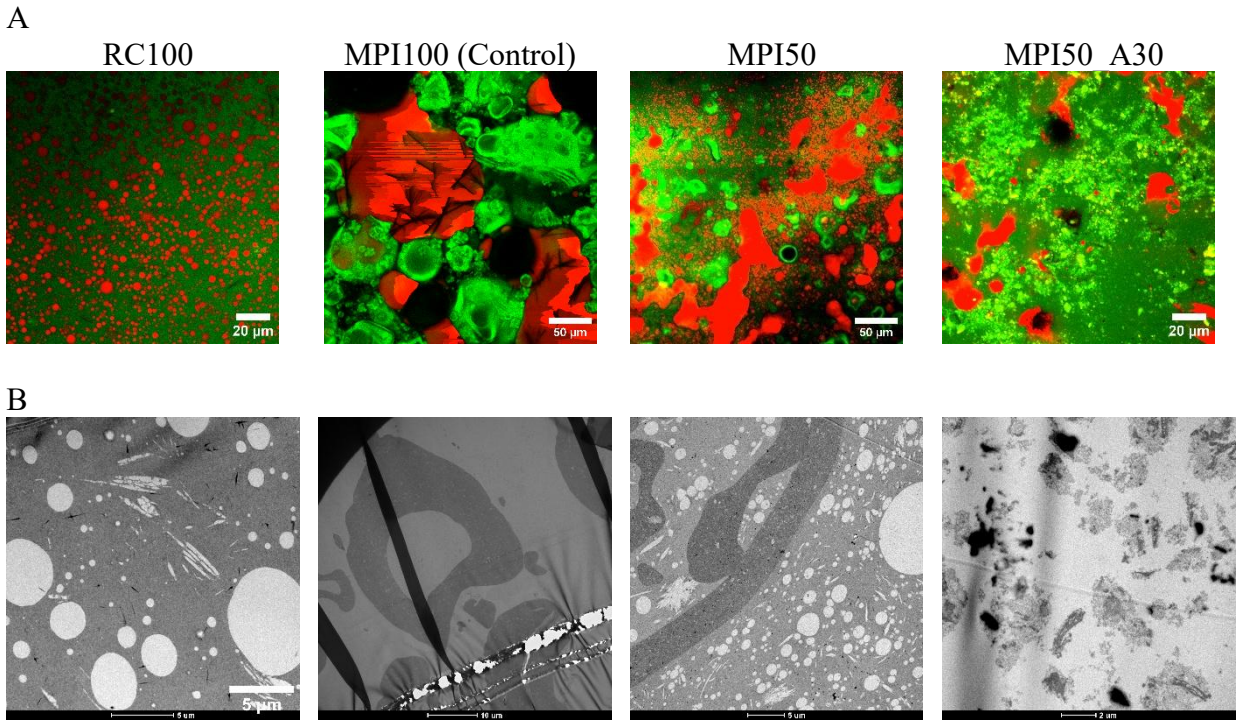
7.3.3. Processed hybrid cheese using Alcalase hydrolysed protein and casein

The mung bean protein hydrolysate obtained after 30 minutes of Alcalase treatment (DH 13.7%) was selected for incorporation into a hybrid cheese formulation with rennet casein at a 50:50 ratio (MPI50_A30).

7.3.3.1. Microstructure of processed hybrid cheese

Both CLSM and TEM microstructure analysis revealed clear structural changes induced by hydrolysis (**Figure 7-7A** & **B**). Compared with the non-hydrolysed MPI50 cheese, the hydrolysed system contained noticeably fewer large protein particles and aggregates. The protein matrix appeared more fragmented, with finer and more uniformly dispersed protein domains embedded within the casein network. These observations confirmed that hydrolysis effectively reduced particle size and improved protein dispersion. Nevertheless, some degree of phase separation between casein and mung bean protein was still evident, suggesting that hydrolysis alleviates the intrinsic incompatibility between the two protein types. Xie et al. (2021) showed that the addition of soy protein hydrolysates inhibited the aggregation of casein micelles, resulting in a coarse and heterogeneous network in Mozzarella cheese. Soy protein hydrolysates with either much larger or much smaller molecular weights, arising from insufficient or excessive hydrolysis, were suggested to be responsible for the poor microstructure. Zhang, Ling, et al. (2024) also reported that increasing the incorporation level of plant protein hydrolysates into Mozzarella cheese led to a weaker casein network due to the interfering effects of the hydrolysates. The authors observed that

higher concentrations (6–8%) of soy or pea protein hydrolysates resulted in an irregular honeycomb structure in Mozzarella cheese. They concluded that low concentrations (2–4%) of soy or pea protein hydrolysates could function as emulsifiers and thickeners, effectively filling the casein network voids and reducing the porous and rough structure of the cheese. However, high levels of soy or pea protein hydrolysates may disrupt the cheese network microstructure and confer a distinctive honeycomb structure to Mozzarella cheese. K. Li et al. (2018) reported that, compared with skim-milk cheese, cheese formulated with highly enzyme-modified soy protein exhibited smaller, denser, and more uniformly distributed casein voids, whereas cheese containing soy protein subjected to a low degree of hydrolysis showed the formation of large casein aggregates. This is consistent with the TEM observations, where the casein network was less apparent in MPI50 cheese made with hydrolyzed protein compared with the non-hydrolyzed cheese sample (**Figure 7-7B**).



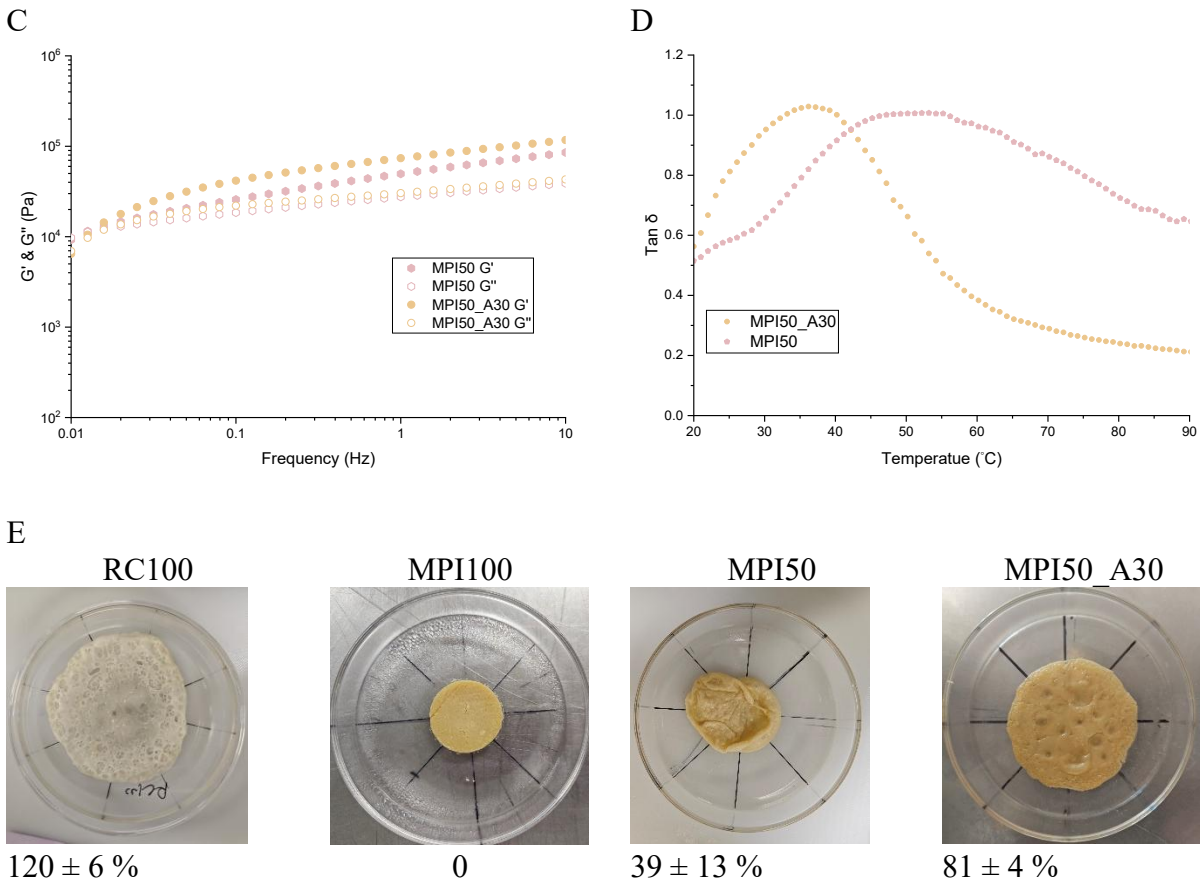


Figure 7-7. Representative CLSM (A) and TEM (B) images of hybrid cheeses formulated with non-hydrolyzed mung bean protein and rennet casein (MPI50) and with 30-min Alcalase-hydrolyzed mung bean protein and rennet casein (MPI50_A30), compared with cheeses formulated solely with rennet casein (RC100) or mung bean protein (MPI100). Rheological properties of MPI50 and MPI50_A30 are shown as storage modulus (G′) and loss modulus (G″) as a function of frequency at 20 °C (γ = 0.1%) (C), and tan δ as a function of temperature (f = 1 Hz, γ = 0.1%) (D). Representative images of MPI50, MPI50_A30, RC100, and MPI100 cheeses after heating at 170 °C for 10 min, together with the corresponding melting index (E).

7.3.3.2. Rheological properties of processed hybrid cheese

The frequency sweep tests showed that G′ was increased with an increase in frequency, with G′ > G″, indicating that both cheese samples are physical gels (**Figure 7-7C**). In addition, no significant differences in G′ and G″ between the hybrid cheese made with non-hydrolysed MPI50 cheese and

MPI50_A30 were observed, suggesting that partial hydrolysis did not markedly affect the linear viscoelastic properties of the matrix.

In contrast, the temperature sweep revealed a marked shift in thermal transition behaviour (**Figure 7-7D**). The tan δ = 1 crossover, which represents the point where the material transitions from a predominantly elastic to a predominantly viscous response, occurred at approximately 35 °C in the hydrolysed hybrid cheese (MPI50_A30) —significantly lower than the ∼55 °C crossover detected in the non-hydrolysed cheese (MPI50). This downward shift suggests that hydrolysis may cause the formation of less intact networks by the disruption of more casein-casein interactions (K. Li et al., 2018; Limit et al., 2024). As a result, the hydrolysed-protein cheese matrix became softer and more easily deformable at lower temperatures. By comparison, the cheese containing non-hydrolysed mung bean protein maintained a more rigid protein network, likely due to larger aggregates and stronger intermolecular associations. This more cohesive structure required higher temperatures to overcome the elastic dominance and transition into a viscous state. Similarly, Limit et al. (2024) observed a rapid decrease in G′ from 20 to 70 °C in fat-free cream cheese containing pea protein or pea protein hydrolysate aggregates, and samples with pea protein hydrolysates exhibited lower G′ than those with pea protein isolate (20–50 °C), indicating stronger disruption of casein–casein interactions and formation of a looser, less connected gel network.

Overall, these findings show that 30-minute enzymatic hydrolysis of mung bean protein modified the thermal transition behaviour of hybrid cheese by enhancing protein dispersion and weakening structural rigidity, while exerting limited influence on linear viscoelastic moduli under frequency sweep conditions.

7.3.3.3. Meltability of processed hybrid cheese

The meltability of this hydrolysed-protein hybrid cheese increased substantially compared with the non-hydrolysed control (81% *vs* 39%), although it remained lower than the meltability observed for the rennet casein reference cheese (RC100, 120%) (**Figure 7-7E**). This demonstrates that controlled enzymatic hydrolysis can enhance the melting performance of plant–protein–containing cheese. Xie et al. (2021) partially hydrolysed soy protein using Flavourzyme and blended it with milk at a 60:40 (v/v) ratio to produce hybrid mozzarella cheese analogues. They reported that hydrolysis at 50 °C with 0.5% (w/v) enzyme for 6 hours (DH 15%) resulted in markedly improved meltability compared with the non-hydrolysed control. The authors attributed this enhancement to moderate proteolysis, which degraded a substantial portion of the soy protein into smaller peptides. This process weakened the protein matrix, thereby promoting greater flow during heating. Zhang, Ling, et al. (2024) investigated the effects of incorporating plant protein hydrolysates on the characteristics of low-fat mozzarella cheese. They reported that increasing the level of hydrolysed plant protein led to improvements in both melt length and overall meltability of the cheese.

Table 7-2. Effects of Alcalase and trypsin hydrolysis at comparable degrees of hydrolysis on molecular characteristics and functional properties of mung bean protein.

	Degree of Hydrolysis (%)	Surface hydrophobicity	D [4, 3] (μm)	SEC-HPLC (%)				Solubility (%)	Water holding capacity (g water/g protein)	Oil holding capacity (g oil/g protein)
				10-50K	5-10K	< 5K	< 1K			
A30	13.74±0.16	63.35 ± 1.26	49.42 ± 2.373	4%	28%	62%	6%	69.6 ± 0.5	1.96 ± 0.75	4.65 ± 0.84
T10	13.27 ± 0.10	168.97 ± 5.03	86.78 ± 2.41	6%	36%	56%	2%	84.6 ± 1.0	1.61 ± 0.76	4.60 ± 0.42

A: Alcalase-treated samples; T: trypsin-treated samples; the numbers following A indicate the hydrolysis time (min).

7.3.4. Alcalase vs trypsin in plant-based cheese

MPI hydrolysates produced using Alcalase and trypsin at comparable degrees of hydrolysis were selected (DH 13.74% after 30 min Alcalase (A30) treatment and DH 13.27% after 10 min trypsin (T10) treatment) to compare the effects of enzyme specificity on hydrolysate characteristics, functional properties, and cheese performance.

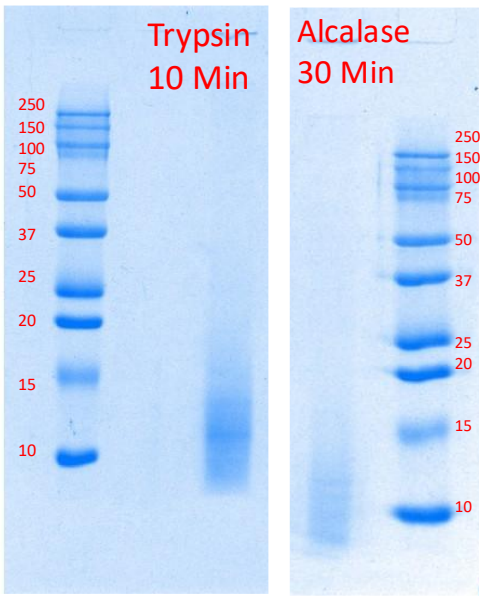
At a similar DH, trypsin-treated hydrolysates exhibited higher surface hydrophobicity (168.97 in T10 *vs.* 63.35 in A30), larger particle size (e.g., D[4,3] 86.78 in T10 *vs*. 49.42 in A30), higher solubility (84.6 in T10 *vs.* 69.6 in A30) (**Table 7-2**), and slightly higher molecular weight compared with Alcalase-treated ones (**Figure 7-8A**). A similar study reported that trypsin hydrolysis resulted in the highest solubility and the greatest increase in surface hydrophobicity of pea protein compared with Alcalase, Neutrase, and Flavourzyme (Shuai et al., 2022).

HPLC analysis indicated that trypsin hydrolysis generated a greater proportion of hydrophobic peptides compared with Alcalase (**Figure 7-8B**). This is consistent with the surface hydroboicity result. In addition, the higher surface hydrophobicity of trypsin digests likely promotes stronger hydrophobic interactions among protein fragments, leading to increased aggregation and the formation of larger particles. CLSM micrographs supported this interpretation, showing more pronounced protein clustering and less uniform dispersion in the trypsin-hydrolysed cheese matrix (**Figure 7-8C**). This aggregated structure contributes to a more rigid and cohesive network, consistent with the higher G′ values observed in rheological measurements (**Figure 7-8E**). A stronger, more elastic network resists deformation during heating, limiting the ability of the matrix to flow and spread—resulting in reduced meltability (**Figure 7-8E & F**). In contrast, Alcalase produced a broader range of smaller peptides with lower overall hydrophobicity, leading to reduced aggregation, finer dispersion, and a more fragmented and weaker protein network. This weaker matrix softens more readily upon heating,

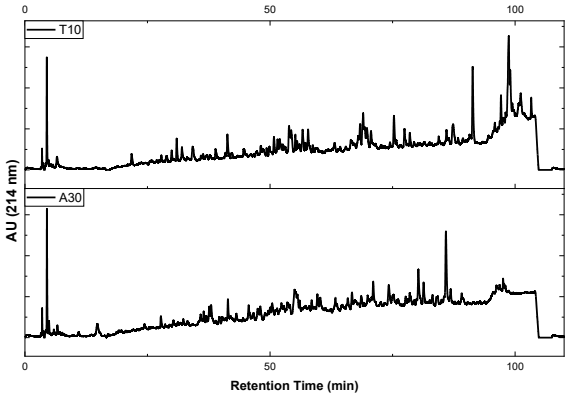
thereby exhibiting superior meltability. Collectively, these findings indicate that the predominance of hydrophobic peptides and aggregation in the trypsin hydrolysates creates a structurally stronger but less heat-responsive matrix, explaining the lower meltability relative to Alcalase-treated samples.

As mentioned previously, Alcalase exhibits broad specificity and preferentially hydrolyses peptide bonds at the C-terminal side of hydrophobic residues, whereas trypsin specifically cleaves peptide bonds at the C-terminal side of Lys and Arg residues (Vogelsang-O'Dwyer et al., 2022). Consequently, even at similar degrees of hydrolysis, the resulting peptides differ markedly in their structural properties. These structural differences play a more important role in determining the functional properties of the final products (Wouters et al., 2016). Therefore, molecular mass, surface hydrophobicity, and the particle size of plant protein hydrolysates were considered key determinants of functionality.

A



B



C

Trypsin (DH 13.27%)

Alcalase (DH 13.74%)

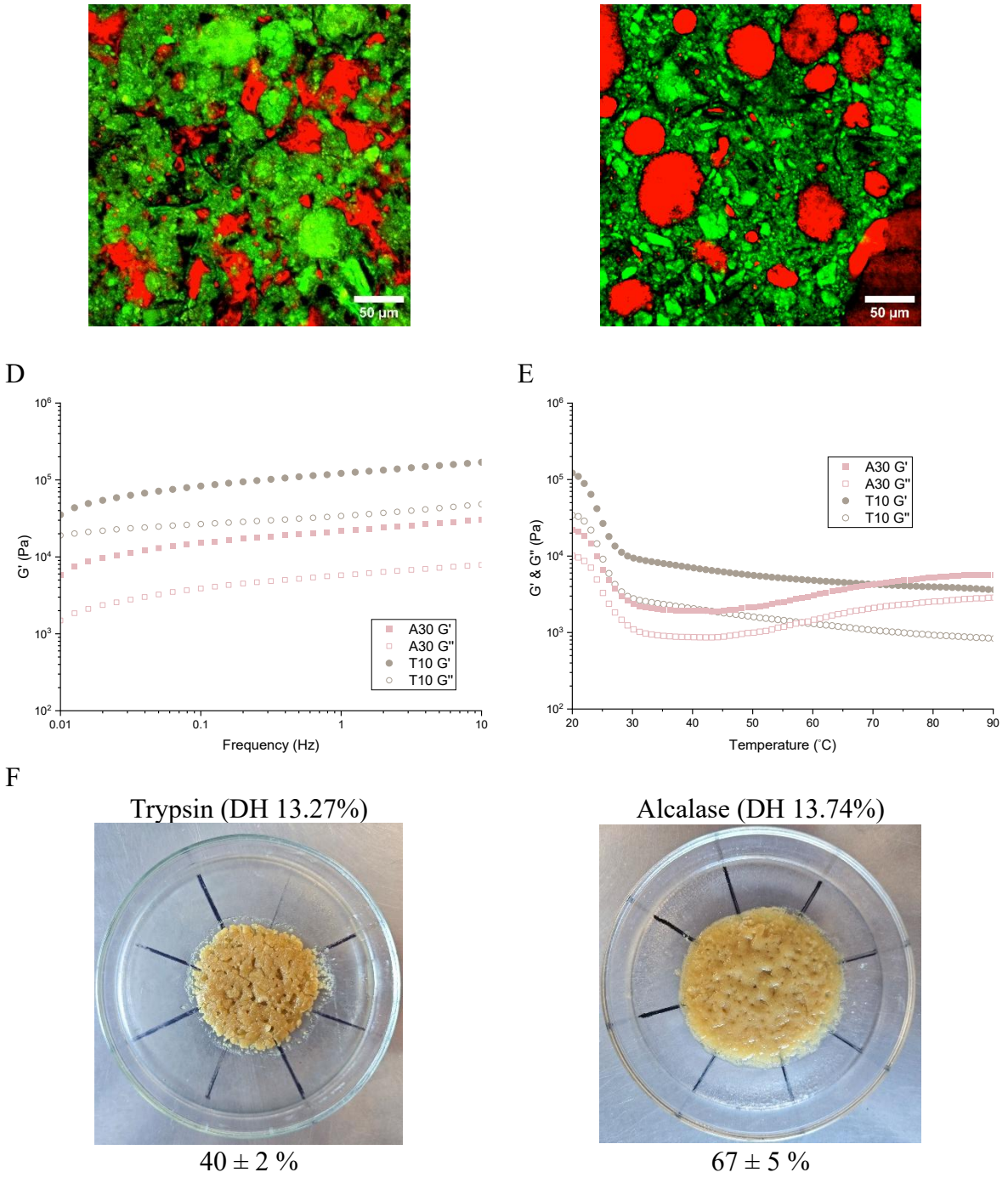


Figure 7-8. Profiles of mung bean protein hydrolysates produced by trypsin or Alcalase at comparable degrees of hydrolysis: SDS-PAGE profiles (A) and RP-HPLC chromatograms at 214 nm (B). Representative CLSM images of the corresponding plant-based cheeses (C). Rheological properties of the cheeses: storage modulus (G′) and loss modulus (G″) as a function of frequency at 20 °C (γ = 0.1%) (D), and as a function of temperature (f = 1 Hz, γ = 0.1%) (E). Representative images of cheeses after heating at 170 °C for 10 min, with the corresponding melting index (F).

7.4. Conclusions

This chapter investigated the effect of enzymatic hydrolysis of MPI on its structural and functional properties and evaluated the resulting hydrolysates in plant-based cheese to improve meltability. Increasing hydrolysis time elevated DH, enhanced surface hydrophobicity and reduced particle size and molecular weight. These structural modifications led to improved protein solubility, decreased water-holding capacity, and no significant changes in oil-holding capacity. In the cheese matrix, hydrolysates became more fragmented and uniformly dispersed, weakening the protein network and altering melting behaviour compared with cheese made from non-hydrolysed MPI. Hybrid cheese formulated with 30 min Alcalase-hydrolysed MPI and rennet casein showed greater disruption of the casein network and softened at lower temperatures, resulting in improved melting performance. At similar DH, cheeses made with Alcalase-treated MPI exhibited better melting than those treated with trypsin, likely due to differences in surface hydrophobicity and particle size that influenced protein aggregation and network rigidity. This study demonstrates that moderate enzymatic hydrolysis is an effective strategy to improve the meltability of plant-based and hybrid cheeses, while also highlighting that enzyme selection critically influences protein structure, network formation, and ultimately cheese performance. For other plant proteins, enzymes should be selected according to the structure, accessible cleavage sites, hydrophobic regions and aggregation behaviour of their major storage proteins.

Chapter 8 Overall discussion, conclusion, and future recommendations

8.1. Overall discussion and conclusions

Plant-based cheese analogues hold promise as sustainable and health-conscious alternatives. However, a fundamental challenge in plant-based cheese design lies in the intrinsic structural and functional differences between plant proteins and casein. Unlike casein, which forms flexible, dynamic networks through weak and reversible interactions, most plant proteins exhibit compact globular structures with stronger intramolecular stabilization, limiting their ability to reorganize into viscoelastic networks. Distinct aggregation pathways and different sensitivities to pH, ionic strength, calcium, and thermal treatment introduce both thermodynamic barriers and kinetic constraints, leading to fundamentally different network formation behaviour (Rashwan et al., 2025). This structural disparity explains why plant-based cheese analogues often struggle to replicate key functional attributes of conventional cheese, particularly meltability and stretchability.

Transforming plant-based cheese systems into a processed cheese model using a Rapid Visco Analyzer enables precise control over temperature, shear rate, and processing conditions, thereby improving reproducibility and allowing meaningful comparisons between formulations. This controlled approach provides a robust platform for systematically investigating structure–function relationships.

A comprehensive suite of analytical techniques was employed to characterise both plant-based and hybrid processed cheese analogues across multiple length scales. Texture and rheological properties were evaluated using a texture analyser and rheometry, while microstructure was examined using confocal laser scanning microscopy (CLSM), scanning electron microscopy (SEM), and transmission electron microscopy (TEM). Molecular-level interactions and structural

changes were further probed using synchrotron-based FTIR and Raman spectroscopy. In addition, melt behaviour was assessed using Schreiber tests and rheological methods. Together, these integrated approaches provide a comprehensive understanding of how protein–protein and protein–lipid interactions, as well as microstructural organisation, govern macroscopic functionality such as texture, meltability, and stretchability. In addition, improving functionality requires targeted structural modification rather than simple formulation adjustment. This work therefore contributes to a more mechanistic understanding of plant-based cheese design and highlights the importance of controlled processing and multi-scale characterisation in developing functional processed cheese analogues.

8.1.1. Influence of plant protein type on structure and function of processed cheese analogues

Plant proteins can be classified according to their natural sources, with cereals, legumes, and oilseeds being the most common ingredients in plant-based cheese products. These sources differ in protein composition and profiles, which influence solubility, gelation, and aggregation behaviour (Kovačević et al., 2024). **In Chapter 3**, nine plant protein sources—soybeans, peas, chickpeas, mung beans, lentils (legumes), quinoa (pseudocereal), canola, hemp seeds (oilseeds), and zein (cereal)—were selected to develop processed cheese analogues. It was hypothesized that the choice of plant protein significantly affects microstructure formation during RVA-based cheese processing, leading to differences in functional properties such as texture, rheological properties, meltability, and stretchability. The results demonstrated that all plant protein-based processed cheese analogues exhibited predominantly elastic behaviour ($G' > G''$), along with lower chewiness and resilience, and limited melting and stretching properties compared to casein cheese. These characteristics were associated with a coarser protein microstructure resulting from increased protein aggregation compared to casein-based cheese. The results are consistent with Grasso et al.

(2021), indicating that plant proteins lack a continuous protein network. Their compact globular structures and covalent interactions hinder their ability to reorganise into viscoelastic networks.

Among the different protein sources, plant protein-based processed cheese analogues exhibited distinct rheological and textural properties that were closely linked to their microstructure. Legume-based cheeses showed higher elastics (G′) values than casein-based cheese, whereas canola-based cheese exhibited the lowest. Zein-based cheese displayed high hardness but softened and became stretchable upon heating due to weakened non-covalent interactions (Mattice & Marangoni, 2020b), while chickpea-, mung bean-, and pea-based cheeses had comparable hardness to casein but lower springiness, cohesiveness, and resilience. These differences were associated with variations in protein aggregation and protein-fat interactions. Most plant protein systems exhibited poor emulsification, characterised by coalesced or irregular fat domains and phase separation, whereas chickpea- and quinoa-based cheeses showed smaller, more spherical fat droplets, indicating improved emulsifying properties. Overall, plant protein-based cheeses formed larger, less continuous protein networks, with legume proteins generating more pronounced aggregates compared to canola, hemp, and quinoa proteins. When ranking physical properties, lentil, hemp, and quinoa proteins most closely resembled casein in rheology and texture, whereas mung bean protein showed the least similarity. These functional differences reflect variations in protein structure and aggregation. Similarly, Hanley et al. (2025) reported that protein source strongly influences the three-dimensional organisation of oil and starch in plant-based cheese analogues, thereby affecting functionality. Their findings highlight that protein solubility and interactions with water, starch, and fat are critical determinants of structure and performance.

8.1.2. Structure-function relationships in hybrid cheeses

8.1.2.1. Comparative effects of mung bean and hemp protein on structure and functionality in hybrid processed cheese analogues

The development of hybrid plant–dairy cheese systems represents a pragmatic strategy to bridge structural and functional gaps. Based on Chapter 3, plant protein-based processed cheese analogues exhibited distinct rheological, microstructural, and textural properties, with hemp protein more closely resembling casein cheese than mung bean protein. Notably, mung bean protein had larger particle size (D[4,3] 118 μm vs. 33 μm for hemp) and lacked disulfide bonds, suggesting potential differences in interactions with casein. **In Chapter 4**, hybrid processed cheese analogues containing either mung bean or hemp protein with rennet casein at various ratios were prepared to investigate spatial distribution, microstructure, and related functional properties. Protein composition and secondary structure, and microstructure were assessed to elucidate the multiscale structure underlying functionality.

The results indicate that plant protein type and concentration significantly influence the physical properties and microstructure of hybrid processed cheese analogues. Increasing plant protein content disrupted the casein network and promoted the formation of independent plant protein networks, resulting in decreased G′ and G″ values, consistent with previous studies reporting weaker structures in mixed systems (Beghdadi et al., 2022; Beliciu & Moraru, 2011; Silva et al., 2019b). Incorporation of ≥30% plant protein led to notable changes in texture and microstructure, including a decrease in β-sheet content and an increase in random coil structures in plant proteins.

However, the behaviour differed depending on protein source. At equivalent incorporation levels, mung bean protein–casein systems exhibited higher tan δ values than hemp protein systems, suggesting a more dominant casein network. This may be attributed to the presence of disulfide

bonds in hemp protein, which can promote interactions with casein upon heating through thiol–disulfide exchange (Hadnađev et al., 2018). In addition, hemp protein formed smaller and more uniformly distributed aggregates within the cheese matrix, leading to greater disruption of the casein network. In contrast, mung bean protein forms larger aggregates, resulting in a more segregated microstructure and less interference with the casein network. Consistent with this, mung bean protein hybrid systems showed superior stretchability and viscoelasticity, whereas hemp protein systems exhibited greater meltability. These differences are likely driven by variations in protein aggregation and structural organisation: mung bean protein–casein hybrid systems promoted microstructural segregation and changes in β-sheet content, while hemp protein–casein hybrid systems showed increased structural disorder and disulfide bond rearrangement. Increasing casein content reduced plant protein aggregation and resulted in a more flexible and heterogeneous network. Such findings highlight that plant proteins cannot be considered interchangeable ingredients; instead, their intrinsic structural characteristics must be strategically matched to the targeted functionality.

8.1.2.2. Molecular insights from Raman microscopy and S-FTIR on mung bean protein-casein and hemp protein-casein hybrid processed cheese analogues

The above results suggest that hybrid systems function not merely as compositional blends, but as interactive molecular systems in which protein–protein compatibility governs final functionality. Understanding these complex interactions requires analytical tools capable of resolving spatial and molecular heterogeneity. Raman microscopy (**Chapter 5**) and synchrotron-based FTIR (S-FTIR) (**Chapter 6**) proved highly effective for visualizing component distribution and probing molecular interactions with minimal sample preparation. Integration with multivariate analysis and machine learning enabled discrimination between protein sources and elucidation of structural transitions.

While FTIR is sensitive to polar functional groups, Raman spectroscopy is more responsive to nonpolar structures, enabling a comprehensive analysis of protein–protein and protein–lipid interactions.

Spectral analysis from both techniques revealed that plant protein type significantly influences molecular structure and network organisation. Mung bean protein–casein systems exhibited enhanced β-sheet content and protein domain separation, indicating stronger aggregation and the formation of a more rigid and segregated network. In contrast, hemp protein–casein systems showed increased structural disorder and disulfide bond rearrangement, suggesting a more flexible and heterogeneous network. These molecular insights are consistent with the physicochemical results in Chapter 4, where mung bean systems showed higher elasticity, hardness, and stretchability but lower meltability, while hemp systems exhibited improved meltability. Overall, the integration of spectroscopic and physicochemical analyses demonstrates that differences in protein interactions and structural organisation underpin the observed functional behaviour in hybrid cheese systems.

8.1.3. Enzymatic modification as a structural engineering tool to improve cheese meltability

Given the inherent rigidity of plant proteins compared with casein, plant-based processed cheese analogues often exhibit coarse, aggregated microstructures and poor meltability. Protein modification therefore represents a feasible strategy to improve their functionality. Enzymatic hydrolysis, in particular, offers a promising approach to tailor the techno-functional properties of plant proteins. **In Chapter 7**, mung bean protein isolate was enzymatically hydrolysed using Alcalase for different durations to enhance the meltability of both plant-based and hybrid cheese analogues, with additional comparison to trypsin-treated proteins.

The results showed that enzymatic hydrolysis of mung bean protein reduced molecular weight and particle size, while increasing surface hydrophobicity. These structural modifications influenced the functionality of the resulting cheese analogues. Specifically, hydrolysis improved meltability in both mung bean-based and mung bean–casein hybrid systems; however, excessive hydrolysis led to reduced elasticity and water-holding capacity due to network fragmentation. Furthermore, enzyme specificity had a greater impact than degree of hydrolysis (DH) alone. Trypsin-generated hydrolysates exhibited higher surface hydrophobicity and a greater tendency to aggregate compared to Alcalase-treated samples, resulting in more rigid networks and poorer meltability in the cheese analogues. Overall, these findings demonstrate that controlled enzymatic modification can tailor functional performance, but optimization must balance solubility, aggregation, and network continuity.

8.1.4. Conclusions

These studies demonstrate that functionality in plant-based and hybrid processed cheese analogues is fundamentally governed by protein structure across multiple scales — from molecular conformation to microstructural organization. Protein source selection, hybridization strategies, and targeted enzymatic modification represent complementary pathways for narrowing this structural–functional gap. Importantly, advanced spectroscopic techniques provide key insights into molecular changes and underlying mechanisms.

Although this study used a controlled laboratory-scale RVA system, the identified roles of protein aggregation, phase continuity and spatial distribution provide a basis for industrial formulation design. Pilot-scale validation should determine whether these relationships remain predictive

under commercial temperature–time profiles, shear conditions, residence times, moisture control and cooling rates.

This PhD work addresses critical knowledge gaps in the structure–function relationships of plant-based and hybrid processed cheese analogues by:

- Systematic comparison of plant protein functionality

This thesis provides a comprehensive comparison of diverse plant protein sources in processed cheese analogue models, demonstrating how protein origin governs rheological, textural, and microstructural properties relative to casein-based systems.

- New insights into hybrid protein systems (plant protein–casein interactions)

It elucidates the mechanisms of interaction in dual-protein hybrid cheese systems, showing that protein compatibility and interaction pathways drive network formation, microstructural organisation, and functional performance.

- Multiscale analytical framework linking molecular structure to functionality

By integrating Raman microscopy and synchrotron-based FTIR with chemometrics and machine learning, this study develops an advanced analytical framework to resolve spatial and molecular heterogeneity and link it to functional outcomes. The application of multivariate analysis and machine learning further enables the discrimination of protein sources and identification of structural transitions, providing a novel approach for analysing complex food matrices.

- Enzymatic modification as a strategy to tailor functionality

The work demonstrates that controlled enzymatic hydrolysis can effectively modify plant protein structure and aggregation behaviour, improving meltability in both plant-based and hybrid

processed cheese analogues. It reveals that enzyme specificity also plays a critical role in determining protein aggregation, network formation, and final functionality, providing new insight into targeted protein modification strategies.

- Mechanistic understanding of structure–function relationships

The thesis establishes clear links between protein physicochemical properties (e.g. aggregation behaviour, particle size, solubility, surface hydrophobicity, and secondary structure) and macroscopic functionality, particularly meltability, stretchability, rheological and textural properties. These findings provide a mechanistic basis for the rational design of plant-based and hybrid cheese systems by highlighting the need to balance protein aggregation and network structure to achieve optimal functionality.

8.2. Future directions

8.2.1. Protein structure and synergistic blending

Our results demonstrate that plant protein type, aggregation, and molecular characteristics strongly influence texture and functionality in plant-based cheese analogues. Building on this, future studies could explore blending proteins with complementary properties to achieve synergistic functionality. Systematic investigations of compatibility between different plant proteins and casein may enable the design of optimized hybrid networks with improved meltability, stretchability, and rheological performance.

8.2.2. Balancing meltability and stretchability

Enzymatic hydrolysis enhanced meltability in mung bean-based cheeses but compromised elasticity. Future work should focus on strategies that balance these properties, such as partial hydrolysis combined with crosslinking (e.g., transglutaminase), controlled aggregation engineering, or exploring alternative enzyme-plant protein combinations. Such approaches could maximize both melt and stretch performance while maintaining structural integrity.

8.2.3. Optimizing processing conditions

Processing parameters, including heating ramps, mixing regimes, or extrusion, may further influence protein network formation and fat–protein interactions. Tailoring these conditions based on protein type and network compatibility could enhance texture and functional performance in both plant-protein cheese and hybrid cheese systems.

8.2.4. Exploring other types of cheese models

Future research should extend beyond processed plant-based cheese systems to explore a broader range of cheese formats, including plant-based and hybrid mozzarella, cheddar, and aged cheese analogues. These systems involve distinct processing conditions, structural architectures, and functional requirements, such as fibrous alignment in mozzarella or proteolysis-driven texture development in aged cheeses. Investigating these diverse cheese types would provide deeper insights into plant protein functionality, particularly in terms of protein–protein and protein–lipid interactions under different thermal, mechanical, and maturation conditions.

Such studies would also enable the development of structure–function relationships across a wider spectrum of cheese applications, facilitating the design of tailored products with specific textural, melting, and sensory properties. Ultimately, expanding research into these categories will support

the creation of more diverse and high-quality plant-based and hybrid cheese products, better meeting consumer expectations and targeting a broader market.

8.2.5. Digestibility and nutritional functionality

Structural modifications introduced through enzymatic hydrolysis or hybridization alter peptide profiles and protein accessibility. Future studies should evaluate *in vitro* digestion, bioaccessibility, and nutritional outcomes to ensure that functional optimization does not compromise protein quality or health benefits. In addition, hybrid cheeses can be strategically formulated to enhance overall protein quality by combining complementary plant and milk proteins, thereby improving the Digestible Indispensable Amino Acid Score (DIAAS) and creating a more balanced and nutritionally complete protein profile.

8.2.6. Pilot-Scale production of plant-based or hybrid cheese analogues

The translation of laboratory-scale formulations to pilot-scale production of plant-based and hybrid cheese analogues is another important development. While small-scale model systems enable controlled investigation of structure–function relationships, scaling up is essential to validate the reproducibility, robustness, and industrial feasibility of these formulations. Differences in processing conditions, such as shear, heating profiles, and mixing efficiency, can significantly influence microstructure and, consequently, functional properties. Therefore, pilot-scale trials are required to optimise processing parameters and ensure that the texture, meltability, and overall quality of the products remain consistent with laboratory findings. In addition, scaling up provides an opportunity to assess product stability, shelf life, and manufacturability under realistic conditions, as well as to prepare sufficient quantities for sensory evaluation and consumer studies.

Bridging this gap between laboratory development and industrial application is critical for the successful commercialisation of plant-based and hybrid cheese products.

8.2.7. Sensory and consumer-relevant evaluation

Ultimately, structural, functional, and nutritional improvements must translate to positive sensory experiences. Integrating molecular-level analyses (e.g., Raman and S-FTIR mapping) with sensory mapping and consumer study will be critical for developing products that are both functional and acceptable to consumers.

In summary, developing high-protein, functionally optimized prototype cheeses will validate structure-driven design principles in practical applications. Hybrid systems, enzyme-modified proteins, and tailored processing strategies can be combined to create next-generation plant-based cheeses with improved texture, meltability, and nutritional performance.

Uncategorized References

Ahrné, L., & Leser, M. E. (2025). Colloidal aspects of cheese and protein-based cheese analogues. *Current Opinion in Colloid & Interface Science*, *79*, 101942. https://doi.org/https://doi.org/10.1016/j.cocis.2025.101942

Alehosseini, E., McSweeney, P. L. H., & Miao, S. (2025). Recent updates on plant protein-based dairy cheese alternatives: outlook and challenges. *Critical Reviews in Food Science and Nutrition*, *65*(30), 6846–6860. https://doi.org/10.1080/10408398.2025.2452356

Ali, B., Khan, K. Y., Majeed, H., Xu, L., Wu, F., Tao, H., & Xu, X. (2017). Imitation of soymilk-cow's milk mixed enzyme modified cheese: their composition, proteolysis, lipolysis and sensory properties. *J Food Sci Technol*, *54*(5), 1273–1285. https://doi.org/10.1007/s13197-017-2534-7

Alrosan, M., Tan, T.-C., Easa, A. M., Alu'datt, M. H., Tranchant, C. C., Almajwal, A. M., Gammoh, S., Maghaydah, S., Dheyab, M. A., Jameel, M. S., & Al-Qaisi, A. (2023). Improving the Functionality of Lentil–Casein Protein Complexes through Structural Interactions and Water Kefir-Assisted Fermentation. *Fermentation*, *9*(2), 194.

Andoyo, R., Dianti Lestari, V., Mardawati, E., & Nurhadi, B. (2018). Fractal Dimension Analysis of Texture Formation of Whey Protein-Based Foods. *International Journal of Food Science*, *2018*, 7673259. https://doi.org/10.1155/2018/7673259

Antuma, L. J., Braitmaier, S. H., Garamus, V. M., Hinrichs, J., Boom, R. M., & Keppler, J. K. (2024). Engineering artificial casein micelles for future food: Preparation rate and coagulation properties. *Journal of Food Engineering*, *366*, 111868. https://doi.org/https://doi.org/10.1016/j.jfoodeng.2023.111868

Atia, M., Wenshui, X., & Guonong, Z. (2004). Effect of soy protein supplementation on the quality of ripening Cheddar-type cheese. *International Journal of Dairy Technology*, *57*(4), 209–214. https://doi.org/https://doi.org/10.1111/j.1471-0307.2004.00107.x

Atik, D. S., & Huppertz, T. (2023). Melting of natural cheese: A review. *International Dairy Journal*, *142*, 105648. https://doi.org/https://doi.org/10.1016/j.idairyj.2023.105648

Auty, M. A. E., Twomey, M., Guinee, T. P., & Mulvihill, D. M. (2001). Development and application of confocal scanning laser microscopy methods for studying the distribution of fat and protein in selected dairy products. *Journal of Dairy Research*, *68*(3), 417–427. https://doi.org/10.1017/S0022029901004873

Balasubramanian, S., Mobasseri, G., Shi, L., Jers, C., Køhler, J. B., Boire, A., Berton-Carabin, C., Mijakovic, I., & Jensen, P. R. (2025). Production of phosphorylated and functional αs1-casein in Escherichia coli. *Trends in Biotechnology*, *43*(9), 2304–2322. https://doi.org/10.1016/j.tibtech.2025.05.015

Barth, A. (2007). Infrared spectroscopy of proteins. *Biochimica et Biophysica Acta (BBA) - Bioenergetics*, *1767*(9), 1073–1101. https://doi.org/https://doi.org/10.1016/j.bbabio.2007.06.004

Beghdadi, A., Picart-Palmade, L., Cunault, C., Marchesseau, S., & Chevalier-Lucia, D. (2022). Impact of two thermal processing routes on protein interactions and acid gelation properties of casein micelle-pea protein mixture compared to casein micelle-whey protein one. *Food Research International*, *155*, 111060. https://doi.org/https://doi.org/10.1016/j.foodres.2022.111060

Beliciu, C. M., & Moraru, C. I. (2011). The effect of protein concentration and heat treatment temperature on micellar casein–soy protein mixtures. *Food Hydrocolloids*, *25*(6), 1448–1460. https://doi.org/https://doi.org/10.1016/j.foodhyd.2011.01.011

Beliciu, C. M., & Moraru, C. I. (2013). Physico-chemical changes in heat treated micellar casein – Soy protein mixtures. *LWT - Food Science and Technology*, *54*(2), 469–476. https://doi.org/https://doi.org/10.1016/j.lwt.2013.06.013

Ben-Harb, S., Panouillé, M., Huc-Mathis, D., Moulin, G., Saint-Eve, A., Irlinger, F., Bonnarme, P., Michon, C., & Souchon, I. (2018). The rheological and microstructural properties of pea, milk, mixed pea/milk gels and gelled emulsions designed by thermal, acid, and enzyme treatments. *Food Hydrocolloids*, *77*, 75–84. https://doi.org/https://doi.org/10.1016/j.foodhyd.2017.09.022

Bittante, G., Patel, N., Cecchinato, A., & Berzaghi, P. (2022). Invited review: A comprehensive review of visible and near-infrared spectroscopy for predicting the chemical composition of cheese. *Journal of Dairy Science*, *105*(3), 1817–1836. https://doi.org/https://doi.org/10.3168/jds.2021-20640

Bobo, J. (2024). Molecular farming navigates a complex regulatory landscape [Perspective]. *Frontiers in Plant Science*, *Volume 15 - 2024*. https://doi.org/10.3389/fpls.2024.1411943

Bouhlal, Y., & Capps, O. (2022). Chapter 16 - Processed cheese: applications, challenges, and market trends. In M. El-Bakry & B. M. Mehta (Eds.), *Processed Cheese Science and Technology* (pp. 491–507). Woodhead Publishing. https://doi.org/https://doi.org/10.1016/B978-0-12-821445-9.00003-0

Braitmaier, H., Wahl, A.-L., Hinrichs, J., & Atamer, Z. (2024). Can plant-based cheese alternatives be characterized by methods for dairy cheese? Extending dairy cheese methods to characterize plant-based cheese alternatives. *International Dairy Journal*, *159*, 106056. https://doi.org/https://doi.org/10.1016/j.idairyj.2024.106056

Bryant, C. M., & McClements, D. J. (1998). Molecular basis of protein functionality with special consideration of cold-set gels derived from heat-denatured whey. *Trends in Food Science & Technology*, *9*(4), 143–151. https://doi.org/https://doi.org/10.1016/S0924-2244(98)00031-4

Campos, N., Paula, I., Perrone, Í., De Oliveira, L. F., Doriguetto, A., Wolfschoon, A., & Stephani, R. (2022). Characterization of the white dots defect ("PIPS") in "Doce de leite". *European Food Research and Technology*, *249*, 1–11. https://doi.org/10.1007/s00217-022-04149-x

Chawanji, A., Holroyd, S. E., & Nickless, E. (2022). Raman confocal microscopy to assess changes in cheddar cheese during maturation [Article]. *International Journal of Dairy Technology*, *75*(4), 882–891. https://doi.org/10.1111/1471-0307.12897

Chen, D., & Campanella, O. H. (2022). Limited enzymatic hydrolysis induced pea protein gelation at low protein concentration with less heat requirement. *Food Hydrocolloids*, *128*, 107547. https://doi.org/https://doi.org/10.1016/j.foodhyd.2022.107547

Chen, H., Xu, B., Wang, Y., Li, W., He, D., Zhang, Y., Zhang, X., & Xing, X. (2023). Emerging natural hemp seed proteins and their functions for nutraceutical applications [Review]. *Food Science and Human Wellness*, *12*(4), 929–941. https://doi.org/10.1016/j.fshw.2022.10.016

Chen, X., Nguyen, X. Y., & McClements, D. J. (2026). Design and fabrication of plant-based casein micelle analogs by controlled heating of potato protein: Factors affecting particle characteristics. *Food Bioscience*, *76*, 108258. https://doi.org/https://doi.org/10.1016/j.fbio.2026.108258

Chuang, B.-F., Chen, S.-Y., Lin, J.-A., & Yen, G.-C. (2025). Modifying pea protein by cold plasma for the development of functional vegan cheese. *Food Bioscience*, *65*, 106017. https://doi.org/https://doi.org/10.1016/j.fbio.2025.106017

Chuang, C.-C., Wegrzyn, T. F., Anema, S. G., & Loveday, S. M. (2019). Hemp globulin heat aggregation is inhibited by the chaperone-like action of caseins. *Food Hydrocolloids*.

Chuang, C. C., Ye, A., Anema, S. G., & Loveday, S. M. (2021). Hemp globulin forms colloidal nanocomplexes with sodium caseinate during pH-cycling. *Food Research International*, *150*(Pt B), 110810. https://doi.org/10.1016/j.foodres.2021.110810

Cobb, J. S., Zai-Rose, V., Correia, J. J., & Janorkar, A. V. (2020). FT-IR Spectroscopic Analysis of the Secondary Structures Present during the Desiccation Induced Aggregation of Elastin-Like Polypeptide on Silica. *ACS Omega*, *5*(14), 8403–8413. https://doi.org/10.1021/acsomega.0c00271

Considine, T., Patel, H. A., Anema, S. G., Singh, H., & Creamer, L. K. (2007). Interactions of milk proteins during heat and high hydrostatic pressure treatments — A Review. *Innovative Food Science & Emerging Technologies*, *8*(1), 1–23. https://doi.org/https://doi.org/10.1016/j.ifset.2006.08.003

Cui, H., Li, S., Roy, D., Guo, Q., & Ye, A. (2023). Modifying quinoa protein for enhanced functional properties and digestibility: A review. *Current Research in Food Science*, *7*, 100604. https://doi.org/10.1016/j.crfs.2023.100604

da Silva, R. R., Odelli, D., Descamps, A., Scudeller, L. A., Doumert, B., Perez, J., Delaplace, G., de Carvalho, A. F., & de Sá Peixoto Junior, P. P. (2025). Multi-scale organization and rheology of casein and pea protein mixed hydrogels formed by acidification: Effects of ratio and temperature.

Food Research International, *209*, 116242. https://doi.org/https://doi.org/10.1016/j.foodres.2025.116242

Dapčević-Hadnađev, T., Hadnađev, M., Lazaridou, A., Moschakis, T., & Biliaderis, C. G. (2018). Hempseed meal protein isolates prepared by different isolation techniques. Part II. gelation properties at different ionic strengths. *Food Hydrocolloids*, *81*, 481–489. https://doi.org/https://doi.org/10.1016/j.foodhyd.2018.03.022

Day, L. (2013). Proteins from land plants – Potential resources for human nutrition and food security. *Trends in Food Science & Technology*, *32*(1), 25–42. https://doi.org/https://doi.org/10.1016/j.tifs.2013.05.005

Day, L., Cakebread, J. A., & Loveday, S. M. (2022). Food proteins from animals and plants: Differences in the nutritional and functional properties. *Trends in Food Science & Technology*, *119*, 428–442. https://doi.org/https://doi.org/10.1016/j.tifs.2021.12.020

Dewantier, G. R., Torley, P. J., & Blanch, E. W. (2023). Identifying Chemical Differences in Cheddar Cheese Based on Maturity Level and Manufacturer Using Vibrational Spectroscopy and Chemometrics. *Molecules*, *28*(24), 8051.

Do, D. T., Ye, A., Singh, H., & Acevedo-Fani, A. (2024). Protein bodies from hemp seeds: Isolation, microstructure and physicochemical characterisation. *Food Hydrocolloids*, *149*, 109597. https://doi.org/https://doi.org/10.1016/j.foodhyd.2023.109597

Dobson, S., & Marangoni, A. G. (2023). Methodology and development of a high-protein plant-based cheese alternative. *Current Research in Food Science*, *7*, 100632. https://doi.org/https://doi.org/10.1016/j.crfs.2023.100632

Dobson, S., & Marangoni, A. G. (2024). Fat stabilization techniques for the reduction of oil loss in high protein plant-based cheese [Article]. *Food Hydrocolloids*, *156*, Article 110362. https://doi.org/10.1016/j.foodhyd.2024.110362

Dobson, S., & Marangoni, A. G. (2025a). Evaluating the effect of plant protein functionalities on the performance of high-protein plant-based cheese. *Food Chemistry*, *492*(Pt 3), 145553. https://doi.org/10.1016/j.foodchem.2025.145553

Dobson, S., & Marangoni, A. G. (2025b). Exploration of structural differences between dairy and plant-based cheese. *Food Structure*, *44*, 100424. https://doi.org/https://doi.org/10.1016/j.foostr.2025.100424

Du, M., Xie, J., Gong, B., Xu, X., Tang, W., Li, X., Li, C., & Xie, M. (2018). Extraction, physicochemical characteristics and functional properties of Mung bean protein. *Food Hydrocolloids*, *76*, 131–140. https://doi.org/https://doi.org/10.1016/j.foodhyd.2017.01.003

Eckhardt, L., Bu, F., Franczyk, A., Michaels, T., & Ismail, B. P. (2024). Hemp (Cannabis sativa L.) protein: Impact of extraction method and cultivar on structure, function, and nutritional quality. *Current Research in Food Science*, *8*, 100746. https://doi.org/10.1016/j.crfs.2024.100746

Espinosa-Marrón, A., Adams, K., Sinno, L., Cantu-Aldana, A., Tamez, M., Marrero, A., Bhupathiraju, S. N., & Mattei, J. (2022). Environmental Impact of Animal-Based Food Production and the Feasibility of a Shift Toward Sustainable Plant-Based Diets in the United States [Mini Review]. *Frontiers in Sustainability*, *3*. https://doi.org/10.3389/frsus.2022.841106

Fact.MR. (2023). *Plant-based Dairy Market Size & Growth Report to 2033*.

Fan, M., Wei, T., Lu, X., Liu, M., Huang, Y., Chen, F., Luo, T., Fan, Y., Liu, R., Deng, Z., & Li, J. (2023). Comprehensive quality evaluation of plant-based cheese analogues [Article]. *Journal of the Science of Food and Agriculture*, *103*(13), 6595–6604. https://doi.org/10.1002/jsfa.12754

Farahmandfar, R., Tehrani, M. M., Razavi, S. M. A., & Najafi, M. B. H. (2011). Effect of Trisodium Citrate Concentration and Soy Cheese on Meltability of Pizza Cheese. *International Journal of Food Properties*, *14*(4), 697–707. https://doi.org/10.1080/10942910903367621

Fellows, A. P., Casford, M. T. L., & Davies, P. B. (2020). Spectral Analysis and Deconvolution of the Amide I Band of Proteins Presenting with High-Frequency Noise and Baseline Shifts. *Applied Spectroscopy*, *74*(5), 597–615. https://doi.org/10.1177/0003702819898536

Ferawati, F., Hefni, M., Östbring, K., & Witthöft, C. (2021). The application of pulse flours in the development of plant-based cheese analogues: Proximate composition, color, and texture properties [Article]. *Foods*, *10*(9), Article 2208. https://doi.org/10.3390/foods10092208

Fox, P. F., Guinee, T.P., Cogan, T.M., McSweeney, P.L.H. (2017a). *Cheese structure, rheology and texture*. Springer. https://doi.org/10.1007/978- 1- 4899- 7681- 9

Freire, P. D. T., Lima Jr, J., Mendes Filho, J., Melo, F., & Barboza, F. (2017). In M. Khan (Ed.), *Raman Spectroscopy and Applications*. IntechOpen. https://doi.org/10.5772/65480

Gałkowska, D., Kapuśniak, K., & Juszczak, L. (2023). Chemically Modified Starches as Food Additives. *Molecules*, *28*(22), 7543.

Gallier, S., Gordon, K. C., & Singh, H. (2012). Chemical and structural characterisation of almond oil bodies and bovine milk fat globules. *Food Chemistry*, *132*(4), 1996–2006. https://doi.org/https://doi.org/10.1016/j.foodchem.2011.12.038

Gandhi, K., Sharma, R., Seth, R., & Mann, B. (2022). Detection of coconut oil in ghee using ATR-FTIR and chemometrics. *Applied Food Research*, *2*(1), 100035. https://doi.org/https://doi.org/10.1016/j.afres.2021.100035

Ganesh, S., Ningtyas, D. W., & Prakash, S. (2022). Investigating the functionality of enzymatically (transglutaminase and alcalase) treated almond protein isolate. *Food Bioscience*, *49*, 101914. https://doi.org/https://doi.org/10.1016/j.fbio.2022.101914

Garcia-Fontanals, L., Llorente, R., Valderrama, J., Bravo, S., & Talens, C. (2023). Hybrid Spreadable Cheese Analogues with Faba Bean and Mealworm (Tenebrio molitor) Flours: Optimisation Using Desirability-Based Mixture Design. *Foods*, *12*(7), 1522.

Gawat, M., Boland, M., Chen, J., Singh, J., & Kaur, L. (2024). Effects of microwave processing in comparison to sous vide cooking on meat quality, protein structural changes, and in vitro digestibility. *Food Chemistry*, *434*, 137442. https://doi.org/https://doi.org/10.1016/j.foodchem.2023.137442

Giri, S. K., Tripathi, M. K., & Kotwaliwale, N. (2018). Effect of composition and storage time on some physico-chemical and rheological properties of probiotic soy-cheese spread. *J Food Sci Technol*, *55*(5), 1667–1674. https://doi.org/10.1007/s13197-018-3078-1

Grasso, N., Bot, F., Roos, Y. H., Crowley, S. V., Arendt, E. K., & O'Mahony, J. A. (2022). The influence of protein concentration on key quality attributes of chickpea-based alternatives to cheese. *Current Research in Food Science*. https://doi.org/https://doi.org/10.1016/j.crfs.2022.09.028

Grasso, N., Bot, F., Roos, Y. H., Crowley, S. V., Arendt, E. K., & O'Mahony, J. A. (2023). Plant-Based Alternatives to Cheese Formulated Using Blends of Zein and Chickpea Protein Ingredients. *Foods*, *12*(7), 1492.

Grasso, N., Roos, Y. H., Crowley, S. V., Arendt, E. K., & O'Mahony, J. A. (2021). Composition and physicochemical properties of commercial plant-based block-style products as alternatives to cheese. *Future Foods*, *4*, 100048. https://doi.org/https://doi.org/10.1016/j.fufo.2021.100048

Grasso, N., Roos, Y. H., Crowley, S. V., & O'Mahony, J. A. (2024). Physicochemical properties of plant-based cheese alternatives fortified with calcium [Article]. *LWT*, *193*, Article 115657. https://doi.org/10.1016/j.lwt.2023.115657

Grasso, N., Thulesen, L., Petersen, I., Skibinska, I., Kilcawley, K., & O'Mahony, J. (2025). Formulation and Key Quality Attributes of a Plant-Based Alternative to Cheese Prototype Prepared Using Zein and Chickpea Protein Ingredients. *Sustainable Food Proteins*, *3*. https://doi.org/10.1002/sfp2.70013

Grossmann, L., & McClements, D. J. (2021). The science of plant-based foods: Approaches to create nutritious and sustainable plant-based cheese analogs. *Trends in Food Science & Technology*, *118*, 207–229. https://doi.org/https://doi.org/10.1016/j.tifs.2021.10.004

Grygorczyk, A., Duizer, L., Lesschaeve, I., & Corredig, M. (2014). Gelation of recombined soymilk and cow's milk gels: Effect of homogenization order and mode of gelation on microstructure

and texture of the final matrix. *Food Hydrocolloids*, *35*, 69–77. https://doi.org/https://doi.org/10.1016/j.foodhyd.2013.04.011

Guidi, S., Formica, F. A., & Denkel, C. (2022). Mixing plant-based proteins: Gel properties of hemp, pea, lentil proteins and their binary mixtures. *Food Research International*, *161*, 111752. https://doi.org/https://doi.org/10.1016/j.foodres.2022.111752

Guinee, T. P. (2011). Cheese Rheology. In J. W. Fuquay (Ed.), *Encyclopedia of Dairy Sciences (Second Edition)* (pp. 685–697). Academic Press. https://doi.org/https://doi.org/10.1016/B978-0-12-374407-4.00082-0

Gunn, S., Sizeland, K. H., Wells, H. C., & Haverkamp, R. G. (2022). Collagen arrangement and strength in sausage casings produced from natural intestines. *Food Hydrocolloids*, *129*, 107612. https://doi.org/https://doi.org/10.1016/j.foodhyd.2022.107612

Hadnađev, M., Dapčević-Hadnađev, T., Lazaridou, A., Moschakis, T., Michaelidou, A. M., Popović, S., & Biliaderis, C. G. (2018). Hempseed meal protein isolates prepared by different isolation techniques. Part I. physicochemical properties. *Food Hydrocolloids*, *79*, 526–533. https://doi.org/https://doi.org/10.1016/j.foodhyd.2017.12.015

Hanley, L., Dobson, S., Stobbs, J., & Marangoni, A. G. (2025). Physicochemical and functional characterization of plant protein isolates and their influence on plant-based mozzarella cheese performance. *Food Hydrocolloids*, *164*, 111222. https://doi.org/https://doi.org/10.1016/j.foodhyd.2025.111222

Harvey, S. (2023). *Precision fermentation cracks stretch-and-melt cheese code but more challenges await*. Retrieved 2023 from https://www.just-food.com/features/precision-fermentation-cracks-stretch-and-melt-cheese-code-but-more-challenges-await/?cf-view

Holroyd, S. E., & Nickless, E. (2024). Understanding mozzarella cheese microstructure with Raman confocal imaging. *International Dairy Journal*, *152*, 105893. https://doi.org/https://doi.org/10.1016/j.idairyj.2024.105893

Holroyd, S. E., Nickless, E., & Watkinson, P. (2023). Raman and mid-infrared spectroscopy to assess changes in Cheddar cheese with maturation [Article]. *International Journal of Dairy Technology*, *76*(2), 408–417. https://doi.org/10.1111/1471-0307.12929

Holt, C., Carver, J. A., Ecroyd, H., & Thorn, D. C. (2013). Invited review: Caseins and the casein micelle: Their biological functions, structures, and behavior in foods1. *Journal of Dairy Science*, *96*(10), 6127–6146. https://doi.org/https://doi.org/10.3168/jds.2013-6831

Hossain Brishti, F., Chay, S. Y., Muhammad, K., Rashedi Ismail-Fitry, M., Zarei, M., Karthikeyan, S., Caballero-Briones, F., & Saari, N. (2021). Structural and rheological changes of texturized mung bean protein induced by feed moisture during extrusion. *Food Chemistry*, *344*, 128643. https://doi.org/https://doi.org/10.1016/j.foodchem.2020.128643

Hu, Y., Cheng, L., Gilbert, E. P., Loo, T. S., Lee, S. J., Harrison, J., & Yang, Z. (2024). Fibrillisation of faba bean protein isolate by thermosonication for process efficacy: Microstructural characteristics, assembly behaviour, and physicochemical properties. *Food Hydrocolloids*, *154*, 110127. https://doi.org/https://doi.org/10.1016/j.foodhyd.2024.110127

Hu, Y., Cheng, L., Lee, S. J., & Yang, Z. (2023). Formation and characterisation of concentrated emulsion gels stabilised by faba bean protein isolate and its applications for 3D food printing. *Colloids and Surfaces A: Physicochemical and Engineering Aspects*, *671*, 131622. https://doi.org/https://doi.org/10.1016/j.colsurfa.2023.131622

Hwang, C.-L., & Yoon, K. (1981). Methods for Multiple Attribute Decision Making. In C.-L. Hwang & K. Yoon (Eds.), *Multiple Attribute Decision Making: Methods and Applications A State-of-the-Art Survey* (pp. 58–191). Springer Berlin Heidelberg. https://doi.org/10.1007/978-3-642-48318-9_3

Itoh, T., Garcia, R. N., Adachi, M., Maruyama, Y., Tecson-Mendoza, E. M., Mikami, B., & Utsumi, S. (2006). Structure of 8Sα globulin, the major seed storage protein of mung bean. *Acta Crystallographica Section D*, *62*(7), 824–832. https://doi.org/https://doi.org/10.1107/S090744490601804X

Jadhav, H. B., Das, M., Das, A., V, G., Choudhary, P., Annapure, U., & Alaskar, K. (2024). Enhancing the functionality of plant-based proteins with the application of ultrasound–A review. *Measurement: Food*, *13*, 100139. https://doi.org/https://doi.org/10.1016/j.meafoo.2024.100139

Johnson, M. E. (2017). A 100-Year Review: Cheese production and quality. *Journal of Dairy Science*, *100*(12), 9952–9965. https://doi.org/https://doi.org/10.3168/jds.2017-12979

Jurowski, K., Noga, M., Kobylarz, D., Niżnik, Ł., & Krośniak, A. (2024). Multimodal Imaging Using Raman Spectroscopy and FTIR in a Single Analytical Instrument with a Microscope (Infrared Raman Microscopy AIRsight, Shimadzu): Opportunities and Applications. *International Journal of Molecular Sciences*, *25*(13). https://doi.org/10.3390/ijms25136884

Kamath, R., Basak, S., & Gokhale, J. (2022). Recent trends in the development of healthy and functional cheese analogues-a review. *LWT*, *155*, 112991. https://doi.org/https://doi.org/10.1016/j.lwt.2021.112991

Kanwal, N., Zhang, M., Law, C. L., khan, S., & Huang, J. (2025). Integrating cellular agriculture with 3D food printing: A pathway to customized, sustainable animal-free dairy foods. *Food Bioscience*, *69*, 107017. https://doi.org/https://doi.org/10.1016/j.fbio.2025.107017

Kapoor, R., Lehtola, P., & Metzger, L. E. (2004). Comparison of Pilot-Scale and Rapid Visco Analyzer Process Cheese Manufacture. *Journal of Dairy Science*, *87*(9), 2813–2821. https://doi.org/https://doi.org/10.3168/jds.S0022-0302(04)73409-8

Kapoor, R., & Metzger, L. E. (2005). Small-scale manufacture of process cheese using a rapid visco analyzer. *Journal of Dairy Science*, *88*(10), 3382–3391. https://doi.org/10.3168/jds.S0022-0302(05)73022-8

Karami, Z., Butkinaree, C., Yingchutrakul, Y., Simanon, N., & Duangmal, K. (2022). Comparative study on structural, biological and functional activities of hydrolysates from Adzuki bean (Vigna angularis) and mung bean (Vigna radiata) protein concentrates using Alcalase and Flavourzyme. *Food Research International*, *161*, 111797. https://doi.org/https://doi.org/10.1016/j.foodres.2022.111797

Khiabanian, N. O., Motamedzadegan, A., Raisi, S. N., & Alimi, M. (2022). Structure–rheology characterization of whey-less Feta cheese containing milk protein concentrate/soy protein isolate. *Korea-Australia Rheology Journal*, *34*(1), 35–49. https://doi.org/10.1007/s13367-022-00020-3

Kim, W., Wang, Y., & Selomulya, C. (2020). Dairy and plant proteins as natural food emulsifiers. *Trends in Food Science & Technology*, *105*, 261–272. https://doi.org/https://doi.org/10.1016/j.tifs.2020.09.012

Kim, W., Wang, Y., Vongsvivut, J., Ye, Q., & Selomulya, C. (2023). On surface composition and stability of β-carotene microcapsules comprising pea/whey protein complexes by synchrotron-FTIR microspectroscopy. *Food Chemistry*, *426*, 136565. https://doi.org/https://doi.org/10.1016/j.foodchem.2023.136565

Klost, M., Giménez-Ribes, G., & Drusch, S. (2020). Enzymatic hydrolysis of pea protein: Interactions and protein fractions involved in fermentation induced gels and their influence on rheological properties. *Food Hydrocolloids*, *105*, 105793. https://doi.org/https://doi.org/10.1016/j.foodhyd.2020.105793

Koca, N., Rodriguez-Saona, L. E., Harper, W. J., & Alvarez, V. B. (2007). Application of Fourier transform infrared spectroscopy for monitoring short-chain free fatty acids in Swiss cheese. *Journal of Dairy Science*, *90*(8), 3596–3603. https://doi.org/10.3168/jds.2007-0063

Koekuyt, H. A., Dobson, S., & Marangoni, A. G. (2025). Lipid complexation improves the mechanical properties and functionality of legume starch gels. *Food Hydrocolloids*, *167*, 111401. https://doi.org/https://doi.org/10.1016/j.foodhyd.2025.111401

Kosikowski, F. (1977). *Cheese and Fermented Milk Foods*. F.V. Kosikowski & Associ.

Kovačević, J., Bechtold, T., & Pham, T. (2024). Plant-Based Proteins and Their Modification and Processing for Vegan Cheese Production. *Macromol*, *4*(1), 23–41.

Lamichhane, P., Kelly, A. L., & Sheehan, J. J. (2018). Symposium review: Structure-function relationships in cheese. *Journal of Dairy Science*, *101*(3), 2692–2709. https://doi.org/https://doi.org/10.3168/jds.2017-13386

Larkin, P. J. (2018). *Infrared and Raman Spectroscopy (Second Edition)*. Elsevier. https://doi.org/https://doi.org/10.1016/B978-0-12-804162-8.00001-X

Li, H., Yang, C., Chen, C., Ren, F., Li, Y., Mu, Z., & Wang, P. (2018). The Use of Trisodium Citrate to Improve the Textural Properties of Acid-Induced, Transglutaminase-Treated Micellar Casein Gels. *Molecules*, *23*(7), 1632.

Li, K., Yang, J., Tong, Q., Zhang, W., & Wang, F. (2018). Effect of enzyme modified soymilk on rennet induced gelation of skim milk [Article]. *Molecules*, *23*(12), Article 3084. https://doi.org/10.3390/molecules23123084

Li, Q., Xia, Y., Zhou, L., & Xie, J. (2013). Evaluation of the rheological, textural, microstructural and sensory properties of soy cheese spreads. *Food and Bioproducts Processing*, *91*, 429–439. https://doi.org/10.1016/j.fbp.2013.03.001

Li, S., Feng, X., Hao, X., Zhu, Y., Zou, L., Chen, X., & Yao, Y. (2023). A comprehensive review of mung bean proteins: Extraction, characterization, biological potential, techno-functional properties, modifications, and applications. *Comprehensive Reviews in Food Science and Food Safety*, *n/a*(n/a). https://doi.org/https://doi.org/10.1111/1541-4337.13183

Li, S., Ye, A., & Singh, H. (2021). Physicochemical changes and age gelation in stored UHT milk: Seasonal variations. *International Dairy Journal*, *118*, 105028. https://doi.org/https://doi.org/10.1016/j.idairyj.2021.105028

Li, Y., Zhang, X., Yang, J. J., Ma, X. Y., Jia, X. D., Du, P., & Li, A. L. (2020). Influence of the addition of Geotrichum candidum on the microbial, chemical, textural, and sensory features of soft soy cheese [Article]. *Journal of Food Processing and Preservation*, *44*(11), Article e14823. https://doi.org/10.1111/jfpp.14823

Limit, D., Austin, L., Wickramaarachchi, P., Mannino, N. C., & Chen, D. (2024). Softening fat-free cream cheese by incorporating aggregates of pea protein hydrolysates. *Food Hydrocolloids*, *147*, 109317. https://doi.org/https://doi.org/10.1016/j.foodhyd.2023.109317

Lingiardi, N., Galante, M., de Sanctis, M., & Spelzini, D. (2022). Are quinoa proteins a promising alternative to be applied in plant-based emulsion gel formulation? *Food Chemistry*, *394*, 133485. https://doi.org/https://doi.org/10.1016/j.foodchem.2022.133485

Liu, C., Bhattarai, M., Mikkonen, K. S., & Heinonen, M. (2019). Effects of Enzymatic Hydrolysis of Fava Bean Protein Isolate by Alcalase on the Physical and Oxidative Stability of Oil-in-Water Emulsions. *Journal of Agricultural and Food Chemistry*, *67*(23), 6625–6632. https://doi.org/10.1021/acs.jafc.9b00914

Liu, F. F., Li, Y. Q., Wang, C. Y., Liang, Y., Zhao, X. Z., He, J. X., & Mo, H. Z. (2022). Physicochemical, functional and antioxidant properties of mung bean protein enzymatic hydrolysates. *Food Chemistry*, *393*, 133397. https://doi.org/10.1016/j.foodchem.2022.133397

Liu, S., Yuan, T. Z., Wang, X., Reimer, M., Isaak, C., & Ai, Y. (2019). Behaviors of starches evaluated at high heating temperatures using a new model of Rapid Visco Analyzer – RVA 4800. *Food Hydrocolloids*, *94*, 217–228. https://doi.org/https://doi.org/10.1016/j.foodhyd.2019.03.015

Liu, Y., Wei, L., Zhang, J., Cao, Z., Yang, G., Zhou, C., Li, Y., & Wang, W. (2025). Tunable techno-functional properties of pea protein gel through microbial transglutaminase synergize pea inner fiber with varying particle sizes and volumetric ratio. *Food Research International*, *221*, 117374. https://doi.org/https://doi.org/10.1016/j.foodres.2025.117374

Loveday, S. M., & Halim, C. (2024). Protein isolates made in the laboratory versus the factory: A case study with mung bean and chickpea. *Sustainable Food Proteins*, *2*(2), 89–98. https://doi.org/https://doi.org/10.1002/sfp2.1027

Lu, D., McGoverin, C., Roy, D., Acevedo-Fani, A., Singh, H., Waterland, M., Zheng, Y., & Ye, A. (2026). Distinguishing plant and milk proteins and their interactions in hybrid cheese using confocal Raman

microscopy with machine learning. *Food Chemistry*, *498*, 147102. https://doi.org/https://doi.org/10.1016/j.foodchem.2025.147102

Lu, D., Roy, D., Acevedo-Fani, A., Singh, H., Waterland, M., & Ye, A. (2026). Physical properties and microstructure of hybrid processed cheeses formulated with plant protein and milk protein ingredients. *Food Hydrocolloids*, *170*, 111688. https://doi.org/https://doi.org/10.1016/j.foodhyd.2025.111688

Lu, D., Roy, D., Acevedo-Fani, A., Singh, H., & Ye, A. (2025). Investigation of various plant protein ingredients for processed cheese analogues: physical properties and microstructure compared with milk proteins. *International Journal of Food Science and Technology*, *60*(1). https://doi.org/10.1093/ijfood/vvae018

Lu, D., Vongsvivut, J., Klein, A. R., McGoverin, C., Waterland, M., Zheng, Y., Acevedo–Fani, A., Roy, D., Singh, H., & Ye, A. (2026). Elucidating protein–lipid microstructure and interactions in hybrid processed cheeses using synchrotron macro ATR-FTIR microspectroscopy. *Food Structure*, *47*, 100511. https://doi.org/https://doi.org/10.1016/j.foostr.2026.100511

Lucey, J. A., & Fox, P. F. (1993). Importance of Calcium and Phosphate in Cheese Manufacture: A Review. *Journal of Dairy Science*, *76*(6), 1714–1724. https://doi.org/https://doi.org/10.3168/jds.S0022-0302(93)77504-9

Lucey, J. A., Johnson, M. E., & Horne, D. S. (2003). Invited Review: Perspectives on the Basis of the Rheology and Texture Properties of Cheese. *Journal of Dairy Science*, *86*(9), 2725–2743. https://doi.org/https://doi.org/10.3168/jds.S0022-0302(03)73869-7

Luo, J., Liu, S., Wang, Y., Chen, Q., & Shi, Y. (2025). Improvement of compositional, textural, and rheological characteristics in plant-based cheese analogs fermented by kefir grain. *Food Chemistry*, *477*, 143519. https://doi.org/https://doi.org/10.1016/j.foodchem.2025.143519

Lyu, Z., Sala, G., & Scholten, E. (2023). Melting properties of vegan cheese: Effect of emulsion and protein addition on the thermal behaviour of starch gels [Article]. *Food Hydrocolloids*, *144*, Article 108917. https://doi.org/10.1016/j.foodhyd.2023.108917

Maltais, A., Remondetto, G. E., Gonzalez, R., & Subirade, M. (2005). Formation of Soy Protein Isolate Cold-set Gels: Protein and Salt Effects. *Journal of Food Science*, *70*(1), C67–C73. https://doi.org/https://doi.org/10.1111/j.1365-2621.2005.tb09023.x

Margolies, B. J., & Barbano, D. M. (2018). Determination of fat, protein, moisture, and salt content of Cheddar cheese using mid-infrared transmittance spectroscopy. *Journal of Dairy Science*, *101*(2), 924–933. https://doi.org/10.3168/jds.2017-13431

Masiá, C., Jensen, P. E., Petersen, I. L., & Buldo, P. (2022). Design of a Functional Pea Protein Matrix for Fermented Plant-Based Cheese [Article]. *Foods*, *11*(2), Article 178. https://doi.org/10.3390/foods11020178

Mattice, K. D., & Marangoni, A. G. (2020a). Evaluating the use of zein in structuring plant-based products. *Current Research in Food Science*, *3*, 59–66. https://doi.org/https://doi.org/10.1016/j.crfs.2020.03.004

Mattice, K. D., & Marangoni, A. G. (2020b). Physical properties of plant-based cheese products produced with zein. *Food Hydrocolloids*, *105*, 105746. https://doi.org/https://doi.org/10.1016/j.foodhyd.2020.105746

Mazac, R., Järviö, N., & Tuomisto, H. L. (2023). Environmental and nutritional Life Cycle Assessment of novel foods in meals as transformative food for the future. *Science of The Total Environment*, *876*, 162796. https://doi.org/https://doi.org/10.1016/j.scitotenv.2023.162796

Mazinani, S., Motamedzadegan, A., Naghizadeh Raeisi, S., & Alimi, M. (2020). Impact of pea protein isolate in partial substitution of milk protein concentrate on the microstructural, rheological, and sensory properties of bacteriologically acidified feta-type cheese [Article]. *Journal of Food Processing and Preservation*, *44*(6), Article e14448. https://doi.org/10.1111/jfpp.14448

Mazinani, S., Motamedzadegan, A., Nghizadeh Raeisi, S., & Alimi, M. (2021). Characterization of bacteriologically acidified feta cheese using soy protein isolate in different substitution percentages:

rheological, microbiological and sensory properties [Article]. *Journal of Food Measurement and Characterization*, *15*(6), 5515–5527. https://doi.org/10.1007/s11694-021-00973-z

McSweeney, P. L. H., Ottogalli, G., & Fox, P. F. (2017). Chapter 31 - Diversity and Classification of Cheese Varieties: An Overview. In P. L. H. McSweeney, P. F. Fox, P. D. Cotter, & D. W. Everett (Eds.), *Cheese (Fourth Edition)* (pp. 781–808). Academic Press. https://doi.org/https://doi.org/10.1016/B978-0-12-417012-4.00031-4

Mefleh, M., Pasqualone, A., Caponio, F., De Angelis, D., Natrella, G., Summo, C., & Faccia, M. (2022). Spreadable plant-based cheese analogue with dry-fractioned pea protein and inulin–olive oil emulsion-filled gel. *Journal of the Science of Food and Agriculture*, *102*(12), 5478–5487. https://doi.org/https://doi.org/10.1002/jsfa.11902

Mendoza, E. M. T., Adachi, M., Bernardo, A. E. N., & Utsumi, S. (2001). Mungbean [Vigna radiata (L.) Wilczek] Globulins: Purification and Characterization. *Journal of Agricultural and Food Chemistry*, *49*(3), 1552–1558. https://doi.org/10.1021/jf001041h

Mession, J.-L., Roustel, S., & Saurel, R. (2017). Interactions in casein micelle – Pea protein system (part I): Heat-induced denaturation and aggregation. *Food Hydrocolloids*, *67*, 229–242. https://doi.org/https://doi.org/10.1016/j.foodhyd.2015.12.015

Michel, S. E. S., Scheermeijer, R., Ambühl, M., & Fernández Farrés, I. (2022). Novel plant-based cream cheese: A tribology perspective [Article]. *Journal of Food Engineering*, *335*, Article 111172. https://doi.org/10.1016/j.jfoodeng.2022.111172

Miller, L. M., & Dumas, P. (2010). From structure to cellular mechanism with infrared microspectroscopy. *Current Opinion in Structure Biology*, *20*(5), 649–656. https://doi.org/10.1016/j.sbi.2010.07.007

Monga, A., Dev, M. J., & Singhal, R. S. (2022). Cottage cheese from blends of fresh green peas (Pisum sativum L.) and dairy milk (pEaneer): Preparation, characterization, and sensory evaluation [Article]. *LWT*, *160*, Article 113263. https://doi.org/10.1016/j.lwt.2022.113263

Moradi, D., Ziarati, P., & Sawicka, B. (2021). Physicochemical and rheological properties of lentil milk/inulin blend—A feta cheese analogue [Article]. *Legume Science*, *3*(4), Article e80. https://doi.org/10.1002/leg3.80

Mounsey, J. S., & O'riordan, E. D. (2001). Characteristics of Imitation Cheese Containing Native Starches. *Journal of Food Science*, *66*(4), 586–591. https://doi.org/https://doi.org/10.1111/j.1365-2621.2001.tb04606.x

Mounsey, J. S., & O'Riordan, E. D. (2008). Alteration of imitation cheese structure and melting behaviour with wheat starch. *European Food Research and Technology*, *226*(5), 1013–1019. https://doi.org/10.1007/s00217-007-0626-8

Movasaghi, Z., Rehman, S., & ur Rehman, D. I. (2008). Fourier Transform Infrared (FTIR) Spectroscopy of Biological Tissues. *Applied Spectroscopy Reviews*, *43*(2), 134–179. https://doi.org/10.1080/05704920701829043

Nascimento, L. G. L., da Silva, R. R., Odelli, D., Doumert, B., Martins, E., Casanova, F., Marie, R., Carvalho, A. F., Delaplace, G., & de Sá Peixoto Junior, P. P. (2024). Acid gelation of high-concentrated casein micelles and pea proteins mixed systems. *Food Research International*, *196*, 114982. https://doi.org/https://doi.org/10.1016/j.foodres.2024.114982

Nickless, E., & Holroyd, S. (2020). Raman imaging of protein in a model cheese system. *Journal of Spectral Imaging*, *9*(1), a9. https://doi.org/DOI:10.1255/jsi.2020.a9

Nielsen, P. M., Petersen, D., & Dambmann, C. (2001). Improved Method for Determining Food Protein Degree of Hydrolysis. *Journal of Food Science*, *66*(5), 642–646. https://doi.org/https://doi.org/10.1111/j.1365-2621.2001.tb04614.x

Noronha, N., Duggan, E., Ziegler, G. R., O'Riordan, E. D., & O'Sullivan, M. (2008). Inclusion of starch in imitation cheese: Its influence on water mobility and cheese functionality. *Food Hydrocolloids*, *22*(8), 1612–1621. https://doi.org/https://doi.org/10.1016/j.foodhyd.2007.11.007

Noronha, N., Duggan, E., Ziegler, G. R., Stapleton, J. J., O'Riordan, E. D., & O'Sullivan, M. (2008). Comparison of microscopy techniques for the examination of the microstructure of starch-

containing imitation cheeses. *Food Research International*, *41*(5), 472–479. https://doi.org/https://doi.org/10.1016/j.foodres.2008.02.008

Notarnicola, B., Tassielli, G., Renzulli, P. A., Castellani, V., & Sala, S. (2017). Environmental impacts of food consumption in Europe. *Journal of Cleaner Production*, *140*, 753–765. https://doi.org/https://doi.org/10.1016/j.jclepro.2016.06.080

Oliveira, K., Callegaro, L., Stephani, R., Almeida, M., & De Oliveira, L. F. (2016). Analysis of Spreadable Cheese by Raman Spectroscopy and Chemometric Tools. *Food Chemistry*, *194*, 441–446. https://doi.org/10.1016/j.foodchem.2015.08.039

Omrani Khiabanian, N., Motamedzadegan, A., Naghizadeh Raisi, S., & Alimi, M. (2020). Chemical, textural, rheological, and sensorial properties of wheyless feta cheese as influenced by replacement of milk protein concentrate with pea protein isolate [Article]. *Journal of Texture Studies*, *51*(3), 488–500. https://doi.org/10.1111/jtxs.12508

Ong, L., Li, X., Ong, A., & Gras, S. L. (2022). New Insights into Cheese Microstructure. *Annual Review of Food Science and Technology*, *13*(Volume 13, 2022), 89–115. https://doi.org/https://doi.org/10.1146/annurev-food-032519-051812

Ong, L., Pax, A. P., Ong, A., Vongsvivut, J., Tobin, M. J., Kentish, S. E., & Gras, S. L. (2020). The effect of pH on the fat and protein within cream cheese and their influence on textural and rheological properties. *Food Chemistry*, *332*, 127327. https://doi.org/10.1016/j.foodchem.2020.127327

Onwulata, C. I., Tunick, M. H., & Thomas-Gahring, A. E. (2014). Rapid Visco Analysis of Food Protein Pastes. *Journal of Food Processing and Preservation*, *38*(5), 2083–2089. https://doi.org/https://doi.org/10.1111/jfpp.12188

Ørskov, K. E., Christensen, L. B., Wiking, L., Hannibal, T., & Hammershøj, M. (2021). Imitation cheese – New insights to relations between microstructure and functionality. *Food Structure*, *29*, 100206. https://doi.org/https://doi.org/10.1016/j.foostr.2021.100206

Ørskov, K. E., Christensen, L. B., Wiking, L., Hannibal, T., & Hammershøj, M. (2023). Detecting interactions between starch and casein in imitation cheese by FTIR and Raman spectroscopy. *Food Chemistry Advances*, *2*, 100322. https://doi.org/https://doi.org/10.1016/j.focha.2023.100322

Ørskov, K. E., Christensen, L. B., Wiking, L., Hannibal, T., & Hammershøj, M. (2024). Microstructural studies of imitation cheese with a shift in continuous phase. *Food Research International*, *184*, 114210. https://doi.org/https://doi.org/10.1016/j.foodres.2024.114210

Ozturk, O. K., Salgado, A. M., Holding, D. R., Campanella, O. H., & Hamaker, B. R. (2023). Dispersion of zein into pea protein with alkaline agents imparts cohesive and viscoelastic properties for plant-based food analogues. *Food Hydrocolloids*, *134*, 108044. https://doi.org/https://doi.org/10.1016/j.foodhyd.2022.108044

Palatzidi, A., Nikoloudaki, O., Tlais, A. Z. A., Zannini, E., O'Mahony, J. A., Tsakalidou, E., Gobbetti, M., & Di Cagno, R. (2025). Fermented plant-based cream cheese analogues formulated using legume flours and avocado pulp. *Future Foods*, *11*, 100580. https://doi.org/https://doi.org/10.1016/j.fufo.2025.100580

Palatzidi, A., Nikoloudaki, O., Torreiro, M. G., Matteucci, C., Ferrentino, G., Scampicchio, M. M., Di Cagno, R., & Gobbetti, M. (2024). Novel formulations for developing fresh hybrid cheese analogues utilizing fungal-fermented brewery side-stream flours. *Current Research in Food Science*, *9*, 100829. https://doi.org/10.1016/j.crfs.2024.100829

Park, J., Rosenau, J. R., & Peleg, M. (1984). Comparison of Four Procedures of Cheese Meltability Evaluation. *Journal of Food Science*, *49*(4), 1158–1170. https://doi.org/https://doi.org/10.1111/j.1365-2621.1984.tb10417.x

Paula Vilela, T., Gomes, A. M., & Ferreira, J. P. (2020). Probing the structure-holding interactions in cheeses by dissociating agents - A review and an experimental evaluation with emmental cheese. *Current Research in Food Science*, *3*, 201–206. https://doi.org/10.1016/j.crfs.2020.07.001

Pax, A. P., Ong, L., Pax, R. A., Vongsvivut, J., Tobin, M. J., Kentish, S. E., & Gras, S. L. (2023). Industrial freezing and tempering for optimal functional properties in thawed Mozzarella cheese. *Food Chemistry*, *405*, 134933. https://doi.org/https://doi.org/10.1016/j.foodchem.2022.134933

Pax, A. P., Ong, L., Vongsvivut, J., Tobin, M. J., Kentish, S. E., & Gras, S. L. (2019). The characterisation of Mozzarella cheese microstructure using high resolution synchrotron transmission and ATR-FTIR microspectroscopy. *Food Chemistry*, *291*, 214–222. https://doi.org/https://doi.org/10.1016/j.foodchem.2019.04.016

Peixoto, P. D., Bouchoux, A., Huet, S., Madec, M. N., Thomas, D., Floury, J., & Gésan-Guiziou, G. (2015). Diffusion and partitioning of macromolecules in casein microgels: evidence for size-dependent attractive interactions in a dense protein system. *Langmuir*, *31*(5), 1755–1765. https://doi.org/10.1021/la503657u

Pennells, J., Watkins, P., Bowler, A. L., Watson, N. J., & Knoerzer, K. (2025). Mapping the AI Landscape in Food Science and Engineering: A Bibliometric Analysis Enhanced with Interactive Digital Tools and Company Case Studies. *Food Eng Rev*, *17*(3), 465–489. https://doi.org/10.1007/s12393-025-09413-w

PM, R., Kumar GV, P., Gaur, A., Singh, L., Hossain, S., Alsulami, T., Rafiq, S. M., & Nayik, G. A. (2024). Microbial transglutaminase in cashew-based vegan cheese: an innovative approach in achieving ideal texture and meltability. *International Journal of Food Science & Technology*, *59*(11), 8290–8297. https://doi.org/https://doi.org/10.1111/ijfs.17539

Popp, A., Lotze-Campen, H., & Bodirsky, B. (2010). Food consumption, diet shifts and associated non-CO2 greenhouse gases from agricultural production. *Global Environmental Change*, *20*(3), 451–462. https://doi.org/https://doi.org/10.1016/j.gloenvcha.2010.02.001

Pratap, D., Singh, R., Ravichandran, C., Ojha, A., Upadhyay, A., Kaur, B. P., & Senthilkumar, T. (2019). Evaluation of physicochemical, antioxidant, and sensory characteristics of khoa prepared from blends of soy and standardized milk. *Journal of Food Processing and Preservation*, *43*(11), e14215. https://doi.org/https://doi.org/10.1111/jfpp.14215

Promjeen, K., Phongthai, S., Singh, K., Chaisan, W., Pakakaew, P., Srichairatanakool, S., Samakradhamrongthai, R. S., & Utama-ang, N. (2025). Optimization of Enzymatic Protein Hydrolysate from Mung Bean (Vigna radiata L.), and Its Functional Properties. *Foods*, *14*(14), 2459.

Promjeen, K., Phongthai, S., Singh, K., Chaisan, W., Pakakaew, P., Srichairatanakool, S., Samakradhamrongthai, R. S., & Utama-Ang, N. (2025). Optimization of Enzymatic Protein Hydrolysate from Mung Bean (Vigna radiata L.), and Its Functional Properties. *Foods*, *14*(14). https://doi.org/10.3390/foods14142459

Prow, L. A., & Metzger, L. E. (2005). Melt Analysis of Process Cheese Spread or Product Using a Rapid Visco Analyzer. *Journal of Dairy Science*, *88*(4), 1277–1287. https://doi.org/https://doi.org/10.3168/jds.S0022-0302(05)72794-6

Qiu, Y., McClements, D. J., Chen, J., Li, C., Liu, C., & Dai, T. (2023). Construction of 3D printed meat analogs from plant-based proteins: Improving the printing performance of soy protein- and gluten-based pastes facilitated by rice protein. *Food Research International*, *167*, 112635. https://doi.org/https://doi.org/10.1016/j.foodres.2023.112635

Ramel, P. R., & Marangoni, A. G. (2017). Characterization of the polymorphism of milk fat within processed cheese products. *Food Structure*, *12*, 15–25. https://doi.org/https://doi.org/10.1016/j.foostr.2017.03.001

Rashwan, A. K., I., O. A., M., A. A., Jianling, M., & and Chen, W. (2025). Plant-based proteins: advanced extraction technologies, interactions, physicochemical and functional properties, food and related applications, and health benefits. *Critical Reviews in Food Science and Nutrition*, *65*(4), 667–694. https://doi.org/10.1080/10408398.2023.2279696

Rinaldoni, A. N., Palatnik, D. R., Zaritzky, N., & Campderrós, M. E. (2014). Soft cheese-like product development enriched with soy protein concentrates [Article]. *LWT*, *55*(1), 139–147. https://doi.org/10.1016/j.lwt.2013.09.003

Rodrigues, A., Maldonado, R., & Freire, M. (2021). Effect of Partial Replacement of Milk Protein by Vegetable Proteins on the Texture of Requeijão. In (pp. 133–150). https://doi.org/10.1007/978-3-030-61817-9_7

Roesch, R. R., & Corredig, M. (2006). Study of the Effect of Soy Proteins on the Acid-Induced Gelation of Casein Micelles. *Journal of Agricultural and Food Chemistry*, *54*(21), 8236–8243. https://doi.org/10.1021/jf060875i

Rosenthal, A., & Thompson, P. (2021). What is cohesiveness?-A linguistic exploration of the food texture testing literature. *Journal of Texture Studies*, *52*, 294–302. https://doi.org/10.1111/jtxs.12586

Sadat, A., Corradini, M. G., & Joye, I. J. (2022). Vibrational and fluorescence spectroscopy to study gluten and zein interactions in complex dough systems. *Current Research in Food Science*, *5*, 479–490. https://doi.org/https://doi.org/10.1016/j.crfs.2022.02.009

Sadat, A., & Joye, I. (2020). Peak Fitting Applied to Fourier Transform Infrared and Raman Spectroscopic Analysis of Proteins. *Applied Sciences*, *10*(17), 5918. https://doi.org/10.3390/app10175918

Saji, R., Ramani, A., Gandhi, K., Seth, R., & Sharma, R. (2024). Application of FTIR spectroscopy in dairy products: A systematic review. *Food and Humanity*, *2*, 100239. https://doi.org/https://doi.org/10.1016/j.foohum.2024.100239

Salgado, A. M., Ozturk, O. K., Hamaker, B. R., & Campanella, O. H. (2023). Matching textural properties of commercial meat and cheese products using zein as the viscoelastic agent and calcium hydroxide as the textural modifier in plant-based formulations [Article]. *Food Hydrocolloids*, *137*, Article 108323. https://doi.org/10.1016/j.foodhyd.2022.108323

Salter, A. M. (2013). Impact of consumption of animal products on cardiovascular disease, diabetes, and cancer in developed countries. *Animal Frontiers*, *3*(1), 20–27. https://doi.org/10.2527/af.2013-0004

Salunke, P., Marella, C., Amamcharla, J. K., Muthukumarappan, K., & Metzger, L. E. (2022). Use of micellar casein concentrate and milk protein concentrate treated with transglutaminase in imitation cheese products—Melt and stretch properties. *Journal of Dairy Science*, *105*(10), 7904–7916. https://doi.org/https://doi.org/10.3168/jds.2022-22253

Salunke, P., & Metzger, L. E. (2022). Functional characteristics of process cheese product as affected by milk protein concentrate and micellar casein concentrate at different usage levels. *International Dairy Journal*, *128*, 105324. https://doi.org/https://doi.org/10.1016/j.idairyj.2022.105324

Sanders, C., Dobson, S., & Marangoni, A. G. (2024a). Effect of saturated and unsaturated fat on the physical properties of plant-based cheese. *Current Research in Food Science*, *9*, 100832. https://doi.org/https://doi.org/10.1016/j.crfs.2024.100832

Sanders, C., Dobson, S., & Marangoni, A. G. (2024b). Influence of protein addition in plant-based cheese. *MRS Bulletin*, *49*(10), 998–1004. https://doi.org/10.1557/s43577-024-00737-2

Sanders, C., Stobbs, J. A., Dobson, S., & Marangoni, A. G. (2025). Impact of protein sources on the functionality of plant-based cheeses formulated with saturated and unsaturated fat. *Physics of Fluids*, *37*(1). https://doi.org/10.1063/5.0238556

Sarker, M. A. H., Pillidge, C., Afshari, R., Chandrapala, J., & Gill, H. (2026). Physicochemical properties of hybrid cheddar-type curd gels made from bovine milk and plant protein isolates. *Food Hydrocolloids*, *171*, 111799. https://doi.org/https://doi.org/10.1016/j.foodhyd.2025.111799

Savello, P. A., Ernstrom, C. A., & Kalab, M. (1989). Microstructure and Meltability of Model Process Cheese Made with Rennet and Acid Casein. *Journal of Dairy Science*, *72*(1), 1–11. https://doi.org/https://doi.org/10.3168/jds.S0022-0302(89)79073-1

Schestkowa, H., Drusch, S., & Wagemans, A. M. (2020). FTIR analysis of β-lactoglobulin at the oil/water-interface. *Food Chemistry*, *302*, 125349. https://doi.org/https://doi.org/10.1016/j.foodchem.2019.125349

Seleet, F., Kassem, J., Bayomim, H., Abd-Rabou, N. S., & Ahmed, N. (2014). Production of Functional Spreadable Processed Cheese Analogue Supplemented with Chickpea. *International Journal of Dairy Science*, *9*, 1–14. https://doi.org/10.3923/ijds.2014.1.14

Shoko, Patience T., Blanch, Ewan W., Torley, Peter J., & Pillidge, C. (2024). Raman Spectroscopy for the Differentiation of Muscles and Tissues in Meat Using Chicken as a Model System. *Journal of Raman Spectroscopy*, *55*(11), 1146–1155. https://doi.org/https://doi.org/10.1002/jrs.6725

Shrestha, S., van 't Hag, L., Haritos, V., & Dhital, S. (2023). Comparative study on molecular and higher-order structures of legume seed protein isolates: Lentil, mungbean and yellow pea. *Food Chemistry*, *411*, 135464. https://doi.org/https://doi.org/10.1016/j.foodchem.2023.135464

Shrestha, S., van 't Hag, L., Haritos, V. S., & Dhital, S. (2023). Lentil and Mungbean protein isolates: Processing, functional properties, and potential food applications [Review]. *Food Hydrocolloids*, *135*, Article 108142. https://doi.org/10.1016/j.foodhyd.2022.108142

Shuai, X., Gao, L., Geng, Q., Li, T., He, X., Chen, J., Liu, C., & Dai, T. (2022). Effects of Moderate Enzymatic Hydrolysis on Structure and Functional Properties of Pea Protein. *Foods*, *11*(15), 2368.

Silva, D. M., Dos Reis, L. G., Tobin, M. J., Vongsvivut, J., Traini, D., & Sencadas, V. (2021). Co-delivery of inhalable therapies: Controlling active ingredients spatial distribution and temporal release. *Materials Science and Engineering*, *122*, 111831. https://doi.org/10.1016/j.msec.2020.111831

Silva, J. V. C., Balakrishnan, G., Schmitt, C., Chassenieux, C., & Nicolai, T. (2018). Heat-induced gelation of aqueous micellar casein suspensions as affected by globular protein addition. *Food Hydrocolloids*, *82*, 258–267. https://doi.org/https://doi.org/10.1016/j.foodhyd.2018.04.002

Silva, J. V. C., Cochereau, R., Schmitt, C., Chassenieux, C., & Nicolai, T. (2019a). Heat-induced gelation of mixtures of micellar caseins and plant proteins in aqueous solution. *Food Research International*, *116*, 1135–1143. https://doi.org/https://doi.org/10.1016/j.foodres.2018.09.058

Silva, J. V. C., Jacquette, B., Amagliani, L., Schmitt, C., Nicolai, T., & Chassenieux, C. (2019b). Heat-induced gelation of micellar casein/plant protein oil-in-water emulsions. *Colloids and Surfaces A: Physicochemical and Engineering Aspects*, *569*, 85–92. https://doi.org/https://doi.org/10.1016/j.colsurfa.2019.01.065

Sim, S. Y. J., SRV, A., Chiang, J. H., & Henry, C. J. (2021). Plant Proteins for Future Foods: A Roadmap. *Foods*, *10*(8), 1967.

Smith, G. P. S., Holroyd, S. E., Reid, D. C. W., & Gordon, K. C. (2017). Raman imaging processed cheese and its components. *Journal of Raman Spectroscopy*, *48*(3), 374–383. https://doi.org/https://doi.org/10.1002/jrs.5054

Smith, G. P. S., McGoverin, C. M., Fraser, S. J., & Gordon, K. C. (2015). Raman imaging of drug delivery systems. *Advanced Drug Delivery Reviews*, *89*, 21–41. https://doi.org/https://doi.org/10.1016/j.addr.2015.01.005

Smith, J. R. (2013). *Assessment of structure and component mobility within Mozzarella cheese*

Smith, R. Y. Y. R. L. J. J. L. (1994). *Protein Structure-Function Relationships in Foods*.

Sözeri Atik, D., & Huppertz, T. (2025). Plant-based cheese analogs: structure, texture, and functionality. *Critical Reviews in Food Science and Nutrition*, 1–17. https://doi.org/10.1080/10408398.2024.2449234

Springmann, M., Godfray, H. C. J., Rayner, M., & Scarborough, P. (2016). Analysis and valuation of the health and climate change cobenefits of dietary change. *Proceedings of the National Academy of Sciences*, *113*(15), 4146–4151. https://doi.org/doi:10.1073/pnas.1523119113

Stehfest, E., Bouwman, L., van Vuuren, D. P., den Elzen, M. G. J., Eickhout, B., & Kabat, P. (2009). Climate benefits of changing diet. *Climatic Change*, *95*(1), 83–102. https://doi.org/10.1007/s10584-008-9534-6

Stocco, G., Gómez-Mascaraque, L. G., Deshwal, G. K., Sanchez, J. C., Molle, A., Pizzamiglio, V., Berzaghi, P., Gergov, G., & Cipolat-Gotet, C. (2024). Exploring the use of NIR and Raman spectroscopy for the prediction of quality traits in PDO cheeses. *Frontiers in Nutrition*, *11*, 1327301. https://doi.org/10.3389/fnut.2024.1327301

Sun, N.-x., Liang, Y., Yu, B., Tan, C.-p., & Cui, B. (2016). Interaction of starch and casein. *Food Hydrocolloids*, *60*, 572–579. https://doi.org/https://doi.org/10.1016/j.foodhyd.2016.04.029

Sutter, R., Assad-Bustillos, M., & Windhab, E. (2023). Zein improves desirable melt-stretch properties in plant-based cheeses made from pea protein [Article]. *Food Hydrocolloids*, *144*, Article 108981. https://doi.org/10.1016/j.foodhyd.2023.108981

Tang, C.-H., & Sun, X. (2010). Physicochemical and Structural Properties of 8S and/or 11S Globulins from Mungbean [Vigna radiata (L.) Wilczek] with Various Polypeptide Constituents. *Journal of Agricultural and Food Chemistry*, *58*(10), 6395–6402. https://doi.org/10.1021/jf904254f

Tang, Q., Roos, Y. H., & Miao, S. (2023). Plant Protein versus Dairy Proteins: A pH-Dependency Investigation on Their Structure and Functional Properties. *Foods*, *12*(2), 368.

Timilsena, Y. P., Vongsvivut, J., Tobin, M. J., Adhikari, R., Barrow, C., & Adhikari, B. (2019). Investigation of oil distribution in spray-dried chia seed oil microcapsules using synchrotron-FTIR microspectroscopy. *Food Chemistry*, *275*, 457–466. https://doi.org/10.1016/j.foodchem.2018.09.043

Tojan, S. (2021). *Hybrid paneer (cottage cheese) : influence of mung bean protein isolate on the texture, microstructure, and gastro-small intestinal digestion in vitro of paneer : a thesis submitted in partial fulfilment of the requirements for the degree of Master of Food Technology, Massey University, Palmerston North, New Zealand* [Masters, Massey University]. http://hdl.handle.net/10179/17297

Tojan, S., Kaur, L., & Singh, J. (2024). Hybrid Paneer: Influence of mung bean protein isolate (Vigna radiata L.) on the texture, microstructure, and in vitro gastro-small intestinal digestion. *Food Chemistry*, *434*, 137434. https://doi.org/https://doi.org/10.1016/j.foodchem.2023.137434

Toplak, M., Read, S., Sandt, C., & Borondics, F. (2021). Quasar: Easy Machine Learning for Biospectroscopy. *Cells*, *10*, 2300. https://doi.org/10.3390/cells10092300

Turetta, F., Leonardi, M., Reniero, R., Alpi, A., & Costanzo, E. (2025). Molecular farming for the food sector. *Trends in Biotechnology*, *43*(5), 989–992. https://doi.org/https://doi.org/10.1016/j.tibtech.2024.09.015

Ushkalova, A. A., Zhao, R., Gu, Y., Wang, C., & Zhang, T. (2025). Partially substituting cheese base with plant proteins to produce processed cheese: Textural, rheological, microstructural and sensory properties. *Journal of Dairy Science*, *108*(5), 4638–4658. https://doi.org/10.3168/jds.2025-26296

Vogelsang-O'Dwyer, M., Sahin, A. W., Arendt, E. K., & Zannini, E. (2022). Enzymatic Hydrolysis of Pulse Proteins as a Tool to Improve Techno-Functional Properties. *Foods*, *11*(9). https://doi.org/10.3390/foods11091307

Vogelsang-O'Dwyer, M., Sahin, A. W., Bot, F., O'Mahony, J. A., Bez, J., Arendt, E. K., & Zannini, E. (2023). Enzymatic hydrolysis of lentil protein concentrate for modification of physicochemical and techno-functional properties. *European Food Research and Technology*, *249*(3), 573–586. https://doi.org/10.1007/s00217-022-04152-2

Vongsvivut, J., Pérez-Guaita, D., Wood, B. R., Heraud, P., Khambatta, K., Hartnell, D., Hackett, M. J., & Tobin, M. J. (2019). Synchrotron macro ATR-FTIR microspectroscopy for high-resolution chemical mapping of single cells [10.1039/C8AN01543K]. *Analyst*, *144*(10), 3226–3238. https://doi.org/10.1039/C8AN01543K

Wahl, A.-L., & Hinrichs, J. (2026). Zein-pea-hybrids as plant-based alternative to cheese: How texture and microstructure are affected by the physical characteristics of the used pea protein. *Food Hydrocolloids*, *172*, 112115. https://doi.org/https://doi.org/10.1016/j.foodhyd.2025.112115

Wang, C.-H., Huang, C.-C., Lin, L.-L., & Chen, W. (2016). The effect of disulfide bonds on protein folding, unfolding, and misfolding investigated by FT–Raman spectroscopy. *Journal of Raman Spectroscopy*, *47*(8), 940–947. https://doi.org/https://doi.org/10.1002/jrs.4935

Wang, X., Cheng, L., Wang, H., & Yang, Z. (2022). Limited Alcalase hydrolysis improves the thermally-induced gelation of quinoa protein isolate (QPI) dispersions. *Current Research in Food Science*, *5*, 2061–2069. https://doi.org/10.1016/j.crfs.2022.10.027

Warncke, M., Keienburg, S., & Kulozik, U. (2021). Cold-Renneted Milk Powders for Cheese Production: Impact of Casein/Whey Protein Ratio and Heat on the Gelling Behavior of Reconstituted Rennet Gels and on the Survival Rate of Integrated Lactic Acid Bacteria. *Foods*, *10*(7), 1606.

Wintersohle, C., Kracke, I., Ignatzy, L. M., Etzbach, L., & Schweiggert-Weisz, U. (2023). Physicochemical and chemical properties of mung bean protein isolate affected by the isolation procedure. *Current Research in Food Science*, *7*, 100582. https://doi.org/10.1016/j.crfs.2023.100582

Wouters, A. G. B., Rombouts, I., Fierens, E., Brijs, K., & Delcour, J. A. (2016). Relevance of the Functional Properties of Enzymatic Plant Protein Hydrolysates in Food Systems. *Comprehensive Reviews in Food Science and Food Safety*, *15*(4), 786–800. https://doi.org/https://doi.org/10.1111/1541-4337.12209

Xie, D., Gao, Y., Du, L., Shen, Y., Xie, J., & Wei, D. (2021). Effect of flavorzyme-modified soy protein on the functional properties, texture and microstructure of Mozzarella cheese analogue. *Journal of Food Processing and Preservation*, *45*(11), e15963. https://doi.org/https://doi.org/10.1111/jfpp.15963

Xu, C., Liu, L., Liu, J., Ye, F., Fang, C., & Lei, L. (2025). Organic Acid-Induced Structural Modifications Improve Melt-Stretch Properties and Mouthfeel of Plant-Based Cheese Alternatives. *Foods*, *14*(21), 3724.

Xu, Y., Li, J., Zhao, J., Wang, W., Griffin, J., Li, Y., Bean, S., Tilley, M., & Wang, D. (2021). Hempseed as a nutritious and healthy human food or animal feed source: a review. *International Journal of Food Science & Technology*, *56*(2), 530–543. https://doi.org/https://doi.org/10.1111/ijfs.14755

Yakoubi, S. (2024). Enhancing plant-based cheese formulation through molecular docking and dynamic simulation of tocopherol and retinol complexes with zein, soy and almond proteins via SVM-machine learning integration. *Food Chemistry*, *452*, 139520. https://doi.org/https://doi.org/10.1016/j.foodchem.2024.139520

Yang, C. (2017). *Plant protein gel formation mechanisms and their applications as delivery systems of bioactive compounds*

Ye, A., & Hewitt, S. (2009a). Phase structures impact the rheological properties of rennet-casein-based imitation cheese containing starch [Article]. *Food Hydrocolloids*, *23*(3), 867–873. https://doi.org/10.1016/j.foodhyd.2008.05.004

Ye, A., Hewitt, S., & Taylor, S. (2009). Characteristics of rennet–casein-based model processed cheese containing maize starch: Rheological properties, meltabilities and microstructures. *Food Hydrocolloids*, *23*(4), 1220–1227. https://doi.org/https://doi.org/10.1016/j.foodhyd.2008.08.016

Yi-Shen, Z., Shuai, S., & FitzGerald, R. (2018). Mung bean proteins and peptides: nutritional, functional and bioactive properties. *Food Nutr Res*, *62*. https://doi.org/10.29219/fnr.v62.1290

Yin, S.-W., Tang, C.-H., Cao, J.-S., Hu, E.-K., Wen, Q.-B., & Yang, X.-Q. (2008). Effects of limited enzymatic hydrolysis with trypsin on the functional properties of hemp (Cannabis sativa L.) protein isolate. *Food Chemistry*, *106*(3), 1004–1013. https://doi.org/https://doi.org/10.1016/j.foodchem.2007.07.030

Yiu, C. C.-Y., Kim, W., Gunawan, I. C., Vongsvivut, J., Wang, Y., & Selomulya, C. (2026). A dual polysaccharide and plant protein system for cheese analog with enhanced meltability and texture. *Food Hydrocolloids*, *171*, 111850. https://doi.org/https://doi.org/10.1016/j.foodhyd.2025.111850

Yun, S., Jeong, S., & Lee, S. (2024). Machine learning-combined rheological and structural characterization of starches for enhanced melt-stretch features in plant-based cheese analogues [Article]. *Food Hydrocolloids*, *157*, Article 110456. https://doi.org/10.1016/j.foodhyd.2024.110456

Zeng, C. (2021). *Development of Vegan Mozzarella-like cheese with extruded fava protein*

Zhai, J., Waddington, L., Wooster, T. J., Aguilar, M.-I., & Boyd, B. J. (2011). Revisiting β-Casein as a Stabilizer for Lipid Liquid Crystalline Nanostructured Particles. *Langmuir*, *27*(24), 14757–14766. https://doi.org/10.1021/la203061f

Zhang, D., Jiang, K., Luo, H., Zhao, X., Yu, P., & Gan, Y. (2024). Replacing animal proteins with plant proteins: Is this a way to improve quality and functional properties of hybrid cheeses and cheese

analogs? *Comprehensive Reviews in Food Science and Food Safety*, *23*(1), e13262. https://doi.org/https://doi.org/10.1111/1541-4337.13262

Zhang, D., Ling, X., Jiang, K., Zhao, X., & Gan, Y. (2024). Development of low-fat Mozzarella cheeses enriched with soy or pea protein hydrolysates: Composition, texture and functional properties during ageing. *International Journal of Dairy Technology*, *77*(1), 165–182. https://doi.org/https://doi.org/10.1111/1471-0307.13021

Zhang, L., Wang, X., Qi, X., Zhang, G., Natalia, V., Liu, L., Chen, Z., Su, Q., Wei, J., & Li, C. (2025). Effects of Sanxan gum on the physical and structural properties of hemp protein plant-based cheese. *LWT*, *224*, 117847. https://doi.org/https://doi.org/10.1016/j.lwt.2025.117847

Zhang, S., Huang, W., Roopesh, M. S., & Chen, L. (2022). Pre-treatment by combining atmospheric cold plasma and pH-shifting to prepare pea protein concentrate powders with improved gelling properties [Article]. *Food Research International*, *154*, Article 111028. https://doi.org/10.1016/j.foodres.2022.111028

Zhang, X., Gao, M., Zhang, Y., Dong, C., Xu, M., Hu, Y., & Luan, G. (2022). Effect of plasticizer and zein subunit on rheology and texture of zein network. *Food Hydrocolloids*, *123*, 107140. https://doi.org/https://doi.org/10.1016/j.foodhyd.2021.107140

Zhang, X., Wang, Q., Liu, Z., Zhi, L., Jiao, B., Hu, H., Ma, X., Agyei, D., & Shi, A. (2023). Plant protein-based emulsifiers: Mechanisms, techniques for emulsification enhancement and applications. *Food Hydrocolloids*, *144*, 109008. https://doi.org/https://doi.org/10.1016/j.foodhyd.2023.109008

Zhang, Y., Herneke, A., Langton, M., Johansson, M., & Corredig, M. (2025). Effect of pH and ionic strength on heat-induced pea protein isolate aggregation and gel formation. *Food Hydrocolloids*, *167*, 111393. https://doi.org/https://doi.org/10.1016/j.foodhyd.2025.111393

Zhang, Z. Y., Jiang, M. Q., & Xiong, H. M. (2023). Optimized identification of cheese products based on Raman spectroscopy and an extreme learning machine [Article]. *New Journal of Chemistry*, *47*(14), 6889–6894. https://doi.org/10.1039/d2nj06350f

Zhao, Y., Ma, C. Y., Yuen, S. N., & Phillips, D. L. (2004). Study of succinylated food proteins by Raman spectroscopy. *Journal of Agricultural and Food Chemistry*, *52*(7), 1815–1823. https://doi.org/10.1021/jf030577a

Zhou, X., Zheng, Y., Zhong, Y., Wang, D., & Deng, Y. (2022). Casein-hempseed protein complex via cross-link catalyzed by transglutaminase for improving structural, rheological, emulsifying and gelation properties [Article]. *Food Chemistry*, *383*, Article 132366. https://doi.org/10.1016/j.foodchem.2022.132366

Zhu, P., Huang, W., & Chen, L. (2022). Develop and characterize thermally reversible transparent gels from pea protein isolate and study the gel formation mechanisms. *Food Hydrocolloids*, *125*, 107373. https://doi.org/https://doi.org/10.1016/j.foodhyd.2021.107373

Zhu, P., Huang, W., Guo, X., & Chen, L. (2021). Strong and elastic pea protein hydrogels formed through pH-shifting method. *Food Hydrocolloids*, *117*, 106705. https://doi.org/https://doi.org/10.1016/j.foodhyd.2021.106705

Zuber, G., Prestrelski, S. J., & Benedek, K. (1992). Application of Fourier transform infrared spectroscopy to studies of aqueous protein solutions. *Analytical Biochemistry*, *207*(1), 150–156. https://doi.org/10.1016/0003-2697(92)90516-a

Zulkurnain, M., Goh, M. H., Karim, A. A., & Liong, M. T. (2008). Development of a soy-based cream cheese [Article]. *Journal of Texture Studies*, *39*(6), 635–654. https://doi.org/10.1111/j.1745-4603.2008.00163.x